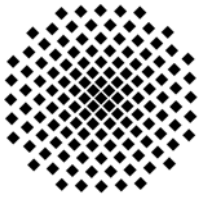

Universität Stuttgart

in collaboration with

Institut für Solare Energieversorgungstechnik
Verein an der Universität Kassel e.V.

Models for Transient Simulations of Decentral Power Generation

- Implementation and Verification in *PowerFactory*

Diplomarbeit by
Martin Braun

01.10.2004 – 31.03.2005

Supervisors:
Prof. Dr. rer. nat. Jürgen H. Werner, ipe
Prof. Dr.-Ing. Jürgen Schmid, ISET
Dr. rer. nat. Thomas Degner, ISET

Institut für Physikalische Elektronik
Prof. Dr. rer. nat. habil. J. H. Werner
Pfaffenwaldring 47
D-70569 Stuttgart

Abstract

As part of the Institut für Solare Energieversorgungstechnik (ISET) e.V. in Kassel, the Design Center for Modular Supply Technology (DeMoTec) has the facilities for testing a variety of low-voltage power grid configurations. These configurations consist of decentralized power generation components in the kilowatt range. Transient simulations of components and grid configurations with MATLAB/Simulink, ATP-EMTP and SIMPLORER support research activities in this field. The aim of this work is to add a fourth tool - *PowerFactory* - which offers additional features for this application. All four simulation tools have their own specific characteristics which make them most suitable for particular applications. This work investigates the features of *PowerFactory* developed by DIgSILENT. The investigation uses components for grid configurations which are available in DeMoTec in order to verify the results of the simulations by measurements.

The island grids which are investigated comprise three components: a bi-directional battery inverter which is able to form a grid, an asynchronous generator which simulates the feed-in of wind power, and a load which represents consumers and their consumption behaviour. In order to allow these components to be used in *PowerFactory*, this work presents the following three parts for the implementation of the components' models:

1. *PowerFactory* does not comprise a generic model for a battery inverter. However, single phase models in MATLAB/Simulink and ATP-EMTP are available which deliver details for the development of a *PowerFactory* model. For the implementation, the available models are enhanced to a three phase model and adjusted to the simulation environment of *PowerFactory*.

2. *PowerFactory* comprises a model for asynchronous generators. This generic model is adjusted to the considered asynchronous generator in DeMoTec. The electrical parameters of the analysed asynchronous generator are measured for this adjustment process and an optimisation process is performed to determine best fitting parameters.

3. A generic model for loads is available in *PowerFactory*. It is adjusted to correspond to the loads used in DeMoTec.

The models implemented in *PowerFactory* form different configurations of island grids. Within these island grids, *PowerFactory* simulates characteristic load changes. The selected components enable measurements of the same load changes in the same grid configurations in DeMoTec. A comparison of the measured and simulated data shows a good congruence with few deviations.

This thesis uses the power system analysis tool *PowerFactory* from DIgSILENT for transient simulations of decentralised power generation components in low-voltage grids which operate with a variable frequency and a variable voltage. Moreover, this thesis verifies the simulation results and illustrates their quality by comparing measured data at DeMoTec with simulated data using *PowerFactory*. Finally, one of the advantages of this simulation tool is presented by simulating a large grid configuration which is not available in the limited laboratory environment of DeMoTec.

Contents

1 Introduction

At present, there are two main developments in the power sector. On the one hand, people in developed countries face the beginning of a structural change in the power sector from a centralized power system with large power plants using fossil and nuclear power to a more decentralized power system with smaller and dispersed power plants partly driven by renewable energy resources. On the other hand, there is an increasing demand for power in developing countries. Especially in remote areas without connection to power grids, an increasing number of island grids for rural electrification are installed.

In order to comply with the emerging challenges of this restructuring process, ISET (Institut für Solare Energieversorgungstechnik e.V.) in Kassel performs considerable research in these topics. For these research activities, a laboratory, called DeMoTec (Design Center for Modular Systems Technology), is equipped with a large variety of different low-voltage decentralised power facilities in the kilowatt range, e.g. diesel generators, wind power simulators, distribution system simulators for low and medium voltage, photovoltaic inverters, battery inverters, batteries, photovoltaic-battery systems and loads. A crossbar switch cabinet connects these facilities for power transfer and an Ethernet network enables communication between them.

In order to support research activities in this field, transient simulations of components and grid configurations are performed with MATLAB/Simulink, ATP-EMTP and SIMPLORER. The aim of this work is to add a fourth tool - *PowerFactory* from DIgSILENT - which offers additional features for this application.

Each of these four simulation tools has its advantages and disadvantages. One feature of *PowerFactory* is the possibility to enlarge grid configurations by additional generic models of grid components ranging from low-voltage to high-voltage. Moreover, a variety of additional tools for analysis of power grids are implemented in *PowerFactory* comprising power flows, short circuits, harmonics, reliabilities and stabilities. Together with interfaces for GIS (geographic information system) and SCADA (supervisory control and data acquisition), this variety of features establishes a wide range of functionalities implemented in *PowerFactory*. However, one disadvantage of *PowerFactory* is the lack of standard generic models for low-voltage power generation components, e.g. photovoltaic, diesel generators and battery inverters. Consequently, they have to be developed individually. Different model studies on wind energy converters improve the functionalities of *PowerFactory* by additional models. Similarly, this work delivers an additional *PowerFactory* model for Sunny Island battery inverters.

This thesis assesses the possibilities of *PowerFactory* by the simulation of switching events in island grid configurations. It uses components for these grid configurations which are available in DeMoTec in order to verify the simulation results by measurements. The investigated three-phase island grids comprise a bi-directional battery inverter which forms the grid, an asynchronous generator which simulates the feed-in of wind power, and different kinds of loads which represent consumers and their consumption behaviour. With these loads, characteristic load changes are simulated. A comparison of the data from the measurement in DeMoTec and the simulation in *PowerFactory* shows the congruency of the simulation to real system behaviour.

This thesis is structured into three main parts. Chapter 2 describes the development of the models of the battery inverter and the adjustment of the asynchronous generator and the loads for their implementation in *PowerFactory*. Simulations of load changes in grid configurations with these models are described in chapter 3. A comparison between the simulated data and the measured data in DeMoTec verifies the applicability of the models and the accuracy of simulations compared to tests in DeMoTec. Finally, chapter 4 describes the simulation of a connection of an asynchronous machine in an enlarged grid configuration, which consists of more components than available in DeMoTec.

2 Models

The following three chapters comprise the description of the three analysed models. Firstly, a model of the three-phase Sunny Island battery inverter is developed. Secondly, a parameter adjustment for the asynchronous generator model is performed and, finally, the parameters of the load model are assessed.

2.1 Battery inverter

In the case of a modularly expandable island grid it is necessary that one of the components is able to guarantee stable power system conditions by keeping the set voltage and frequency in order to supply different consumers. High power quality is characterised by a sinusoidal voltage of a certain frequency with low harmonic distortion. One component which is able to perform this task is a battery inverter. It uses a battery as a buffer to balance the fluctuating energy generation by solar or wind energy and the fluctuating energy demand. Additionally, the analysed battery inverter is able to manage the demand and the supply side. Therewith, an optimization of the total system behaviour is possible.

In this thesis the bi-directional battery inverter Sunny Island 4500 from SMA is analysed. The three phase system analysed is shown in figure 1. It is connected with a 14 kWh battery bank as storage. The technical specifications of one battery inverter representing one phase of the three phase system is presented in table 1.

Figure 1: Three phase Sunny Island system in DeMoTec. The three one phase Sunny Island battery inverters (yellow boxes) are connected to the AC-Bus (red) and to the battery bank at the bottom.

Table 1: Technical specifications of the Sunny Island 4500 battery inverter from SMA [SMA04]

Continuous output power	3300 VA
AC output power for 30 min (ambient air temperature 25 °C)	4500 VA
Maximal output power for 20 sec	6600 VA
Maximal efficiency	$\geq$ 90 %
Nominal battery voltage	60 V
Nominal battery current	60 A
Nominal RMS output voltage	230 V
Nominal RMS output current	16 A
Nominal frequency	50 Hz or 60 Hz
Range of RMS output voltage	200 V - 260 V
Range of frequency	48 Hz - 62 Hz
Harmonic distortion in output voltage	< 3 %
Voltage ripple	< 5 %
Weight	45 kg

The Sunny Island battery inverter has three different operating modes (cf. [SMA04]). These are the grid-tied mode, the grid-forming mode and the droop mode. In grid tied mode, the Sunny Island complies with the voltage and frequency which is defined by an additional component of the island grid that itself forms the grid. In grid-forming mode, in contrast, the Sunny Island keeps the voltage and the frequency of the grid autonomously at a constant level. In this mode, all other components in the grid have to operate as grid-controlled power generators or consumers. The task of the grid former is the stabilization of the frequency and the voltage of the grid. A grid former is considered to be a voltage source. In contrast, other grid components operated in parallel or supporting mode are considered to be current sources. However, the focus of this thesis is on the droop mode which is an advanced grid-forming mode. In droop mode, the Sunny Island varies the grid's frequency f depending on its current active power supply P (cf. Figure 2), and the grid's voltage U depending on its current reactive power supply Q (cf. Figure 3). In case that the active power supply rises, the frequency is reduced starting from the nominal frequency f_0. The slope of this droop is a frequency reduction Δf of -2 % of the nominal frequency or 1 Hz when reaching an active power supply of the nominal active power P_N. In case that the reactive power supply rises, the voltage is reduced starting from the nominal RMS voltage U_0. The slope of this droop is a voltage reduction of 6 % of the nominal RMS voltage with reaching a reactive power supply of the nominal reactive power Q_N.

The Sunny Island battery inverter also tries to affect the grid's frequency according to its battery state. If the available power on the AC bus of the system is higher than the power demanded, all Sunny Islands will charge their batteries and let the idle frequency slightly rise, analogous to the amount of energy stored in their batteries. The other way around, if the available power is less than the power demanded, the missing amount will be fed into the AC bus by the Sunny Islands, slightly reducing the AC frequency.

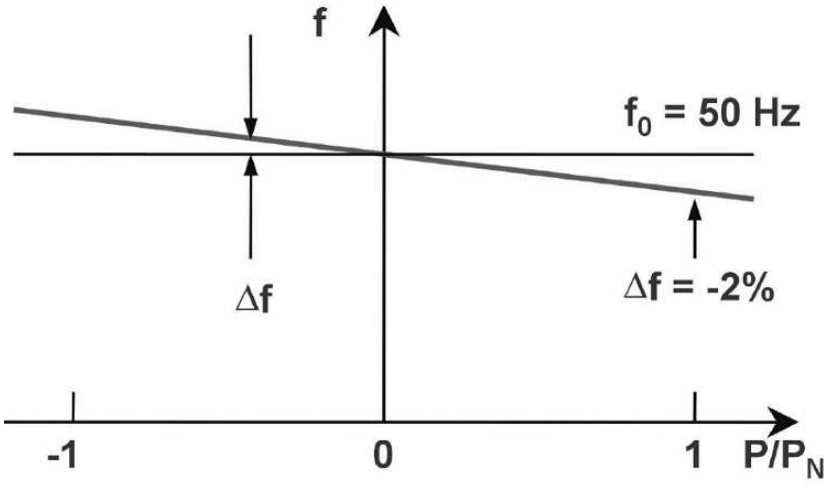

Figure 2: Frequency-active power droop [SMA04]

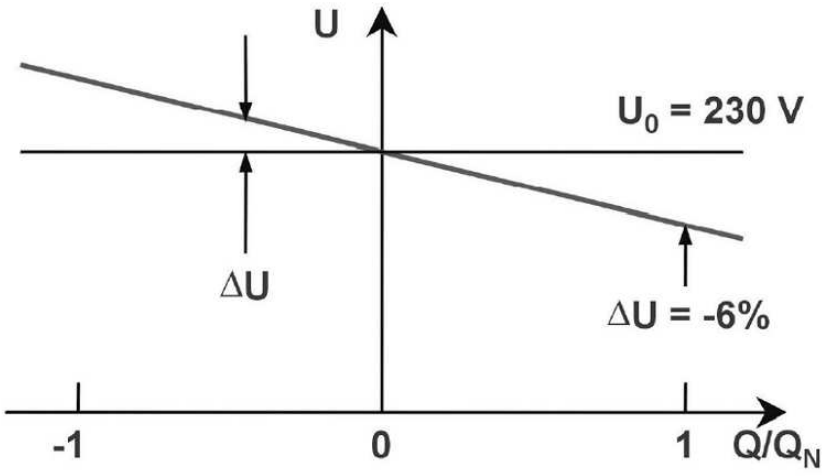

Figure 3: Voltage-reactive power droop [SMA04]

The droop mode with a frequency droop and a voltage droop allows to connect several Sunny Islands in parallel each acting as a grid-forming device. Also other grid-forming elements can be connected if they are capable of automatically synchronizing themselves to the grid or have a droop characteristic. Therewith, the droop mode enables a simple expandability of supply systems. Additionally, it is possible to distribute the share of load automatically by using different slopes for the droops.

Figure 4 shows the principle structure of the Sunny Island battery inverter (cf. [Eng01]). The battery is connected with the grid via a bidirectional Cuk-Converter [Cuk77] which is connected to the DC link of the inverter. It boosts the DC voltage of the battery to a higher DC voltage. Therewith, it substitutes a transformer. The link between the Cuk-Converter and

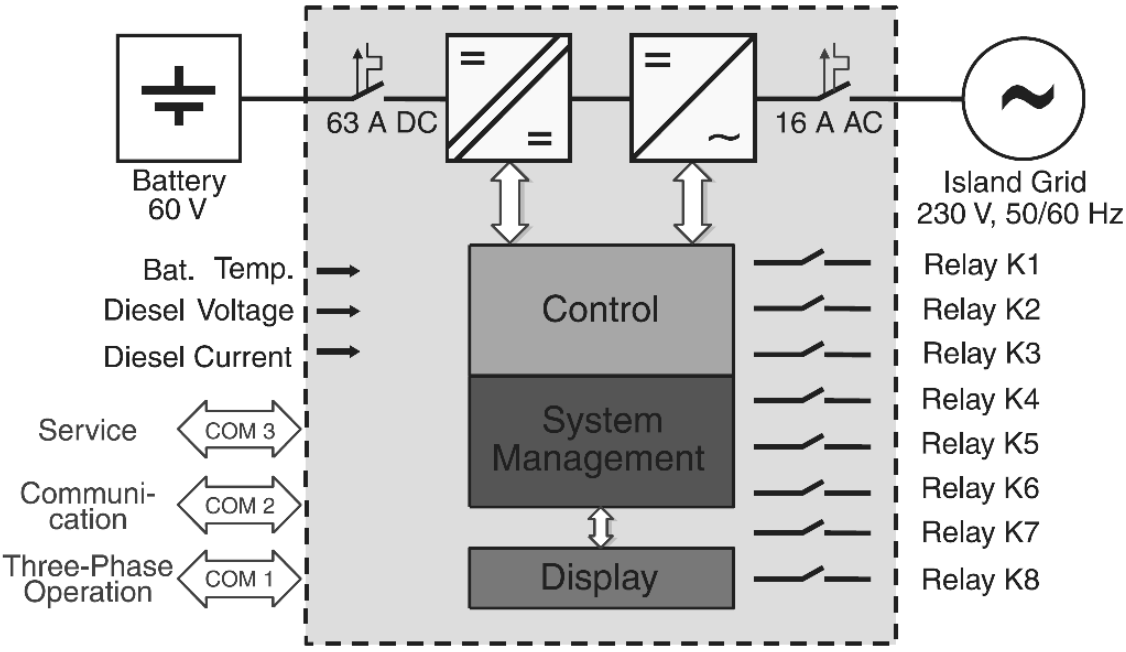

Figure 4: Structure of the Sunny Island 4500 battery inverter [SMA]

the AC grid is a single phase inverter. This inverter can be operated in the above mentioned different operation modes. The voltage output of the inverter is controlled by the controller which is described below. The topology of the inverter is a bridge circuit connected with the battery centre. Therewith, a supply of unbalanced loads becomes possible. However, it leads to a unbalanced discharge of the two halves of the battery requiring separate load control. Input signals, e.g. the temperature of the battery or information by power line, are used for the operation control which controls the battery, power generating components and consumers via relays.

2.1.1 Droop Control

[Eng05] derives the applicability of the conventional grid control concept with frequency and voltage droops in low voltage grids. This concept enables redundancy as well as expandable

distributed systems and avoids extensive communication.

The coupling of the voltage sources can be assumed to be inductive or resistive. In case the voltage source inverters are coupled directly, the coupling is inductive because of the inductances of the filter for pulse suppression and of decoupling reactors.

A coupling of two inverters (cf. [Eng01]) with the voltage phasors $\underline{U}_1$ and $\underline{U}_2$ with an inductivity $L = L_1 + L_2$ (cf. Figure 5) in a grid with a frequency of ω results in an active power P_1 and a reactive power Q_1 of the inverter with the voltage phasor $\underline{U}_1$ of

$$P_1 = \frac{U_{RMS}(U_{RMS}-\Delta U)}{\omega L} sin\delta \approx f(\delta) \quad (1)$$

$$Q_1 = \frac{U_{RMS}^2}{\omega L} - \frac{U_{RMS}(U_{RMS}-\Delta U)}{\omega L} cos\delta \approx f(\Delta U)\,. \quad (2)$$

In these two equation the RMS voltage U_{RMS} resulting from the voltage phasor $\underline{U}_1$ is used as well as the difference between the RMS voltages of the two voltage sources ΔU and the phase shift δ between the voltage phasors $\underline{U}_1$ and $\underline{U}_2$. For small angles δ, the active power mainly

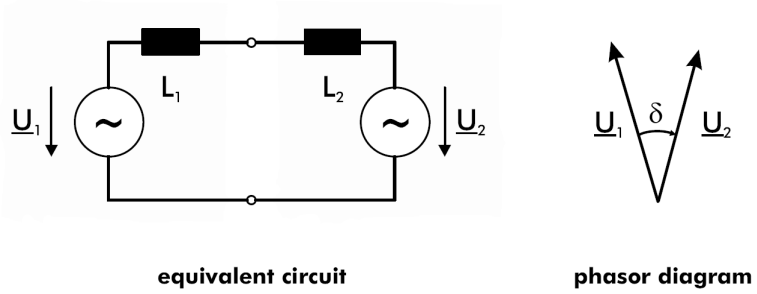

Figure 5: Equivalent circuit and phasor diagram of inductive coupled voltage sources [Eng05]

depends on the angle δ while the reactive power mainly depends on the voltage difference ΔU. This dependence leads to a decoupling which enables a separate influence on active and reactive power. Assuming standard values for the inductance L, even small differences in voltage and phase cause high currents between the inverters which cannot be neglected. Therefore, a fast control is required. This high sensitivity is the reason for the impossibility of inverters with fixed frequency and fixed voltage to operate in parallel because there are always deviations due to tolerances of the sensors, references, temperature drift, ageing and unequal crystals.

The described approach is appropriate for direct coupling of inverters and in case of a coupling with high voltage cables because in both cases the influence of the resistances is negligible compared to the influence of the inductivities [AG71, pages 663-672]. However, in low voltage grids, a coupling with low voltage cables (cf. [Eng01]) results in a main influence of the resistances R compared to the inductances (cf. figure 6). Resistive coupling results in the equations for the power

$$P_1 = \frac{U_{RMS}^2}{R} - \frac{U_{RMS}(U_{RMS}-\Delta U)}{R} cos\delta \approx f(\Delta U) \quad (3)$$

$$Q_1 = \frac{U_{RMS}(U_{RMS}-\Delta U)}{R} sin\delta \approx f(\delta) \quad (4)$$

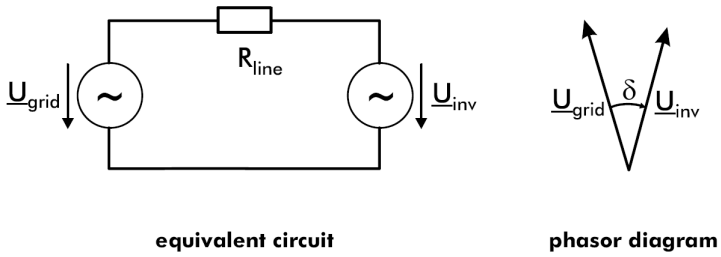

Figure 6: Equivalent circuit and phasor diagram of resistive coupled voltage sources [Eng05]

which show an inverted interdependence compared to an inductive coupling. In case of a resistive coupling, for small angles δ, the active power mainly depends on the voltage difference ΔU while the reactive power mainly depends on the angle δ.

The comparison of the droop concepts for the low voltage level in [Eng05] shows that assuming inductive coupling is advantageous compared to resistive coupling because it is compatible with the high voltage level, compatible with rotating generators representing traditional control techniques in the power grid and allows active power dispatch. Resistive coupling does not have these advantages of inductive coupling. Thus, it is not compatible to the public power grid. Despite of these advantages of inductive coupling, active power consumption results in an exchange of reactive power depending on the location of extraction. An approach would be to compensate the low voltage lines in order to achieve a voltage control with lower need for reactive power by reducing the phase shift between inverter voltage and grid voltage. Nevertheless, droops for inductive coupling should be applied even in low voltage grids because simulations showed no problems within a distance of several kilometres and no significant influence to the active power distribution (cf. [Eng01]).

2.1.2 Parallel operation

The frequency droop determines the active power of a battery inverter and the voltage droop determines the reactive power. Droop controlled components have characteristics to power changes which are comparable to a primary controlled public power grid. The slope of the droop of the grid-forming components defines the power distribution between them [Leo80].

For parallel operation, it is necessary that all inverters have the same frequency and the voltage as well as the phase differences are very small in order to reduce losses due to power exchanges and to ensure a stable operation. For stable operation, the three parameters have to be adjusted to ensure voltage stability, frequency stability and phase angle stability. In order to achieve parallel operation without the need for communication to synchronize, each inverter needs an own reference for voltage and frequency, which tend to have tolerances. Additionally, each inverter has to control its frequency, phase and voltage exactly. Therefore, the inverter needs information about the time dependent grid voltage and its current.

Figure 7 shows the control approach *selfsync*^{TM}. The *selfsync*^{TM} control approach comprises the four parts power acquisition, decoupling, droops and voltage reference. First of all,

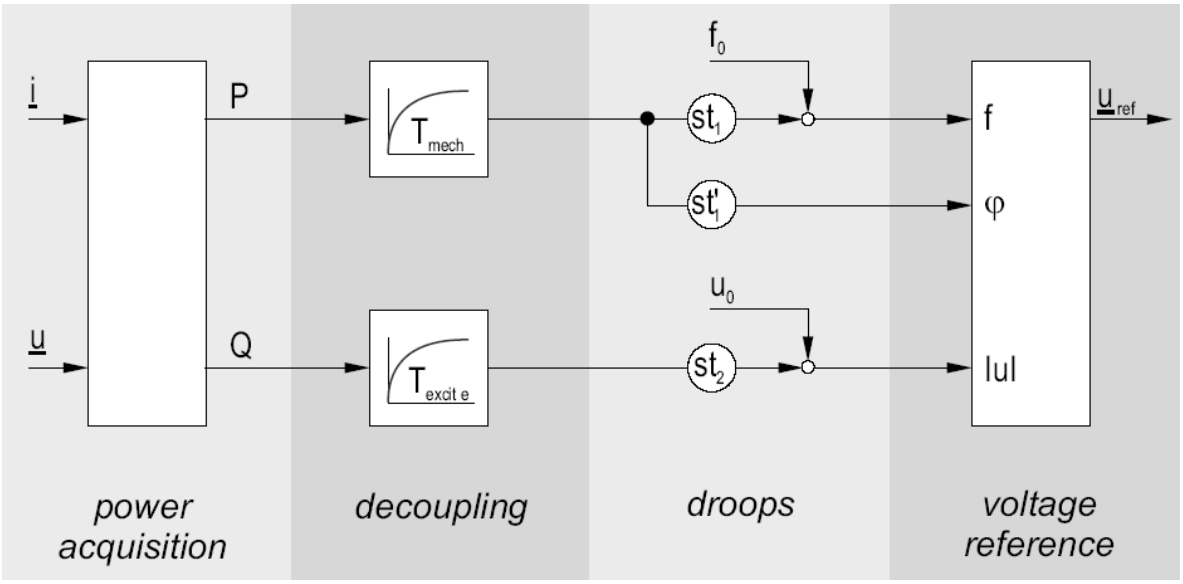

Figure 7: Control approach *selfsync*^{TM} [Eng01, Eng05]. This approach is divided into four parts. Firstly, the active and reactive power is acquired from the current and the voltage. Secondly, the values are decoupled. Thirdly, the droops influence the frequency, phase and voltage amplitude which define in the last part the voltage reference.

the power acquisition determines the active power P and the reactive power Q using the voltage $\underline{u}$ and the current $\underline{i}$. These values are decoupled by using first order time lags with the time constants T_{mech} and T_{excite}. This decoupling helps the power acquisition to consider even fast and non linear current changes by smoothing them. These lags are analogous to the time constant of the torque of inertia T_{mech} and the excitation time constant T_{excite} which occur in rotating generators. The delayed values of the active and reactive power are the input for the droops. Each droop is defined by its slope and its rated valued. The frequency droop has a rated value f_0 and the slope st_1, the voltage droop has a rated value u_0 and the slope st_2, and the phase control has a slope st_1', which is defined by grid stability considerations. These droops generate the voltage reference signal $\underline{u}_{ref} = |u| \times sin(2\pi ft) + \varphi$.

Inverters using this control approach are able to expand existing grids without compatibility problems. The compatibility of *selfsync*^{TM} with rotating generators is shown in [Van01] and with the grid in [Har04].

2.1.3 Sunny Island Model in *PowerFactory*

One task of this thesis is the development of a model implemented in *PowerFactory* from DIgSILENT which enables the simulation of a three phase Sunny Island system. For simplification, the real system components battery, Cuk-converter, and inverter (cf. figure 4) with its pulse width modulation are considered to generate a sinusoidal AC voltage. Therefore, the implemented model uses a controlled AC voltage source representing these components of the battery inverter.

Figure 8 shows the analysed grid in *PowerFactory*. The elements of the grid are described in

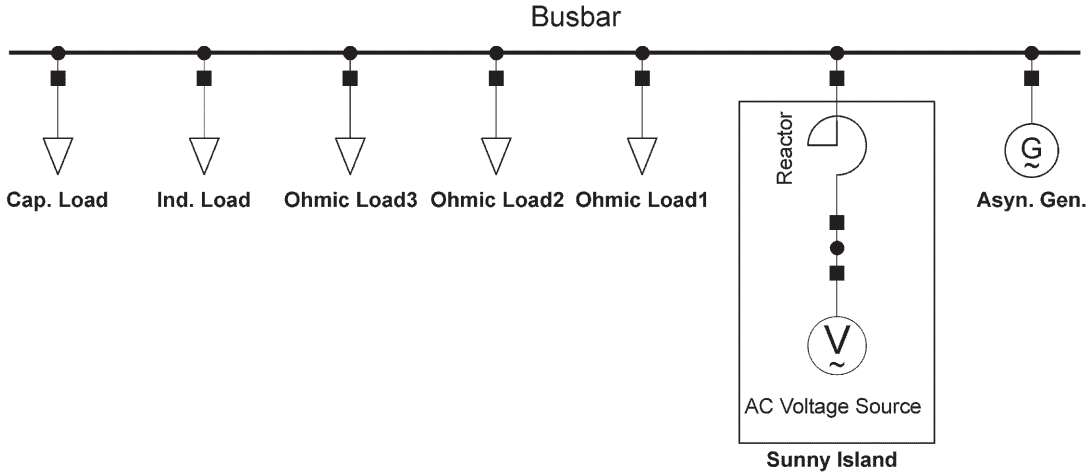

Figure 8: Analysed grid in *PowerFactory*. The grid comprises different components which are connected via the busbar. On the left hand side, there are ohmic, inductive and capacitive loads. In the centre, there is the Sunny Island battery inverter comprising the AC voltage source and the output reactor. On the right hand side, there is the asynchronous generator.

the following chapters. First of all the Sunny Island battery inverter is described in this chapter. The controlled voltage of the voltage source is the input to the output reactor of the Sunny Island which is directly connected to the analysed grid. The main structure of the Sunny Island battery inverter model is shown in figure 9. Its purpose is the control of the AC voltage source. Unfortunately, it is not possible to specify all the parameter values which are used in the model because they are confidential data of SMA. Thus, they are not publishable.

The main structure of the model (cf. figure 9) is divided into the three phases (A,B,C) represented by three rows. The first column of the structure shows the current and voltage measurement of each phase. The points of measurement are the output reactor of the Sunny Island for the current ‘imeas’ [kA] and the AC voltage source output for the voltage ‘umeas’ [kV]. In the second row these measured signals are the input to calculate the active power ‘Pgrid’ [W] and the reactive power ‘Qgrid’ [VAr]. This calculation is performed within the block ‘PQdetermination’. Another output signal is the measured current ‘I_Load’ [A]. The third column of the main structure contains the droop controllers of the Sunny Island, one for each phase, a master droop controller ‘Droop Master’ for phase A and a slave droop controller ‘Droop Slave’ for phase B and phase C. The master droop controller generates output signals for the voltage of each phase which result from the droop characteristics. While the generated voltage for phase A is directly given to the controller, which is visible in the fourth column of the main structure, the output signals of phase B and phase C ‘U_syn’ are synchronizing signals which guarantee the same phase and frequency behaviour for all three phases. The synchronizing signals are input signals for the slave droop controls of phase B and phase C which generate the respective voltage for their phase. These voltage signals ‘Uinv’ are the input of the ‘Controller’ in the fourth column. Each controller comprises a voltage controller and a subordinated current controller for the capacity current of the filter which consists of a

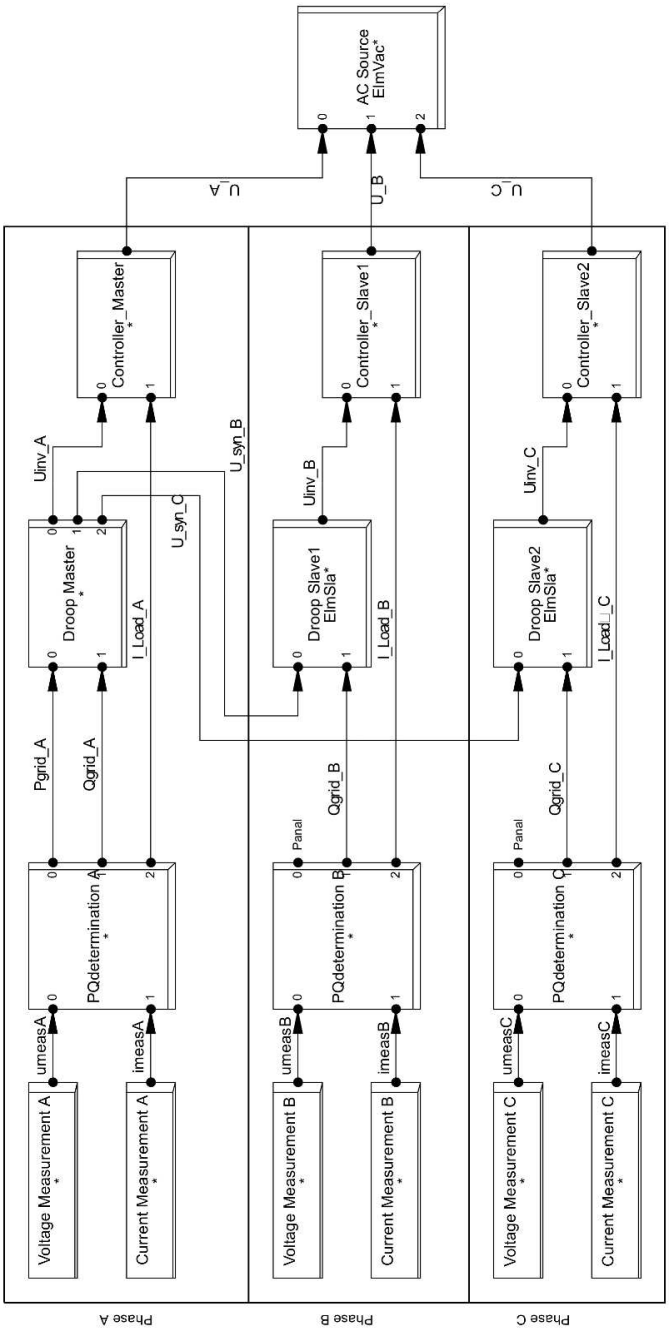

Figure 9: Main structure of the Sunny Island Model in *PowerFactory*. The three phases of the AC voltage source on the right-hand side are controlled by three similar rows representing the respective phase. In the first column the voltage and current measurement takes place. The measured values are the input of the 'PQdetermination'-calculation in the second column which provides the measured power to the droop elements in the third row. The droop element of the respective phase defines how the output voltage has to look like. Together with the measured current, the respective reference voltage is the input of the controller. The controller controls the voltage and the capacitor current of the included filter. The output of these controllers define the generated voltage of the AC voltage source.

capacity and a inductivity. The output signals of these controllers ‘U_A’, ‘U_B’ and ‘U_C’ are the generated voltages for the AC voltage source. In the following chapters, the elements of column two three and four are described in more detail.

Determination of active and reactive power Using single phase inverters requires a fast power measurement because no phasors are available. [Bur01] developed a method for this task based on a ‘verallgemeinerter Integrator’ (VI) developed in [Bur97]. The principal structure is shown in figure 10 consisting of a proportional element K_U/ω_N and two integrators with the slope ω_N in feedback loops. Its resonance frequency ω_N can be adjusted to 50 Hz corresponding

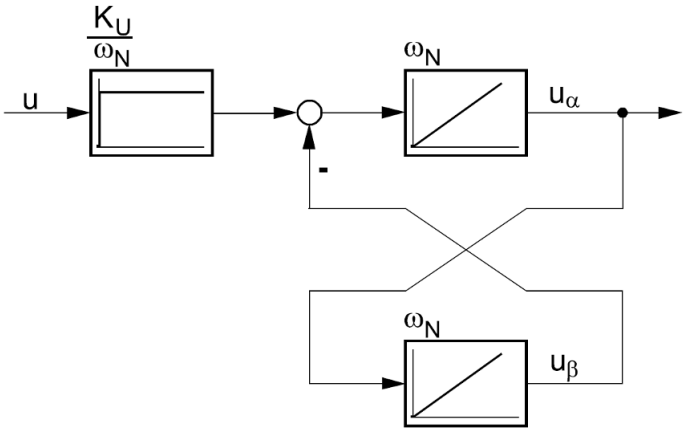

Figure 10: Verallgemeinerter Integrator [Bur01] consisting of a proportional element K_U/ω_N and two integrators with the slope ω_N in feedback loops. The output signals of the integrators are u_α and u_β.

to the grid frequency. In case that the VI is excited by an input signal u of this resonance frequency, the amplitude increases continually. This behaviour is an integral behaviour.

The challenge of single phase power measurement is that only sinusoidal signals of voltage and current are available over the time, in contrast to phasors that are available in three phase systems. However, phasors require orthogonal components. This is achieved by using VIs with additional feedback loops (cf. figure 11). This method generates the orthogonal components i_α and i_β for the current phasor as well as the orthogonal components u_α and u_β for the voltage phasor. This orthogonality results from a 90° phase difference between the output signals of the two integrators. Further characteristics of this method are a filter characteristic resulting in an output of the fundamental oscillation and no drift of the integrators resulting from the feedback loops. Therefore, the integrator gains are adjusted to the grid frequency ω_N. The proportional element determines the damping. In steady state, the α - component is identical to the fundamental oscillation of the input signal. In case of a constant component of the input signal, it does not influence the α - component, only the β - component.

Generally, the apparent power phasor $\vec{S}$ is calculated with the equation

$$\vec{S} = P + jQ = \frac{1}{2}\vec{u}\vec{i}^{\star} = \frac{1}{2}(u_\alpha + ju_\beta)(i_\alpha - ji_\beta)\,. \tag{5}$$

Therein orthogonal components express the phasors of the voltage and current. The complex result of the product of voltage and current is separated into a real and imaginary part. Therewith,

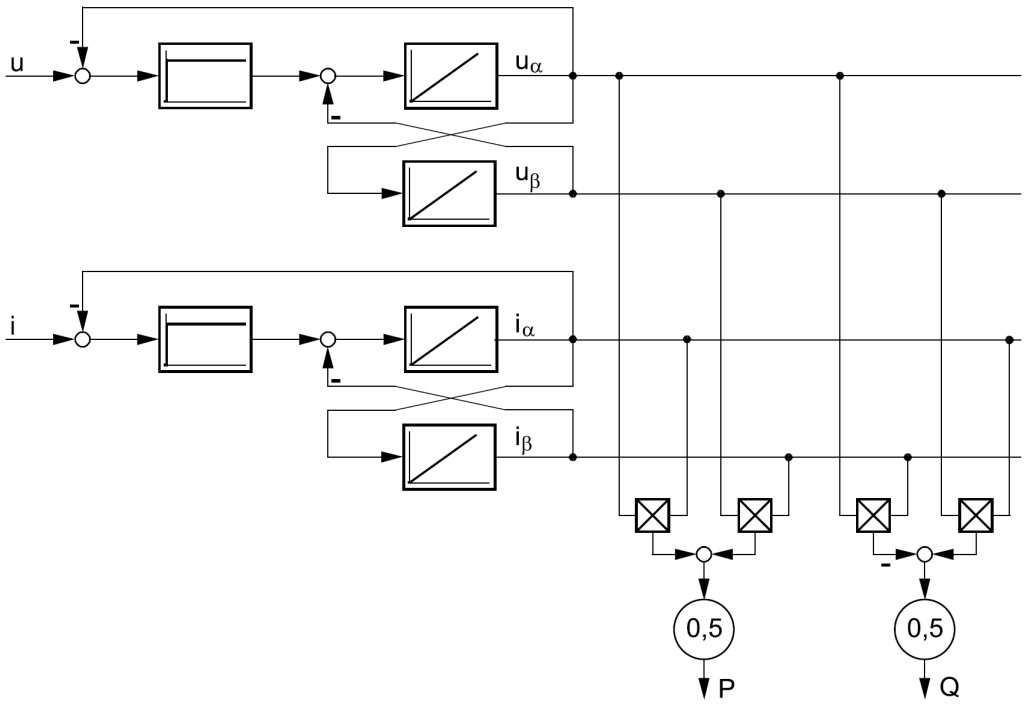

Figure 11: Determination of the active power P and the reactive power Q via two VIs from the measurement of the voltage u and the current i [Bur01].

the real part is assigned to the active power

$$P = \frac{1}{2}(u_\alpha i_\alpha + u_\beta i_\beta) \tag{6}$$

and the imaginary part to the reactive power

$$Q = \frac{1}{2}(u_\beta i_\alpha - u_\alpha i_\beta)\,. \tag{7}$$

Additionally, this method gives results for the magnitude of the voltage

$$\hat{u} = |u| = \sqrt{u_\alpha^2 + u_\beta^2} \tag{8}$$

and the magnitude of the current

$$\hat{i} = |i| = \sqrt{i_\alpha^2 + i_\beta^2}\,. \tag{9}$$

From these magnitudes, the root mean square values of the voltage

$$U_{rms} = \hat{u}/\sqrt{2} \tag{10}$$

and the current

$$I_{rms} = \hat{i}/\sqrt{2} \tag{11}$$

can be calculated. The determination of the power and the magnitudes is achieved in less than one time period of the grid frequency. Due to its filter characteristic, this system mainly determines the values for the fundamental oscillation.

In *PowerFactory*, this power acquisition displayed in column 2 of figure 9 is implemented with the block definition 'MeasurementDeviceUItoPQ.BlkDef' (cf. figure 11):

```
Name:
Measurement Device UItoPQ

Output Signals:
Panal,Qanal,imeaskA

Input Signals:
umeas,imeas

State Variables:
x1,x2,x3,x4,x5,x6

Internal Variables:
UVI1,UVI2,UVI3,UVI4,UVI5,UA,UB,IVI1,IVI2,IVI3,IVI4,IVI5,IA,IB,
Umeas,Imeas,PanalkW,QanalkVAr,Urms,Irms,Urms_act,Irms_act

Additional equations:
!Initialization
inc(x1) = 0
inc(x2) = 0
inc(x3) = 0
inc(x4) = 0
inc(x5) = 0
inc(x6) = 0
inc(UA) = 0
inc(UB) = 0
inc(IA) = 0
inc(IB) = 0
inc(Panal) = 0
inc(Qanal) = 0
inc(PanalkW) = 0
inc(QanalkW) = 0
inc(imeaskA) = 0

!Conversion from kV and kA to V and A
Umeas = 1000 * umeas
Imeas = 1000 * imeas
imeaskA = imeas

! Verallgemeinerter Integrator for voltage
UVI1 = Umeas - UA
UVI2 = sqrt(2) * UVI1
UVI3 = UVI2 - UB
UVI4 = 100 * pi() * UVI3
```

```
UVI5 = 100 * pi() * UA
UA = '\Library\Models\Global_Macros\1/s.BlkDef'(UVI4;x1;;)
UB = '\Library\Models\Global_Macros\1/s.BlkDef'(UVI5;x2;;)

! Verallgemeinerter Integrator for current
IVI1 = Imeas - IA
IVI2 = sqrt(2) * IVI1
IVI3 = IVI2 - IB
IVI4 = 100 * pi() * IVI3
IVI5 = 100 * pi() * IA
IA = '\Library\Models\Global_Macros\1/s.BlkDef'(IVI4;x3;;)
IB = '\Library\Models\Global_Macros\1/s.BlkDef'(IVI5;x4;;)

! Output of active power
Panal = 0.5 * (UA*IA + UB*IB)
PanalkW = Panal / 1000

! Output of reactive power
Qanal = 0.5 * (UB*IA - UA*IB)
QanalkVAr = Qanal / 1000

! Output of RMS voltage
Urms_act = sqrt( (UA*UA + UB*UB) / 2 )
Urms='\Library\Models\Global_Macros\(1/(1+sT)).BlkDef'
 (Urms_act;x5;0.1;)

! Output of RMS current
Irms_act = sqrt( (IA*IA + IB*IB) / 2 )
Irms='\Library\Models\Global_Macros\(1/(1+sT)).BlkDef'
     (Irms_act;x6;0.1;)
```

After the initialization of the state variables and the signals, the measured values of the voltage and the current are converted from kV and kA to V and A. Then, the following two blocks define the VI for the voltage and the VI for the current. Afterwards, the output of the power in the next two block follows the calculation given in equation 6 and 7. Finally, the last two blocks of the block definition calculate the output of the root mean square values of the voltage and the current according to equation 10 and 11.

Master Droop Controller The implementation of the droop control is based on the concepts described in chapter 2.1.1 and chapter 2.1.2. Also the ATP-EMTP simulation described in [Eng03] is taken into account. In *PowerFactory*, two different droop controllers are used to represent the Master-Slave concept of the three phase Sunny Island system. They are displayed in column three of figure 9. Each droop controller of the respective phase defines the voltage by the droop characteristic based on the measured reactive power. However, only the Master defines the phase by the droop characteristic based on the measured active power as well as the phase. The Master synchronizes the Slave droop controllers with the phase in order to guarantee as little deviations of the phases as possible. Therefore, two different block definitions are

implemented. The block definition for the Master is the ‘Master Droop Controller.BlkDef’:

```
Name:
Master Droop Controller

Output Signals:
U_A,U_Bsyn,U_Csyn

Input Signals:
Pgrid,Qgrid

State Variables:
x1,x2,x3

Parameters:
Pnom,Qnom,Unom,fnom,Ti,kpf,kqu,kpph,fbat

Internal Variables:
Pfstatic,QUstatic,A0,W0Hz,F0Hzcon,A0cor,Uabs,
Plag,Qlag,Pphstatic

Additional equations:

!Definition of variables:
vardef(Unom) = ’V’; ’Nominal Effective Voltage’
vardef(fnom) = ’Hz’;’Nominal Frequency’
vardef(Pnom) = ’W’;’Nominal Active Power’
vardef(Qnom) = ’VAr’;’Nominal Reactive Power’
vardef(Ti) = ’s’; ’Time constant of first order lag’
vardef(kpf) = ’Hz/Pnom’; ’Active Power / Frequency droop’
vardef(kqu) = ’%Unom/Qnom’; ’Reactive Power / Voltage droop’
vardef(kpph) = ’rad/Pnom’; ’Active Power / Phase droop’
vardef(fbat) = ’Hz’; ’Deviation of Frequency by
 Battery Management’

!Initialization:
inc(x1)=0
inc(x2)=0
inc(x3)=0
inc(U_A)= Unom / 1000 * sqrt(2) * sin (0*pi()/3)
inc(U_Bsyn)= Unom / 1000 * sqrt(2) * sin (-2*pi()/3)
inc(U_Csyn)= Unom / 1000 * sqrt(2) * sin (-4*pi()/3)
inc(Pgrid) = 0
inc(Qgrid) = 0

!Decoupling:
!First order lag of the active power
Plag = ’\Library\Models\Global_Macros\(1/(1+sT)).BlkDef’
 (Pgrid;x2;Ti;)
!First order lag of the reactive power
Qlag = ’\Library\Models\Global_Macros\(1/(1+sT)).BlkDef’
```

```
 (Qgrid;x3;Ti;)

!Determination of the droops:
!Active Power / Frequency static
Pfstatic = kpf * Plag / Pnom
!Reactive Power / Voltage static
QUstatic = kqu / 100 * Qlag / Qnom
!Active Power / Phase static
Pphstatic = kpph * Plag / Pnom

!Frequency adjustment:
!Grid frequency control [Hz]
F0Hzcon = fnom + Pfstatic + fbat
!Grid angular frequency [1/s]
W0Hz = 2 * pi() * F0Hzcon
!grid angle [rad]
A0 = '\Library\Models\Global_Macros\1/s.BlkDef'(W0Hz;x1;;)

!Phase correction
A0cor = A0 + Pphstatic

!Voltage adjustment:
Uabs = (1 + QUstatic)

!Voltage output:
U_A = Uabs / 1000 * Unom * sqrt(2) * sin( A0cor )
U_Bsyn = sin( A0cor - 2*pi()/3 )
U_Csyn = sin( A0cor - 4*pi()/3 )
```

In this block definition, the calculations performed after the 'Definition of variables' and the 'Initialization' process correspond to the control approach displayed in figure 7:

1. 'Decoupling': The measured active power 'Pgrid' and the measured reactive power 'Qgrid' are decoupled by first order time lags.

2. 'Determination of the droops': The decoupled power values 'Plag' and 'Qlag' determine the deviation of the frequency 'Pfstatic', the voltage 'QUstatic' and the phase 'Pphstatic' based on their rated values 'Pnom' and 'Qnom'. Additionally, the droop parameters for the frequency droop 'kpf', the voltage droop 'kqu' and the phase droop 'kpph' define the deviations.

3. 'Frequency adjustment': The nominal grid frequency 'f_nom' is adjusted by the frequency droop 'Pfstatic' and a correction factor for frequency 'fbat' which is needed because the battery management is not simulated. The frequency is transformed into a grid angle 'A0' by using an integrator. This calculation is derived from the equation between the frequency f or the angular frequency

$$\omega = 2\pi f = d\alpha/dt \,. \tag{12}$$

   and the derivative of the angle α.

4. ‘Phase correction’: The phase correction enables a more stable operation of battery inverters in parallel. Therefore the angle ‘A0’ determined in the block ‘Frequency adjustment’ is corrected by the phase droop ‘Pphstatic’.

5. ‘Voltage adjustment’: The voltage droop ‘QUstatic’ determines the relative adjustment of the magnitude of the voltage which is given in per unit values.

6. ‘Voltage output’: The voltage of phase A ‘U_A’ is defined by the droop adjustments. The adjusted magnitude of the voltage ‘Uabs’ given in per unit values is multiplied with the nominal root mean square value of the voltage ‘Unom’ and a correction factor ‘sqrt(2)’ to get the magnitude. The magnitude is also downscaled to get voltage values in the kV scale which is the internal calculation scale of *PowerFactory*. Additionally, the adjusted angle is used in a sinusoidal function. In contrast, the voltage signals of phase B ‘U_Bsyn’ and the voltage signals of phase C ‘U_Csyn’ are the synchronizing signals containing the synchronized sinusoidal function with the grid angle and a symmetrical phase shift of 120° or $2\pi/3$ and 240° or $4\pi/3$.

Slave Droop Controller The ‘Slave Droop Controller’ gets the synchronizing signals ‘U_syn’ from the ‘Master Droop Controller’ and the signals of the reactive power measurements ‘Qgrid’ of phase B and phase C. Therewith, the ‘Slave Droop Controller’ determines the voltage of the phase ‘U_out’ analogously to the ‘Master Droop Controller’. However, it only requires the parts for the voltage and reactive power because the frequency is included in the synchronizing signal. The block definition for the Slave is the ‘Slave Droop Controller.BlkDef’:

```
Name:
Slave Droop Controller

Output Signals:
U_out

Input Signals:
U_syn,Qgrid

State Variables:
x

Parameters:
Qnom,Unom,Ti,kqu

Internal Variables:
QUstatic,Uabs,Qlag

Additional equations:

!Definition of variables:
vardef(Unom) = 'V'; 'Nominal Effective Voltage'
vardef(Qnom) = 'VAr';'Nominal Reactive Power'
```

```
vardef(Ti) = 's'; 'Time constant of first order lag'
vardef(kqu) = '%Unom/Qnom'; 'Reactive Power / Voltage droop'

!Initialization:
inc(x)=0
inc(U_out) = U_syn
inc(Qgrid) = 0

!Decoupling:
!First order lag of the reactive power
Qlag = '\Library\Models\Global_Macros\(1/(1+sT)).BlkDef'
 (Qgrid;x;Ti;)

!Determination of the droops:
!Reactive Power / Voltage droop
QUstatic = kqu / 100 * Qlag / Qnom

!Voltage adjustment:
Uabs = (1 + QUstatic) !Grid voltage control of magnitude

!Voltage output:
U_out = Uabs / 1000 * Unom * sqrt(2) * U_syn
```

Controller and filter For one phase systems, [Eng01] derives an appropriate voltage control structure based on a 'verallgemeinerter Integrator' (VI). This control structure is based on the field-oriented control but does not need a Park-transformation. Three phase systems can be set up by three one phase systems which have a phase shift of 120°. The big advantage of this control structure is an easy supply of unbalanced loads.

Figure 12 displays the control structure shown in column four of figure 9. This control structure is implemented in *PowerFactory* together with the block definition 'Controller/Filter dis.BlkDef' which contains the additional equations for the initialization of the signals and state variables:

```
Name:
Controller/Filter dis

Upper Limitation:
Limiting Parameter:
y_max

Lower Limitation:
Limiting Parameter:
y_min

Output Signals:
int1_out,int2_out,Uinv_out

Input Signals:
```

```
Uinv,I_Load,int1_in,int2_in

State Variables:
x1,x2,x3,x4

Parameters:
VI_P1,FilterReactor_L,FilterReactor_R,FilterCapacitor_R,
Current_P,Factor1000,VI_P3a,VI_P3b,uadapt,
FilterCapacitor_C,VI_P2,Inv_Tdelay,y_min,y_max

Internal Variables:
I_C,Iref,U_L,o1,o11,si011,si021,si03,si04,si05,si06,si07,
si08,si09,si10,si11,si12,si13,si14,si15,si16,si18,si19,
si20,si21

Additional equations:
inc(x1)=0
inc(x2)=0
inc(x3)=0
inc(x4)=0
inc(Uinv_out) = Uinv
inc(I_Load) = 0
inc(int1_out) = 0
inc(int1_in) = 0
inc(int2_out) = 0
inc(int2_in) = 0
inc(int3_out) = 0
inc(int3_in) = 0
inc(int4_out) = 0
inc(int4_in) = 0
```

The proportional element ‘Factor1000’ in figure 12 is needed to scale the units A and V of the current and voltage to kA and kV and vice versa. This is necessary because *PowerFactory* calculates internally with kA and kV. The input signals ‘Uinv’ from the droop controller and ‘I_Load’ from the current measurement are delivered in kV and kA while this structure is implemented without scaling factors. Because the output signal ‘Uinv_out’ defines the voltage of the AC voltage source, which is an internal *PowerFactory* model, it is necessary to convert it into kV.

The voltage controller in the upper left part of the structure enables a precise control of the amplitude and the phase of the sinusoidal voltage by using a VI which is adjusted by the proportional elements ‘VI_P1’, ‘VI_P3a’ and ‘VI_P3b’ to the grid frequency. The VI is extended with the proportional element ‘VI_P2’. The real Sunny Island uses Euler integrators in its discretised control structure. However, *PowerFactory* does not support the use of Euler integrators. This results from the *PowerFactory* concept that state variables can not be defined for normal functions so that the recursive behaviour of Euler integrators can not be modelled appropriately. Nevertheless, in order to model the discrete control implemented in the real Sunny Island, sample and hold elements are used. This approach is an approximation for the real discretisation.

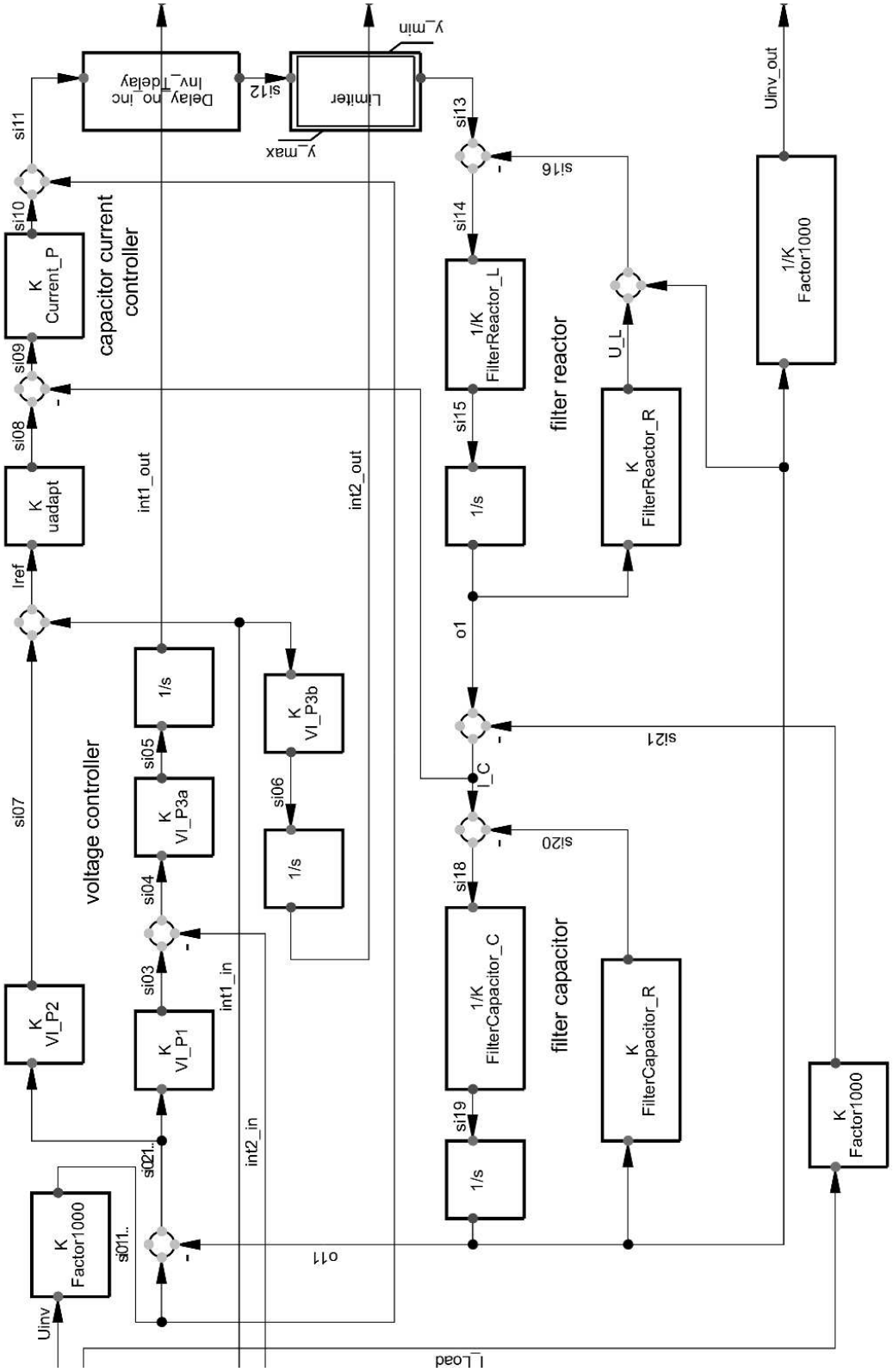

Figure 12: Controller and filter structure of the Sunny Island model in *PowerFactory*. This control structure comprises a voltage controller on the upper left side as well as a subordinated current controller. The controlled current is the capacity current of the filter in the lower part of the control structure which consists of a capacity and a inductivity.

In order to use these sample and hold elements, the output signals of the integrators ‘int1_out’ and ‘int2_out’ are given to the block definition ‘Discretization.BlkDef’ displayed in figure 13:

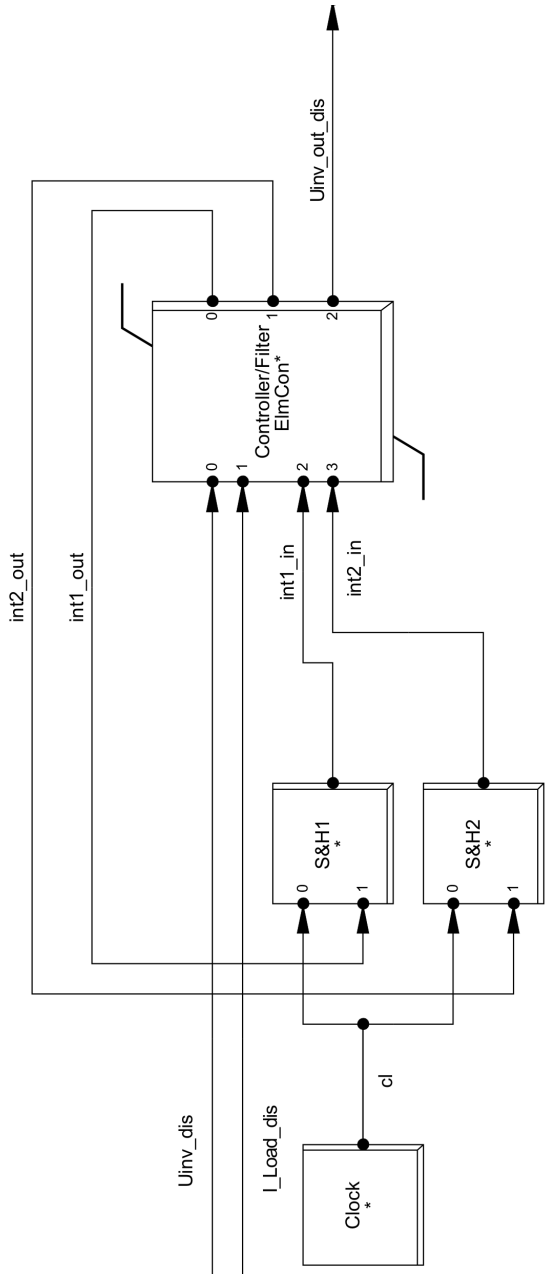

Figure 13: Discretisation structure of the Sunny Island Model in *PowerFactory*. It is used to discretise the integrators of the VI in figure 12

```
Name:
Discretization

Output Signals:
Uinv_out_dis
```

```
Input Signals:
Uinv_dis,I_Load_dis

State Variables:

Parameters:

Internal Variables:
cl,int1_in,int1_out,int2_in,int2_out

Additional equations:
inc(I_Load_dis) = 0
inc(Uinv_out_dis) = Uinv_dis
inc(cl) = 0
```

The block definition for the discretisation is implemented into the main structure of the model in column four as the block Controller for each of the three phases (cf. figure 9). It consists of two additional blocks ‘Clock’ and ‘S&H’ which discretise the integrators of the VI in the voltage controller of figure 12. Therefore, the block definition ‘Controller/Filter dis.BlkDef’ is included in the block definition for the discretisation. The ‘Clock’ gives the time signal ‘cl’ to the sample and hold elements ‘S&H’. It defines within which time period the ‘S&H’-element has to hold the sample value of the beginning of the time period. This behaviour results in a step function. The two ‘S&H’-elements are used for the respective integrator of the voltage controller. This additional effort of using discretisation is performed because it results in a behaviour of the voltage which is not simulated in case of time-continuous integrators. The important behaviour is the influence of the active power to the voltage. Theoretically, the voltage of the Sunny Island should not change in case of a change in the active power because the controller does not consider a behaviour like this. However, an increase of the active power results in a decrease of the voltage. This behaviour results in the simulation only in case that a discretisation is used, albeit the influence is not as big in simulation as it is in the measured real situation.

In order to improve the speed of the controller in figure 12, a subordinate control of the capacitor current ‘I_C’ with the proportional element ‘Current_P’ is implemented. The upper part of figure 12 displays the cascaded control with a subordinate control of the capacitor current. This corresponds to a subordinate control of the voltage which lags 5 ms behind the current. Two advantages of this cascaded control are reasons for its application. On the one hand, the control of the LC-filter as a second order system, which is displayed in the lower part of figure 12, is simplified by controlling the capacitor current ‘I_C’ resulting in a first order system. On the other hand, the use of the capacitor current instead of the voltage increases the speed by the actual time lag of 5 ms and enables therewith a fast reaction to a change of the output voltage. The model of the filter capacitor in the lower left part of figure 12 comprises a capacity ‘FilterCapacitor_C’ and a resistivity ‘FilterCapacitor_R’. In the lower right part of figure 12, the model of filter reactor consists of an inductivity ‘FilterReactor_L’ and a resistivity ‘FilterReactor_R’. The voltage signal is delayed for the lag ‘Inv_Tdelay’ and limited by the upper value ‘y_max’ and the lower value ‘y_min’.

2.1.4 Assumptions for the *PowerFactory* model

Because of the scope of this thesis, several assumptions simplify the model of the battery inverter. The aim of the thesis is not to accomplish a model which is as accurate as possible but to develop a model which is able to simulate the characteristic behaviour of the battery inverter. Therefore, the approach is not a simulation of every electrical constituent of the battery inverter. This is not possible because there is a variety of influence factors to the constituents and tolerances of the constituents which go far beyond the scope of this thesis. The following simplifications outline the scope of the implemented *PowerFactory* model.

Voltage source The real system components of the Sunny Island battery inverter the battery, the Cuk-converter, and the inverter (cf. figure 4) are considered to generate a sinusoidal AC voltage. Therefore, the implemented model uses a controlled AC voltage source representing these components of the battery inverter. This simplification is not reducing the accuracy in an improper way because modern power electronics in these components generate a sinusoidal AC voltage signal which has only little deviations from the ideal curve. The remaining deviations are interesting for power quality analyses, which are beyond the scope of this thesis. Therefore, they are not considered in the simulations performed in the following chapters.

Sinusoidal synchronizing signals Since the 'Master Droop Controller' defines the grid angle and therewith the frequency and phase for all three phases, the 'Slave Droop Controller' only adjusts the magnitude of the voltage to the phase-dependent reactive power supply. In reality, the synchronizing signals are signals defining the zero-crossing of the voltage curve. However, in this thesis, the synchronizing signals are sinusoidal signals which are identical for each phase. The use of sinusoidal signals simplifies the model without loosing the characteristic behaviour of the modelled Master-Slave characteristic.

Sinusoidal voltage without offset Additionally, the model has no voltage offset controller which is implemented in the real battery inverter because the voltage generated with the droop controller block definitions is a sinusoidal wave without an offset. In real systems, this offset results from the pulse width modulation where the voltage drops at the power electronic components [Wue95, pages 319-320]. The voltage offset controller reduces these inevitable voltage drifts. However, the *PowerFactory* model of the battery inverter does not include the pulse width modulation of the inverter. Consequently, the voltage offset controller is not required. Moreover, the time constant of the voltage offset controller in the region of seconds exceeds the focus of this thesis which is in the region of milliseconds.

Battery management not modelled Another part of the real system which is beyond the scope of this thesis is the battery management system of the Sunny Island. This battery management influences the frequency with a deviation from the droop controlled frequency of up to 0.5 Hz which is 50 % of the droop controlled deviation of 1 Hz at rated active power. In the scope of this thesis, it is not reasonable to simulate this battery management because it depends

on the loads as well as on the state of the battery determined by the battery management. Since the battery bank of the analysed Sunny Islands is used only sporadically, the battery management is not optimised to determine the state of the battery properly. Because of this uncertainty, the battery management is not implemented in the model. Nevertheless, the parameter 'Deviation of Frequency by Battery Management' in the 'Master Droop Controller' is used to adjust the simulation manually to the measurements. Indeed, it is not possible to simulate several large load changes with one deviation parameter because the influence of the battery management is significant in these cases. However, for smaller load changes the adjustment parameter is sufficient because the battery management changes the frequency only in small ranges.

The parameters of the droop controllers are adjusted to the real behaviour of the Sunny Islands. However, the power supply of the voltage source used in the *PowerFactory* model is not limited theoretically. Therefore, the user of the model has to consider the appropriate size of the loads connected with the voltage source according to table 1 in order to get reasonable results.

2.2 Asynchronous Generator

The asynchronous generator analysed in this thesis is manufactured by VEM motors GmbH. Figure 14 shows the generator on the left side and its asynchronous driving motor on the right side. The whole machine set is controlled in the control cabinet which is displayed in figure 15. Table 2 lists the technical data of the asynchronous generator and figure 16 shows its torque speed characteristic according to VEM data sheets.

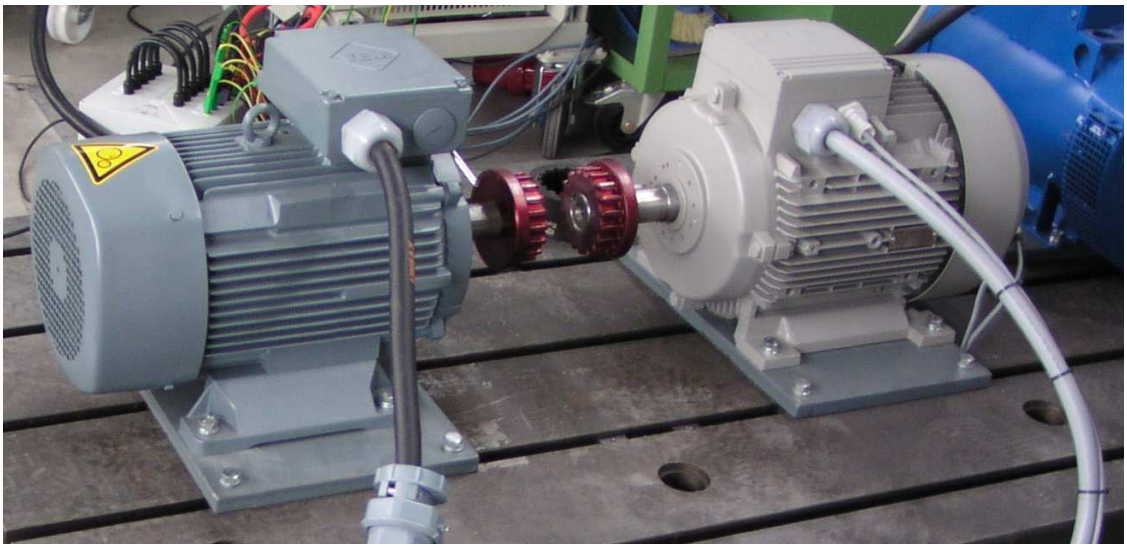

Figure 14: Picture of the VEM asynchronous generator on the left side and the drive asynchronous motor on the right side.

Figure 15: Control cabinet of the analysed machine set containing controls for an asynchronous machine and a synchronous machine.

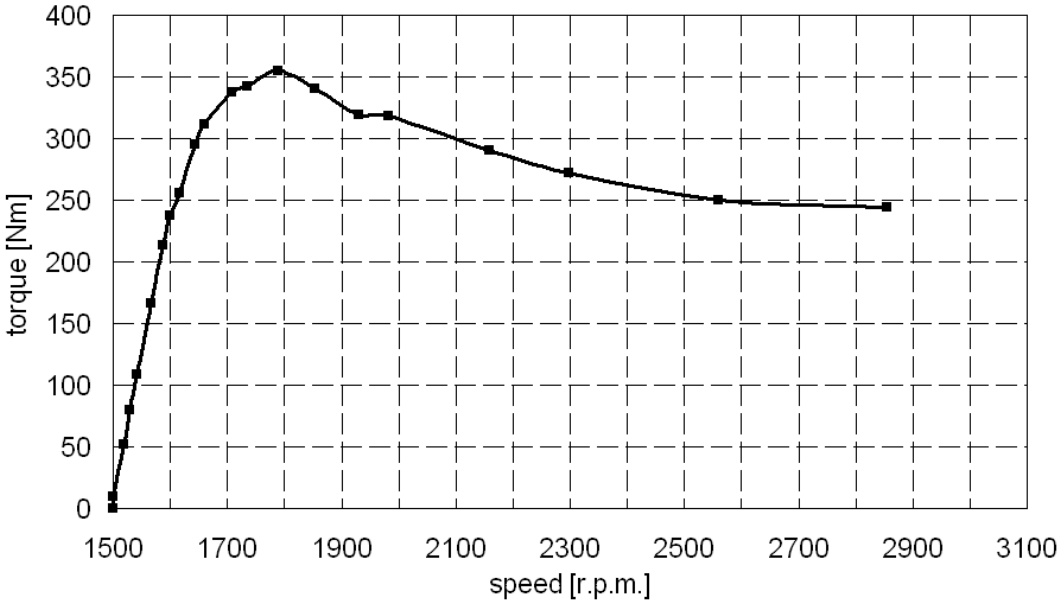

Figure 16: Torque speed characteristic of the VEM asynchronous generator given in VEM datasheets.

Table 2: Technical specifications of the analysed VEM asynchronous generator according to VEM data sheets.

Manufacturer	VEM motors GmbH
Type	G21R 160 M4 HW
Induction machine type	single fed squirrel-cage machine
Number of pole pairs p_z	2
Connection	star
Rated electrical active power $P_{e,r}$	11 kW
Rated electrical apparent power S_r	13.2 kW
Rated mechanical active power $P_{m,r}$	12.6 kW
Rated power factor $cos\varphi$	0.83
Rated efficiency η_r	87.6 %
Rated electrical frequency f_r	50 Hz
Rated mechanical speed n_r	1545 r.p.m.
Rated voltage U_r	400 V
Rated current I_r	19 A
Locked rotor current	5.8 p.u.
Maximum current	58.5 A
Rated torque M_r	72.7 Nm
Stalling torque M_s	4.5 p.u.
Locked rotor torque	3.4 p.u.
Maximum torque	184 Nm
Slip at stalling point	0.193
Stator resistance R_s	0.55 Ω
Rotor resistance R_{rA}	0.38 Ω
Stator leakage reactance X_s	0.73 Ω
Rotor leakage reactance X_{rA}	0.96 Ω
Magnetizing reactance X_m	26.1 Ω
Torque of inertia J	0.035 kg m^2
Weight	92 kg

2.2.1 *PowerFactory* Model of the Asynchronous Generator

The generic *PowerFactory* model of a asynchronous machine is basically a classical induction machine model (cf. [Cra00]). The equivalent circuit diagram is shown in figure 17. This generic model represents the voltages and currents of the stator as instantaneous phasors in a steady reference frame. In contrast, voltages and currents of the rotor are represented in a reference frame which rotates with mechanical frequency. These two reference frames are connected by a 'rotating transformer' without a winding ratio. Therefore, the rotor impedance is referred to the stator side. Altogether, the stator resistance Rs, the stator leakage reactance Xs, the magnetizing reactance Xm and the rotor impedance $Zrot$ characterize the model [DIg03].

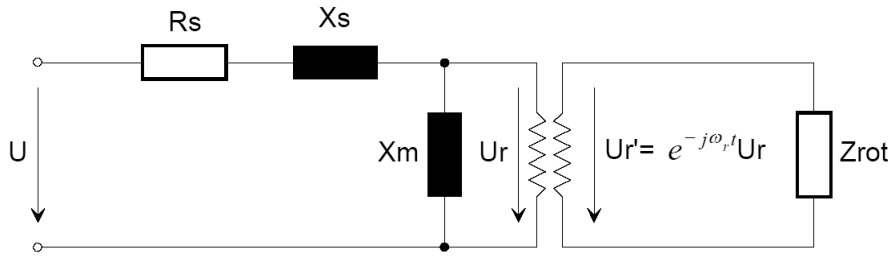

Figure 17: Equivalent circuit diagram of the induction machine model in *PowerFactory* [DIg03]

The rotor impedance comprises ohmic and inductive elements whose configuration depends on the type of induction machine. The analyzed VEM asynchronous generator has a single fed single cage rotor. Thus, the rotor impedance given in figure 18 is the applied one. It comprises the rotor resistance RrA and the rotor reactance XrA [DIg03].

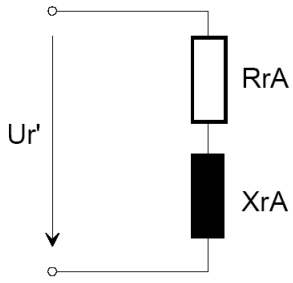

Figure 18: Rotor impedance of the single cage rotor [DIg03]

Besides these electrical parameters it is alternatively possible to specify the asynchronous generator by its 'slip-torque/current characteristic'. However, it is not possible to use this option in case of the VEM asynchronous generator because the calculation of the generators characteristics with the data of the manufacturer results in the error massage 'the iteration has no convergence'. Therefore, the electrical parameters are used to specify the model in this thesis.

2.2.2 Determination of the Input Parameters of the Asynchronous Generator on the Basis of Data from the Manufacturer

The model used in *PowerFactory* is a motor model which can be converted into a generator model. However, the specification data has to be entered for motor characteristics. This leads to a deviating input data compared to the manufacturer's specification (cf. table 2) which is given for a generator model.

With the assumption of a generator model, the apparent power is the result of the mechanical active power which drives the generator. Therewith, the losses represented by the efficiency η_r lead to a higher mechanical active power $P_{m,r}$ of 12.6 kW compared to the electrical active power $P_{e,r}$ of 11 kW. With the assumption of a motor model, the mechanical power is the result of the apparent power used to drive the motor. Therewith, the losses represented by the efficiency lead to a higher electrical active power of 11 kW compared to the mechanical active power

$$P_{m,r} = P_{e,r}\eta_r \tag{13}$$

of 9.6 kW.

In case of a generator model the rated mechanical speed n_r is 1545 r.p.m. according to table 2 with a rated slip of 3 %. In contrast, in case that the same machine is considered as a motor model, a rated slip of 3 % corresponds to a rated mechanical speed of 1455 r.p.m..

The reduction of the rated mechanical active power $P_{m,r}$ results in a reduction of the rated mechanical torque

$$M_r = \frac{P_{m,r}p_z}{(1-s_r)\omega_r} \tag{14}$$

to 63 Nm. The rated mechanical torque is calculated with the rated slip

$$s_r = \frac{n_1 - n_r}{n_1}, \tag{15}$$

with the rated mechanical speed n_r and the synchronous speed

$$n_1 = \frac{f_r \times 60 \text{ sec/min}}{p_z}, \tag{16}$$

the number of pole pairs p_z and the rated angular velocity

$$\omega_r = 2\pi f_r \tag{17}$$

with the rated frequency f_r. Equation 14 results in a rated mechanical torque of 63 Nm instead of 72.7 Nm[1] given by the manufacturer. Therewith, the stalling torque would be 5.6 p.u. instead of 4.5 p.u. given in table 2. This complies with the stalling torque of 355 Nm (cf. torque

[1]The calculation of this value is not unreproducible with the given manufacturer's data. However it is assumed to be the used value for the p.u. values of the torque parameters.

characteristics in figure 16). Moreover, the locked rotor torque of 245 Nm given in figure 16 changes from 3.4 p.u. to 3.9 p.u. by use of the rated mechanical torque for a motor model.

Additionally, the input parameters of the resistances and reactances are in p.u. values and not in Ohm. Therefore, they are related to the rated impedance Z_r which results from the rated voltage U_r and the rated apparent power S_r by the equation

$$Z_r = U_r^2/S_r = (400\ \text{V})^2/13200\ \text{VA} = 12.12\ \Omega. \tag{18}$$

Including the described changes, the input parameters are listed in the third column of table 3. The adapted input parameters are compared to the original data from the manufacturer listed in the second column.

Table 3: Adapated values of manufacturer's data which are necessary to comply with the built in motor model

Parameters	Manufacturer data	Adapted data for a motor model
Rated mechanical power	12.6 kW	9.6 kW
Stator resistance	0.55 Ω	0.0454 p.u.
Rotor resistance	0.38 Ω	0.0314 p.u.
Stator leakage reactance	0.73 Ω	0.0602 p.u.
Rotor leakage reactance	0.96 Ω	0.0792 p.u.
Magnetizing reactance	26.1 Ω	2.1533 p.u.
Rated electrical frequency	50 Hz	
Rated voltage	400 V	
Rotor type	single cage	
Number of pole pairs	2	
Connection	star	
Torque of inertia	0.035 kg m^2	

However, *PowerFactory* calculates parameters of the generator given in table 2 from the electrical parameters. These calculated parameters deviated from the manufacturer's data. Table 4 shows that there are quite significant differences. Especially, the torque characteristic represented by the stalling torque and the locked rotor torque does not correspond to the manufacturers data.

2.2.3 Determination of the Input Parameters of the Asynchronous Generator on the Basis of Measurements

In respect of such discrepancy, the electrical parameters of the VEM asynchronous generator are measured in DeMoTec following the tests illustrated in [Zwi02]. These three tests comprise a direct measurement of the stator resistance, locked rotor (corresponding to a short circuit) and unlocked rotor (corresponding to an open circuit) tests. The measurements are not exact because they are based on several simplifications, e.g. no consideration of temperature dependent or

Table 4: Comparison of the data of the analyzed VEM asynchronous generator given by the manufacturer (column 2) and calculated by *PowerFactory* (column 3) with the usage of the input parameters given in table 3.

Parameters	Manufacturer Data	Calculated by *PowerFactory* with adapted data for motor model
Rated electrical apparent power	13.2 kW	12.2 kW
Rated power factor ($cos\varphi$)	0.83	0.85
Rated efficiency	87.6 %	91.9 %
Rated mechanical speed	1455 r.p.m.	1456 r.p.m.
Locked rotor current	5.8 p.u.	6.4 p.u.
Locked rotor torque	3.9 p.u.	1.5 p.u.
Stalling torque	5.6 p.u.	3.1 p.u.
Slip at stalling point	0.193	0.215

speed dependent characteristics. However, they are performed in order to discover possible measurement faults of the manufacturer.

Stator resistance measurement A Thomson-Bridge (Siemens Direct-Reading Single Knob Bridges M273-A1) measures the resistivity of each of the three windings at the terminal box. For this measurement, the generator is switched off. The results are 0.498 Ohm for winding U, 0.498 Ohm for winding V and 0.504 Ohm for winding W. With the arithmetic average the stator resistivity is assumed to be

$$R_s = 0.5\ \Omega\ . \tag{19}$$

The Thomson-Bridge seems to work precisely because it measures standard resistances of 0.1 and 0.3 Ohm within their tolerance of 1 %.

Short circuit test The locked rotor or short circuit test is performed with a slip $s = 1$ which corresponds to a mechanical speed $n = 0$. This situation occurs in the moment of starting. Locking the rotor simulates this state of the machine. In this condition of the machine, the current at rated voltage is 5.8 times higher than the rated current (cf. table 2). A measurement at a lower voltage reduces the risk of overloading. Therefore, the asynchronous machine is connected to the public grid via a variable transformer. The transformer increases the voltage from zero up to a value which generates the nominal current. A grid analyser EURO-QUANT manufactured by HAAG Elektronische Messgeräte GmbH measures the RMS voltage, the RMS current and the active power which are the input of the asynchronous motor with a locked rotor at its stator side. The measured data are given in table 5. In case of a locked rotor, the equivalent circuit diagram in figure 17 is simplified by the assumption that the magnetizing reactance X_m is negligible because it is more than ten times bigger than the rotor impedance Z_{rot} which is

Table 5: RMS Voltage, RMS current and active power measured for the three phases at the stator side of the analysed asynchronous machine with a locked rotor. Additionally, the average value is calculated.

Phase	L1	L2	L3	Arithmetic average
RMS voltage U_{sc} [V]	42.8	43.2	43.5	43.2
RMS current I_{sc} [A]	18.3	19.5	19.1	19.0
Active power P_{sc} [W]	360	400	400	390

in parallel (cf. table 2). With this assumption, the resistance of the asynchronous motor with locked rotor is

$$R_{sc} = R_s + R_{rA} \tag{20}$$

and the reactance is

$$X_{sc} = X_s + X_{rA}\,. \tag{21}$$

Equation 20 determines the rotor resistance

$$R_{rA} = R_{sc} - R_s \tag{22}$$

with the short circuit resistance

$$R_{sc} = P_{sc}/I_{sc}^2 \tag{23}$$

which results from the situation that the active power is directly converted within the resistances. The values of the arithmetic average in table 5 determine the rotor resistance to be

$$R_{rA} = P_{sc}/I_{sc}^2 - R_s = 390\ \mathrm{W}/(19\ \mathrm{A})^2 - 0.5\Omega = 0.58\Omega\,. \tag{24}$$

Equation 20 and 21 determine the complex impedance $\vec{Z}_{sc} = R_{sc} + jX_{sc}$ of the asynchronous motor with a locked rotor. The magnitude of the impedance

$$Z_{sc} = U_{sc}/I_{sc} \tag{25}$$

uses the arithmetic average values of table 5. Therewith, the reactance of the asynchronous motor is determined by

$$X_{sc} = \sqrt{(Z_{sc}^2 - R_{sc}^2} \tag{26}$$

$$= \sqrt{(U_{sc}/I_{sc})^2 - R_{sc}^2} \tag{27}$$

$$= \sqrt{(U_{sc}/I_{sc})^2 - (P_{sc}/I_{sc}^2)^2} \tag{28}$$

$$= \sqrt{(43.2\ \mathrm{V}/19\ \mathrm{A})^2 - (390\ \mathrm{W}/(19\ \mathrm{A})^2)^2} = 2\ \Omega\,. \tag{29}$$

With the assumption that the reactance X_{sc} is distributed equal to its two components the stator leakage reactance X_s and the rotor leakage reactance X_{rA} so that

$$X_s = \ 1\ \Omega \tag{30}$$

and

$$X_{rA} = \ 1\ \Omega\,. \tag{31}$$

Open circuit test The 'unlocked rotor' or 'open circuit' test is performed for a slip $s = 0$ which corresponds to a mechanical speed that is identical to the synchronous speed. However, due to losses, e.g. resulting from friction, the mechanical speed is a bit smaller than the synchronous speed. The measurement device Braun MOBIPORT C156.61 measures the mechanical speed with an optical reflection probe. It displays a value of the mechanical speed of 1499.3 rpm at a grid frequency of 50 Hz. Therewith it is slightly lower than the ideal value of 1500 r.p.m. for open circuit operation. During the measurement, the asynchronous motor has no load so that the rotor can rotate freely. The grid analyser EURO-QUANT measures the RMS voltage and the RMS current which are the input of the asynchronous motor in open circuit operation at its stator side. Table 6 lists the measured data. In case of a asynchronous machine

Table 6: RMS voltage and RMS current measured for the three phases at the stator side of the analysed asynchronous machine with a unlocked rotor without load. Additionally, the average value is calculated.

Phase	L1	L2	L3	Arithmetic average
RMS voltage U_{oc} [V]	230.6	232.7	232.8	232.0
RMS current I_{oc} [A]	6.0	7.0	7.3	6.8

in open circuit operation, the equivalent circuit diagram in figure 17 is simplified by the assumption that the rotor impedance Z_{rot} is negligible because the current in the windings of the rotor are small compared to the currents through the stator windings. Moreover, it is assumed that the resistance R_s and the reactance X_s of the stator winding are negligible compared to the magnetizing reactance X_m because the magnetizing reactance is more than ten times bigger than the stator impedance (cf. table 2). With these assumptions, the magnetizing reactance can be calculated on basis of Ohm's law to be

$$X_m = U_{oc}/I_{oc} = 232\ \text{V}/6.8\ \text{A} = 34.1\ \Omega \tag{32}$$

with the arithmetic average values of table 6.

The results of these measurements are presented in table 7. This table shows that the mea-

Table 7: Electrical parameters from the measurement compared to the manufacturer's data.

Parameters	Manufacturer data	Measured data
Stator resistance	0.55 Ω	0.50 Ω
Rotor resistance	0.38 Ω	0.58 Ω
Stator leakage reactance	0.73 Ω	1.00 Ω
Rotor leakage reactance	0.96 Ω	1.00 Ω
Magnetizing reactance	26.1 Ω	34.1 Ω

sured values of the stator resistance and the rotor leakage reactance are similar to the manufacturer's data. In contrast, the rotor resistance, the stator leakage reactance and the magnetizing

reactance differ significantly from the manufacturer's data. Using these values as input parameters for the *PowerFactory* model of the asynchronous generator leads to the calculated parameters in table 8. This table shows that the discrepancy between the manufacturer and the

Table 8: Comparison of the data of the analysed VEM asynchronous generator given by the manufacturer (column 2) and calculated by *PowerFactory* (column 3) with the usage of the measured input parameters given in table 7.

Parameters	Manufacturer Data	Calculated by *PowerFactory* with measured electrical parameters
Rated electrical apparent power	13.2 kW	11.9 kW
Rated power factor ($cos\varphi$)	0.83	0.89
Rated efficiency	87.6 %	90.8 %
Rated mechanical speed	1455 r.p.m.	1429 r.p.m.
Locked rotor current	5.8 p.u.	5.4 p.u.
Locked rotor torque	3.9 p.u.	1.6 p.u.
Stalling torque	5.6 p.u.	2.7 p.u.
Slip at stalling point	0.193	0.284

calculated data in case of the locked rotor torque, the stalling torque and the slip at stalling point is not significantly better compared to table 4 resulting from the manufacturer's data.

2.2.4 Determination of the Input Parameters of the Asynchronous Generator by Adjusting them to the Torque Speed Characteristic

A third approach is performed in order to adjust the electrical parameters to the torque-slip characteristic given by the manufacturer. The resulting electrical parameters of this adjustment process are listed in table 9. With these adjusted parameters the torque slip characteristic is

Table 9: Electrical parameters from the adjustment process compared to the manufacturer's data.

Parameters	Manufacturer data	Measured data
Stator resistance	0.55 Ω	0.99 Ω
Rotor resistance	0.38 Ω	0.38 Ω
Stator leakage reactance	0.73 Ω	0.73 Ω
Rotor leakage reactance	0.96 Ω	0.96 Ω
Magnetizing reactance	26.1 Ω	12.1 Ω

improved. The other parameters of the asynchronous generator calculated by *PowerFactory* on the basis of the adjusted electrical parameters are listed in table 10. This table shows that the locked rotor current, the stalling torque and the slip at stalling point are adjusted to the manufacturer's data. However, it is not possible to improve the locked rotor torque without

Table 10: Comparison of the data of the analysed VEM asynchronous generator given by the manufacturer (column 2) and calculated by *PowerFactory* (column 3) with the usage of the adjusted input parameters given in table 9.

Parameters	Manufacturer Data	Calculated by *PowerFactory* adjusted to torque speed characteristics
Rated electrical apparent power	13.2 kW	28.4 kW
Rated power factor ($cos\varphi$)	0.83	0.42
Rated efficiency	87.6 %	79.6 %
Rated mechanical speed	1455 r.p.m.	1481 r.p.m.
Locked rotor current	5.8 p.u.	5.8 p.u.
Locked rotor torque	3.9 p.u.	2.6 p.u.
Stalling torque	5.6 p.u.	5.6 p.u.
Slip at stalling point	0.193	0.194

deteriorating the stalling torque or the slip at stalling point. Consequently, it is not possible to adjust the electrical parameters to the torque speed characteristic given in figure 16. Moreover, the calculated parameters for the rated electrical apparent power and the rated power factor have a deviation from the manufacturer's data which is not acceptable.

2.2.5 Pragmatical Determination of the Input Parameters of the Asynchronous Generator on the Basis of Data from the Manufacturer

The result of each of the three approaches using manufacturer's data, using self-measured data, or using electrical parameters which are adjusted to the torque speed characteristic is not satisfying. Consequently a pragmatical approach is applied. This fourth approach adjusts the electrical parameters of the manufacturer so that the measured data of the asynchronous generator in connection with the Sunny Island battery inverter and loads correspond to the simulated data of the same configuration in a way that the active and reactive power are as similar as possible. Within this adjustment process, only the magnetizing reactance is changed from 26.1 Ω to 28.7 Ω. This change influences the calculated parameters in column three of table 4 only marginally so that the rated apparent power is 12.0 kW instead of 12.2 kW and the rated power factor is 0.87 instead of 0.85.

2.3 Loads

Besides the Sunny Island battery inverter and the VEM asynchronous generator the model comprises different kinds of loads. The loads used in DeMoTec are displayed in figure 19. It shows cabinets for ohmic, inductive and capacitive three phase load. With jumpers it is possible to set different values between 50 VA and 11550 VA for the loads. In case of the inductive load the measurements show that a inductive load of 1000 VAr has an ohmic load of 50 W in addition.

Figure 19: Picture of the Loads in DeMoTec. The two cabinets on the left side show ohmic loads and the cabinet on the right side shows an inductive load on the left and a capacitive load on the right.

The model takes this characteristic into account. The generic *PowerFactory* model of a 'General Load Type' is specified as a three phase load with a neutral phase which is star-connected. Another specification is a voltage dependence for active and reactive power of the value '2'. This is necessary because the analyzed loads have a constant impedance. The equation for the apparent power

$$\vec{S} = 3 \times \vec{U} \cdot \vec{I} \tag{33}$$

defined by the voltage $\vec{U}$ and the current $\vec{I}$ together with the ohmic law

$$\vec{U} = \vec{Z} \cdot \vec{I} \tag{34}$$

defined by the impedance $\vec{Z}$ and the current $\vec{I}$ results in the equation for the apparent power

$$\vec{S} = 3\frac{\vec{U}^2}{\vec{Z}} \tag{35}$$

which shows a proportionality between the power and the squared voltage as well as a reciprocal proportionality between the power and the impedance. In case of an ohmic impedance $\vec{Z} = R$, the active power

$$P = 3U^2/R \propto U^2 \tag{36}$$

is proportional to the squared voltage because the resistance is constant. The proportionality of the power to the squared voltage is expressed in *PowerFactory* with the value '2' for the voltage dependence. In case of an inductivity L or a capacity C, the impedance $\vec{Z}$ in equation 35 shows a dependence on the frequency f for the reactive power Q. The reactive power of an inductivity is

$$Q = 3\frac{U^2}{2\pi f L} \propto \frac{U^2}{f} \tag{37}$$

while the reactive power of a capacity is

$$Q = -3U^2 2\pi f\, C \propto U^2 f\ . \tag{38}$$

These dependencies are transfered to the model in *PowerFactory* by a value '-1' for the frequency dependence of the reactive power in case of an inductive load and by a value '1' in case of a capacitive load. The time constant for this characteristic is assumed to be '0 s' because of very low time constants L/R and R/C of less than 1 ms. Moreover, the influence of these voltage and frequency dependencies on the power is only of few percentage points at maximum.

The models described in this chapter are verified in the next chapter by a comparison of the simulated and the measured data of load changes in different grid configurations.

3 Model verification

This chapter compares measured data of real grid configurations in DeMoTec and results of simulations performed with *PowerFactory* using the models described in chapter 2. The comparison shows the quality of the simulations. Chapter 3.2 describes this comparison for the case of the Sunny Island battery inverter (cf. chapter 2.1) connected with loads (cf. chapter 2.3). In this first configuration, the investigation focusses on different kinds of ohmic, inductive and capacitive load changes in balanced and unbalanced connection. Chapter 3.3 compares the measured data with the simulated data in grid configurations enlarged with the asynchronous generator desribed in chapter 2.2. Figure 20 shows the investigated grid configuration comprising the different kinds of loads on the left hand side and the Sunny Island battery inverter as well as the asynchronous generator on the right hand side. These components are connected with switches (black squares at the busbar) which connect and disconnect the respective component at the specified time. The data of the measurement as well as the data of the simulation are the respective signals measured or calculated at the point of measurement which considers the output signals of the battery inverter.

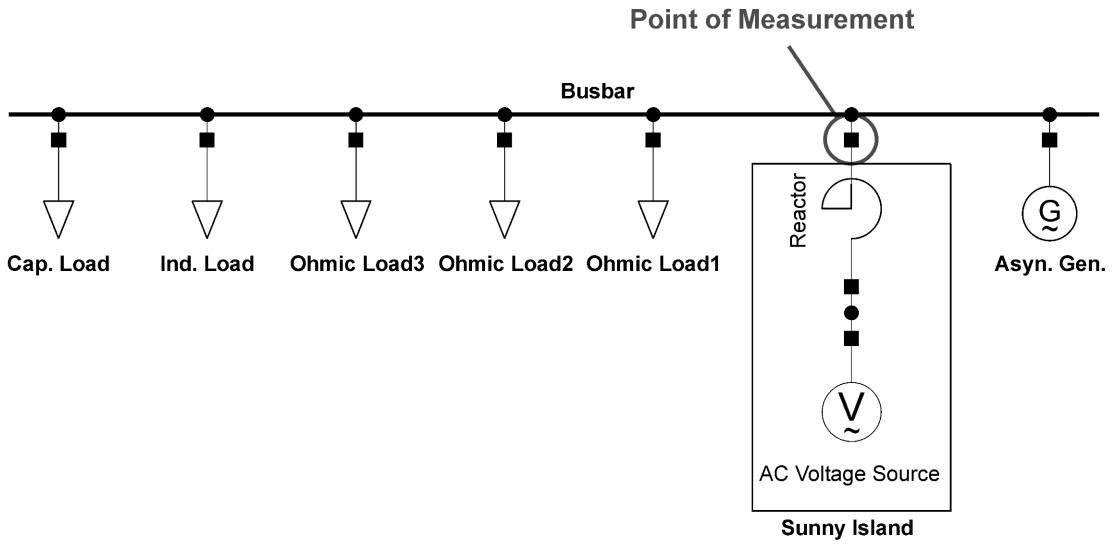

Figure 20: Analysed grid in *PowerFactory*. The grid comprises different components which are connected to the busbar via switches (black squares). On the left hand side, there are ohmic, inductive and capacitive loads. In the centre, there is the Sunny Island battery inverter comprising the AC voltage source and the output reactor. On the right hand side, there is the asynchronous generator.

Additionally, chapter 3.4 describes the parallel operation of two battery inverters. Depending on the ratio between the active power droops of the two battery inverters, the active power is distributed between the two systems. This chapter compares the simulated and the measured data for different droop ratios. Moreover, the chapter analyses the stability of a parallel operation in case of deviations between the two battery inverters. These deviation are different target frequencies and different target voltages.

The following paragraphs contain basic notes how the measurement is performed in De-

MoTec, how *PowerFactory* simulates the same configurations, and how the measured and simulated data are compared in the following chapters.

Measurement The grid analyser EURO-QUANT manufactured by HAAG Elektronische Messgeräte GmbH records the signals at the point of measurement. The resolution of the signals measured by the EURO-QUANT is 16 Bit with a sampling rate of 51.2 kHz for standard measurements and 12 Bit with a sampling rate of 1 - 100 kHz for transient measurements [HAA03]. In the performed measurements the transients of voltage and current are recorded every 0.1 ms, while the frequency, the RMS voltage, the RMS current, the active power and the reactive power are recorded every second. The EURO-QUANT uses a symmetrical differential amplifier for the measurement of voltage signals and Rogowski coils for the measurement of current signals.

Simulation *PowerFactory* from DIgSILENT uses the models of chapter 2 for the simulation of the analysed load changes in the respective grid configurations measured in DeMoTec. The software has three different simulation functions which can be selected for the respective simulation purpose.

1. The *basic function* uses a symmetrical steady-state network model for mid-term and long-term transients under balanced network conditions. It calculates electromechanical transients with root mean square values.
2. A *three phase function* extends the basic function by considering unbalanced network conditions.
3. The *electromagnetic transient function* uses a dynamic network model. It enables to calculate short-term electromagnetical transients besides the electromechanical transients in balanced and unbalanced network conditions.

Resulting from the short-term scope of this thesis, the following simulations use the electromagnetic transient function with the simulation option ‘Instantaneous Values (Electromagnetic Transients)’. *PowerFactory* uses a Newton-Raphson based iteration of network and dynamic model equations combined with a non-linear representation of electromechanical models. The integration step size for the calculation is set to a fixed value of 0.01 ms. With

- a ‘Maximum Error of the State Equations’ of 0.1 % ,
- a ‘Maximum Number of Successive State Iterations’ of 10, and
- a ‘Damping Factor (EMT)’ of 0.9,

the control of the integration is accomplished. The iteration is controlled by

- a ‘Maximum Iteration Error of Nodal Equations’ of 1 VA,
- a ‘Maximum Error of Model Equations’ of 0.1 % ,
- a ‘Maximum Number of Iterations’ of 25, and
- a ‘Iteration Limit to Recompute Jacobian Matrix’ of 5.

Comparison The resolution of time in the simulation (0.01 ms) differs from the resolution of time in the measurements (1 s or 0.1 ms). Thus, a comparison between the data of different resolutions needs an adjustment. The comparison of the data in the following chapters shows two types of adjustments.

On the one hand, the *figures* show the comparison between transients of voltage and current in a time range of less than 0.2 s with the highest resolutions of both types of data.

On the other hand, the *tables* show the comparison between frequency, RMS current, RMS voltage, active power and reactive power. The signals compared in the tables have a resolution of 1 s in case of the measurement data and 0.01 ms in case of the simulation data. Additionally, the simulation runs only for 1 s. Consequently, a graphical comparison is not appropriate. The delays in the simulation are small enough so that the steady state before the considered event and the steady state after the considered event are included in the data of the simulation. Because of the described resolution discrepancy, the tables show the steady state before the event at 0 ms with '< 0 ms' and the steady state after the event with '> 0 ms'. With this designation, the listed values of the measured data show the mean value of the seconds before and the mean value of the seconds after the event, while the listed values of the simulated data show the mean value of the milliseconds before and the mean value of the milliseconds one second after the event at the end of the simulation. The mean values of the

- the frequency are rounded to 0.01 Hz,
- the RMS voltage are rounded to 0.1 V,
- the RMS current are rounded to 0.05 A,
- the active power are rounded to 1 W, and
- the reactive power are rounded to 1 VAr.

Chapter 3.2 and chapter 3.3 show the comparison of the measured and simulated data for different types of load changes in the grid. The types of load changes are

- a balanced change of an ohmic load,
- a balanced change of an inductive load,
- a balanced change of a capacitive load,
- an unbalanced change of an ohmic load,
- an unbalanced change of an inductive load, and
- an unbalanced change of a capacitive load.

Appendix A lists figures of the measured and simulated signals systematically. In the following chapters, only selected figures from the whole list are displayed and discussed.

However, prior to the detailed comparison of the data, a synopsis shows the main results of the comparison.

3.1 Synopsis of the Verification

The comparison between the measured data and the simulated data shows how well the signals fit together. This illustrates the quality of the simulation. As this chapter compares the data for the three basic types of load changes, namely ohmic, inductive and capacitive load changes, a good fit verifies the model for load changes which consist of a mix of ohmic, inductive and capacitive loads. Additionally, the analysis of balanced and unbalanced load changes verifies the model for load changes which occur asymmetrically distributed over the three phases.

Generally, the measured values show variations between each phase, even in balanced situations. This asymmetric behaviour results from tolerances of real system components, measurement errors and influences which are not considered in this work. Consequently, there is always a small deviation between the measured and simulated values. This deviation results from the battery inverter model with simplifications of constituents and influences.

These simplifications are, for instance, the reason for a faster recovery of the simulated voltage signal from voltage drops compared to the measured voltage signal. This results from the assumption of an ideal voltage source which adjusts rapidly. However, the real power electronics control needs longer to control disturbances. Another influence, which is not considered in the model, is the battery management. The battery management causes a lower level of the frequency of the measured values compared to the simulated ones. An overview of the simplifications of the model is presented in chapter 2.1.4.

The following paragraphs highlight certain configurations, components, effects and switching events. They do not exclude each other but can be combined. There is no overall structure but each paragraph describes an important issue which occurs once or several times in the subsequent comparison.

Battery inverter connected with loads The measured data of transient currents in case of the battery inverter in connection with loads show offsets and a jagged signal of 2450 Hz with an amplitude of 0.1 A. In contrast, the simulated data of transient currents show a smoothed signal and no offset resulting from an ideal sine wave. However, considering the possibilities and the scope of the simulation, the simulated transient current fits sufficiently.

Battery inverter connected with asynchronous generator and loads Without additional components, the asynchronous generator feeds an active power of 1268 W per phase into the grid. With this power, the asynchronous generator loads the battery of the battery inverter and delivers the power consumption of the battery inverter. However, it needs a reactive power of 1630 VAr per phase. The asynchronous generator operates below its rated operation point. Therefore, the power factor is 0.61 which is below the rated power factor 0.83 given in table 2.

The jagged transient current signal is more smooth and results from a harmonic with a lower frequency compared to the configuration without an asynchronous generator. Additionally, the current signal is more deformed than without the asynchronous generator. One reason for this deformation is the operation of the asynchronous generator below its rated operation point. In contrast, the simulated signal of the transient currents is an ideal sine wave which results from

the assumption of an ideal voltage source for the battery inverter and an ideal asynchronous generator model. However, considering the possibilities of simulation, the simulated data fits sufficiently to the measured data. Nevertheless, some peaks of the sine waves do not fit well because the maximum value deviates up to 3 A between the measured and simulated data. One reason of these deviations is that the measured transient currents of the battery inverter in connection with the asynchronous generator show fluctuations. The analysis of more than 60 seconds of the measured current signals shows deviations of up to 3 A between the minimum and maximum tops of the transient current's sine waves in steady state situations.

The current of all three phases changes not at the same time to the next steady state amplitude, but it tunes due to the inertia of the asynchronous generator. However, the measured current decays more slowly compared to the simulated current. The measured oscillations are not simulated accurately but both current signals are tuning and finally reaching similar current signals.

The voltage progression before and after the load change shows a good fit. In contrast to the situation without the asynchronous generator, the measured transient voltage signal shows an harmonic similar to the harmonic of the transient currents.

The simulated values of the active as well as the reactive power flow between the asynchronous generator and the battery inverter are adjusted to the measured values by applying the respective torque to the asynchronous generator model in *PowerFactory*. Therefore, the simulated as well as the measured values show a good correspondence in case of an operation without additional components. In case of additional components, deviations occur which partly results from the influence of the frequency and the voltage to the active power output of the asynchronous generator. However these influences are not modelled appropriately as the asynchronous generator model is not an accurate representation of the real asynchronous generator (cf. chapter 2.2). Therefore, the comparison of the measured and simulated data in case of the connection of unbalanced inductive or capacitive loads shows significant deviations.

Ohmic Loads The frequency shows a decline by connecting an ohmic load and an increase by connecting a component which feeds active power into the grid (cf. paragraph 'Master Droop Controller' in chapter 2.1.3). Additionally, the battery management reduces the frequency with increasing power supply so that the measured values are lower than the simulated ones because the simulation does not consider the battery management.

Inductive Loads After the connection event, the transient currents have a superposed direct current which causes a deviation of the mean value from zero. This offset decays over some time periods of the current. In the simulation, this offset occurs similarly because it is characteristic for the connection of inductivities. Altogether, qualitatively, the measured and simulated currents fit well.

The RMS voltage shows a decline after connecting an inductive load. This decline is caused by the droop control described in chapter 2.1.3 which changes the grid voltage depending on the supplied reactive power. The additional voltage reduction results at least partly from the discretisation effect.

Capacitive Loads After the connection event, the current oscillates and tunes within 20 ms. Qualitatively, the measured and simulated currents fit well.

The voltage progression before and after the load change shows a good fit. The following 20 ms after the connection of the capacitive load show an oscillation and tuning which is similar to the behaviour of the transient currents. The simulated voltages do not follow the oscillations of the measured voltages exactly but qualitatively well. As in the case of the transient current, it is not possible to simulate the oscillations accurately because there are many influences which are out of scope of the simulations in this thesis.

The RMS voltage shows an increase by connecting a capacitive load. This increase is caused by the droop control described in chapter 2.1.3. The additional voltage increase is at least partly explainable with the discretisation effect.

Unbalanced Loads A connection as well as a disconnection at phase A shows the same behaviour of the transient current and the transient voltage as in the balanced case. However, phase B and phase C are not affected. A connection or disconnection at phase B or phase C shows the respective behaviour of the transient currents and transient voltages at the respective phase, while the respective other phases are not affected.

The frequency in case of unbalanced load changes shows the same behaviour as in balanced load changes. The battery management influences the measured values so that a direct comparison with the simulated values is not possible. The values depend on the power at phase A. In case that an ohmic load is connected to the battery inverter at phase A, the frequency declines, whereas no dependence is recognizable at phase B and phase C. This results from the implemented droop control concept described in chapter 2.1.3. In this concept, the 'Master Droop Controller' adjusts the frequency to the active power at phase A while the other phases are not considered in the control concept. Consequently, the change of the active power supply at phase B or phase C does not result in a change of the frequency by the 'Master Droop Controller'.

The behaviour of RMS voltage, active power and reactive power before and after a connection or disconnection of unbalanced loads is similar to the behaviour of balanced loads. However, only the phase where the load changes shows the respective behaviour.

Discretisation effect [Wil99] describes a characteristic dependence between an increase of the load and a decline of the output voltage. The slope of this dependency is influenced by the resolution of the digital controller. The lower the resolution the steeper the slope. However, the slope in the simulation is less than the measured one. Without the discretisation, the voltage does not change in case of active power changes. The effect is stronger for the measured system than for the simulated one because the implemented discretisation is only an approach to simulate the Euler integrators of the real system.

Active power The active power has two influences. One influence is the ohmic load in the grid and the other influence is the voltage dependence described in equation 36 in chapter 2.3.

Altogether, the simulation shows a good correspondence to the theoretical values. The deviation of the measured and the simulated values from the theoretical values is less than 3% and mostly around 1 %. However, the inaccuracy of the asynchronous generator model results in significant higher deviations in case of unbalanced load changes.

Reactive power The reactive power has three influences. Its first influence is the reactive load in the grid, its second influence is the voltage dependence and its third influence is the frequency dependence. The last two influence factors for inductivities are described in equation 37 and for capacities in equation 38 in chapter 2.3. A comparison of the simulation and the measurement shows a good correspondence to the theoretical values. The deviation is less than 3% and mostly around 1 %. However, the inaccuracy of the asynchronous generator model results in significant higher deviations in case of unbalanced load changes.

Disconnecting behaviour The loads are disconnected by load switches. These load switches have a characteristic disconnection behaviour. The disconnection of two power exchanging components is achieved by the load switch when the current between the components is zero. However, the command for disconnection, which opens the contacts of the load switch, can be given earlier. In case of an ohmic or inductive load, the current of all three phases is not zero at the same time of the command for disconnection, but each phase follows its respective sine wave until it crosses zero. In contrast, in case of a capacitive load, the current of all three phases is immediately at zero at the time of the command for disconnection.

This behaviour results from the extinction characteristic of the arc which is created at the moment of separating the contacts. The extinction of the arc eventuates in the zero-crossing of the current because the arc is then without energy and collapses. An arc extinguishes in case that the voltage, which is applied to the contacts, is equal to or lower than the voltage over the arc. In this case, no current flows in the arc which causes a collapse of the ionisation channel of the arc.

In case of an ohmic load, the applied voltage is the output voltage of the battery inverter less the voltage over the resistance of the load and the resistance of the arc. Consequently, the extinction occurs at zero-crossing of the voltage and the current, which are correlated, because the voltage over the resistance of the arc is not influenced by the ohmic load in a way that it crosses zero before the zero-crossing of the voltage.

In case of an inductive load, the inductivity allows no abrupt current change. Because of the characteristic of an inductivity, the inductivity reverses its voltage to maintain the current and drives the current through the arc. Due to the reverse voltage at the inductivity, the applied voltage is even higher than in case of an ohmic load. This reverse voltage even sustains the arc. Consequently, the extinction occurs at zero-crossing of the current.

In case of an capacitive load, the capacity allows no abrupt voltage change. Because of this characteristic, in the first moment, the capacity stores a voltage which is similar to the voltage which is applied in the moment before the switching event. Consequently, a similar voltage is applied on both sides of the arc which results in a low voltage over the arc. This low voltage is not able to drive current through the arc. Therefore, the arc extinguishes immediately.

The real disconnection characteristic of the switch is not simulated by the generic switch models of *PowerFactory*. The only discrimination available in the switch model is between an extinction at zero-crossing or an immediate extinction. For the simulation of a disconnection of an ohmic or an inductive load, the option 'extinction at zero-crossing' is selected. In contrast, for the simulation of a disconnection of a capacitive load, the option 'immediately' is selected. The simulated current shows a similar behaviour to the measured data. However, the measured current is a bit faster at zero compared to the simulated current and the measured current is partly deformed. These differences occur because the switching characteristics of the load switches are not considered in detail in *PowerFactory*. As *PowerFactory* does not model the arc characteristic in its switch models, the different behaviours of the extinction of the arc have to be defined manually for different loads. This is possible in case of pure loads but not for mixed loads. However, mixed loads which do not have mainly capacities can be assumed to be switched with zero-crossing of the current.

Battery inverters in parallel operation In case that the two battery inverters have different active power droops, the active power distribution between the two battery inverters shows a similar behaviour in case of the measurement as well as the simulation. The active power supply deviates between 0.2 % and 3.2 % between the simulation and the measurement.

An unbalanced droop ratio results in a transient behaviour in the time after the connection of the ohmic load. The transient behaviour shows an equal distribution of the active power in the moment after the connection. However, over the following hundreds of milliseconds, the distribution tunes to the target droop ratio. The measurement and the simulation show the same behaviour, but the simulation needs a bit longer for the tuning.

After this synopsis of simulation results, the following chapters present a more detailed comparison between the measurement and the simulation. The good quality of their correspondence results in a verification of the models implemented in *PowerFactory*.

3.2 Battery inverter connected with loads

In the grid configuration considered in this chapter, the Sunny Island battery inverter forms the grid and supplies the power for the connected loads by converting the stored energy in the batteries. The asynchronous generator is not considered in this chapter.

3.2.1 Balanced change in ohmic load

The Sunny Island battery inverter forms the grid in open circuit. At the time t = 0 ms it is connected to a 3 kW balanced ohmic load.

Transient currents Figure 21 shows the transient currents of the three phases A, B and C of the battery inverter measured at the point of measurement (cf. figure 20). This figure displays the main differences between the measured data and the simulated data. The measured data

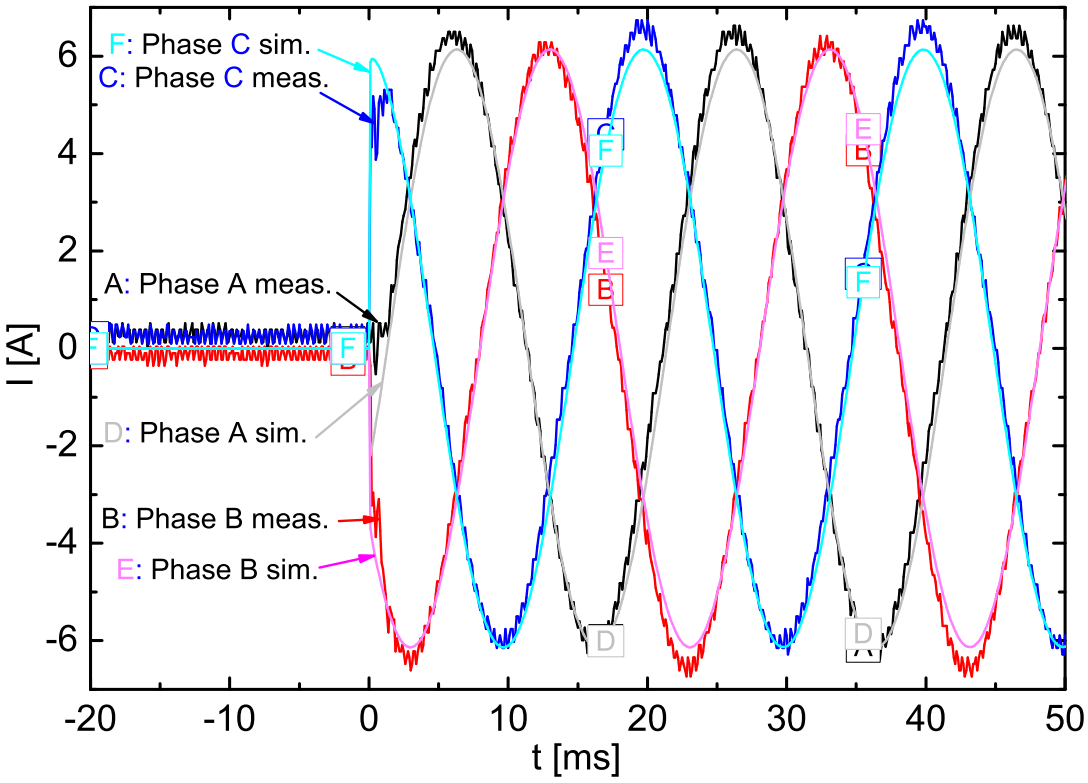

Figure 21: Transient currents I of the battery inverter in open circuit which is connected at the time t = 0 ms to a 3 kW ohmic load. Comparison between the measured (meas.) values in darker colours (A,B,C) and the simulated (sim.) values in brighter colours (D,E,F).

show an offset and a jagged signal, which has a frequency of 2450 Hz and an amplitude of 0.1 A. In contrast, the simulated data show a smoothed signal and no offset resulting from an ideal sine wave. Due to these two main differences, there is always a small deviation between the measured and simulated values. This deviation results from the scope of the battery inverter model which has simplifications of constituents and influences causing these deviations. However, considering the possibilities and the scope of the simulation, the simulated data fits sufficiently. The amplitude and the phase of the simulated data comply quantitatively, while the signal progression at the transition from no load to the 3 kW ohmic load complies qualitatively with the measured data.

Transient voltages Figure 22 shows the transient voltages of the three phases A, B and C of the battery inverter. The voltage progression before and after the load change shows a good correlation between measured and simulated data. At the time t = 0 ms, a voltage drop occurs. In the simulated data, it decays rapidly in far less than 1 ms in contrast to the measured data which needs more than 1 ms for its decay. This deficit in the simulation causes the current deviation in the 2 ms after the switching event (cf. figure 21) which shows a lower value for the measured current compared to the simulated one. The deficit in the simulation results from

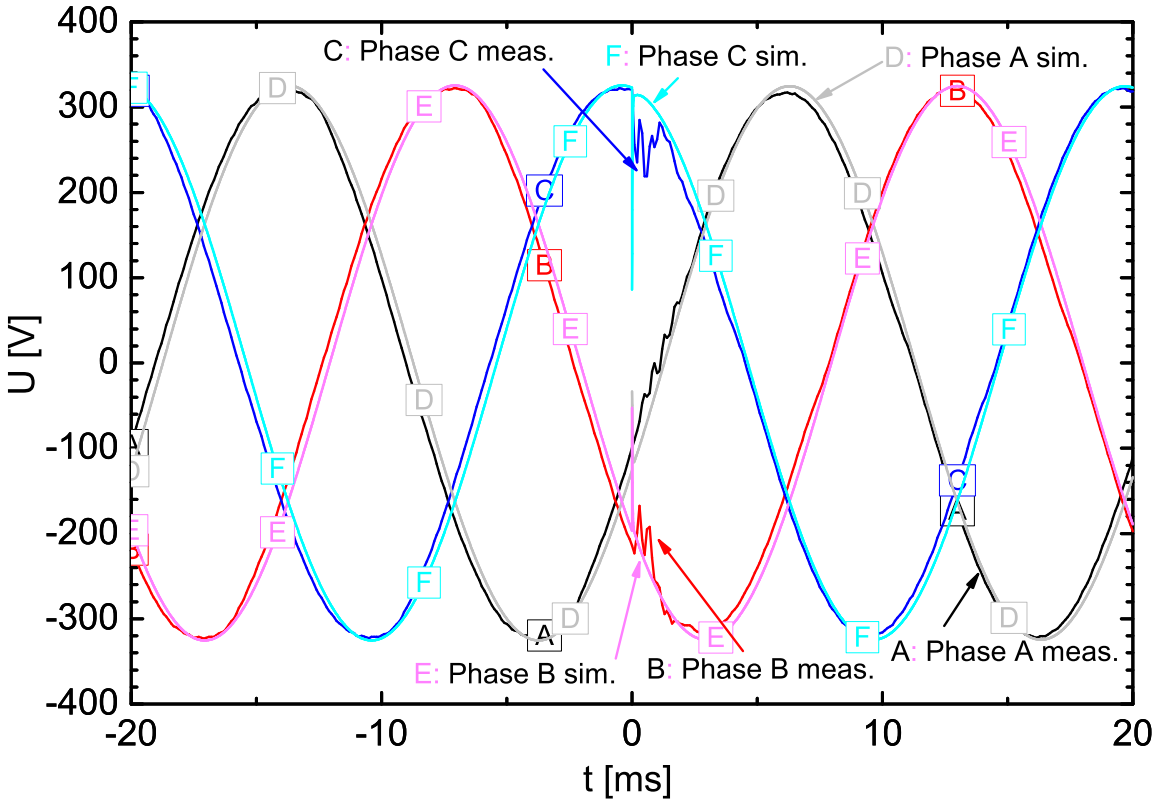

Figure 22: Transient voltages U of the battery inverter in open circuit which is connected at the time t = 0 ms to a 3 kW ohmic load. Comparison between the measured (meas.) values in darker colours (A,B,C) and the simulated (sim.) values in brighter colours (D,E,F).

the assumption of an ideal voltage source which adjusts rapidly. A change of the simulation time step shows that the voltage drop decreases with increasing time steps and the recovery time increases. Nevertheless, the real power electronics control needs longer to control the disturbance but the voltage drop is not as big as in the simulation. In comparison, the simulation sampling rate is 100 kHz while the frequency of the pulse-width modulation is approximately 16 kHz. The reason for this voltage drop is the subordinated voltage control which is described in paragraph 'Controller and filter' in chapter 2.1.3.

Table 11 lists the steady state values before and after the load change. The values of this table are those of phase A because a balanced situation is analysed. Phase B and phase C show the same values in case of the simulated values. However, in case of the measured values, all phases vary a bit from each other.

Frequency The frequency (cf. table 11) shows a decline by connecting the ohmic load. This decline is caused by the 'Master Droop Controller' (cf. chapter 2.1.3) which changes the grid frequency of 50 Hz by the frequency deviation

$$\Delta f = -1 \text{ Hz} \times P/P_{nom} \tag{39}$$

Table 11: Comparison of the data of phase A between the measured and the simulated signals of the battery inverter in open circuit which is connected at the time t = 0 ms to a 3 kW ohmic load.

Signals	Measured < 0 ms	> 0 ms	Simulated < 0 ms	> 0 ms
Frequency [Hz]	49.90	49.44	50	49.72
RMS voltage [V]	229.5	226.7	230.1	229.9
RMS current [A]	0.1	4.40	0.0	4.35
Active power [W]	3	1000	0	999
Reactive power [VAr]	70	70	0	-3

with the supplied active power P and the rated active power $P_{nom} = 3600$ W. The supplied active power at the time $t < 0$ ms is assumed to be 0 W resulting in a frequency deviation $\Delta f = 0$ Hz. Connecting 1 kW ohmic load at each phase results in a theoretical frequency deviation of $\Delta f = -1 \times 1000/3600$ Hz = - 0.28 Hz. This behaviour is given for the simulated frequency which changes from 50 Hz to 49.72 Hz. The measured frequency does not comply with these values because of the influence of the battery management, which is not modelled. This battery management additionally reduces the frequency with increasing power supply so that the measured values are lower than the simulated ones.

RMS voltage The RMS voltage (cf. table 11) shows a decline by connecting the balanced 3 kW ohmic load. This behaviour can not be explained by the droop control because the voltage only changes in case of reactive power changes. [Wil99] describes a characteristic dependence between an increase of the load and a decline of the output voltage. The slope of this dependency is influenced by the resolution of the digital controller. The lower the resolution the steeper the slope. In the model of the Sunny Island battery inverter the voltage controller is discretised to simulate this behaviour (cf. chapter 2.1.3). Nevertheless, the slope in the simulation is less than the measured one. Without the discretisation, the voltage does not change in case of active power changes. This discretisation requires with 0.01 ms a high resolution of the simulation so that the implementation of this dependency can take effect because the frequency of digital controller is 8.33 kHz. However, if the described effect is not relevant, the discretisation can be substituted by a dynamic model. Additionally, the simulation step size of 0.01 ms can be changed to 0.2 ms which reduces the time for the simulation significantly.

RMS current In the open circuit operation of the battery inverter, the measured current (cf. table 11) is higher than the expected value of 0 A. This results from a direct current which fluctuates between -1 A and 1 A with a time period of more than a second in the measured data. The mean value is the listed 0.1 A. One reason of this current in open circuit is the sensitivity of the measurement equipment which is calibrated for measurements in tens of amperes. The simulation does not consider this offset. Consequently, the simulated value is 0 A. In connection with the balanced 3 kW ohmic load, the RMS current has similar values in the measured and the simulated case.

Active power The active power (cf. table 11) in open circuit operation has a theoretical value of 0 W. However, a low active power is measured. The active power has the voltage dependence described in equation 36 in chapter 2.3. With this dependency, the active power of the measurement of the battery inverter in connection with a balanced 3 kW load should be $1000 \times (226.7/230)^2$ W $= 972$ W (compared to 1000 W in table 11) and the simulation should result in $1000 \times (229.9/230)^2$ W $= 999$ W (compared to 999 W in table 11).

Reactive power The measured reactive power has a mean value of 70 VAr (cf. table 11) which results from a stochastically fluctuating measurement of 0 - 200 VAr. The expected value of 0 VAr shows the simulation data in open circuit situation. By adding the ohmic load, the reactive power in the simulation is slightly negative. There is no significant change between the two considered steady states because a pure ohmic load is added.

Disconnecting behaviour of the current Figure 23 shows the comparison between the measured and the simulated transient current in case of a disconnection of a 3 kW ohmic load which is the only connected load. The figure shows that the current of all three phases is not zero at the same time but that each phase follows its respective sine wave until it crosses zero. This is the characteristic disconnecting behaviour of the used load switch in case of an ohmic load. Therefore, switching off the load in the simulation is specified by disconnection at zero-crossing.

This behaviour results from the extinction characteristic of the arc which is created at the moment of separating the contacts. The extinction of the arc eventuates in the zero-crossing of the current because the arc is then without energy and collapses. An arc extinguishes in case that the voltage, which is applied to the contacts, is equal to or lower than the voltage over the arc. In this case, no current flows in the arc which causes a collapse of the ionisation channel of the arc. Due to this behaviour, the arc can be represented by an assumed resistance.

In case of an ohmic load, the applied voltage is the output voltage of the battery inverter less the voltage over the resistance of the load and the resistance of the arc. Consequently, the extinction occurs at zero-crossing of the voltage or rather the current because the voltage over the resistance of the arc is not influenced by the ohmic load in a way that it gets negative.

However, the real characteristic is not simulated by the generic switch models of *PowerFactory*. The only discrimination available in the switch model is between an extinction at zero-crossing or an immediate extinction. For the described simulation, the option ‘extinction at zero-crossing’ is selected. The simulated current shows a similar behaviour to the measured data. However, the measured current of phase B and phase C is a bit faster at zero compared to the simulated current. Additionally, the measured current of phase B has a lower peak compared to the simulated one. These differences occur because the switching characteristics of the load switches are not considered in detail but assumed to be zero-crossing.

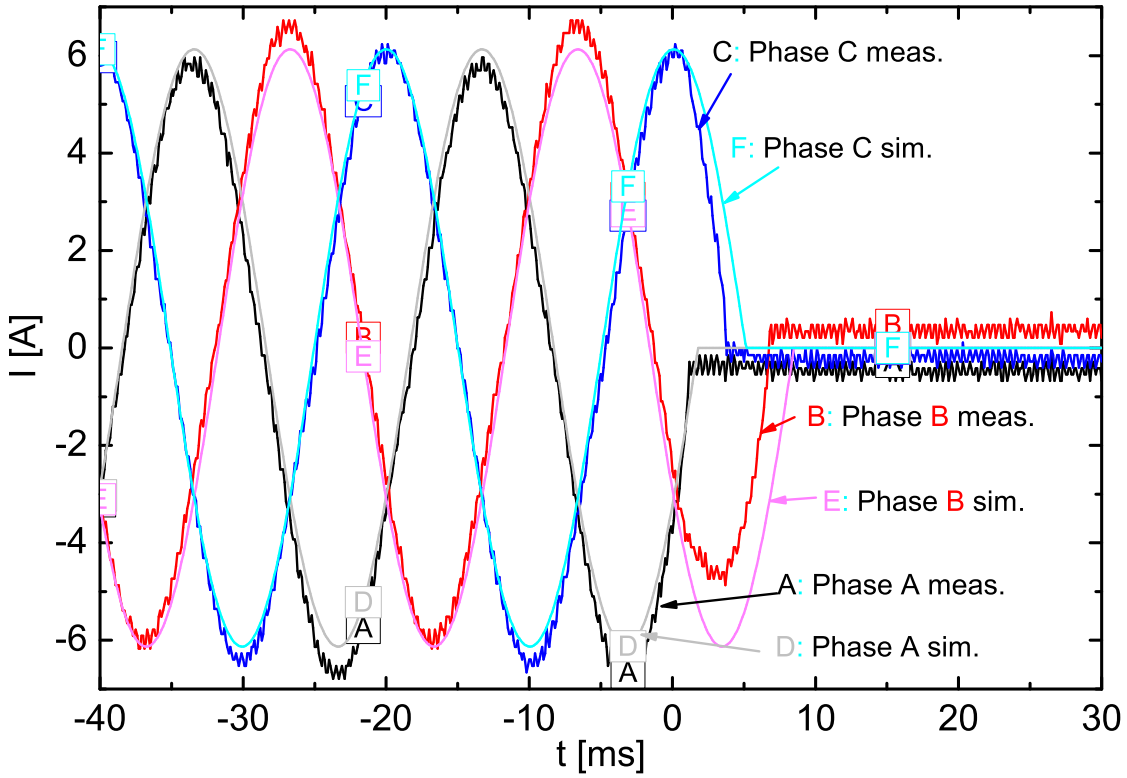

Figure 23: Transient currents I of the battery inverter supplying a 3 kW ohmic which is disconnected at the time t = 0 ms. Comparison between the measured (meas.) values in darker colours (A,B,C) and the simulated (sim.) values in brighter colours (D,E,F).

3.2.2 Balanced change in inductive load

The Sunny Island battery inverter forms the grid in connection with a balanced 3 kW ohmic load. At the time t = 0 ms the battery inverter is connected to a 3 kVAr balanced inductive load.

Transient currents Figure 24 shows the transient currents of the three phases A, B and C of the battery inverter measured at the point of measurement (cf. figure 20). After the connection event, the current has a superposed direct current which causes a deviation of the mean value from zero. This offset decays over some time periods of the current. This offset characteristic occurs also in the simulated data because it is characteristic for the connection of inductivities. Altogether, qualitatively, the measured and simulated currents fit well. However, the measured current shows a signal deformation in the first two periods, especially phase A and phase B, which is not part of the simulation signals. Consequently, the deformation results from additional influences which are not considered. Additionally, the simulated transient currents of the first two peaks of the sine waves after the load change are up to 30 % lower than the measured ones.

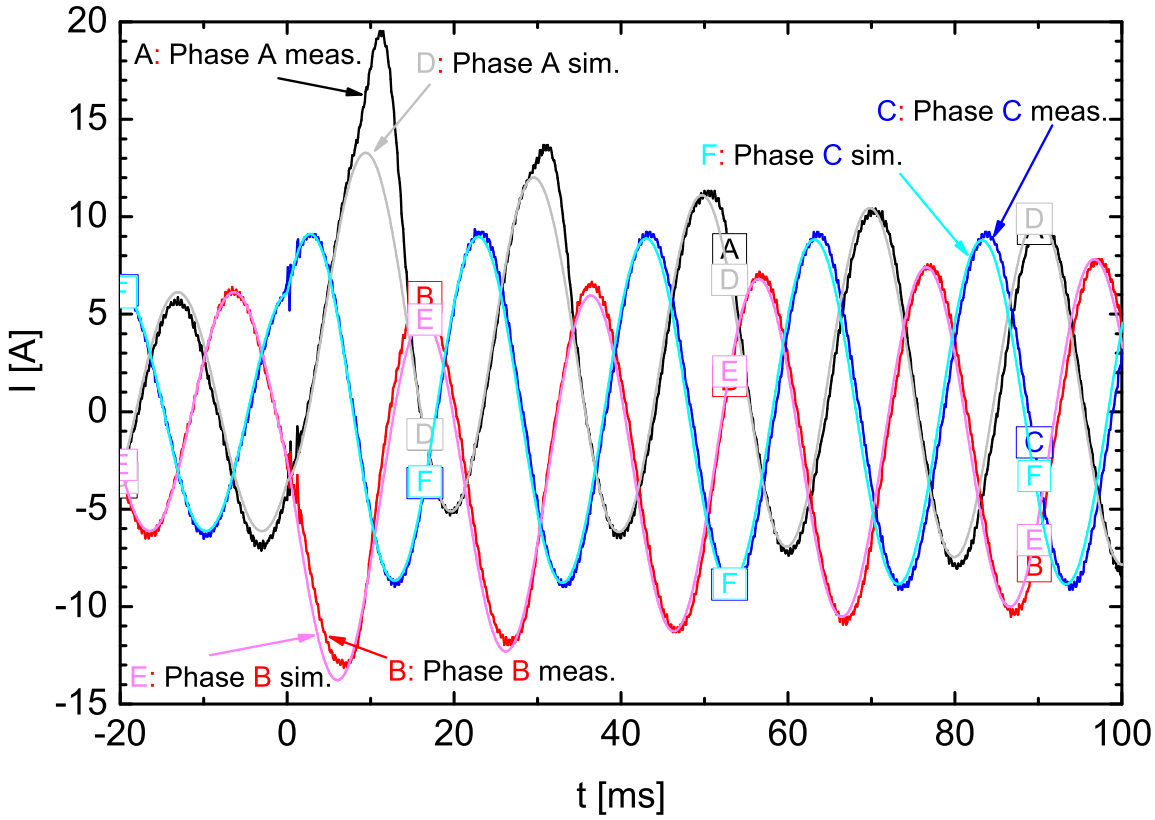

Figure 24: Transient currents I of the battery inverter supplying a 3 kW ohmic load which is connected at the time t = 0 ms to a 3 kVAr inductive load. Comparison between the measured (meas.) values in darker colours (A,B,C) and the simulated (sim.) values in brighter colours (D,E,F).

Transient voltages The transient voltages show no particular transient behaviour. Additionally, the measured and the simulated voltages show no significant difference. Therefore, it is not displayed here but in the appendix in figure 62.

Table 12 lists the steady state values before and after the load change. The values of this table are those of phase A because a balanced situation is analysed. Phase B and phase C show the same values in case of the simulated values. However, in case of the measured values, all phases vary a bit from each other.

Frequency The frequency before and after the connection of the balanced inductive load is equal in the measured data as well as in the simulated data. However, the battery management causes a 0.27 Hz lower level of the frequency of the measured values compared to the simulated ones.

RMS voltage The RMS voltage listed in table 12 shows a decline after connecting the inductive load. This decline is caused by the droop control which changes the grid voltage of 230 V

Table 12: Comparison of the data of phase A between the measured and the simulated signals of the battery inverter supplying a 3 kW ohmic load which is connected at the time t = 0 ms to a 3 kVAr inductive load.

Signals	Measured < 0 ms	> 0 ms	Simulated < 0 ms	> 0 ms
Frequency [Hz]	49.45	49.45	49.72	49.72
RMS voltage [V]	227.2	221.5	229.8	225.2
RMS current [A]	4.35	6.20	4.35	6.20
Active power [W]	985	987	1000	1012
Reactive power [VAr]	70	965	-3	961

by the voltage deviation

$$\Delta U = -6\ \% \times U_{nom} \times Q/Q_{nom} \tag{40}$$

with the supplied reactive power Q, the rated reactive power $Q_{nom} = 3600$ VAr and the rated RMS voltage $U_{nom} = 230$ V. The connection of a 1 kW inductive load at each phase results in a theoretical voltage deviation of $\Delta U = -6\ \% \times 230 \times 965/3600$ V = - 3.7 V for the measured values and a voltage deviation of $\Delta U = -6\ \% \times 230 \times 1012/3600$ V = - 3.9 V for the simulated values. However, this is neither the case for the measured data, which changes by 5.7 V from 227.2 V to 221.5 V, nor the case for the simulated data, which changes by 4.6 V from 229.8 V to 225.2 V. The additional voltage dip of 2.0 V in case of the measured values and 0.7 V in case of the simulated values is explainable with the discretisation effect described in the paragraph on the RMS voltage in chapter 3.2.1. As mentioned there, the effect is stronger for the measured system than for the simulated one.

RMS current The RMS current in the example of the connection event of an inductive load is equal in the measured and the simulated case. This match supports the good representation of the current values by the simulation.

Active power The active power has two influences. One influence is the ohmic load in the grid and the other influence is the voltage dependence described in equation 36 in chapter 2.3. With these dependencies, the active power of the measurement of the battery inverter in connection with a balanced 3 kW load should be $1000 \times (227.2/230)^2$ W $= 975$ W (compared to 985 W in table 12) and the simulation should result in $1000 \times (229.8/230)^2$ W $= 998$ W (compared to 1000 W in table 12). After adding the inductivity with an active power of 50 W per phase at rated conditions, the measurement should be $1050 \times (221.5/230)^2$ W $= 973$ W (compared to 987 W in table 12) and the simulation should result in $1050 \times (225.2/230)^2$ W $= 1007$ W (compared to 1012 W in table 12). Altogether, the simulation shows a good correspondence to the theoretical values. In contrast, the measurement shows a higher deviation from the theoretical values and the adding of the inductive load results in an increase instead of a decrease of the active power. The deviation of the measured values from the theoretical values is approximately 1 % .

Reactive power The reactive power has three influences. Its first influence is the inductive load in the grid, its second influence is the voltage dependence and its third influence is the frequency dependence. The last two influence factors for inductivities are described in equation 37 in chapter 2.3. According to these influences the reactive power after adding the inductive load should be $1000 \times (221.5/230)^2 \times (50/49.45)$ VAr $= 938$ VAr (compared to 965 VAr in table 12) and the simulation should result in $1000 \times (225.2/230)^2 \times (50/49.72)$ VAr $= 964$ VAr (compared to 961 VAr in table 12). The simulation shows a good correspondence to the theoretical values. However, the measured ones show a deviation of approximately 3 %.

Disconnecting behaviour of the current Figure 25 shows the comparison between the measured and the simulated transient current in case of a disconnection of the 3 kVAr inductive load in connection with the battery inverter and an ohmic base load of 3 kW. The figure shows that

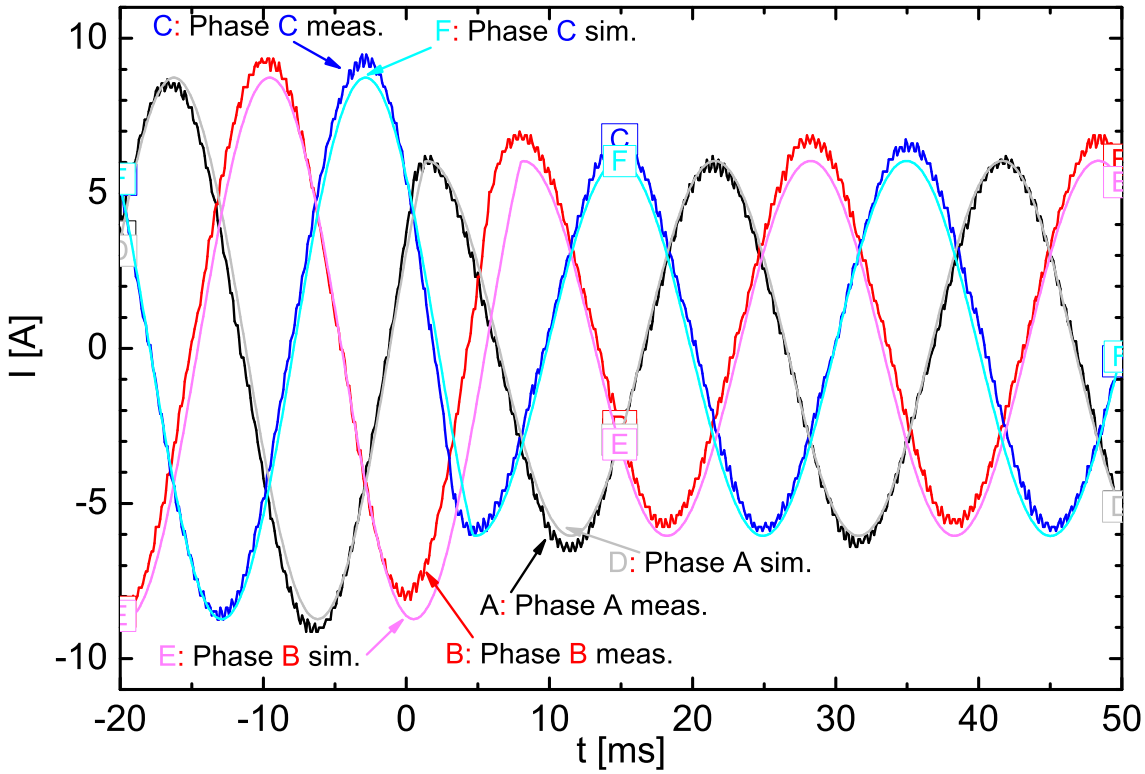

Figure 25: Transient currents I of the battery inverter supplying a 3 kW ohmic and a 3 kVAr inductive load. The 3 kVAr inductive load is disconnected at the time t = 0 ms. Comparison between the measured (meas.) values in darker colours (A,B,C) and the simulated (sim.) values in brighter colours (D,E,F).

the current of all three phases changes not at the same time to the next steady state amplitude but that each phase follows its respective sine wave until the current of the inductive load crosses zero. This is the characteristic disconnecting behaviour of the used load switch in case of an inductive load (cf. the disconnecting of an ohmic load described in chapter 3.2.1). Therefore, the disconnection of the load in the simulation is specified by a zero-crossing of the current of

the inductive load.

This behaviour results from the extinction characteristic of the arc which is created at the moment of separating the contacts. In case of an inductive load, the inductivity allows no abrupt current change. Because of the characteristic of an inductivity, the inductivity reverses its voltage to maintain the current and drives the current through the arc. Due to the reverse voltage at the inductivity, the applied voltage is even higher than in case of an ohmic load. This reverse voltage even sustains the arc. Consequently, the extinction occurs at zero-crossing of the current.

The simulated current shows a similar behaviour to the measured data. However, the measured current of phase B is a bit faster at the next steady state value compared to the simulated current.

3.2.3 Balanced change in capacitive load

The Sunny Island battery inverter forms the grid in connection with a balanced 3 kW ohmic load. At the time t = 0 ms the battery inverter is connected to a 3 kVAr balanced capacitive load.

Transient currents Figure 26 shows the transient currents of the three phases A, B and C of the battery inverter measured at the point of measurement (cf. figure 20). After the connection event, the current oscillates and tunes within 20 ms. Qualitatively, the measured and simulated currents fit well. The transients in figure 26 are difficult to recognize in detail. Therefore, they are displayed separately in figure 65, figure 66 and figure 67 in the appendix.

Transient voltages Figure 27 shows the transient voltages of the three phases A, B and C of the battery inverter. The voltage progression before and after the load change shows a good correlation between measured and simulated data. The following 20 ms after the connection of the capacitive load show an oscillation and tuning which is similar to the behaviour of the transient currents. The simulated voltages do not follow the oscillations of the measured voltages exactly but qualitatively well. As in the case of the transient current, it is not possible to simulate the voltages accurately because there are many influences which are out of scope of the simulations in this thesis.

Table 13 lists the steady state values before and after the load change. The values of this table are of phase A because a balanced situation is analysed. Phase B and phase C show the same values in case of the simulated values. However, in case of the measured values, all phases vary a bit from each other.

Frequency The frequency before and after the connection of the balanced capacitive load is similar in the measured data as well as in the simulated data because no active power is changed. However, the battery management causes an approximately 0.3 Hz lower level of the frequency of the measured values compared to the simulated ones.

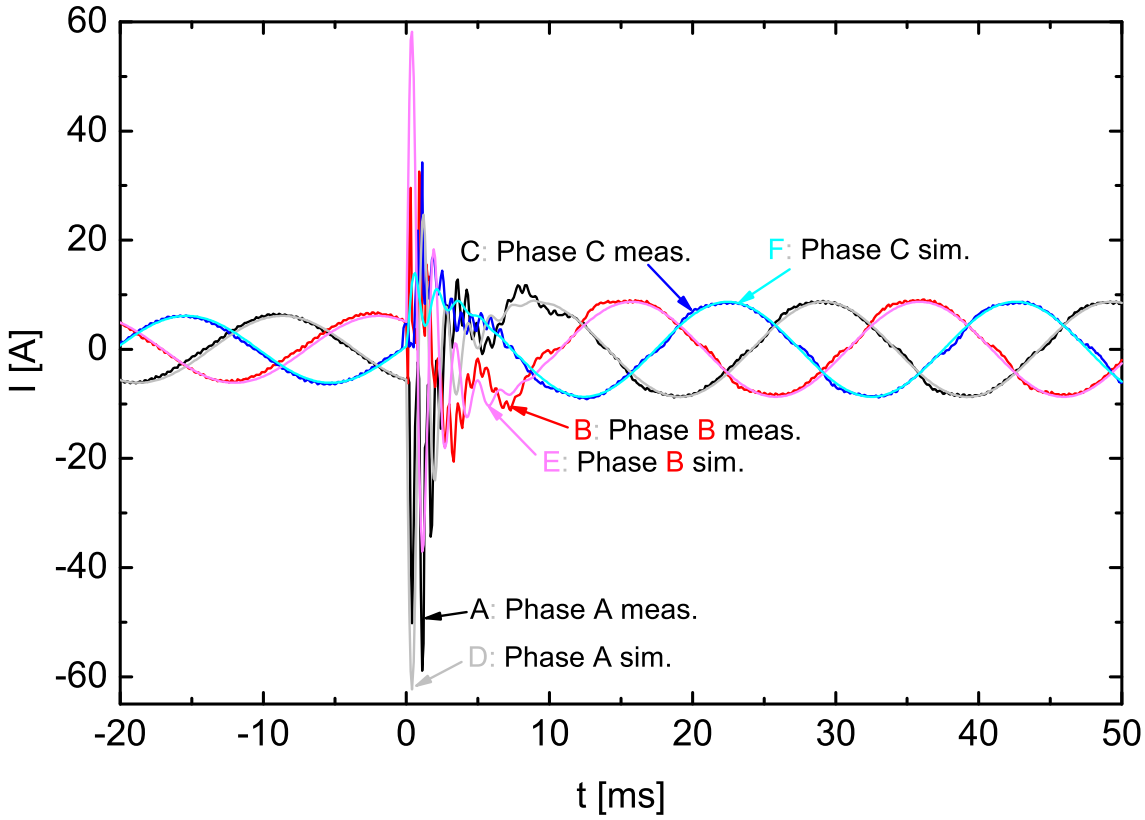

Figure 26: Transient currents I of the battery inverter supplying a 3 kW ohmic load which is connected at the time t = 0 ms to a 3 kVAr capacitive load. Comparison between the measured (meas.) values in darker colours (A,B,C) and the simulated (sim.) values in brighter colours (D,E,F).

RMS voltage The RMS voltage in table 13 shows an increase by connecting the capacitive load. This increase is caused by the droop control described in chapter 3.2.2. Connecting 1 kVAr capacitive load at each phase results in a theoretical voltage deviation of $\Delta U = -6\,\% \times 230 \times (-1055)/3600$ V = + 4.0 V with the actual reactive power of -1055 VAr. Theoretically, the droop control changes the voltage then from 230 V to 234 V but it changes to 236.1 V (cf. table 13). In case of the simulated values, the connection of 1 kVAr capacitive load at each phase results in a theoretical voltage deviation of $\Delta U = -6\,\% \times 230 \times (-1040)/3600$ V = + 4.0 V with the actual reactive power of -1040 VAr. Theoretically, the droop control changes the voltage then from 230 V to 234 V but it changes to 234.8 V (cf. table 13). The additional voltage increase is at least partly explainable with the discretisation effect described in the paragraph on the RMS voltage in chapter 3.2.1. As mentioned there, the effect is stronger for the measured system than for the simulated one.

RMS current The RMS current in the example of the connection event of an inductive load is similar in the measured and the simulated case. This match supports the good representation of the current values by the simulation.

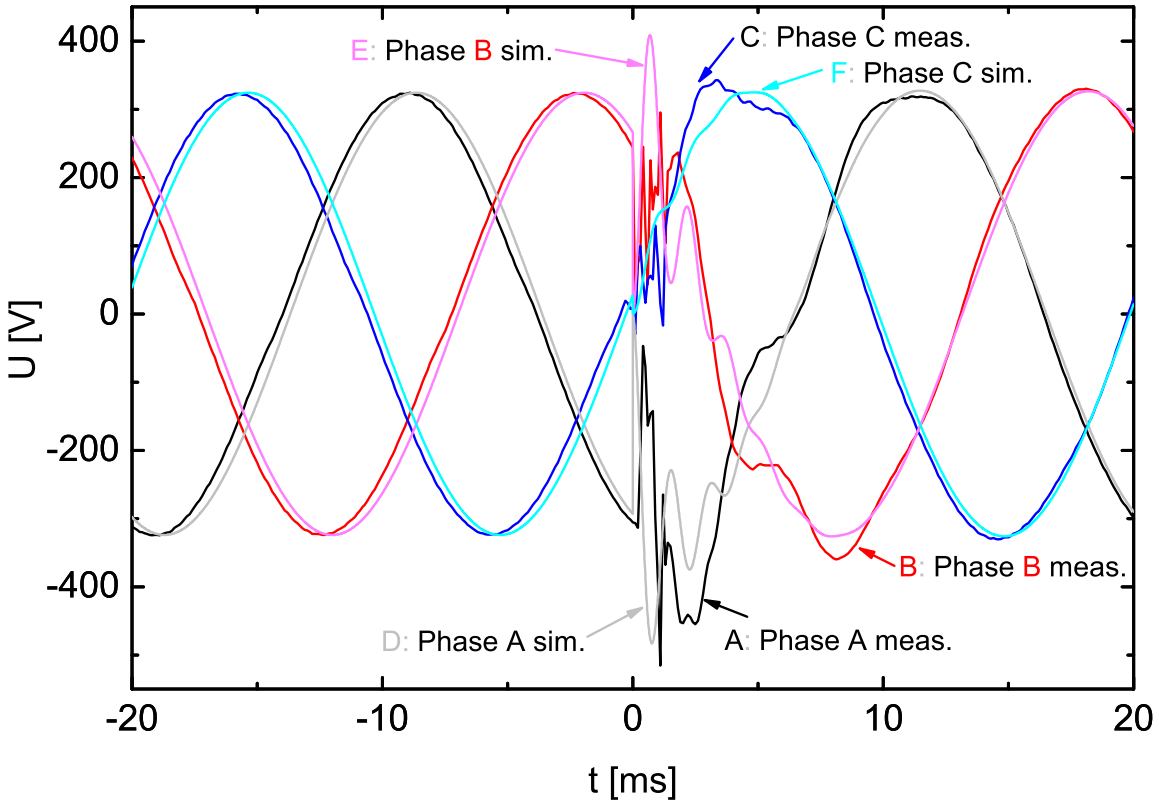

Figure 27: Transient voltages U of the battery inverter supplying a 3 kW ohmic load which is connected at the time t = 0 ms to a 3 kVAr capacitive load. Comparison between the measured (meas.) values in darker colours (A,B,C) and the simulated (sim.) values in brighter colours (D,E,F).

Active power The active power has two influences. One influence is the ohmic load in the grid and the other influence is the voltage dependence described in equation 36 in chapter 2.3. With these dependencies, the active power of the measurement of the battery inverter in connection with a balanced 3 kW load should be $1000 \times (227.2/230)^2$ W $= 975$ W (compared to 980 W in table 13) and the simulation should result in $1000 \times (229.8/230)^2$ W $= 998$ W (compared to 1000 W in table 13). After adding the capacitive load with an active power of 0 W per phase at rated conditions, the active power of the measurement should be $1000 \times (236.1/230)^2$ W $= 1054$ W (compared to 1044 W in table 13). The simulation should result in $1000 \times (234.8/230)^2$ W $= 1042$ W (compared to 1042 W in table 13). Altogether, the simulation as well as the measurement show a good correspondence to the theoretical values. The measurement has a deviation of less than 1 % to the theoretical values calculated on basis of the voltage dependence of the active power.

Reactive power The reactive power has three influences. Its first influence is the inductive load in the grid, its second influence is the voltage dependence and its third influence is the frequency dependence. The last two influence factors are described in equation 38 in chapter 2.3. According to these influences the reactive power after adding the capacitive load should

Table 13: Comparison of the data of phase A between the measured and the simulated signals of the battery inverter supplying a 3 kW ohmic load which is connected at the time t = 0 ms to a 3 kVAr capacitive load.

Signals	Measured < 0 ms	> 0 ms	Simulated < 0 ms	> 0 ms
Frequency [Hz]	49.42	49.40	49.72	49.71
RMS voltage [V]	227.2	236.1	229.8	234.8
RMS current [A]	4.30	6.30	4.35	6.25
Active power [W]	980	1044	1000	1042
Reactive power [VAr]	70	-1055	-3	-1040

be $-1000 \times (236.1/230)^2 \times (49.4/50)$ VAr $= -1041$ VAr (compared to - 1055 VAr in table 13) and the simulation should result in $-1000 \times (234.8/230)^2 \times (49.71/50)$ VAr $= -1036$ VAr (compared to - 1040 VAr in table 13). The simulation shows a good correspondence to the theoretical values with a deviation of approximately 1 %.

Disconnecting behaviour of the current Figure 28 shows the comparison between the measured and the simulated transient current in case of a disconnection of the 3 kVAr capacitive load in connection with the battery inverter and an ohmic base load of 3 kW. The simulated current shows a similar behaviour to the measured data with little deviations. The figure shows that the current of all three phases changes at the same time to the next stead state amplitude. This behaviour is in contrast to the analysed cases of the disconnection of an ohmic (cf. chapter 3.2.1) and an inductive (cf. chapter 3.2.2) load. In the latter cases, each phase follows its respective sine wave until it crosses zero. In contrast, switching off the capacitive load in the simulation is specified by an immediate disconnection of the current of the capacitive load.

This behaviour results from the extinction characteristic of the arc which is created at the moment of separating the contacts. In case of an capacitive load, the capacitive allows no abrupt voltage change. Because of this characteristic of a capacity, the capacity applies a voltage to the arc which is similar to the voltage which is applied in the moment before the switching event. The loaded capacity stores this voltage in the first moment. Consequently, a similar voltage is applied on both sides of the arc which results in a low voltage over the arc. This low voltage is not able to drive current through the arc. Therefore, the arc extinguishes immediately.

However, *PowerFactory* does not model the arc characteristic in its switch models so that the different behaviours of the extinction of the arc have to be defined manually for different loads. This is possible in case of pure loads but not for mixed loads. However, mixed loads which do not have mainly capacities can be assumed to be switched with zero-crossing of the current. The simulated current shows a similar behaviour to the measured data with little deviations.

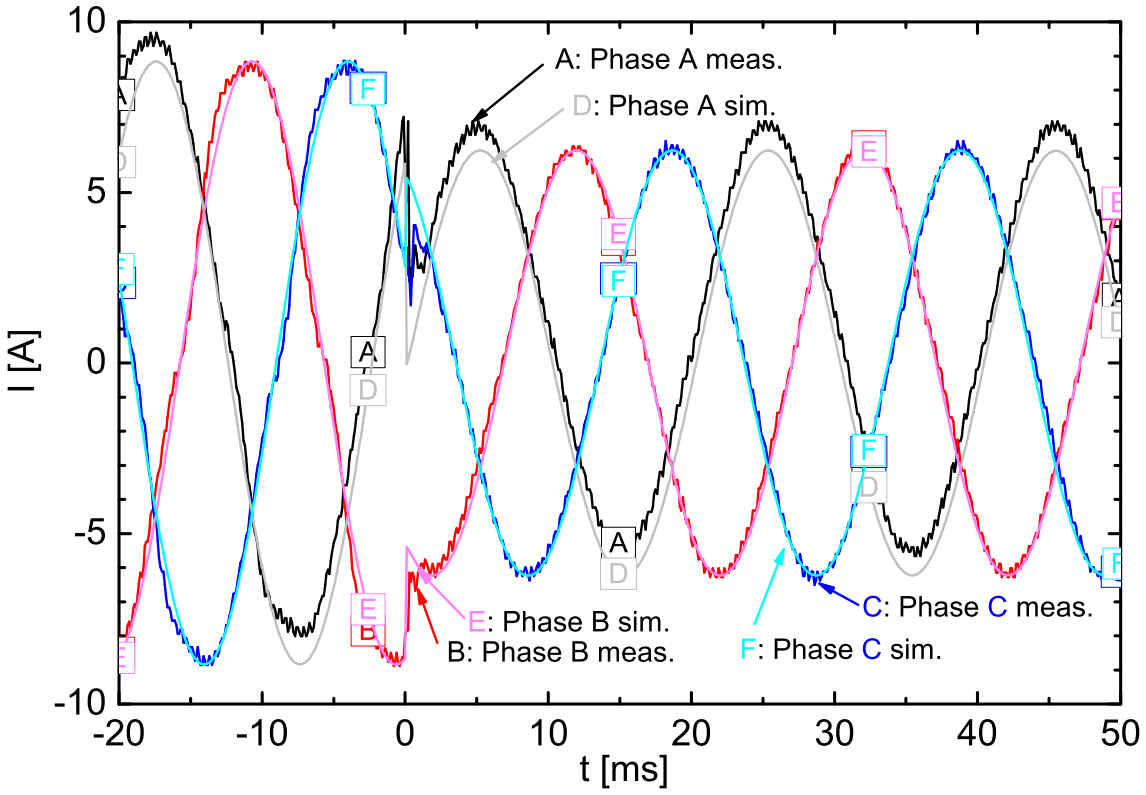

Figure 28: Transient currents I of the battery inverter supplying a 3 kW ohmic and a 3 kVAr capacitive load. The 3 kVAr capacitive load is disconnected at the time $t = 0$ ms. Comparison between the measured (meas.) values in darker colours (A,B,C) and the simulated (sim.) values in brighter colours (D,E,F).

3.2.4 Unbalanced change in ohmic load

The Sunny Island battery inverter forms the grid in open circuit. At the time $t = 0$ ms it is connected to a 1 kW ohmic load at one phase. Firstly, a 1 kW ohmic load is connected to the battery inverter at phase A. Secondly, a 1 kW ohmic load is connected to the battery inverter at phase B, and, finally, at phase C.

Transient Currents Figure 29 shows the comparison of the measured and simulated transient currents. It displays that phase B and phase C are not affected while phase A shows the same behaviour of the transient current as described in chapter 3.2.1. Figure 71 shows the connection of phase B and figure 72 shows the connection of phase C (cf. Appendix). They also show the same behaviour of the transient currents.

Transient Voltages In case of an unbalanced connection as well as an unbalanced disconnection of an ohmic load, the transient voltages show no particular behaviour. It is similar to the behaviour displayed in figure 22 in chapter 3.2.1. The simulated values fit well to the measured ones. Therefore, there is no need to display them in this work.

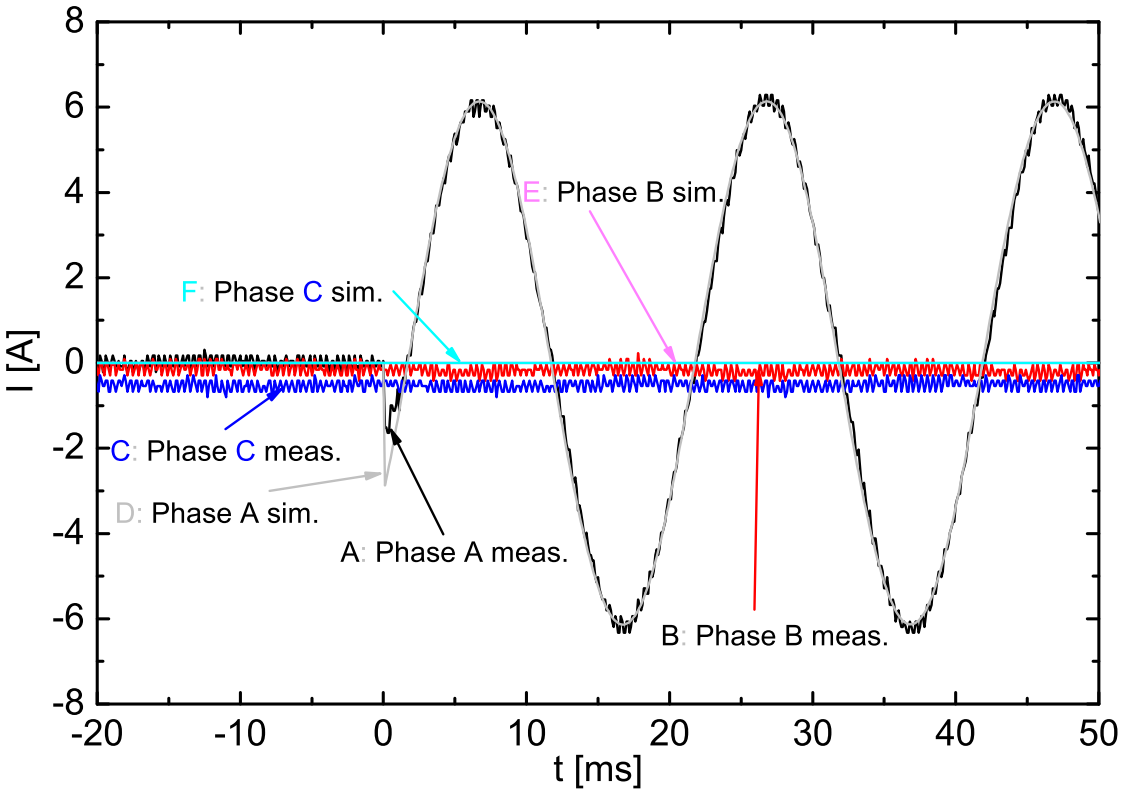

Figure 29: Transient currents I of the battery inverter in open circuit which is connected at the time t = 0 ms to a 1 kW ohmic load at phase A. Comparison between the measured (meas.) values in darker colours (A,B,C) and the simulated (sim.) values in brighter colours (D,E,F).

Frequency The frequency shows the expected behaviour similar to the described one in chapter 3.2.1. As mentioned therein, the battery management influences the measured values so that a direct comparison with the simulated values is not possible. The values depend on the power at phase A. In case that an ohmic load is connected to the battery inverter at phase A, the frequency declines, whereas no dependence is recognizable at phase B and phase C. This results from the implemented droop control concept described in chapter 2.1.3. In this concept, the 'Master Droop Controller' adjusts the frequency to the active power at phase A while the other phases are not considered in the control concept. Consequently, the change of the active power supply at phase B or phase C does not result in a change of the frequency by the 'Master Droop Controller'.

RMS voltage Table 14 lists the steady state values of the RMS voltages of the three phases (in the columns) for a connection sequence (in the rows) in case of the measured values and in case of the simulated values. The connection sequence starts with the open circuit where no load is connected to the battery inverter. The measured values show a little asymmetry whereas the simulated ones are all 230.1 V. By adding unbalanced ohmic loads in the following connection sequence, the discretisation effect described in chapter 3.2.1 causes the voltage to decline. This

Table 14: Comparison of the data between the measured and the simulated RMS voltage signals of the battery inverter in connection with unbalanced ohmic loads. Four different steady states are considered: open circuit; 1 kW at phase A; 1 kW at phase A,B; and 1 kW at phase A,B,C

RMS voltage at phase	A	B	C	A	B	C
	measured [V]			simulated [V]		
Open circuit	229.6	229.3	229.4	230.10	230.10	230.10
1 kW at phase A	227.2	228.4	228.5	229.85	230.05	230.05
1 kW at phase A,B	227.2	226.5	228.4	229.85	229.85	230.05
1 kW at phase A,B,C	227.3	226.4	226.4	229.85	229.85	229.85

decline is larger in case of the measured values compared to the simulated ones. A connection of a 1 kW ohmic load at phase A causes the voltage at all phases to decline. However, the voltage of phase A has a larger decline compared to the voltage of phase B and phase C. The voltage of phase A stays at this value even in the next sequence steps. By adding a 1 kW ohmic load at phase B, only the voltage of phase B declines. The same happens in case of adding a 1 kW ohmic load at phase C. In this case, only the voltage of phase C declines. While the simulated values show a symmetrical behaviour at the balanced situation in the end, the measured values of phase B and phase C deviate from phase A. The influence of this asymmetric behaviour of the measured values is not included in the models of this thesis. The declining characteristic is equal in the measured as well as in the simulated case. However, the absolute values of the decline are different. This behaviour is at least partly explainable with the discretisation effect described in the paragraph on the RMS voltage in chapter 3.2.1. As mentioned there, the effect is stronger for the measured system than for the simulated one.

RMS current The RMS current shows the same behaviour as described in chapter 3.2.1. Only the measured RMS current after the load connection is 4.30 - 4.35 A at the respective phase instead of 4.40 A at each phase. This value is reached in case that a 1 kW ohmic load is connected at the respective phase.

Active power The simulated values of the active power are similar to those described in chapter 3.2.1. However, the measured values are in the range of 975 - 995 W which is considerable lower than the measured values in case of a balanced ohmic load.

Reactive power The reactive power shows the same behaviour as described in chapter 3.2.1. This results from the independence of the reactive power on an ohmic load.

Disconnecting behaviour of the current The disconnecting behaviour is similar to the behaviour described in chapter 3.2.1. However, it only takes place for one phase instead of all three phases. The respective transient currents caused by a disconnection of ohmic loads at single phases are illustrated in the appendix in figure 73, figure 74 and figure 75.

3.2.5 Unbalanced change in inductive load

The Sunny Island battery inverter forms the grid in connection with a balanced ohmic load. At the time t = 0 ms it is connected to a 1 kVAr inductive load at one phase.

Transient Currents Figure 30 shows the comparison of the measured and simulated transient currents in case of a connection of a 1 kVAr inductive load at phase A. It displays that phase B

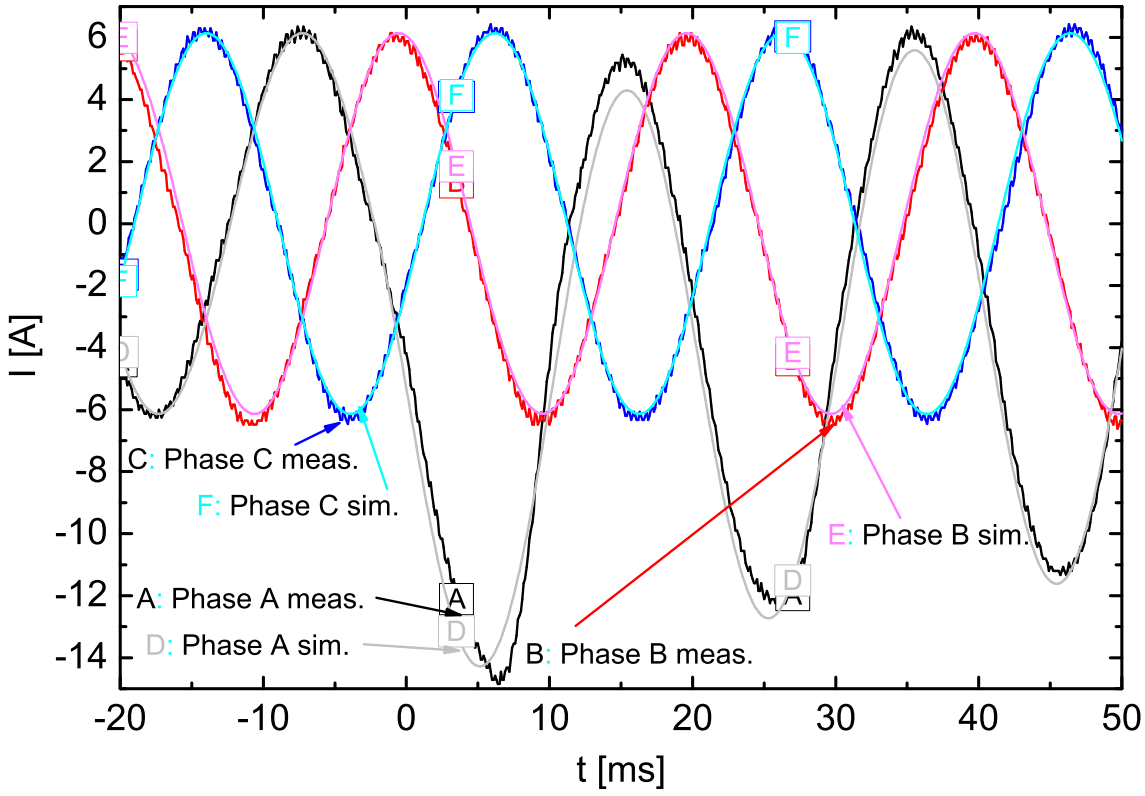

Figure 30: Transient currents I of the battery inverter in connection with a 1 kW ohmic load at each phase. The battery inverter is connected at the time t = 0 ms to a 1 kVAr inductive load at phase A. Comparison between the measured (meas.) values in darker colours (A,B,C) and the simulated (sim.) values in brighter colours (D,E,F).

and phase C are not affected while phase A shows the same behaviour of the transient current as described in chapter 3.2.2. The decay of the offset is illustrated by figure 77 (cf. Appendix). Figure 78 (cf. Appendix) shows the connection of phase B which displays a similar behaviour. Consequently, this behaviour also occurs in case of an inductive load connection at phase C (cf. chapter 3.2.2) because of the symmetric characteristics.

Transient Voltages In case of an unbalanced connection as well as an unbalanced disconnection of an ohmic load, the transient voltages show no particular behaviour. It is similar to the behaviour described in chapter 3.2.2. The simulated values fit well to the measured ones.

Therefore, there is no need to display them in this work.

Table 15 lists the steady state values before and after the load change. The values of this

Table 15: Comparison of the data of phase A between the measured and the simulated signals of the battery inverter supplying a 3 kW ohmic load which is connected at the time t = 0 ms to a 1 kVAr inductive load at phase A.

Signals	Measured < 0 ms	> 0 ms	Simulated < 0 ms	> 0 ms
Frequency [Hz]	49.45	49.44	49.72	49.72
RMS voltage [V]	227.3	221.6	229.9	225.2
RMS current [A]	4.30	6.15	4.35	6.20
Active power [W]	980	970	1000	1012
Reactive power [VAr]	70	955	-3	961

table are those of phase A. Phase B and phase C show no change caused by the load change at phase A. Similar values occur in case of the connection of a 1 kVAr inductive load at phase B or phase C. In this case, the respective other values show no change. Nevertheless, the measured values are a little asymmetric.

Frequency The frequency before and after the connection of the balanced inductive load is similar in the measured data as well as in the simulated data. However, the battery management causes a 0.27 Hz lower level of the frequency of the measured values compared to the simulated ones.

RMS voltage In table 15, the RMS voltage of phase A shows a decline by connecting the inductive load. This decline is caused by the droop control and it is the same as described in chapter 3.2.2. Connecting 1 kW inductive load at phase A results in a theoretical voltage deviation of $\Delta U = -6\ \% \times 230 \times 970/3600$ V = - 3.7 V for the measured values and a voltage deviation of $\Delta U = -6\ \% \times 230 \times 1012/3600$ V = - 3.9 V for the simulated values. However, this is neither the case for the measured data, which changes by 5.7 V from 227.3 V to 221.6 V, nor the case for the simulated data, which changes by 4.7 V from 229.9 V to 225.2 V. The additional voltage dip of 2.0 V in case of the measured values and 0.8 V in case of the simulated values is at least partly explainable with the discretisation effect described in the paragraph on the RMS voltage in chapter 3.2.1. As mentioned there, the effect is stronger for the measured system than for the simulated one. The described behaviour is similar in case of adding the inductive load to phase B or phase C.

RMS current The RMS current in the example of the connection event of an inductive load is similar in the measured and the simulated case. Similar values are measured and simulated in case of adding the inductive load to phase B or phase C.

Active power The influences to the active power are described in chapter 3.2.1. The active power of the measurement of the battery inverter in connection with a balanced 3 kW load should be $1000 \times (227.3/230)^2$ W $= 976$ W (compared to 980 W in table 15) and the simulation should result in $1000 \times (229.9/230)^2$ W $= 999$ W (compared to 1000 W in table 15). After adding the inductive load at phase A with an active power of 50 W at rated conditions, the measurement should be $1050 \times (221.6/230)^2$ W $= 974$ W (compared to 970 W in table 15) and the simulation should result in $1050 \times (225.2/230)^2$ W $= 1007$ W (compared to 1012 W in table 15). Altogether, the measurement as well as the simulation show a good correspondence to the theoretical values. The connection of the inductive load results in an increase of the active power in case of the simulation instead of a decrease of the active power in case of the measurement. However, the deviation is in the range of acceptable 1 %.

Reactive power The influences to the reactive power are described in chapter 3.2.2. According to these influences, after adding the inductive load, the reactive power should be $1000 \times (221.6/230)^2 \times (50/49.44)$ VAr $= 938$ VAr (compared to 955 VAr in table 15) and the simulation should result in $1000 \times (225.2/230)^2 \times (50/49.72)$ VAr $= 964$ VAr (compared to 961 VAr in table 15). The simulation shows a good correspondence to the theoretical values. However, the measured ones show a deviation of approximately 2 %.

Disconnecting behaviour of the current The disconnecting behaviour of the current is similar to the described one in chapter 3.2.2. However, it concerns only one phase. Figure 79 in the appendix shows the comparison between the measured and the simulated transient current in case of a disconnection of the 1 kVAr inductive load at phase A in connection with the battery inverter and an ohmic base load of 3 kW. Additionally, figure 80 in the appendix shows that a disconnection of a 1 kVAr inductive load at phase B has a similar behaviour as well as a similar match of the measured and the simulated values. The behaviour of phase B is representative to the behaviour of phase C.

3.2.6 Unbalanced change in capacitive load

The Sunny Island battery inverter forms the grid in connection with a balanced ohmic load. At the time t = 0 ms it is connected to a 1 kVAr inductive load at one phase.

Transient Currents Figure 31 shows the comparison of the measured and simulated transient currents in case of a connection of a 1 kVAr capacitive load at phase A. It displays that phase B and phase C are not affected while phase A shows the same behaviour of the transient current as described in chapter 3.2.3. Figure 83 (cf. Appendix) shows the connection of phase B which displays a similar behaviour. Consequently, this behaviour also occurs in case of an capacitive load connection at phase C because of the symmetric characteristics.

Transient Voltages Figure 82 in the appendix shows the comparison of the measured and simulated transient voltages in case of a connection of a 1 kVAr capacitive load at phase A. It

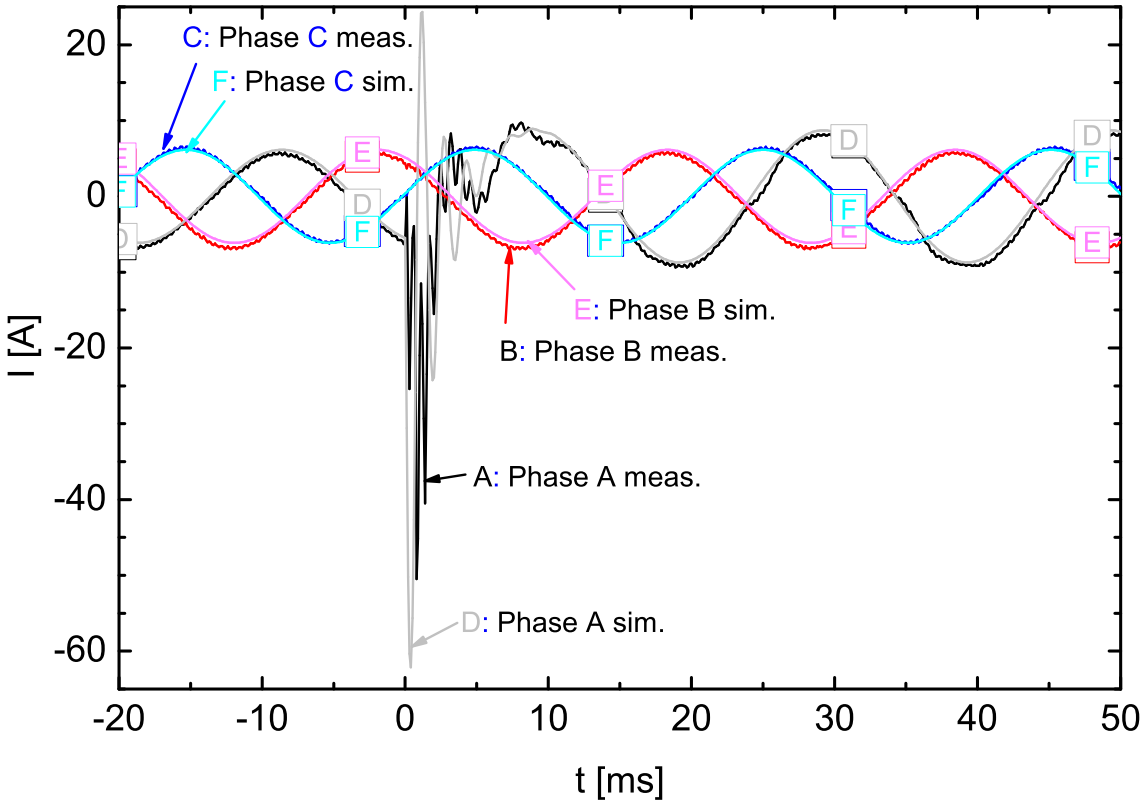

Figure 31: Transient currents I of the battery inverter in connection with a 1 kW ohmic load at each phase. The battery inverter is connected at the time t = 0 ms to a 1 kVAr capacitive load at phase A. Comparison between the measured (meas.) values in darker colours (A,B,C) and the simulated (sim.) values in brighter colours (D,E,F).

displays that phase B and phase C are not affected while phase A shows the same behaviour of the transient voltage as described in chapter 3.2.3. Figure 84 in the appendix shows the connection of phase B which displays a similar behaviour. Consequently, this behaviour also occurs in case of a capacitive load connection at phase C because of the symmetric characteristics. Additionally, the appendix shows in figure 86 and figure 88 the disconnection of the capacitive load at phase A as well as phase B. These figures show a behaviour of the measured and the simulated transient voltages with less disturbances compared to the case of the load connection.

Table 16 lists the steady state values before and after the load change. The values of this table are those of phase A. Phase B and phase C show no change (only the measured values are a little asymmetric) caused by the load change. Similar values occur in case of the connection of a 1 kVAr inductive load at phase B or phase C. In this case, the respective other values show no change.

Frequency The frequency before and after the connection of the balanced capacitive load is similar in the measured data as well as in the simulated data because no active power is changed.

Table 16: Comparison of the data of phase A between the measured and the simulated signals of the battery inverter supplying a 3 kW ohmic load which is connected at the time t = 0 ms to a 1 kVAr capacitive load at phase A.

Signals	Measured < 0 ms	> 0 ms	Simulated < 0 ms	> 0 ms
Frequency [Hz]	49.44	49.41	49.72	49.72
RMS voltage [V]	227.2	236.1	229.8	234.8
RMS current [A]	4.30	6.30	4.35	6.25
Active power [W]	977	1060	1000	1042
Reactive power [VAr]	70	-1047	-3	-1040

However, the battery management causes an approximately 0.3 Hz lower level of the frequency of the measured values compared to the simulated ones.

RMS voltage In table 16, the RMS voltage of phase A shows a similar behaviour as the voltage of phase A listed in table 13 commented in chapter 3.2.3. However, the RMS voltage of phase B and phase C is not influenced by adding a capacitive load at phase A. The described behaviour is similar in case of adding the capacitive load to phase B and phase C. In these cases, the respective other phases are not influenced.

RMS current The RMS current in the example of the connection event of an capacitive load at phase A is similar in the measured and the simulated case. The respective other phases (phase B and phase C) do not change by the load change.

Active power The influences to the active power are described in chapter 3.2.1. However, the RMS voltage of phase B and phase C is not influenced by adding a capacitive load at phase A. The active power of the measurement of the battery inverter in connection with a balanced 3 kW load should be $1000 \times (227.2/230)^2$ W $= 975$ W (compared to 977 W in table 16) and the active power of the simulation should result in $1000 \times (229.8/230)^2$ W $= 998$ W (compared to 1000 W in table 16). After adding the capacitive load with an active power of 0 W per phase at rated conditions, the measured active power should be $1000 \times (236.1/230)^2$ W $= 1054$ W (compared to 1060 W in table 16) and the simulated active power should result in $1000 \times (234.8/230)^2$ W $= 1042$ W (compared to 1042 W in table 16). Altogether, the simulation as well as the measurement show a good correspondence to the theoretical values. The absolute values fit well with a deviation of less than 1 %. In case of adding a capacitive load to phase B or phase C, the behaviour is similar with no influence to the respective other phases.

Reactive power The influences to the reactive power are described in chapter 3.2.2. However, the RMS voltage of phase B and phase C is not influenced by adding a capacitive load at phase A. According to equation 38 in chapter 2.3, after adding the capacitive load at phase A, the measured reactive power of phase A should be $1000 \times (236.1/230)^2 \times (49.41/50)$ VAr $=$

1041 VAr (compared to 1047 VAr in table 16) and the simulation should result in $1000 \times (234.8/230)^2 \times (49.72/50)$ VAr $= 1036$ VAr (compared to 1040 VAr in table 16). The simulation shows a good correspondence to the theoretical values with a deviation of less than 1 %. In case of adding a capacitive load to phase B or phase C, the behaviour is similar with no influence to the respective other phases.

Disconnecting behaviour of the current Figure 32 shows the comparison between the measured and the simulated transient current in case of a disconnection of the 1 kVAr capacitive load at phase A in connection with the battery inverter and an ohmic base load of 3 kW. The simulated current shows a similar behaviour to the measured data with little deviations. A disconnection at phase B or C shows the same behaviour (cf. figure 87 in the Appendix).

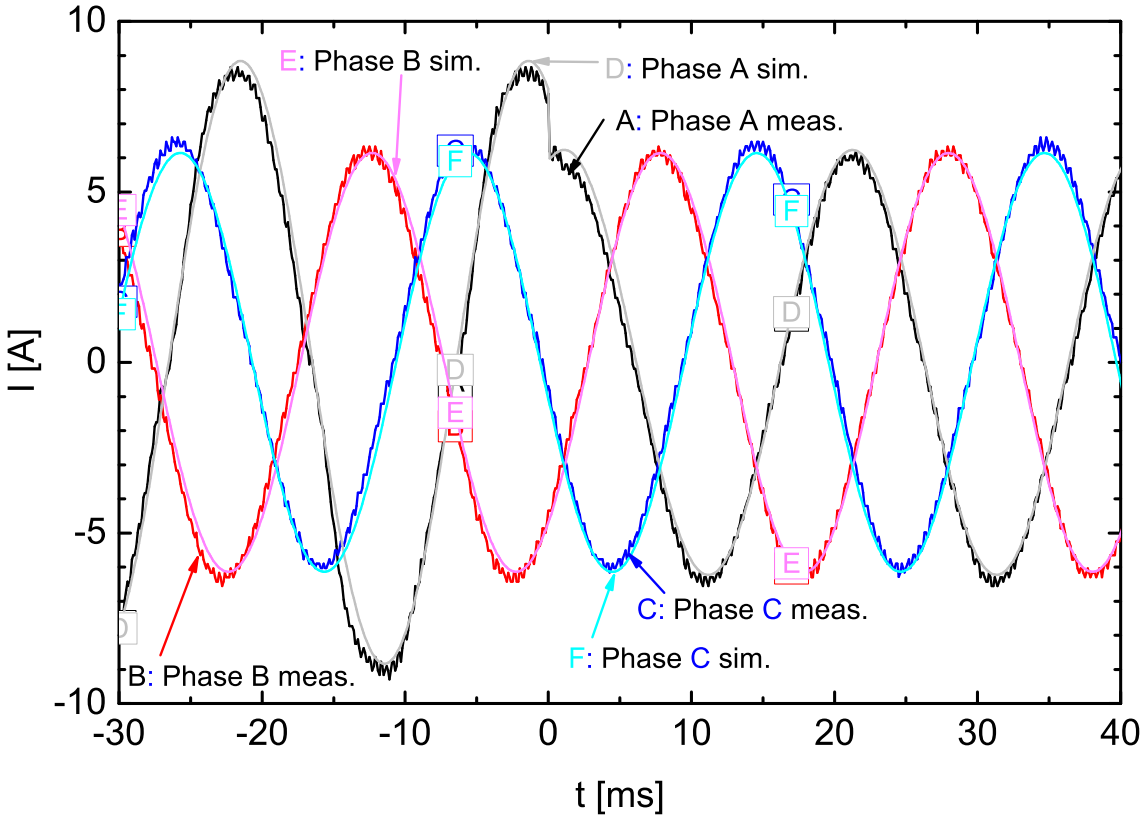

Figure 32: Transient currents I of the battery inverter in connection with a 1 kW ohmic load at each phase and a 1 kVAr capacitive load at phase A. The capacitive load at phase A is disconnected at the time t = 0 ms. Comparison between the measured (meas.) values in darker colours (A,B,C) and the simulated (sim.) values in brighter colours (D,E,F).

3.3 Battery inverter connected with asynchronous generator and loads

In this chapter the Sunny Island battery inverter is connected to the asynchronous generator which has a fixed target torque. Without additional components the asynchronous generator

feeds an active power of 1268 W per phase into the grid. With this power, the asynchronous generator loads the battery of the battery inverter and delivers the power consumption of the battery inverter. However, it needs a reactive power of 1630 VAr per phase. The asynchronous generator operates below its rated operation point. Therefore, the power factor is 0.61 which is below the rated power factor 0.83 given in table 2.

3.3.1 Balanced change in ohmic load

The Sunny Island battery inverter forms the grid. It operates in connection with the asynchronous generator. At the time t = 0 ms a 3 kW balanced ohmic load is connected to the system.

Transient currents Figure 33 shows the transient currents of the three phases A, B and C of the battery inverter measured at the point of measurement (cf. figure 20). This figure (with

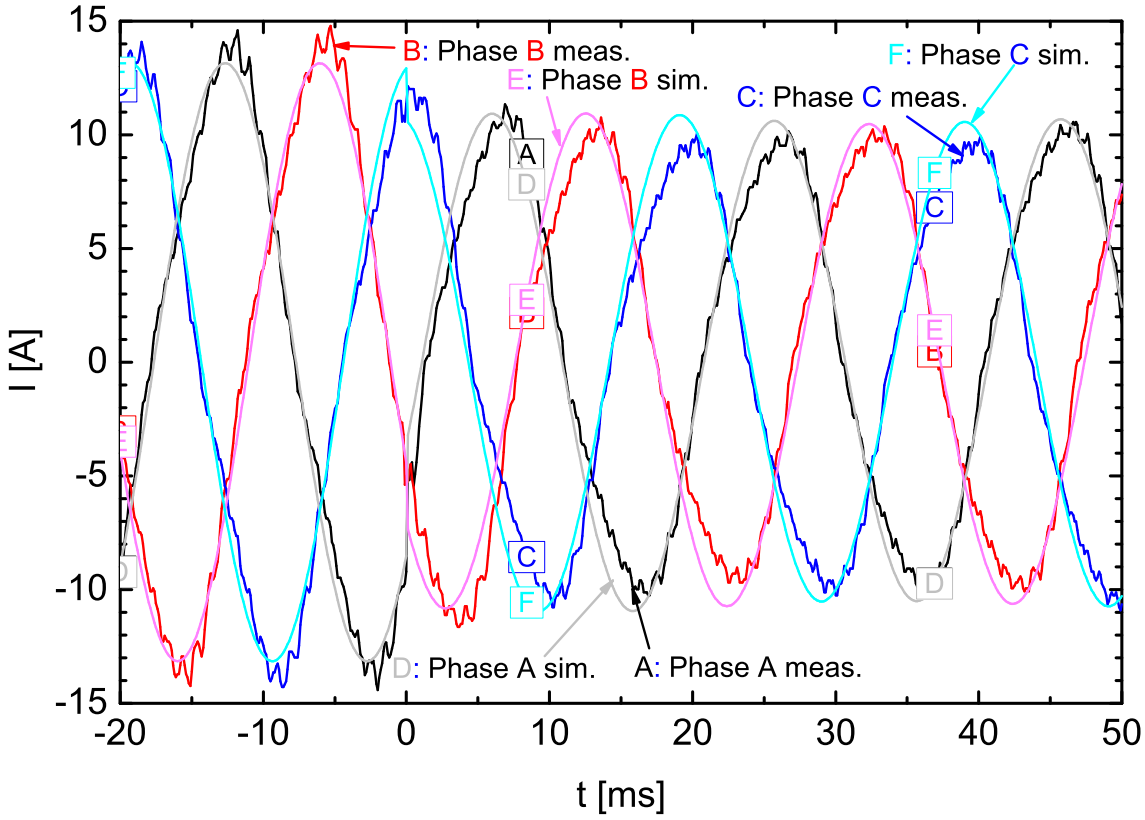

Figure 33: Transient currents I of the battery inverter in connection with the asynchronous generator which is connected at the time t = 0 ms to a 3 kW ohmic load. Comparison between the measured (meas.) values in darker colours (A,B,C) and the simulated (sim.) values in brighter colours (D,E,F).

asynchronous generator) shows a different measured transient current signal compared to the one displayed in figure 21 (without asynchronous generator) . The jagged signal is more smooth and results from a harmonic with a lower frequency. Additionally, the signal is more deformed than without the asynchronous generator. In contrast, the simulated signal of the transient currents is an ideal sine wave which results from the assumption of an ideal voltage source for the

battery inverter and an ideal asynchronous generator model. However, considering the possibilities of simulation, the simulated data fits sufficiently. The phase of the simulated data complies quantitatively, while the amplitude and the signal progression at the transition from no load to the 3 kW ohmic load complies qualitatively with the measured data.

However, some peaks of the sine waves to not fit well because the maximum value deviates up to 3 A between the measured and simulated data. One reason of these deviations shows figure 34 with an example of a steady state situation. The figure displays the positive peaks of the sinusoidal current signals. In this figure, the measured transient currents of the battery

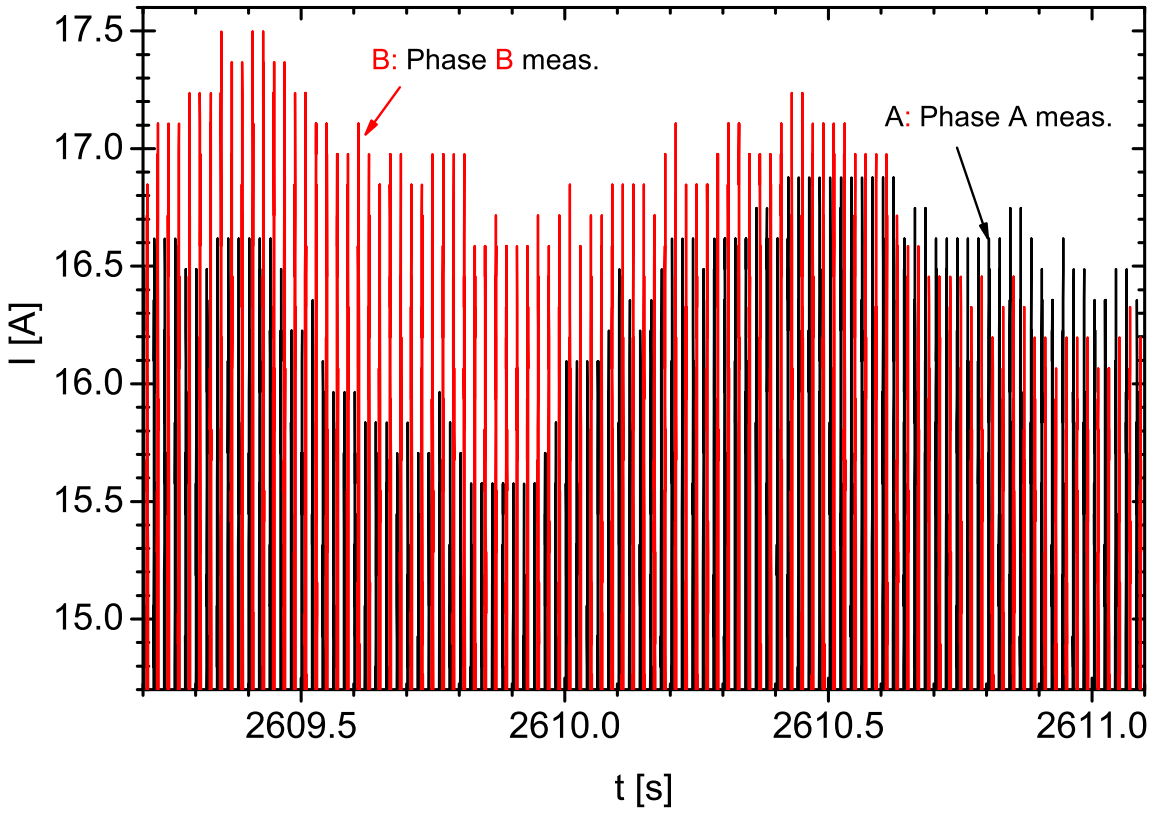

Figure 34: Fluctuations of the transient currents I of phase A and phase B of the battery inverter in connection with the asynchronous generator, a balanced 3 kW ohmic load and a 3 kVAr inductive load. The figure displays the positive peaks of the sinusoidal current signals.

inverter in connection with the asynchronous generator show fluctuations. The analysis of more than 60 seconds of the measured current signals shows deviations of up to 3 A between the minimum and maximum tops of the transient current's sine waves in steady state situations.

Transient voltages Figure 35 shows the transient voltages of the three phases A, B and C of the battery inverter. The voltage progression before and after the load change shows a good correlation between measured and simulated data. In comparison to the situation without the asynchronous generator (cf. figure 22), the measured transient voltage signal shows a harmonic similar to the harmonic of the transient currents. At the time t = 0 ms, a voltage dip occurs. In

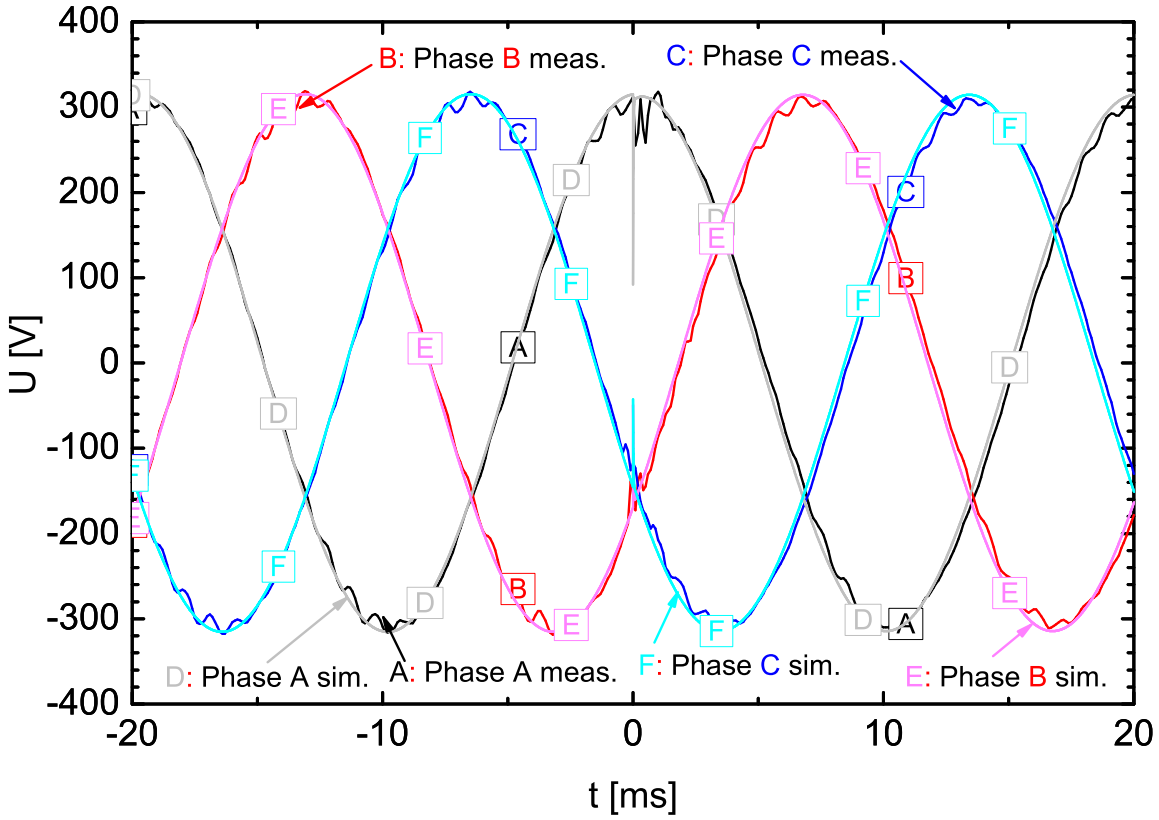

Figure 35: Transient voltages U of the battery inverter in connection with the asynchronous generator which is connected at the time t = 0 ms to a 3 kW ohmic load. Comparison between the measured (meas.) values in darker colours (A,B,C) and the simulated (sim.) values in brighter colours (D,E,F).

the simulated data it decays more rapidly compared to the measured data because of the simplifications in the models, e.g. the use of an ideal voltage source for the battery inverter.

Table 17 lists the steady state values before and after the load change. The values of this table are those of phase A because a balanced situation is analysed. Phase B and phase C show the same values in case of the simulated values. However, in case of the measured values, all phases vary a bit from each other.

Frequency The frequency (cf. table 17) shows a decrease after connecting the ohmic load. The active power of the measured data at the time $t < 0$ ms is -1268 W. This measured active power theoretically results in a frequency deviation $\Delta f = (-1) \times (-1268)/3600$ Hz = 0.35 Hz from the grid frequency of 50 Hz. Connecting 1 kW ohmic load at each phase results in a theoretical frequency deviation of $\Delta f = (-1) \times (-330)/3600$ Hz = 0.09 Hz at the time $t > 0$ ms. However, the measured frequency is lower because of the influence of the battery management. The simulated values of the frequency deviation of 0.34 Hz and 0.09 Hz comply with the theoretical values of $\Delta f = -1 \times -1260/3600$ Hz = 0.35 Hz at the time $t < 0$ ms and $\Delta f = (-1) \times (-327)/3600$ Hz = 0.09 Hz at the time $t > 0$ ms.

Table 17: Comparison of the data of phase A between the measured and the simulated signals of the battery inverter in connection with the asynchronous generator which is connected at the time t = 0 ms to a 3 kW ohmic load.

Signals	Measured < 0 ms	> 0 ms	Simulated < 0 ms	> 0 ms
Frequency [Hz]	50.15	49.88	50.34	50.09
RMS voltage [V]	220.6	220.0	222.2	222.1
RMS current [A]	9.30	7.50	9.25	7.50
Active power [W]	-1268	-330	-1260	-327
Reactive power [VAr]	1620	1620	1627	1631

RMS voltage The RMS voltage (cf. table 17) shows a small decline by connecting the balanced 3 kW ohmic load. This behaviour caused by the discretisation effect is explained in chapter 3.2.1. The same reason causes the RMS voltage of the measured values to be lower than the simulated values.

RMS current The RMS current values in table 17 show similar values in case of measured as well as simulated data before and after the load change. The reduction of the RMS current from 9.3 A to 7.5 A is caused by adding a balanced 3 kW ohmic load to the system consisting of the battery inverter and the asynchronous generator. Before adding the load, the active power of the asynchronous generator flows to the battery of the battery inverter. After adding the load, the asynchronous generator additionally supplies the consumed active power of the ohmic load. This new power flow between the asynchronous generator and the load reduces the power flow to the battery inverter and, therewith, the current.

Active power The simulated values of the active power flow (cf. table 17) between the asynchronous generator and the battery inverter are adjusted to the measured values by applying the respective torque to the asynchronous generator model in *PowerFactory*. Therefore, the simulated as well as the measured values show a good correspondence. Due to the dependence of the active power consumption of the ohmic load on the voltage, the difference between the measured and simulated active power before and after the load change is not 1000 W per phase but lower because the voltage is significantly lower. Equation 36 in chapter 2.3 defines that the active power of the load in case of the measurement should be $1000 \times (220/230)^2$ W $= 915$ W (compared to $-330 + 1268 = 938$ W in table 17). In case of the simulation the active power of the load should result in $1000 \times (222.1/230)^2$ W $= 932$ W (compared to $-327 + 1260 = 933$ W in table 17). There is a good fit for the simulated values but a deviation of 2.5 % for the measured values.

Reactive power The reactive power of the simulated data is adjusted to the measured data by changing the electrical parameters of the asynchronous generator model appropriately (cf.

chapter 2.2). Therefore, the values are similar. There is no significant change of the reactive power due to the load change because it is a pure ohmic load.

Disconnecting behaviour of the current Figure 36 shows the comparison between the measured and the simulated transient current in case of the disconnection of the 3 kW ohmic load in connection with the battery inverter and the asynchronous generator. The figure displays that

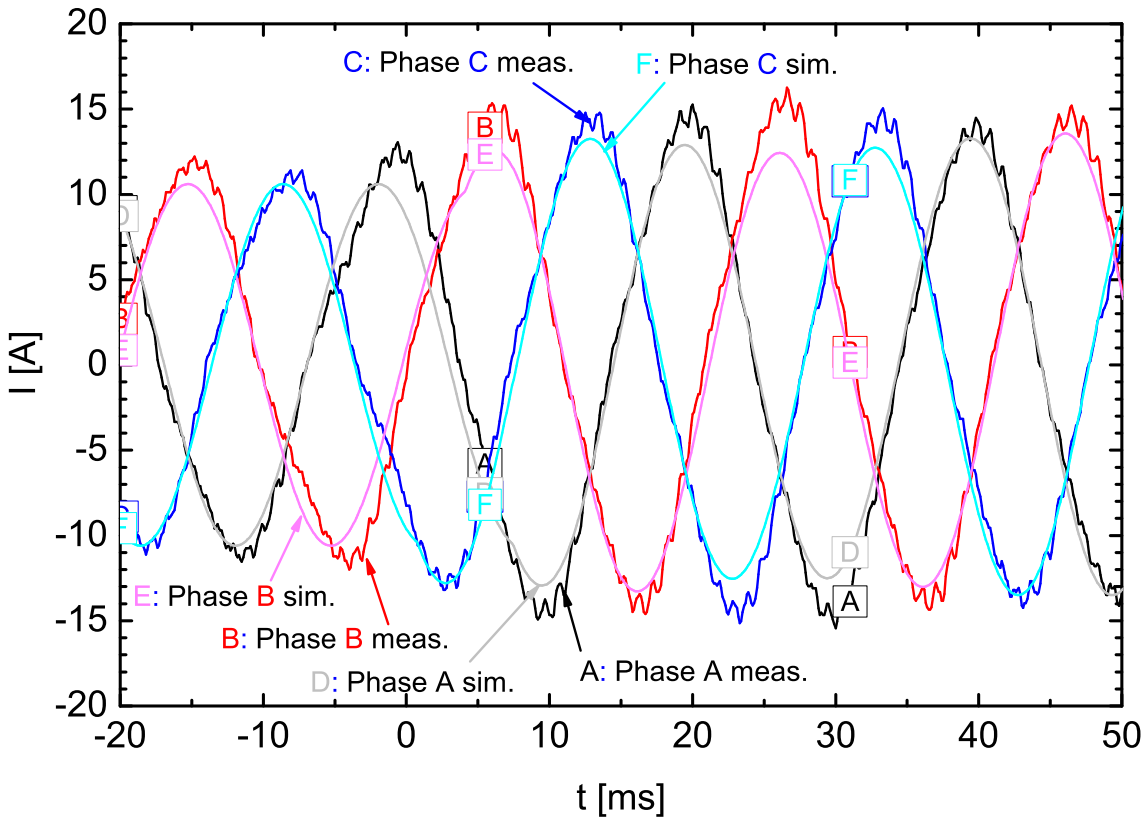

Figure 36: Transient currents I of the battery inverter in connection with the asynchronous generator supplying a 3 kW ohmic load. The 3 kW ohmic load is disconnected at the time t = 0 ms. Comparison between the measured (meas.) values in darker colours (A,B,C) and the simulated (sim.) values in brighter colours (D,E,F).

the current of all three phases changes not at the same time to the next stead state amplitude but that it tunes. This tuning is illustrated with figure 92 in the appendix. It shows that the measured oscillations are not simulated accurately but that both current signals are tuning and finally reaching similar current signals. Switch off the load in the simulation is specified by disconnection at zero-crossing (cf. chapter 3.2.1).

3.3.2 Balanced change in inductive load

The Sunny Island battery inverter forms the grid. It operates in connection with the asynchronous generator and the balanced 3 kW ohmic load. At the time t = 0 ms, a 3 kVAr balanced inductive load is connected to the system.

Transient currents Figure 37 shows the transient currents of the three phases A, B and C of the battery inverter measured at the point of measurement (cf. figure 20). After the connection

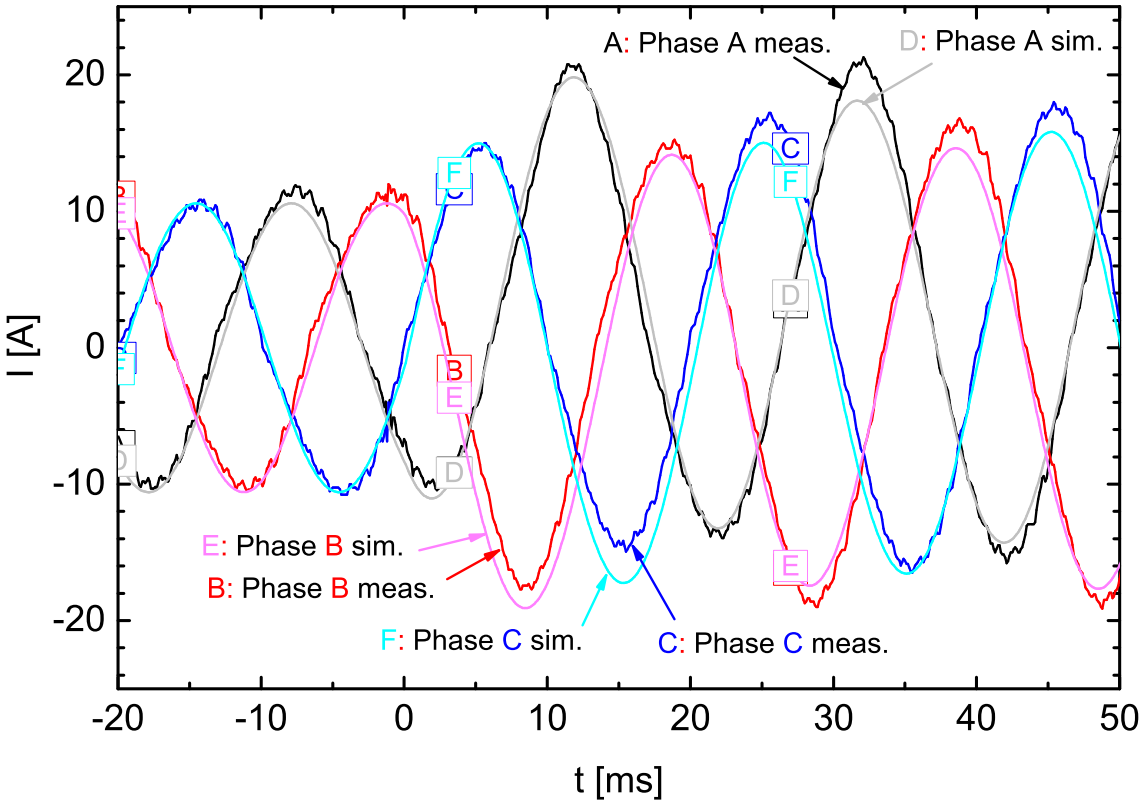

Figure 37: Transient currents I of the battery inverter in connection with the asynchronous generator and the balanced 3 kW ohmic load which is connected at the time t = 0 ms to a 3 kVAr inductive load. Comparison between the measured (meas.) values in darker colours (A,B,C) and the simulated (sim.) values in brighter colours (D,E,F).

event, the current has a superposed direct current which causes a deviation of the mean value from zero. This offset decays over some periods of the current as displayed in figure 38 for the 150 ms after the load change. The offset characteristic occurs also in the simulated data. Altogether, qualitatively, the measured and simulated currents fit sufficiently. The remaining deviations between the measured and the simulated values partly result from the fluctuations of the measured current which is described in chapter 3.3.1.

Transient voltages The transient voltages show no particular transient behaviour. Additionally, the measured and the simulated voltages show no significant difference. Therefore, it is not displayed here but in the appendix in figure 96. However, the measured voltage signal shows a harmonic as described in chapter 3.3.1.

Table 18 lists the steady state values before and after the load change. The values of this table are those of phase A because a balanced situation is analysed. Phase B and phase C show

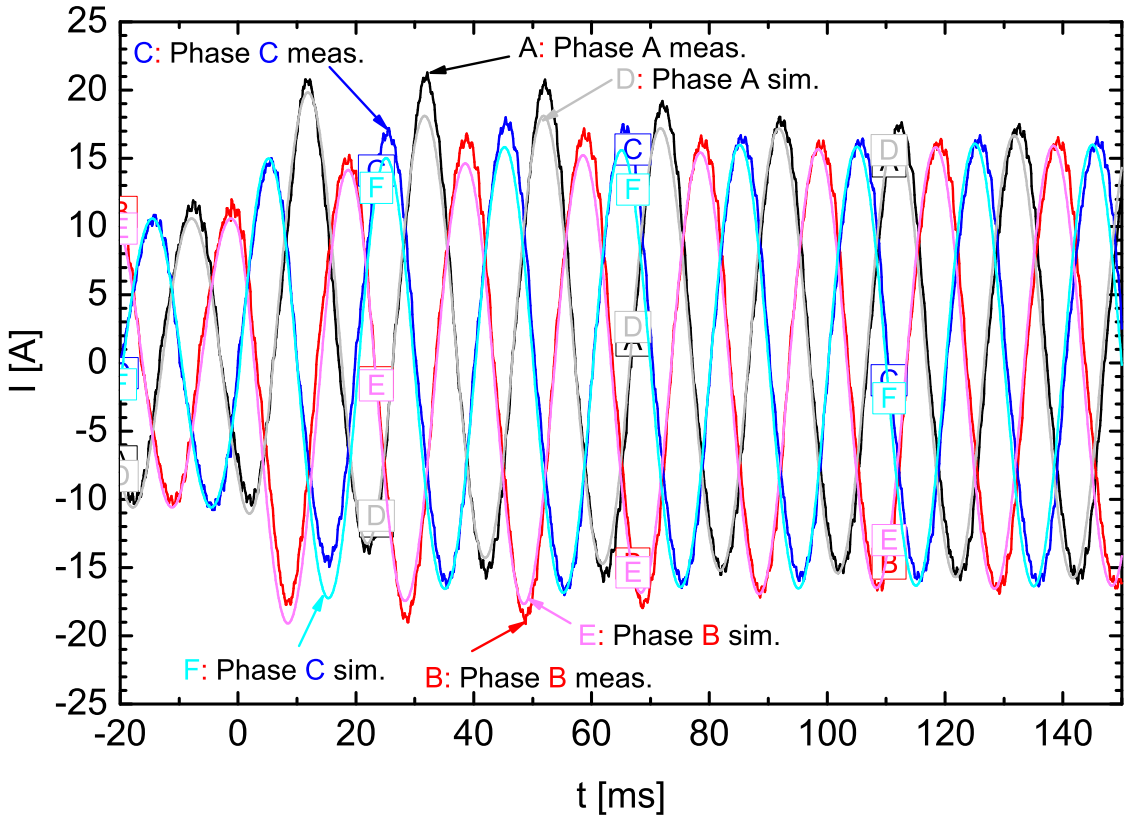

Figure 38: Decay of the transient currents I of the battery inverter in connection with the asynchronous generator and the balanced 3 kW ohmic load which is connected at the time t = 0 ms to a 3 kVAr inductive load. Comparison between the measured (meas.) values in darker colours (A,B,C) and the simulated (sim.) values in brighter colours (D,E,F).

the same values in case of the simulated values. However, in case of the measured values, all phases vary a bit from each other.

Frequency The frequency before and after the connection of the balanced inductive load is equal in the measured data as well as in the simulated data. However, the battery management causes a 0.2 Hz lower level of the frequency of the measured values compared to the simulated ones. The active power of the measured data at the time $t < 0$ ms is -350 W. This measured active power theoretically results in a frequency deviation $\Delta f = (-1) \times (-350)/3600$ Hz = 0.10 Hz from the grid frequency of 50 Hz. Connecting 1 kVAr inductive load with an ohmic load of 50 W at each phase results in a theoretical frequency deviation of $\Delta f = (-1) \times (-355)/3600$ Hz = 0.10 Hz at the time $t > 0$ ms. However, the measured frequency is lower because of the influence of the battery management. The active power of the simulated data at the time $t < 0$ ms is -315 W. This simulated active power theoretically results in a frequency deviation $\Delta f = (-1) \times (-315)/3600$ Hz = 0.10 Hz from the grid frequency of 50 Hz. Connecting 1 kVAr inductive load with an ohmic load of 50 W at each phase results in a theoretical frequency deviation of $\Delta f = (-1) \times (-300)/3600$ Hz = 0.09 Hz at the time $t > 0$ ms. The

Table 18: Comparison of the data of phase A between the measured and the simulated signals of the battery inverter in connection with the asynchronous generator and the balanced 3 kW ohmic load which is connected at the time t = 0 ms to a 3 kVAr inductive load.

Signals	Measured < 0 ms	> 0 ms	Simulated < 0 ms	> 0 ms
Frequency [Hz]	49.88	49.88	50.08	50.08
RMS voltage [V]	220.0	215.2	222.1	217.8
RMS current [A]	7.50	11.45	7.50	11.45
Active power [W]	-350	-355	-315	-300
Reactive power [VAr]	1620	2445	1630	2472

simulated values of the frequency comply with the theoretical values.

RMS voltage The RMS voltage (cf. table 18) shows a decline by connecting the inductive load. This decline is caused by the droop control as described in chapter 3.2.2. In case of the measured values, the supplied reactive power at the time $t < 0$ ms is 1620 VAr resulting in a voltage deviation $\Delta U = -6\ \% \times 230 \times 1620/3600$ V = - 6.2 V compared to measured - 10.0 V. Connecting 1 kVAr inductive load at each phase corresponds to a supplied reactive power at the time $t > 0$ ms of 2445 VAr resulting in a voltage deviation $\Delta U = -6\ \% \times 230 \times 2445/3600$ V = - 9.4 V compared to measured - 14.8 V. In case of the simulated values, the supplied reactive power at the time $t < 0$ ms is 1630 VAr resulting in a voltage deviation $\Delta U = -6\ \% \times 230 \times 1630/3600$ V = - 6.2 V compared to simulated - 7.9 V. Connecting 1 kVAr inductive load at each phase results in a supplied reactive power at the time $t > 0$ ms of 2472 VAr resulting in a voltage deviation $\Delta U = -6\ \% \times 230 \times 2472/3600$ V = - 9.5 V compared to simulated - 12.2 V. At least one reason for the additional voltage dip in case of the measured values as well as the simulated values is the discretisation effect described in the paragraph on the RMS voltage in chapter 3.2.1. As mentioned there, the effect is stronger for the measured system than for the simulated one.

RMS current The RMS current in the example of the connection event of an inductive load is equal in the measured and the simulated case. This match supports the good representation of the current values by the simulation.

Active power With the dependencies described in chapter 3.2.2, the active power of the measurement of the battery inverter in connection with the asynchronous generator and the balanced 3 kW ohmic load should be -1268 W$+1000 \times (220/230)^2$ W $= -353$ W (compared to -350 W in table 18) and the simulation should result in -1260 W$+ 1000 \times (222.1/230)^2$ W $= -327$ W (compared to -315 W in table 18). After adding the inductivity with an active power of 50 W per phase at rated conditions, the measurement should be -1268 W $+ 1050 \times (215.2/230)^2$ W $= -349$ W (compared to - 355 W in table 18) and the simulation should result in -1260 W $+ 1050 \times (217.8/230)^2$ W $= -318$ W (compared to -300 W in table 18). Altogether, the mea-

surement shows a good correspondence to the theoretical values. In contrast, the simulation shows a significant deviation from the theoretical values. This deviation partly results from the influence of the frequency and the voltage to the active power output of the asynchronous generator, which is not considered in this work.

Reactive power The reactive power has three influences which are described in chapter 3.2.2. According to these influences the reactive power after adding the inductive load should be 1620 VAr $+ 1000 \times (215.2/230)^2 \times (50/49.88)$ VAr $= 2498$ VAr (compared to 2445 VAr in table 18) and the simulation should result in 1630 VAr$+1000\times(217.8/230)^2\times(50/50.08)$ VAr $= 2525$ VAr (compared to 2472 VAr in table 18). The influence of the frequency and the voltage to the reactive power output of the asynchronous generator is not considered in this calculation. However, both, the measured and the simulated values, are 53 VAr lower than the theoretical values. This additional deviation can be attributed to the asynchronous generator whose reactive power decreases by this load change.

Disconnecting behaviour of the current Figure 39 shows the comparison between the measured and the simulated transient current in case of a disconnection of the 3 kVAr inductive load in connection with the battery inverter, the asynchronous generator and an ohmic base load of 3 kW. The figure shows that the current of all three phases changes not at the same time to the next stead state amplitude but that each phase decays without an interruption of its sine wave. The simulated current shows a similar behaviour as the measured data. However, the measured current decays more slowly compared to the simulated current.

3.3.3 Balanced change in capacitive load

The Sunny Island battery inverter forms the grid. It operates in connection with the asynchronous generator and the balanced 3 kW ohmic load. At the time t = 0 ms a 3 kVAr balanced capacitive load is connected to the system.

Transient currents Figure 40 shows the transient currents of the three phases A, B and C of the battery inverter measured at the point of measurement (cf. figure 20). After the connection event, the current oscillates and tunes within 15 ms. Qualitatively, the measured and simulated currents fit well. However, the measured sine wave before and after the transient (0-15 ms) is more deformed than the measured current signals without the asynchronous generator in figure 26. The transients in figure 40 are difficult to recognize in detail. Therefore, they are displayed separately in figure 100, figure 101 and figure 102 in the appendix. The deviation between the simulated and measured values is partly caused by the fluctuations of the measured current signals (cf. the paragraph on transient currents in chapter 3.3.1.

Transient voltages Figure 41 shows the transient voltages U of the three phases A, B and C of the battery inverter. The voltage progression before and after the load change shows a good correlation between measured and simulated data. However, the measured voltage signal shows

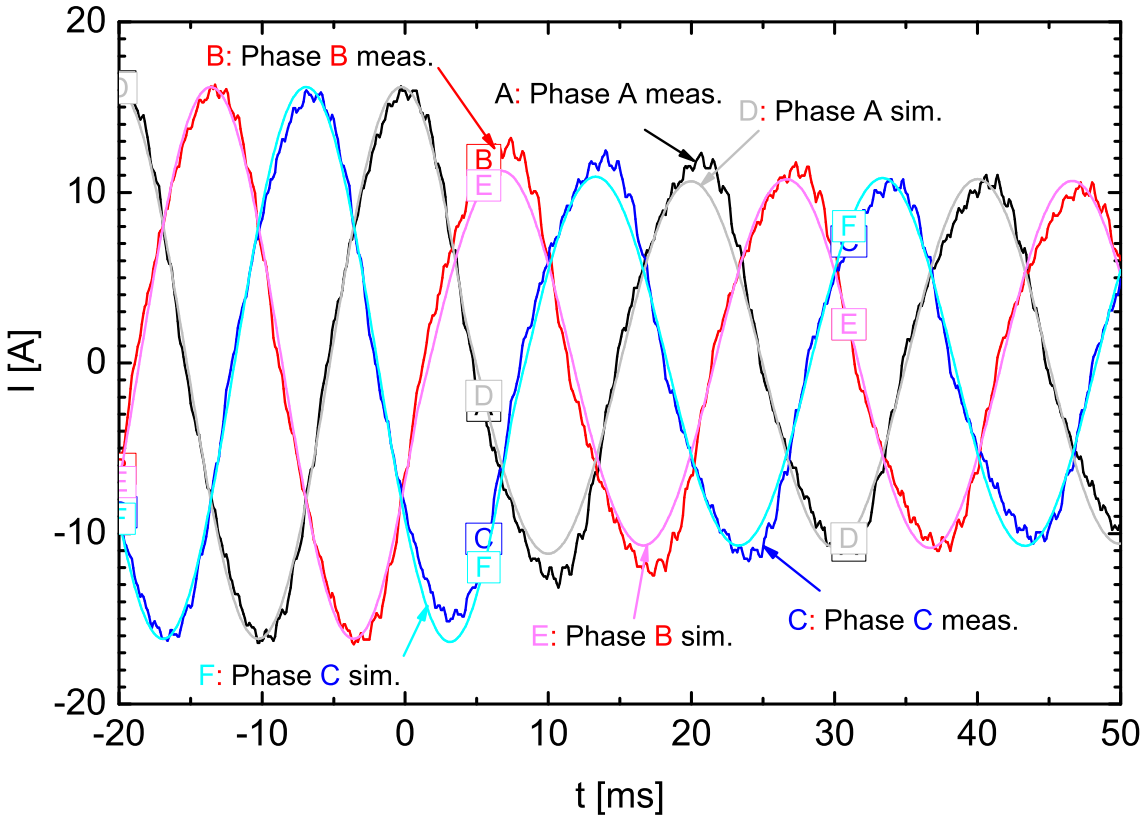

Figure 39: Transient currents I of the battery inverter in connection with the asynchronous generator supplying a 3 kW ohmic and a 3 kVAr inductive load. The 3 kVAr inductive load is disconnected at the time t = 0 ms. Comparison between the measured (meas.) values in darker colours (A,B,C) and the simulated (sim.) values in brighter colours (D,E,F).

a harmonic as described in chapter 3.3.1. The following 20 ms after the connection of the capacitive load show a behaviour which is similar to the behaviour of the transient currents. The simulated voltages do not follow the oscillations of the measured voltages exactly but qualitatively well. As in the case of the transient current, it is not possible to simulate the voltages accurately because there are many influences which are out of scope of the simulations in this thesis.

Table 19 lists the steady state values before and after the load change. The values of this table are those of phase A because a balanced situation is analysed. Phase B and phase C show the same values in case of the simulated values. However, in case of the measured values, all phases vary a bit from each other.

Frequency The frequency before and after the connection of the balanced capacitive load is similar in the measured data as well as in the simulated data because no active power is changed. However, the battery management causes an approx. 0.17 Hz lower level of the frequency of the measured values compared to the simulated ones.

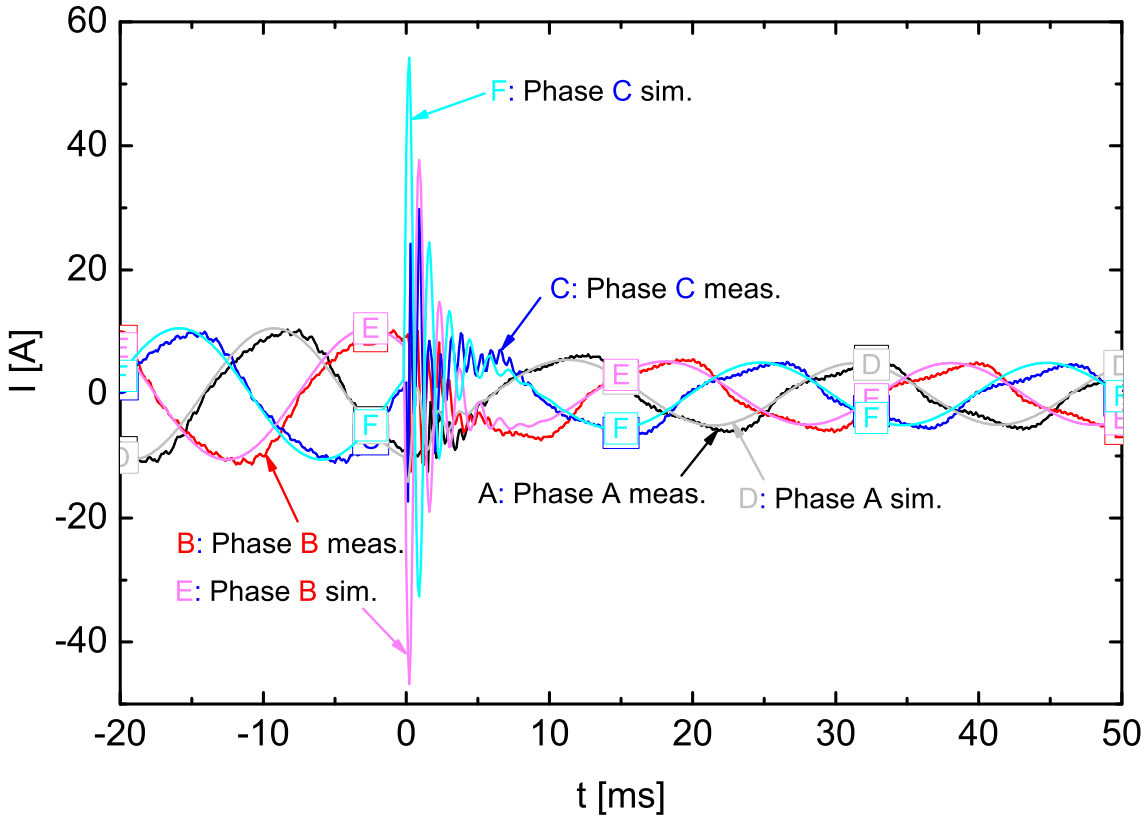

Figure 40: Transient currents I of the battery inverter in connection with the asynchronous generator and the balanced 3 kW ohmic load which is connected at the time t = 0 ms to a 3 kVAr capacitive load. Comparison between the measured (meas.) values in darker colours (A,B,C) and the simulated (sim.) values in brighter colours (D,E,F).

RMS voltage The voltage (cf. table 19) shows an increase by connecting the capacitive load as described in chapter 3.2.3. In case of the measured values, the supplied reactive power at the time $t < 0$ ms is 1605 VAr and results in a voltage deviation $\Delta U = -6\,\% \times 230 \times 1605/3600$ V = - 6.2 V compared to measured - 9.9 V. Connecting 1 kVAr capacitive load at each phase causes a supplied reactive power at the time $t > 0$ ms of 730 VAr and results in a voltage deviation $\Delta U = -6\,\% \times 230 \times 730/3600$ V = - 2.8 V compared to measured - 4.8 V.

In case of the simulated values, the supplied reactive power at the time $t < 0$ ms is 1631 VAr and results in a voltage deviation $\Delta U = -6\,\% \times 230 \times 1631/3600$ V = - 6.2 V compared to simulated - 7.9 V. Connecting 1 kVAr capacitive load at each phase causes a supplied reactive power at the time $t > 0$ ms of 719 VAr and results in a voltage deviation $\Delta U = -6\,\% \times 230 \times 719/3600$ V = - 2.8 V compared to simulated - 3.4 V. The additional voltage increase is at least partly explainable with the discretisation effect described in the paragraph on the RMS voltage in chapter 3.2.1. As mentioned there, the effect is stronger for the measured system than for the simulated one.

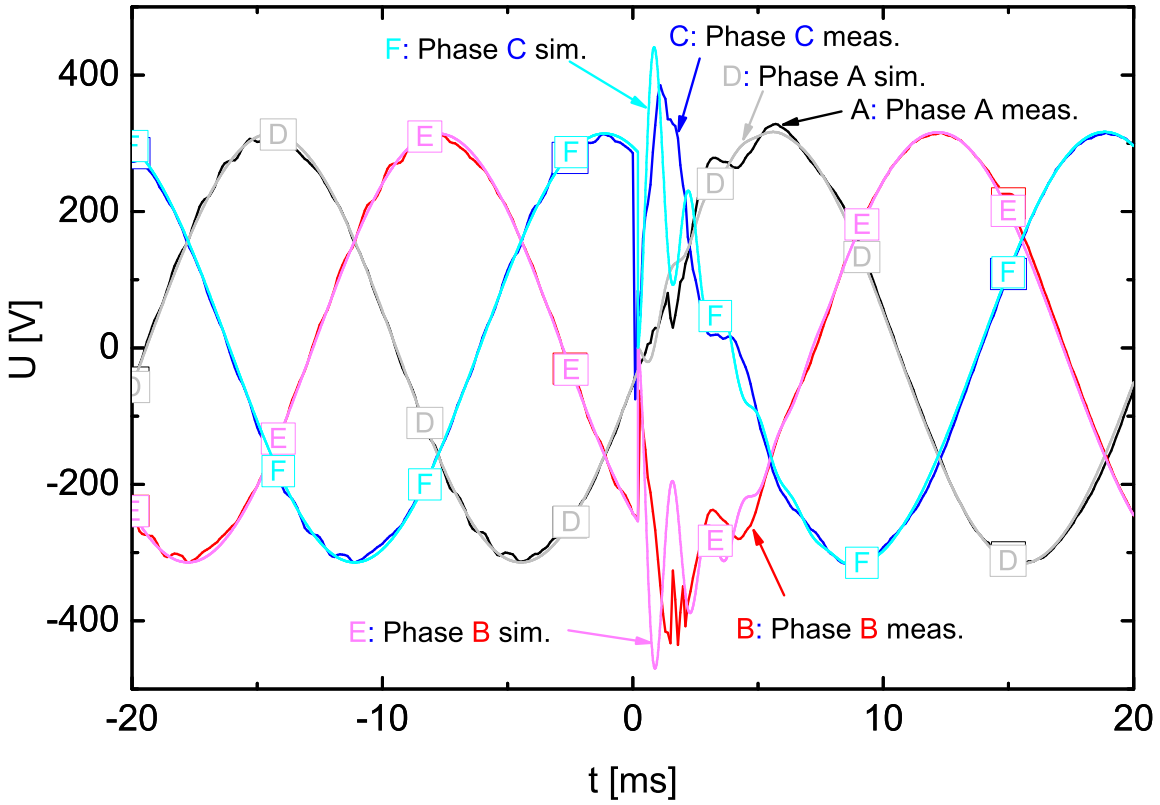

Figure 41: Transient voltages U of the battery inverter in connection with the asynchronous generator and the balanced 3 kW ohmic load which is connected at the time t = 0 ms to a 3 kVAr capacitive load. Comparison between the measured (meas.) values in darker colours (A,B,C) and the simulated (sim.) values in brighter colours (D,E,F).

RMS current The RMS current in the example of the connection event of a capacitive load is similar in the measured and the simulated case.

Active power With the dependencies described in chapter 3.2.2, the active power of the measurement of the battery inverter in connection with the asynchronous generator and the balanced 3 kW ohmic load should be $-1268\ \text{W} + 1000 \times (220.1/230)^2\ \text{W} = -352\ \text{W}$ (compared to -350 W in table 19) and the simulation should result in $-1260\ \text{W} + 1000 \times (222.1/230)^2\ \text{W} = -327\ \text{W}$ (compared to -310 W in table 19). After adding the capacity without a resistance, the measurement should be $-1268\ \text{W} + 1000 \times (225.2/230)^2\ \text{W} = -309\ \text{W}$ (compared to - 300 W in table 19) and the simulation should result in $-1260\ \text{W} + 1000 \times (226.6/230)^2\ \text{W} = -289\ \text{W}$ (compared to -275 W in table 19). Altogether, the measurement as well as the simulation shows a significant deviation from the theoretical values. Not considered in this calculation is the influence of the frequency and the voltage to the active power output of the asynchronous generator.

Reactive power The reactive power has three influences which are described in chapter 3.2.2. According to these influences the reactive power after adding the capacitive load should be

Table 19: Comparison of the data of phase A between the measured and the simulated signals of the battery inverter in connection with the asynchronous generator and the balanced 3 kW ohmic load which is connected at the time t = 0 ms to a 3 kVAr capacitive load.

Signals	Measured < 0 ms	> 0 ms	Simulated < 0 ms	> 0 ms
Frequency [Hz]	49.92	49.90	50.08	50.08
RMS voltage [V]	220.1	225.2	222.1	226.6
RMS current [A]	7.45	3.50	7.50	3.40
Active power [W]	-350	-300	-310	-275
Reactive power [VAr]	1605	730	1631	719

1605 VAr$-1000\times(225.2/230)^2\times(49.9/50)$ VAr $= 648$ VAr (compared to 730 VAr in table 19) and the simulation should result in 1631 VAr $- 1000 \times (226.6/230)^2 \times (50.08/50)$ VAr $= 659$ VAr (compared to 719 VAr in table 19). The influence of the frequency and the voltage to the reactive power output of the asynchronous generator is not considered in this calculation. However, the measured values are 82 VAr higher than the theoretical values and the simulated values are 60 VAr higher than the theoretical values. This additional deviation can be attributed to the asynchronous generator whose reactive power increases by this load change. Another reason are the deficits of the asynchronous generator model.

Disconnecting behaviour of the current Figure 42 shows the comparison between the measured and the simulated transient current in case of a disconnection of the 3 kVAr capacitive load in connection with the battery inverter, the asynchronous generator and an ohmic base load of 3 kW. The figure shows that the current of all three phases changes at the same time. While different influences deform the measured current signals, the simulated current signal shows an ideal sine wave. Therefore, the simulated signal changes sharply at the time of the switching event in contrast to the measured signal which changes more smoothly. The time until the current reaches its new steady state is longer for the measured signals than for the simulated ones. Consequently, the simulated current values are higher than the measured current values in the first 25 ms after the switching event. This tuning to the next steady state is illustrated in more detail in figure 104 in the appendix. This figure shows the transient currents for a longer time t.

3.3.4 Unbalanced change in ohmic load

The Sunny Island battery inverter is connected to the asynchronous generator. At the time t = 0 ms it is connected to a 1 kW ohmic load at one phase. Firstly, a 1 kW ohmic load is connected to the battery inverter at phase A. Secondly, a 1 kW ohmic load is connected to the battery inverter at phase B, and, finally, at phase C.

Transient Currents Figure 43 shows the comparison of the measured and simulated transient currents. It displays that phase B and phase C are not significantly affected while the current of

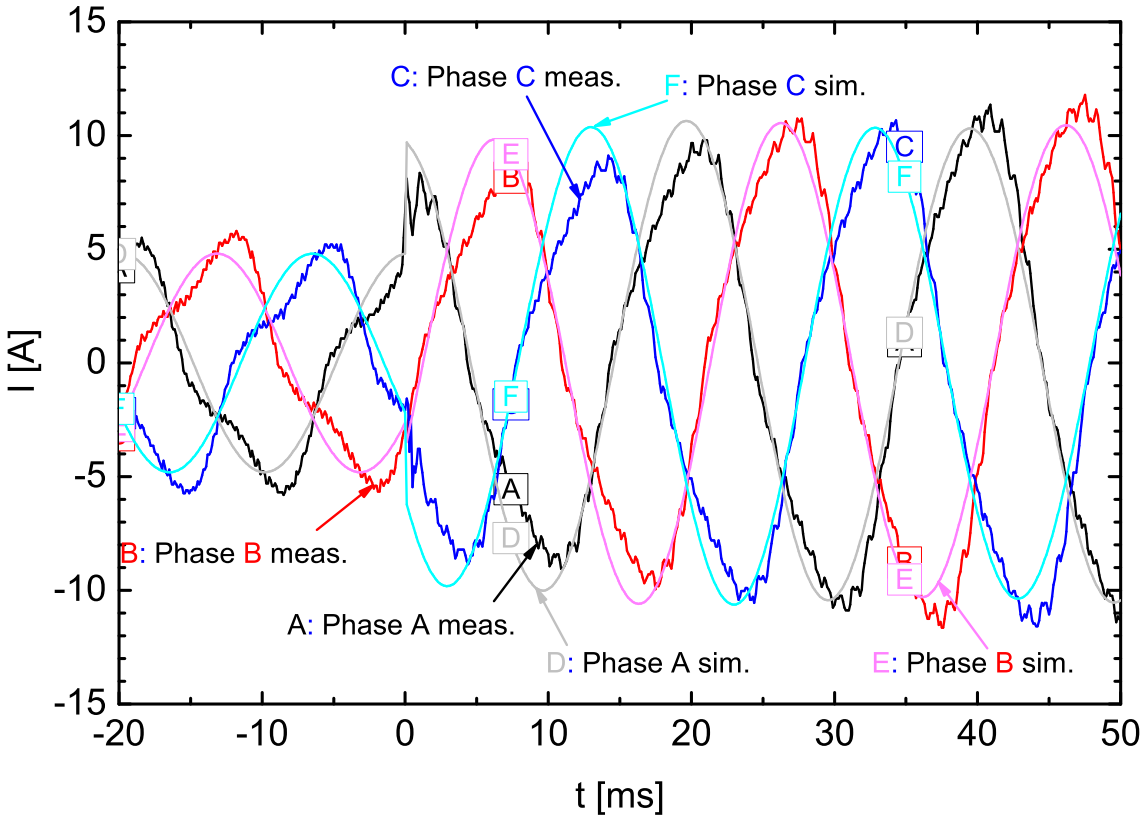

Figure 42: Transient currents I of the battery inverter in connection with the asynchronous generator supplying a 3 kW ohmic and a 3 kVAr capacitive load. The 3 kVAr capacitive load is disconnected at the time t = 0 ms. Comparison between the measured (meas.) values in darker colours (A,B,C) and the simulated (sim.) values in brighter colours (D,E,F).

phase A tunes to the new steady state. The figure shows that the phases oscillated independent on each other. These oscillations occur in case of the measured signals as well as in case of the simulated signals. However, due to influences which are not considered in the simulation, the oscillations of the measured and simulated values do not comply exactly. In the appendix, figure 105 shows the connection of phase A in the 50 ms after the connection. Additionally, figures are listed in the appendix illustrating the transient currents of the measurement and the simulation in case of a connection of phase B (figure 108 and figure 109) and phase C (figure 110 and figure 111). They show a similar behaviour of the transient currents. The deviation between the simulated and measured values is partly caused by the fluctuations of the measured current signals (cf. the paragraph on transient currents in chapter 3.3.1.

Transient Voltages In case of an unbalanced connection as well as an unbalanced disconnection of an ohmic load, the transient voltages show no particular behaviour. The simulated values fit well to the measured ones. An example is given in figure 107 in the appendix.

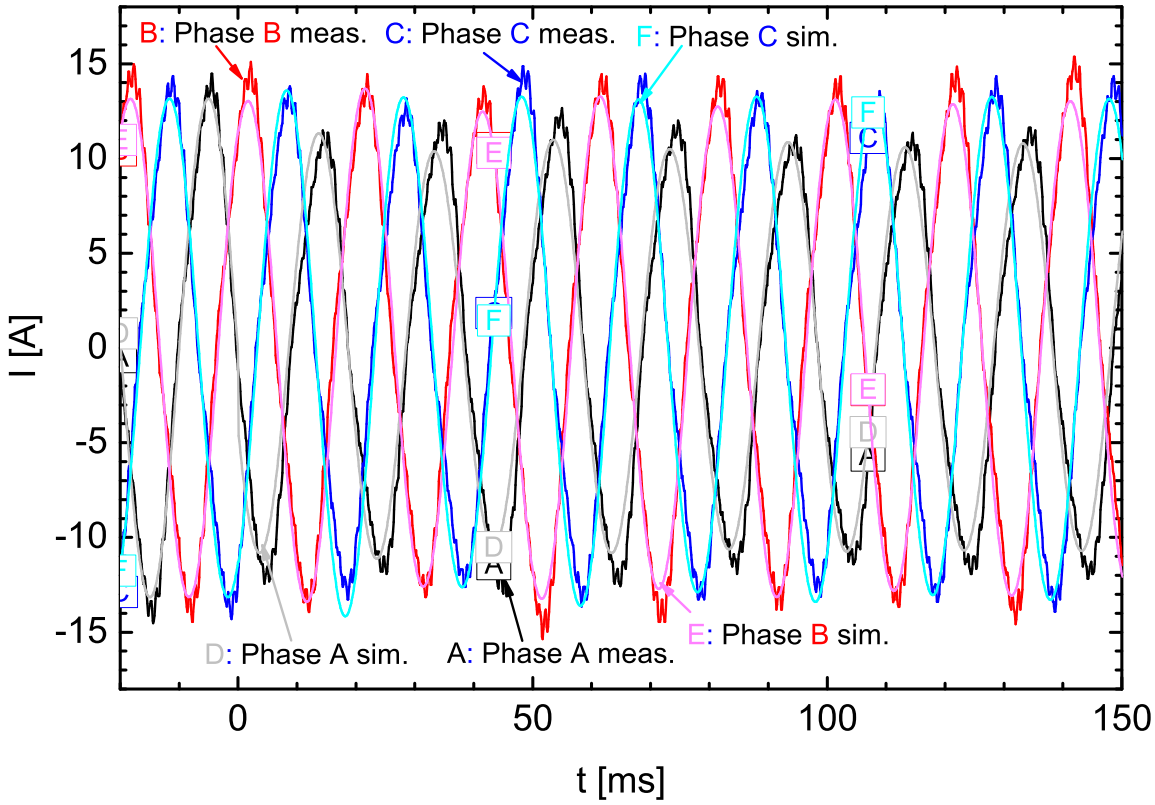

Figure 43: Transient voltages U of the battery inverter which is connected with the asynchronous generator. At the time t = 0 ms a 1 kW ohmic load is connected to phase A. The transients of the following 150 ms are displayed. Comparison between the measured (meas.) values in darker colours (A,B,C) and the simulated (sim.) values in brighter colours (D,E,F).

Frequency The frequency shows the expected behaviour similar to the described one in chapter 3.3.1. As mentioned therein, the battery management influences the measured values so that a direct comparison with the simulated values is not possible. The values depend on the power at phase A. In case that ohmic load is connected to the battery inverter at phase A, the frequency declines, whereas no dependence is recognizable at phase B and phase C. This results from the implemented droop control concept described in chapter 2.1.3. In this concept, the 'Master Droop Controller' adjusts the frequency to the active power at phase A while the other phases synchronise to this frequency.

RMS voltage Table 20 lists the steady state values of the RMS voltages of the three phases (in the columns) for a connection sequence (in the rows) in case of the measured values and in case of the simulated values. The steady state values of the measured RMS voltages show the same behaviour as described in chapter 3.2.4. However, due to the asynchronous generator, the voltage level is generally lower. In contrast, the behaviour of the simulated RMS voltages is different to the measured ones.

Table 20: Comparison of the data between the measured and the simulated RMS voltage signals of the battery inverter connected to the asynchronous generator supplying unbalanced ohmic loads. Four different steady states are considered: open circuit; 1 kW at phase A; 1 kW at phase A,B; and 1 kW at phase A,B,C

RMS voltage at phase	A	B	C	A	B	C
	measured [V]			simulated [V]		
Open circuit	220.6	220.7	221.1	222.20	222.20	222.20
1 kW at phase A	220.1	220.4	221.0	222.05	222.30	222.10
1 kW at phase A,B	220.1	219.8	220.9	221.95	222.20	222.20
1 kW at phase A,B,C	220.1	219.9	220.3	222.10	222.10	222.10

RMS current The RMS current shows the same behaviour as described in chapter 3.3.1. However, in the unbalanced case the value is reached only in the phase where a 1 kW ohmic load is connected to while the other phases are not influenced significantly.

Active power The measured values of the active power are similar to those described in chapter 3.2.1. However, in the case of unbalanced loads, only single phases are considered.

Reactive power The reactive power shows the same behaviour as described in chapter 3.3.1. This results from the independence of the reactive power on an ohmic load.

Disconnecting behaviour of the current The disconnecting behaviour is similar to the behaviour described in chapter 3.3.1. However, it only takes place for one phase instead of all three phases. The respective transient currents caused by a disconnection of ohmic loads at single phases are illustrated in the appendix for phase A (figure 112 and figure 113), phase B (figure 114 and figure 115) and phase C (figure 116 and figure 117).

3.3.5 Unbalanced change in inductive load

The Sunny Island battery inverter is connected to the asynchronous generator. At the time t = 0 ms it is connected to a 1 kVAr inductive load at one phase.

Transient Currents Figure 44 shows the comparison of the measured and simulated transient currents in case of a connection of a 1 kVAr inductive load at phase A. It displays that phase B and phase C are not affected while phase A shows the same behaviour of the transient current as described in chapter 3.3.2. The decay of the offset is illustrated by figure 119 (cf. Appendix). This behaviour is similar in case of a connection of an inductive load at phase B as well as phase C because of the symmetric characteristics (cf. chapter 3.2.5).

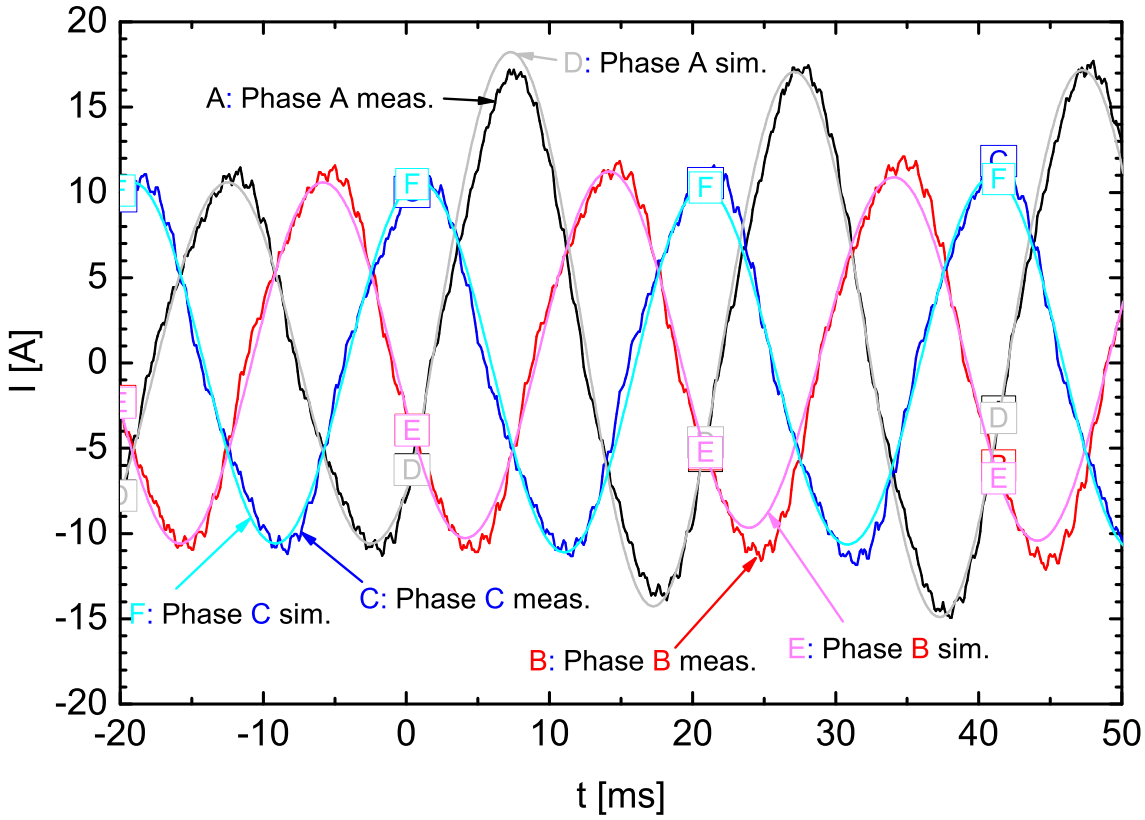

Figure 44: Transient currents I of the battery inverter which is connected with the asynchronous generator supplying a 1 kW ohmic load at each phase. At the time t = 0 ms, a 1 kVAr inductive load is connected to phase A. Comparison between the measured (meas.) values in darker colours (A,B,C) and the simulated (sim.) values in brighter colours (D,E,F).

Transient Voltages In case of an unbalanced connection as well as an unbalanced disconnection of an ohmic load, the transient voltages show no particular behaviour (cf. figure 96 in the appendix). The simulated values fit well to the measured ones.

Table 21 lists the steady state values before and after the load change. The values of this table are those of phase A. Phase B and phase C show no significant change caused by the load change. Only the measured values are a little asymmetric. Similar values occur in case of the connection of a 1 kVAr inductive load at phase B or phase C. In this case, the respective other values show no change.

Frequency The frequency before and after the connection of the balanced inductive load is equal in the measured data as well as in the simulated data. However, the battery management causes a 0.18 Hz lower level of the frequency of the measured values compared to the simulated ones.

Table 21: Comparison of the data of phase A between the measured and the simulated signals of the battery inverter which is connected with the asynchronous generator supplying a 3 kW ohmic load. At the time t = 0 ms, a 1 kVAr inductive load is connected to phase A.

Signals	Measured < 0 ms	> 0 ms	Simulated < 0 ms	> 0 ms
Frequency [Hz]	49.90	49.90	50.08	50.08
RMS voltage [V]	220.0	216.5	222.0	218.3
RMS current [A]	7.50	10.40	7.50	11.00
Active power [W]	-350	-375	-315	-320
Reactive power [VAr]	1610	2220	1630	2375

RMS voltage In table 21, the RMS voltage of phase A shows a decline by connecting the inductive load. This decline is caused by the droop control and it is the same as described in chapter 3.2.2. The supplied reactive power results in a theoretical voltage deviation of $\Delta U = -6\ \% \times 230 \times 2220/3600$ V = - 8.5 V (compared to - 13.5 V in table 21) for the measured values and a voltage deviation of $\Delta U = -6\ \% \times 230 \times 2375/3600$ V = - 9.1 V (compared to - 11.7 V in table 21) for the simulated values. The additional voltage dip is at least partly explainable with the discretisation effect described in the paragraph on the RMS voltage in chapter 3.2.1. As mentioned there, the effect is stronger for the measured system than for the simulated one. The described behaviour is similar in case of adding the inductive load to phase B or phase C.

RMS current The RMS current in the example of the connection event of an inductive load is similar in the measured and the simulated case for the steady state before the switching event. However, after the switching event, the measured RMS current of 10.4 A is lower than the simulated RMS current of 11.0 A. Similar values are measured and simulated in case of adding the inductive load to phase B or phase C.

Active power With the dependencies described in chapter 3.2.1, the active power of the measurement of the battery inverter in connection with the asynchronous generator and a 1 kW ohmic load at phase A should be -1268 W $+ 1000 \times (220/230)^2$ W $= -353$ W (compared to -350 W in table 21) and the simulation should result in -1260 W $+ 1000 \times (222.0/230)^2$ W $= -328$ W (compared to -315 W in table 21). After adding the inductivity with an active power of 50 W at rated conditions, the measurement should be -1268 W $+ 1050 \times (216.5/230)^2$ W $= -338$ W (compared to - 375 W in table 21) and the simulation should result in -1260 W $+ 1050 \times (218.3/230)^2$ W $= -314$ W (compared to -320 W in table 21). Altogether, the measurement as well as the simulation shows a significant deviation from the theoretical values. The influence of the frequency and the voltage to the active power output of the asynchronous generator is not considered in this calculation.

Reactive power The reactive power has three influences which are described in chapter 3.2.2. According to these influences the reactive power after adding the inductive load should be

$1610\ \text{VAr} + 1000 \times (216.5/230)^2 \times (50/49.9)\ \text{VAr} = 2497\ \text{VAr}$ (compared to 2220 VAr in table 21) and the simulation should result in $1630\ \text{VAr} + 1000 \times (218.3/230)^2 \times (50/50.08)\ \text{VAr} = 2529\ \text{VAr}$ (compared to 2472 VAr in table 21). The influence of the frequency and the voltage to the reactive power output of the asynchronous generator is not considered in this calculation. However, both, the measured and the simulated values, are significantly lower than the theoretical values. This additional deviation can be attributed to the asynchronous generator whose reactive power decreases by this load change. Another reason are the deficits of the asynchronous generator model.

Disconnecting behaviour of the current Figure 45 shows the comparison between the measured and the simulated transient current in case of a disconnection of the 1 kVAr inductive load at phase A in connection with the battery inverter, the asynchronous generator and an ohmic base load of 3 kW. The simulated current shows a similar behaviour to the measured

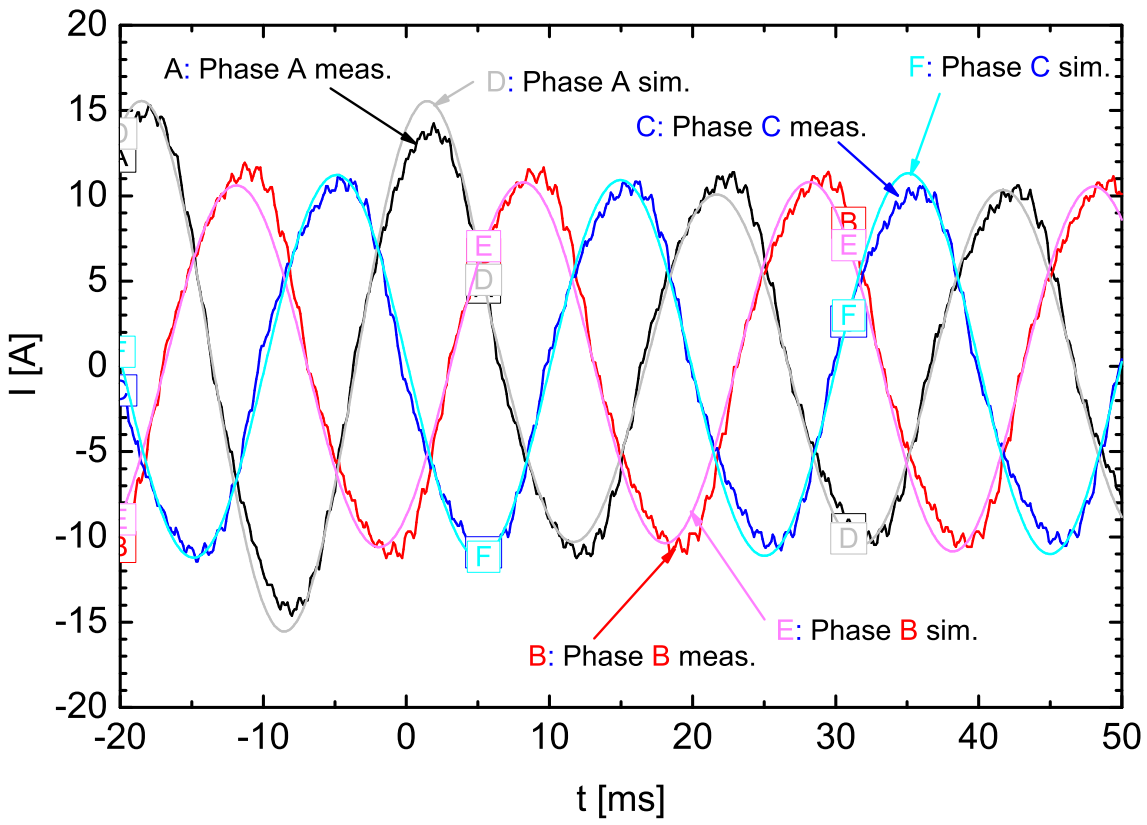

Figure 45: Transient currents I of the battery inverter which is connected with the asynchronous generator supplying a 1 kW ohmic load at each phase and a 1 kVAr inductive load at phase A. The inductive load at phase A is disconnected at the time t = 0 ms. Comparison between the measured (meas.) values in darker colours (A,B,C) and the simulated (sim.) values in brighter colours (D,E,F).

data. This behaviour is similar in case of the other phases.

3.3.6 Unbalanced change in capacitive load

The Sunny Island battery inverter forms the grid. It operates in connection with the asynchronous generator and the balanced 3 kW ohmic load. At the time t = 0 ms it is connected to a 1 kVAr capacitive load at one phase.

Transient Currents Figure 46 shows the comparison of the measured and simulated transient currents in case of a connection of a 1 kVAr capacitive load at phase A. It displays that phase B

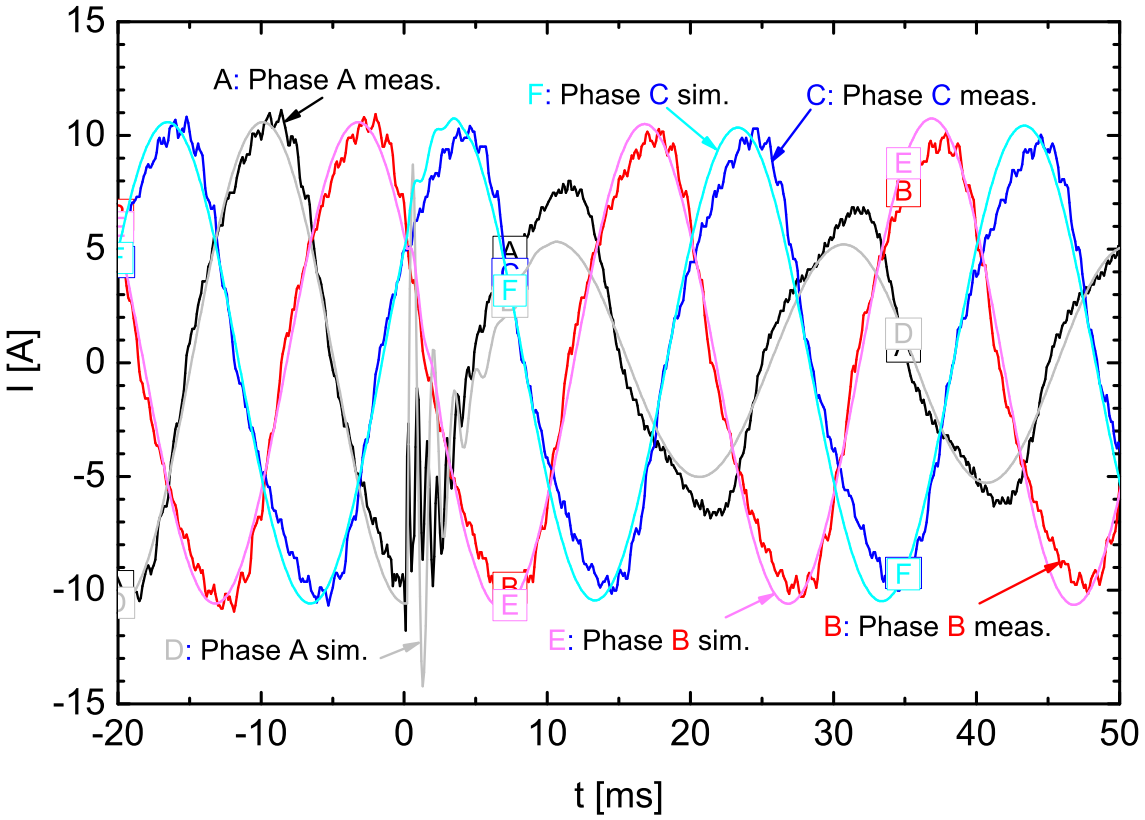

Figure 46: Transient currents I of the battery inverter which is connected with the asynchronous generator supplying a 1 kW ohmic load at each phase. At the time t = 0 ms, a 1 kVAr capacitive load is connected to phase A. Comparison between the measured (meas.) values in darker colours (A,B,C) and the simulated (sim.) values in brighter colours (D,E,F).

and phase C are not affected while phase A shows the same behaviour of the transient current as described in chapter 3.3.3. This behaviour also occurs in case of an capacitive load connection at phase B and phase C because of the symmetric characteristics.

Disconnecting behaviour of the current Figure 47 shows the comparison between the measured and the simulated transient currents in case of a disconnection of the 1 kAr capacitive load at phase A in connection with the battery inverter, the asynchronous generator and an ohmic base load of 3 kW. The simulated current shows a similar behaviour to the measured data. This behaviour is similar in case of the other phases.

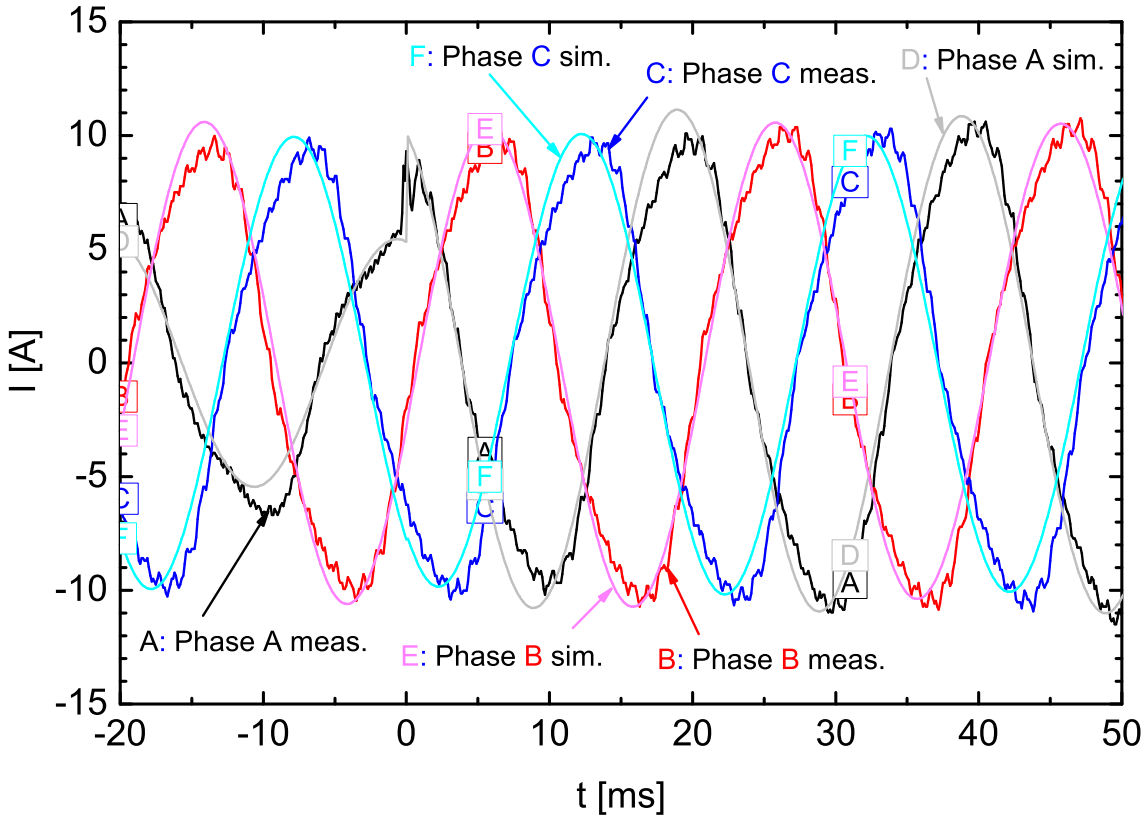

Figure 47: Transient currents I of the battery inverter which is connected with the asynchronous generator supplying a 1 kW ohmic load at each phase and a 1 kVAr capacitive load at phase A. The capacitive load at phase A is disconnected at the time t = 0 ms. Comparison between the measured (meas.) values in darker colours (A,B,C) and the simulated (sim.) values in brighter colours (D,E,F).

Transient Voltages Figure 123 in the appendix shows the comparison of the measured and simulated transient currents in case of a connection of a 1 kVAr capacitive load at phase A. It displays that phase B and phase C are not affected while phase A shows the same behaviour of the transient voltage as described in chapter 3.3.3. This behaviour also occurs in case of an capacitive load connection at phase B and phase C because of the symmetric characteristics. Additionally, figure 125 in the appendix shows the disconnection of the capacitive load at phase A. The figure illustrates a behaviour of the measured and the simulated transient voltages with less disturbances compared to the case of the load connection.

Table 22 lists the steady state values before and after the load change. The values of this table are those of phase A. Phase B and phase C show no change (only the measured values are a little asymmetric) caused by the load change. Similar values occur in case of the connection of a 1 kVAr capacitive load at phase B or phase C. In this case, the respective other values show no change.

Table 22: Comparison of the data of phase A between the measured and the simulated signals of the battery inverter which is connected with the asynchronous generator supplying a 3 kW ohmic load which is connected at the time t = 0 ms to a 1 kVAr capacitive load at phase A.

Signals	Measured < 0 ms	> 0 ms	Simulated < 0 ms	> 0 ms
Frequency [Hz]	49.91	49.89	50.08	50.08
RMS voltage [V]	220.1	223.8	222.1	226.0
RMS current [A]	7.45	4.50	7.50	3.85
Active power [W]	-350	-305	-310	-250
Reactive power [VAr]	1600	975	1630	830

Frequency The frequency before and after the connection of the capacitive load is similar in the measured data as well as in the simulated data because no active power is changed. However, the battery management causes an approximately 0.18 Hz lower level of the frequency of the measured values compared to the simulated ones.

RMS voltage The voltage (cf. table 22) shows an increase by connecting the capacitive load as described in chapter 3.3.3. In case of the measured values, the supplied reactive power at the time $t < 0$ ms is 1600 VAr resulting in a voltage deviation $\Delta U = -6\,\% \times 230 \times 1600/3600$ V = - 6.1 V compared to measured - 9.9 V. Connecting 1 kVAr capacitive load at phase A results in a supplied reactive power at the time $t > 0$ ms of 975 VAr causing a voltage deviation $\Delta U = -6\,\% \times 230 \times 975/3600$ V = - 3.7 V compared to measured - 6.2 V.

In case of the simulated values, the supplied reactive power at the time $t < 0$ ms is 1630 VAr resulting in a voltage deviation $\Delta U = -6\,\% \times 230 \times 1630/3600$ V = - 6.2 V compared to simulated - 7.9 V. Connecting 1 kAr capacitive load at phase A results in a supplied reactive power at the time $t > 0$ ms of 830 VAr causing a voltage deviation $\Delta U = -6\,\% \times 230 \times 830/3600$ V = - 3.2 V compared to simulated - 4.0 V.

The additional voltage increase is at least partly explainable with the discretisation effect described in the paragraph on the RMS voltage in chapter 3.2.1. As mentioned there, the effect is stronger for the measured system than for the simulated one.

RMS current The RMS current in the example of the connection event of a capacitive load at phase A in the measured case deviates from the simulated case. This deviation results from the asynchronous generator which is not simulated accurately as described in chapter 2.2.

Active power With the dependencies described in chapter 3.2.2, the active power of the measurement of the battery inverter in connection with the asynchronous generator and the balanced 3 kW ohmic load is similar as described in chapter 3.3.5. After adding the capacity without a resistance, the measurement should be -1268 W$+1000 \times (223.8/230)^2$ W $= -321$ W (compared to - 305 W in table 22) and the simulation should result in -1260 W$+1000 \times (226.0/230)^2$ W $=$

-294 W (compared to -250 W in table 22). Altogether, the measurement as well as the simulation shows a significant deviation from the theoretical values. Not considered in this calculation is the influence of the frequency and the voltage to the active power output of the asynchronous generator. Another reason for the deviation are the deficits of the asynchronous generator model.

Reactive power The reactive power has three influences which are described in chapter 3.2.2. According to these influences the reactive power after adding the capacitive load should be 1600 VAr $- 1000 \times (223.8/230)^2 \times (49.89/50.00)$ VAr $= 648$ VAr (compared to 975 VAr in table 22) and the simulation should result in 1630 VAr$-1000\times(226/230)^2\times(50.08/50)$ VAr $=$ 662 VAr (compared to 830 VAr in table 22). The influence of the frequency and the voltage to the reactive power output of the asynchronous generator is not considered in this calculation. However, the measured values are 327 VAr higher than the theoretical values and the simulated values are 168 VAr higher than the theoretical values. Consequently, this additional deviation can be attributed to the asynchronous generator whose reactive power increases by this load change. However, the deviation between the difference of 327 VAr in the measured values and the difference of 168 VAr in the simulated values results from the asynchronous generator which is not simulated accurately as described in chapter 2.2.

3.4 Enlarged grid configuration with two battery inverters and a load

This chapter describes the behaviour of two three-phase Sunny Island battery inverters which are operated parallel in droop mode. An 18 kW ohmic load is connected to the two battery inverters. As described in chapter 2.1.2, the slope of the droop defines the distribution of the power supply by the generating components. Three different parameter settings are chosen in this chapter. Table 23 lists the different frequency droop slopes of the two parallel Sunny Island battery inverters. The following paragraphs analyse these different droop ratios.

Table 23: Analysed frequency droop slopes.

Battery inverter	Sunny Island 1	Sunny Island 2
Droop ratio 1:1	- 1 Hz / 3600 W	- 1 Hz / 3600 W
Droop ratio 2:1	- 1 Hz / 3600 W	- 0.5 Hz / 3600 W
Droop ratio 3:1	- 1 Hz / 3600 W	- 0.33 Hz / 3600 W

3.4.1 Droop ratio 1:1

With a droop ratio of 1:1, the active power should be distributed symmetrically between the two battery inverters.

Transient currents and voltages Figure 48 shows the transients currents of the battery inverter Sunny Island 1 which operates in parallel with the battery inverter Sunny Island 2 at the time of the connection of the 18 kW ohmic load. It shows the same behaviour as the one de-

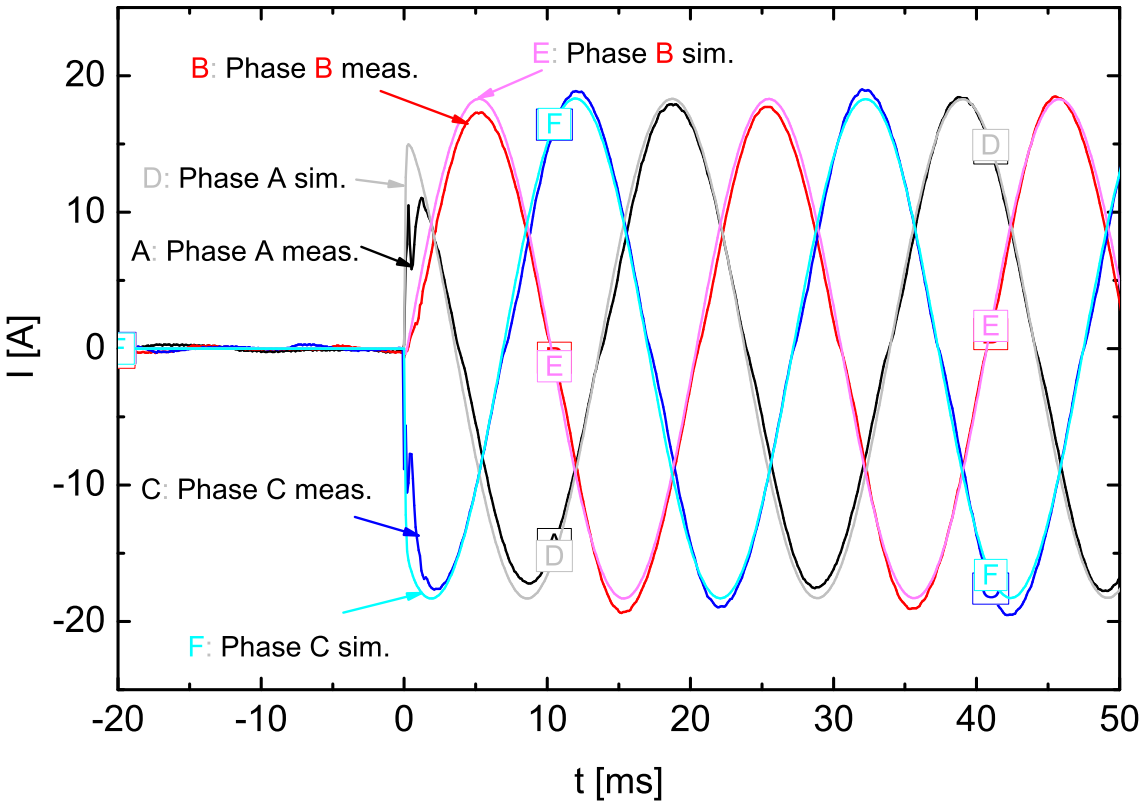

Figure 48: Transient currents I of the battery inverter Sunny Island 1 which operates in parallel with battery inverter Sunny Island 2 with a droop ratio of 1:1. They are connected at the time t = 0 ms to a 18 kW ohmic load. Comparison between the measured (meas.) values in darker colours (A,B,C) and the simulated (sim.) values in brighter colours (D,E,F).

scribed in chapter 3.2.1. Due to the symmetries in case of a droop ratio of 1:1, the transients currents of the battery inverter Sunny Island 2 show the same behaviour (cf. figure 127 in the appendix). This similarity also occurs in case of the transient voltages (cf. figure 127 and figure 129 in the appendix).

RMS currents and voltages Table 24 lists the RMS current and the RMS voltage of the battery inverters after the connection of the 18 kW ohmic load. The whole system is assumed to be purely ohmic because a deviation between the voltage and the current signal of 1.8° is so small that it is not necessary to consider in the following comparison. With this simplification, the active power listed in the last row of table 24 is calculated as the product of the RMS current and the RMS voltage. The active power shows a deviation between the simulated and measured values of 1.2 % in case of Sunny Island 1 and 0.2 % in case of Sunny Island 2. Because of the discretisation effect described in chapter 3.2.1, the voltage of the measurement is lower.

Table 24: Average steady state of one phase after the load change in case of a droop ratio of 1:1

Battery inverter	Sunny Island 1		Sunny Island 2	
	simulated	measured	simulated	measured
RMS current [A]	13.0	13.3	13.0	13.2
RMS voltage [V]	229.2	226.7	229.2	226.2
Active power [W]	2980	3015	2980	2986

Consequently, the current has to increase in order to be able to supply the same load. Therefore, the measured current is slightly higher and the measured voltage is slightly lower than the simulated ones.

3.4.2 Droop ratio 2:1

With a droop ratio of 2:1, the active power supply should be distributed between the two battery inverters, so that the battery inverter Sunny Island 1 supplies one third of the active power while the battery inverter Sunny Island 2 supplies two thirds.

Transient currents and voltages Figure 130 and figure 133 in the appendix show the transients currents of the two parallel battery inverters which have the same behaviour as described in chapter 3.2.1. However, the active power distribution is not yet achieved in the first milliseconds after the load change. This distribution tunes as displayed in figure 131, which shows the decline of the current values of Sunny Island 1, and figure 134, which shows the increase of the current values of Sunny Island 2 (cf. appendix). A comparison of the transient currents of phase A between the two battery inverters Sunny Island 1 (SI1) and Sunny Island 2 (SI2) shows figure 49. The comparison shows the decline of the current values of Sunny Island 1 and the increase of the current values of Sunny Island 2. The deviation between the measured and simulated current values is explained in the next paragraph which describes the RMS voltages and currents as well as the steady state after this tuning. The transient voltages (cf. figure 132 and figure 135 in the appendix) show he same behaviour as described in chapter 3.2.1.

RMS currents and voltages Table 25 lists the RMS current, the RMS voltage and the active power of the battery inverters after the connection of the 18 kW ohmic load. The active power shows a deviation between the simulated and measured values of 0.3 % in case of Sunny Island 1 and 2.6 % in case of Sunny Island 2. Because of the discretisation effect described in chapter 3.2.1, the voltage of the measurement is lower. Consequently, the current has to increase in order to be able to supply the same load. Therefore, the measured current is slightly higher and the measured voltage is slightly lower than the simulated ones. The active power supply of the two battery inverters shows a ratio of $3944/1972 = 2/1$ in case of the simulated values or a ratio of $4047/1967 = 2.06/1$ in case of the measured values. These ratios represents the power distribution defined by the droop ratio of 2:1.

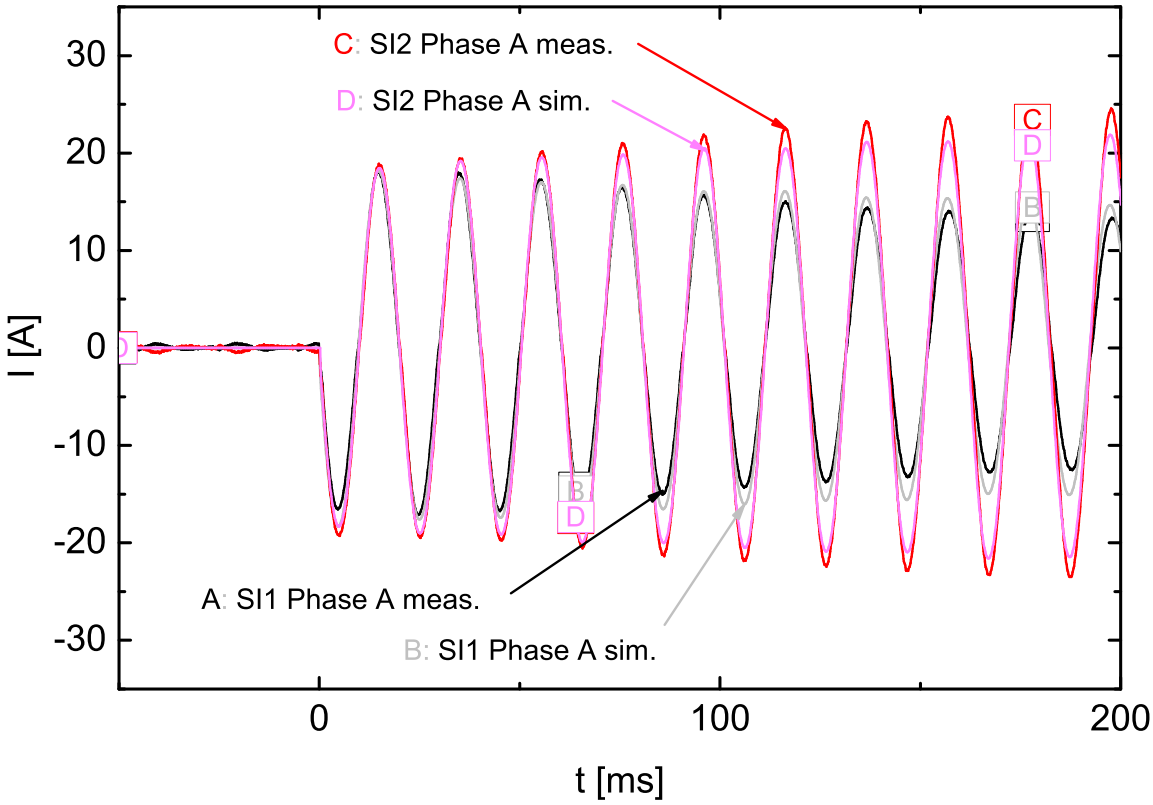

Figure 49: Comparison of the transient currents I of phase A between the two battery inverters Sunny Island 1 (SI1) and Sunny Island 2 (SI2) which operate with a droop ratio of 2:1. They are connected at the time t = 0 ms to a 18 kW ohmic load. Comparison between the measured (meas.) values in darker colours (A,B,C) and the simulated (sim.) values in brighter colours (D,E,F).

3.4.3 Droop ratio 3:1

With a droop ratio of 3:1, the active power supply should be distributed between the two battery inverters, so that the battery inverter Sunny Island 1 supplies one fourth of the active power while the battery inverter Sunny Island 2 supplies three fourths.

Transient currents and voltages Figure 136 and figure 139 in the appendix show the transients currents of the two parallel battery inverters which have the same behaviour as described in chapter 3.2.1. However, the active power distribution is not yet achieved in the first milliseconds after the load change. This distribution tunes as displayed in the appendix in figure 137, which shows the decline of the current values of Sunny Island 1, and in figure 140, which shows the increase of the current values of Sunny Island 2. The slope of the described increase and decline is steeper for a droop ratio of 3:1 because the active power is distributed more unbalanced. A comparison of the transient currents of phase A between the two battery inverters Sunny Island 1 (SI1) and Sunny Island 2 (SI2) shows figure 50. The comparison shows the decline of the current values of Sunny Island 1 and the increase of the current values of Sunny Island 2. The deviation between the measured and simulated current values is explained in the

Table 25: Average steady state of one phase after the load change in case of a droop ratio of 2:1

Battery inverter	Sunny Island 1		Sunny Island 2	
	simulated	measured	simulated	measured
RMS current [A]	8.6	8.7	17.2	17.9
RMS voltage [V]	229.3	226.1	229.3	226.1
Active power [W]	1972	1967	3944	4047

next paragraph which describes the RMS voltages and currents as well as the steady state after this tuning. Additionally, the simulated transient currents tune not as fast as the measured transient currents. The transient voltages (cf. figure 138 and figure 141 in the appendix) show he same behaviour as described in chapter 3.2.1.

RMS currents and voltages Table 26 lists the RMS current, the RMS voltage and the active power of the battery inverters after the connection of the 18 kW ohmic load. The active power

Table 26: Average steady state of one phase after the load change in case of a droop ratio of 3:1

Battery inverter	Sunny Island 1		Sunny Island 2	
	simulated	measured	simulated	measured
RMS current [A]	6.5	6.6	19.3	20.2
RMS voltage [V]	229.3	225.6	229.3	226.0
Active power [W]	1490	1489	4425	4565

shows a deviation between the simulated and measured values of 1.6 % in case of Sunny Island 1 and 3.2 % in case of Sunny Island 2. Because of the discretisation effect described in chapter 3.2.1, the voltage of the measurement is lower. Consequently, the current has to increase in order to be able to supply the same load. Therefore, the measured current is slightly higher and the measured voltage is slightly lower than the simulated ones. The active power supply of the two battery inverters shows a ratio of $4425/1513 = 2.97/1$ in case of the simulated values or a ratio of $4565/1489 = 3.07/1$ in case of the measured values. These ratios represents the power distribution defined by the droop ratio of 3:1.

3.4.4 Stability of parallel battery inverters

The last chapter on parallel operation analyses the parallel operation of two battery inverters with a difference of their target frequency and a difference of their target voltage. These differences result from tolerances of the constituents of the battery inverters. The two battery inverters are connected via a low-voltage cable which has an assumed resistance of 21 mΩ and an assumed reactance of 2.6 mΩ. Additional to the two battery inverters and the low-voltage cable, no other components are considered in this parallel operation.

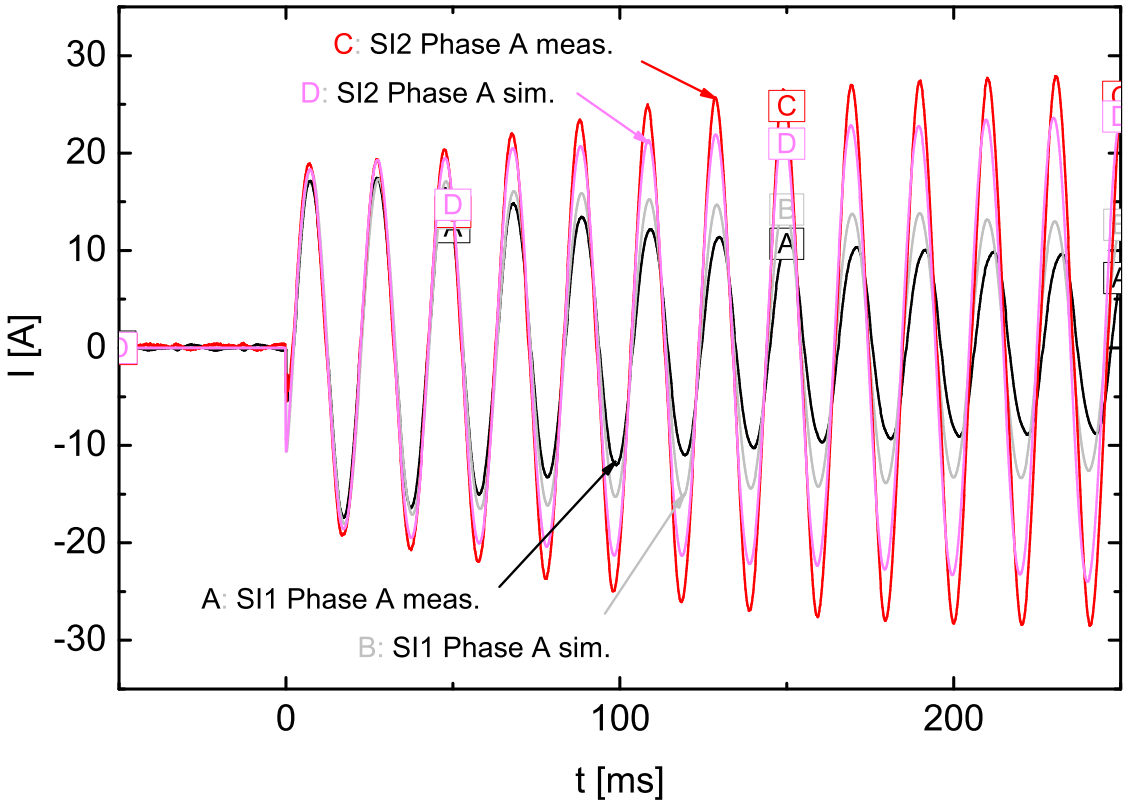

Figure 50: Comparison of the transient currents I of phase A between the two battery inverters Sunny Island 1 (SI1) and Sunny Island 2 (SI2) which operate with a droop ratio of 3:1. They are connected at the time t = 0 ms to a 18 kW ohmic load. Comparison between the measured (meas.) values in darker colours (A,B,C) and the simulated (sim.) values in brighter colours (D,E,F).

Frequency difference The target frequency of Sunny Island 1 is set to 50 Hz while the target frequency of Sunny Island 2 is set to 50.3 Hz. The simulation shows that the operation is stable and that a constant active power of 540 W per phase flows from Sunny Island 2 to Sunny Island 1. This active power flow results from the phase difference which is caused by the frequency difference according to equation 1. The steady state grid frequency is the mean frequency 50.15 Hz resulting from the two target frequencies.

Voltage difference The target voltage of Sunny Island 1 is set to 230 V while the target voltage of Sunny Island 2 is set to 231 V. The simulation shows that the operation is stable and that a constant reactive power of 100 VAr per phase flows from Sunny Island 2 to Sunny Island 1. This reactive power flow results from the voltage difference which according to equation 2.

Voltage and frequency difference The target voltage of Sunny Island 1 is set to 230 V while the target voltage of Sunny Island 2 is set to 231 V. Additionally, the target frequency of Sunny Island 1 is set to 50 Hz while the target frequency of Sunny Island 2 is set to 50.3 Hz. The simulation shows that the operation is stable and that a constant reactive power of 100 VAr per

phase flows from Sunny Island 2 to Sunny Island 1 as well as a constant active power of 540 W per phase from Sunny Island 2 to Sunny Island 1. This behaviour results from the superposition law which is applicable for these independent dependencies.

These three simulations show that the battery inverters work in parallel without loosing their stability even in case that the target values of frequency and voltage have small differences.

As summarised in the synopsis of this chapter, the comparison of the simulation and the measurement shows a good correlation. Consequently, the comparison verifies the models. After this verification the models are used in larger grid configurations. A case study in the following chapter demonstrates the application of the verified battery inverter model.

4 Case Study: Simulation of an enlarged grid configuration

The Sunny Island battery inverter is a central component of island grids because it can form such grids and controls the power flow. Those island grids, so called Microgrids, comprise power generation components, e.g. photovoltaic generators, diesel generators and small-scale wind energy converters. One example is the remote power supply on Kythnos as illustrated in figure 51. The first approach for the case study is the simulation of the island grids on Kythnos.

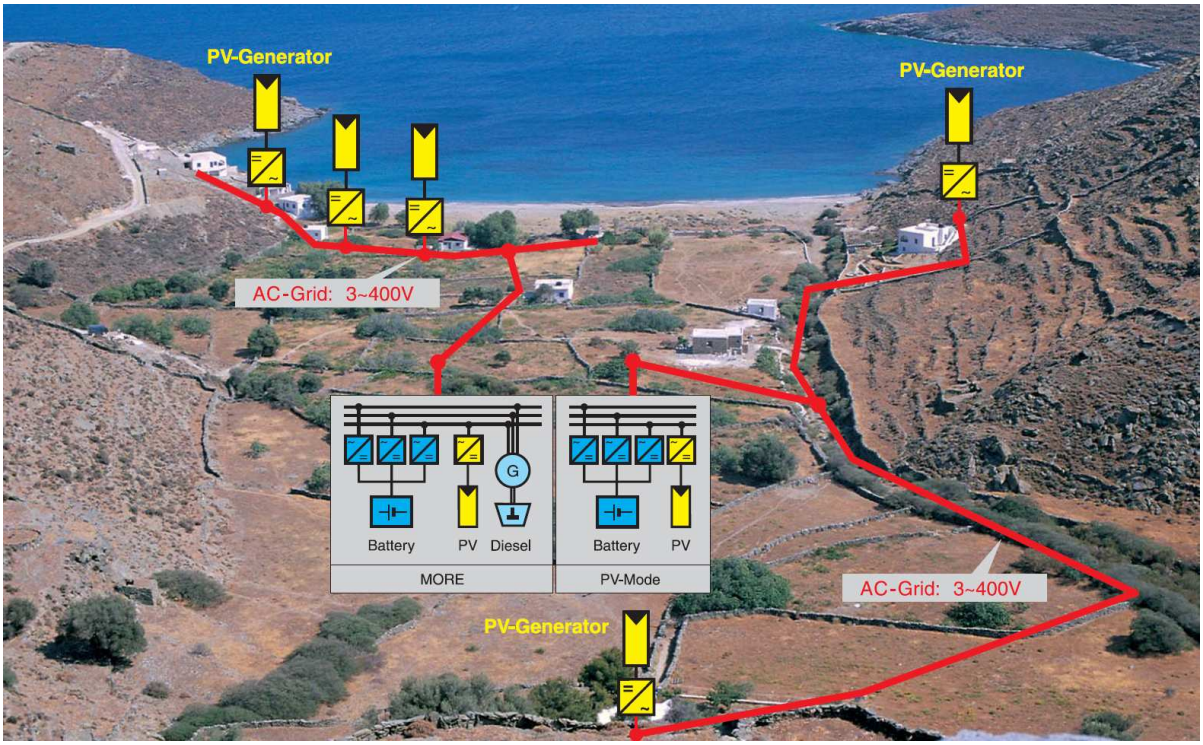

Figure 51: Modular island grids on Kythnos [SMA].

However, several approaches to simulate photovoltaic generators and diesel generators with simple models fail. Because of the scope of this work the models are not developed, however, it is recommended to develop them in future works in order to be able to simulate island grids. Nevertheless, the case study analyses a fictitious island grid without active power generation components. It is assumed that the time of simulation is at night when photovoltaic modules do not generate power and that the synchronous generator is deactivated for maintenance.

4.1 Description of the grid configuration

This chapter describes the transient behaviour after a connection of an asynchronous machine in a grid configuration which can not be verified in DeMoTec with its actual available components. Figure 52 shows the analysed grid configuration. The grid comprises four busbars. Three of these four busbars (‘SI 1’, ‘SI 2’ and ‘SI 3’) are controlled by three phase Sunny Island battery inverters, in contrast to busbar ‘Remote 4’. The loads and asynchronous machines in figure 52

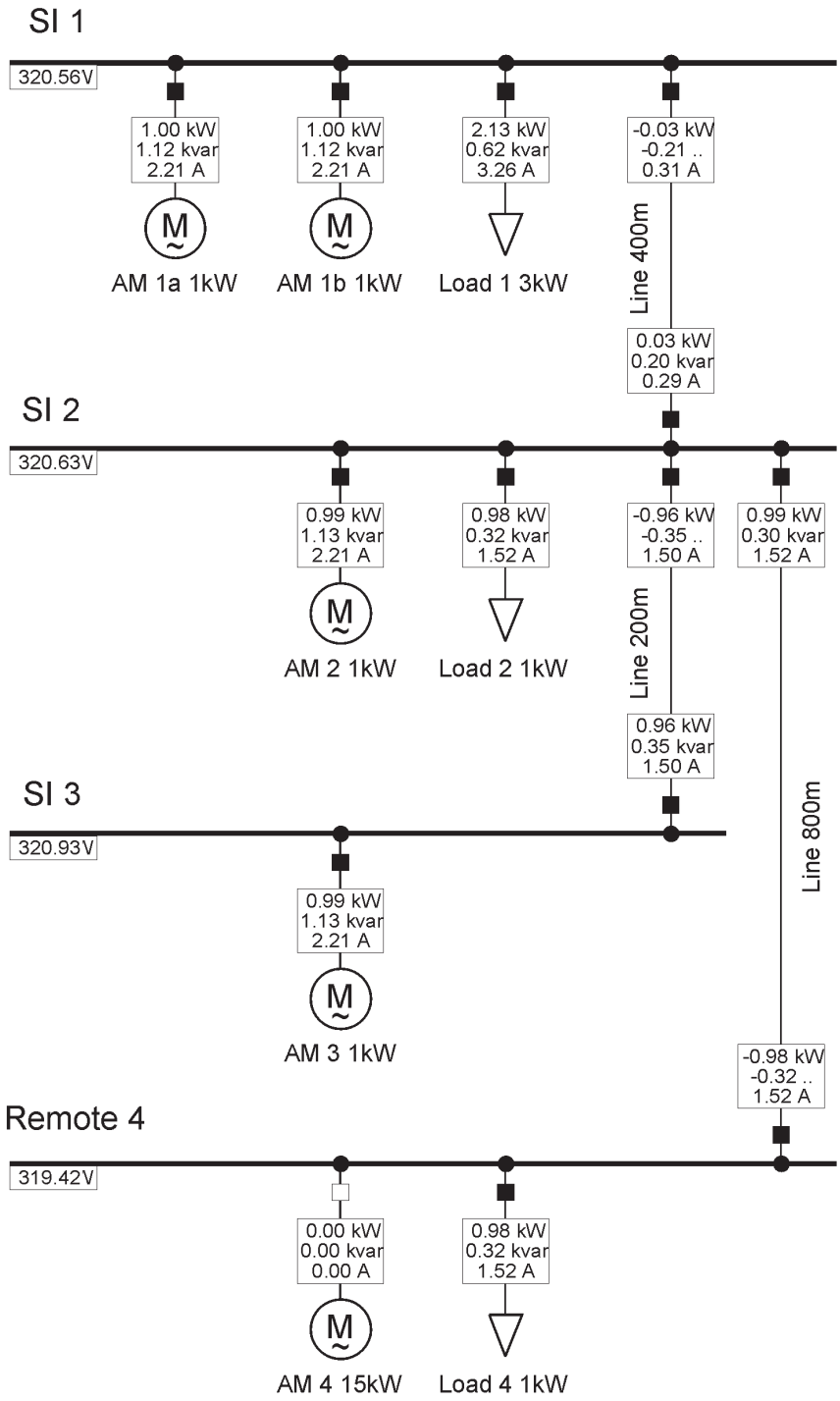

Figure 52: Load flow in case study grid before the connection of the asynchronous machine at busbar ‘Remote 4’. Each busbar ‘SI 1’, ‘SI 2’ and ‘SI 3’ presents one three phase Sunny Island battery inverter (the battery inverter itself is not displayed). Additionally, the busbar ‘Remote 4’ presents a grid node without a battery inverter. The box on the left side shows the amplitude of the voltage at the respective busbar. These four busbars are connected via low-voltage cable. At each busbar, asynchronous machines and loads present consumers. The boxes at the respective grid components show the active power, the reactive power and the magnitude of the positive sequence current.

represent standardised consumers. All these components are connected via low-voltage cables of different length between the busbars.

Sunny Island battery inverters This grid configuration uses the same model for the battery inverter as described in previous chapters. Table 27 lists the droop slopes of the three Sunny Island battery inverters. The battery inverter 'Sunny Island 1' has only half the slope of the other

Table 27: Droop slopes of the three Sunny Island battery inverters.

Battery inverter	f/P-Droop	U/Q-Droop
Sunny Island 1:	- 0.5 Hz / 3600 W	- 3 % U_{rated} / 3600 VAr
Sunny Island 2:	- 1 Hz / 3600 W	- 6 % U_{rated} / 3600 VAr
Sunny Island 3:	- 1 Hz / 3600 W	- 6 % U_{rated} / 3600 VAr

two battery inverters because it is assumed to have a bigger battery which allows to control a higher power flow compared to the other two.

Cables All busbars are connected via low-voltage cables with a cross section of 25 mm^2. The rated voltage of these cables is 400 V and the rated current is 100 A. They are used in an AC power grid with a rated frequency of 50 Hz. The assumed model parameters of this type of line lists table 28. In addition, figure 52 shows the lengths of the cables.

Table 28: Model parameters of the low-voltage cable

Parameter	Value
Cable/Overhead line:	Non-armoured cable
Phases:	3
Number of Neutrals:	1
Resistance per Length R' (1,2-Sequence):	0.708 Ω/km
Reactance per Length X' (1,2-Sequence):	0.087 Ω/km
Resistance per Length R0' (0-Sequence):	2.832 Ω/km
Reactance per Length X0' (0-Sequence):	0.348 Ω/km
Resistance per Length Rn' (Neutral):	0.708 Ω/km
Reactance per Length Xn' (Neutral):	0.087 Ω/km
Capacitance per Length C' (1,2-Sequence):	0.51 μF/km
Capacitance per Length C0' (0-Sequence):	0.2125 μF/km
Capacitance per Length Cn' (Neutral):	0.51 μF/km

Loads Generally, the loads in this grid configuration have a voltage dependence on the active power of 1.6, while the voltage dependence on the reactive power is 1.8. Moreover, the reactive

power is mixed capacitive and inductive reactive power. The ratio of the mixture is 200 % inductive reactive power over capacitive reactive power. This considered reactive power results from an inductive power factor of 0.95, which defines each load.

At busbar 'SI 1', an unbalanced load is connected to the battery inverter 'Sunny Island 1'. Phase A of this load consumes an active power of 500 W, phase B an active power of 1000 W, and phase C an active power of 1500 W. In contrast, the loads at busbar 'SI 2' and 'Remote 4' are balanced loads with an active power consumption of 1 kW.

Asynchronous machines Two different types of asynchronous machines are connected to the grid. The four asynchronous machines at the busbars 'SI 1', 'SI 2' and 'SI 3' are of the same 1.5 kW type which is described in table 29. They consume 1 kW active power and are connected to the grid over the whole simulation time. At busbar 'Remote 4', the 15 kW asynchronous machine is of a different type which is described in table 30.

Table 29: Technical specifications of the 1.5 kW asynchronous machine.

Number of pole pairs p_z	2
Connection	star
Rated mechanical active power $P_{m,r}$	1.5 kW
Rated electrical apparent power S_r	2.44 kW
Rated power factor $cos\varphi$	0.82
Rated electrical frequency f_r	50 Hz
Rated mechanical speed n_r	1405 r.p.m.
Rated voltage U_r	400 V
Locked rotor current	4.9 p.u.
Stalling torque M_s	2.6 p.u.
Locked rotor torque	2.2 p.u.
Acceleration time constant	0.0505 s

4.2 Description of the transient simulation of the connection event

The 15 kW asynchronous machine is connected at the time $t = 0$ s consuming 15 kW active power.

Load flow analysis Figure 53 shows the analysed grid configuration after the connection of the asynchronous machine 'AM 4 15kW' to the busbar 'Remote 4'. This figure illustrates the difference to the load flow situation before the connection event which is displayed in figure 52. Before the connection event, there is no significant load flow between the busbars with the exception of approximately 1 kW active power and 0.3 kVAr reactive power which flow from busbar 'SI 3' over busbar 'SI 2' to busbar 'Remote 4'. This power flow supplies the load

Table 30: Technical specifications of the 15 kW asynchronous machine.

Number of pole pairs p_z	2
Connection	star
Rated mechanical active power $P_{m,r}$	15 kW
Rated electrical apparent power S_r	19.83 kW
Rated power factor $cos\varphi$	0.85
Rated electrical frequency f_r	50 Hz
Rated mechanical speed n_r	1455 r.p.m.
Rated voltage U_r	400 V
Locked rotor current	7.7 p.u.
Stalling torque M_s	3.2 p.u.
Locked rotor torque	2.8 p.u.
Acceleration time constant	0.1083 s

'Load 4 1kW'. The amplitudes of the voltage at the respective busbars shows similar values around 320 V because the fall of voltage at the cables is low due to small power flows.

The connection of the asynchronous machine 'AM 4 15kW' changes this situation significantly. After the connection, the additional power consumption of the connected asynchronous machine, besides the power consumption of the load at busbar 'Remote 4' and the losses from the cables, increases the power flows to busbar 'Remote 4'. The three battery inverters share the power supply according to the setting of their droop slopes. Sunny Island 1 supplies 7.9 kW to the other busbars, while Sunny Island 2 supplies 5.6 kW. Consequently, Sunny Island 2 supplies 18.3 kW - 7.8 kW - 5.6 kW = 4.9 kW to busbar 'Remote 4'. These big power flows result in bigger voltage drops at the cables. Due to the increased reactive power supply, the voltage at the busbars is more than 10 V smaller than before the connection event. Especially, the amplitude of the voltage of busbar 'Remote 4' drops from 319 V to 285 V or by approximately 11 %.

Frequency The frequency of the grid has the same steady state value at each busbar. Before the connection event, the frequency is 49.83 Hz. After the connection event, the frequency decreases to 49.43 Hz because of the additional active power supply for the asynchronous machine.

Transient currents Figure 54 shows the transient currents of the battery inverter Sunny Island 1. The figure illustrates the supply of the unbalanced 'Load 1 3kW' which results in unbalanced current amplitudes. Phase A has the lowest amplitude and phase C has the highest amplitude according to the unbalanced load which has the lowest power consumption at phase A and the highest power consumption at phase C. Due to the parallel operation of the three battery inverters, the other two also supply a part of this unbalanced power. This can be derived from figure 143 and figure 144 in the appendix. However, the distance over cables leads to a damping of their contribution.

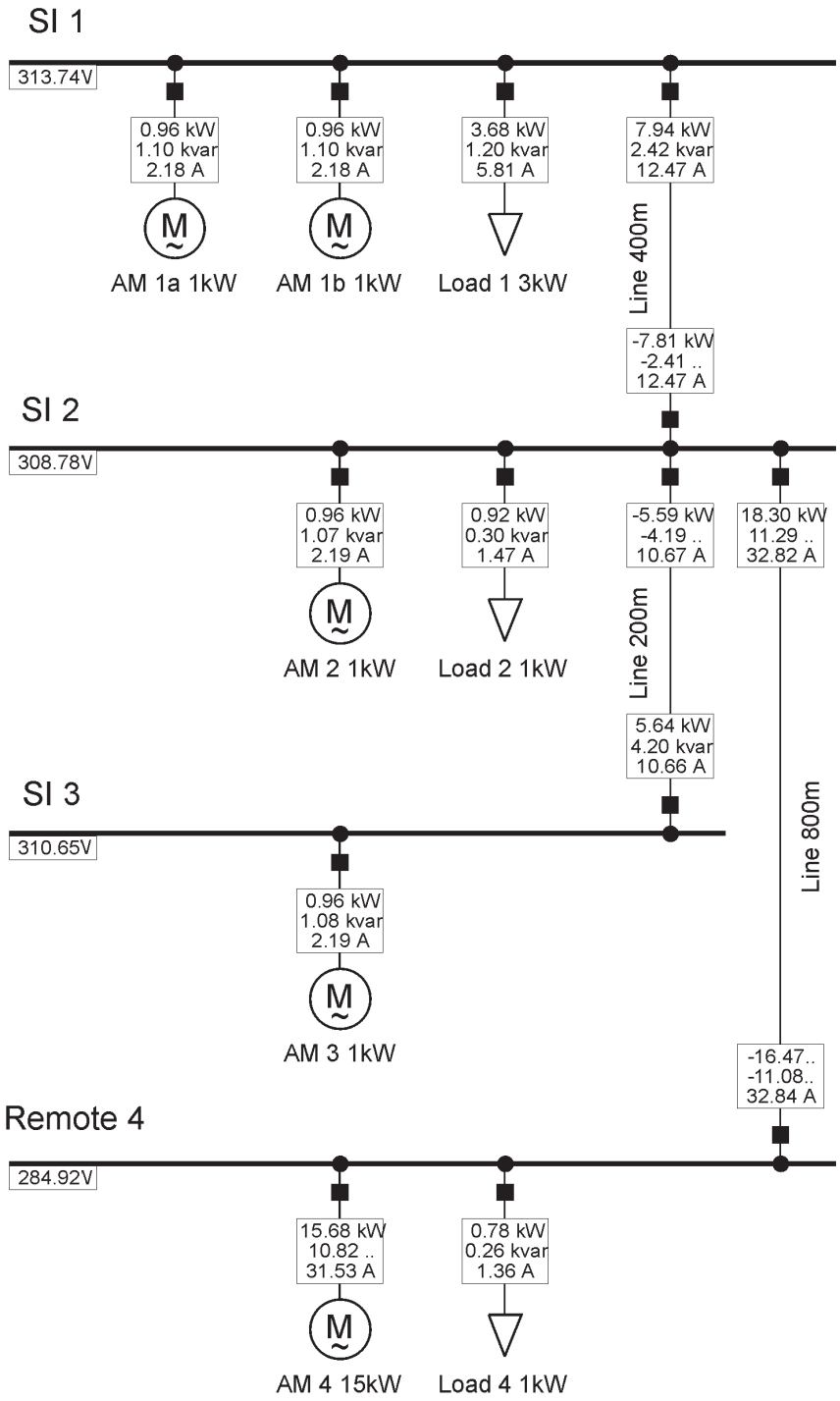

Figure 53: Load flow in case study grid after the connection of the asynchronous machine at busbar 'Remote 4'. Each busbar 'SI 1', 'SI 2' and 'SI 3' presents one three phase Sunny Island battery inverter (the battery inverter itself is not displayed). Additionally, the busbar 'Remote 4' presents a grid node without a battery inverter. The box on the left side shows the amplitude of the voltage at the respective busbar. These four busbars are connected via low-voltage cable. At each busbar, asynchronous machines and loads present consumers. The boxes at the respective grid components show the active power, the reactive power and the magnitude of the positive sequence current.

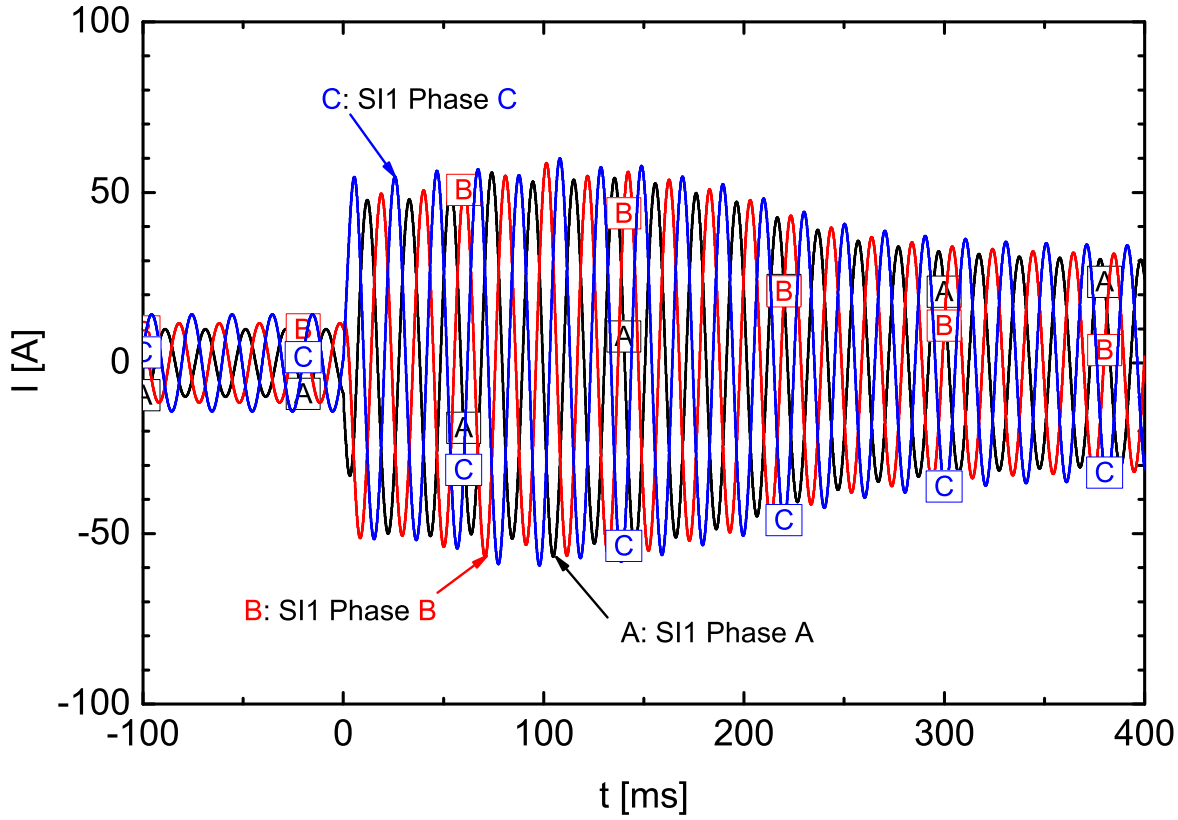

Figure 54: Transient currents I of the battery inverter Sunny Island 1 (SI1). The connection of the 15 kW asynchronous machine is at the time t = 0 ms.

Moreover, these figures of the transient currents show the behaviour of the starting of the asynchronous machine with higher currents at the beginning followed by a decay until the current reaches its steady state. A comparison of figure 142, figure 143 and figure 144 shows that the starting currents of the battery inverters are damped by the cables. This causes battery inverter 'Sunny Island 2' to have the highest starting currents which are four times higher than the steady state values. In comparison, 'Sunny Island 3' has the second highest starting currents which are three times higher than the steady state values because 'Sunny Island 3' has an additional cable distance of 200 m. Consequently, 'Sunny Island 1' with an additional cable distance of 400 m has the lowest starting currents which are only two times higher than the steady state values.

A comparison between the transient currents of phase A of the three battery inverters shows figure 55. The respective comparison of the other two phases is displayed in figure 146 and figure 147 in the appendix. Two different effects are illustrated by these figures. On the one hand, the figures show that the amplitudes of Sunny Island 1 have the double value of the amplitudes of the other two battery inverters in steady state situation. This results from the droop slope settings which defines a power distribution so that Sunny Island 1 supplies 200 % of the power of the other two battery inverters. On the other hand, the figures show that Sunny Island 2 supplies the biggest part to the power supply in the first 50 ms, while Sunny Island 1

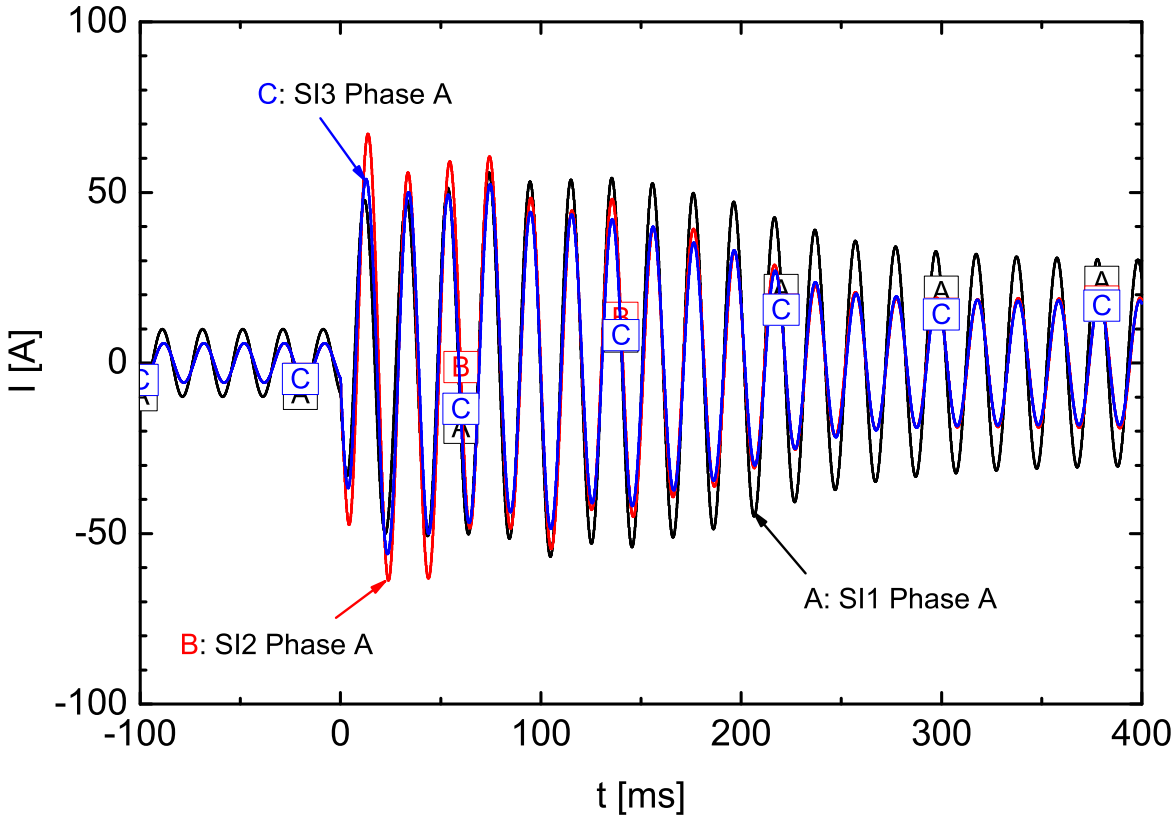

Figure 55: Comparison of the transient currents I of phase A of the three battery inverters SI1, SI2 and SI3. The connection of the 15 kW asynchronous machine is at the time t = 0 ms.

supplies the smallest part. This delayed power supply results from the damping of the cables so that battery inverters in greater distance react more delayed. However, the effect only occurs in the first 50 ms after the connection event. Afterwards, the power distribution tunes to values defined by the droop slopes of the battery inverters.

Transient voltages Figure 56 shows the transient voltages of the battery inverter Sunny Island 1. Additionally, figure 149 and figure 150 in the appendix display the transient voltages of the other two battery inverters. The figures of the transient voltages show in the first milliseconds after the connection event small disturbances of the ideal sinusoidal wave form. This behaviour is similar in case of all three battery inverters.

RMS voltages Figure 57 shows the RMS voltages of the battery inverter Sunny Island 1. The figures displays a voltage drop after the connection of the asynchronous machine. This voltage drop decays over the following second until the voltage reaches its new steady state. In contrast to figure 152 and figure 153 in the appendix, which display the same behaviour for the other two battery inverters, figure 57 illustrates the unbalanced supply of the unbalanced load because the voltage of the three phases has different values according to the reactive power supply of ‘Load 1 3kW’. Moreover, a comparison of these three figures shows that the minimum of the

voltage drop is different, the farther the respective battery inverter is away from the load change, the smaller the voltage drop due to the described damping effects.

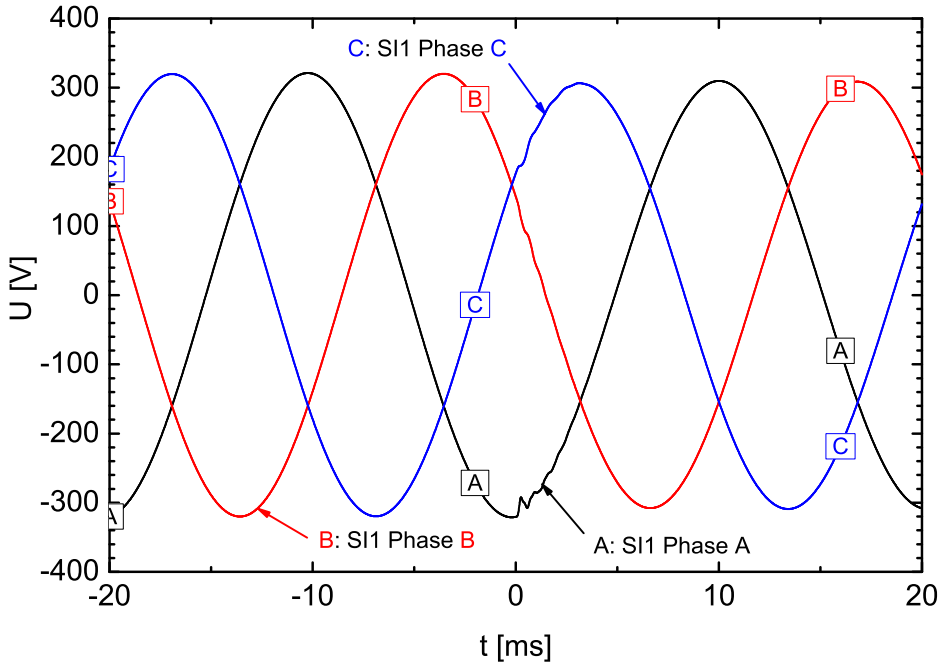

Figure 56: Transient voltages U of the battery inverter Sunny Island 1 (SI1). The connection of the 15 kW asynchronous machine is at the time t = 0 ms.

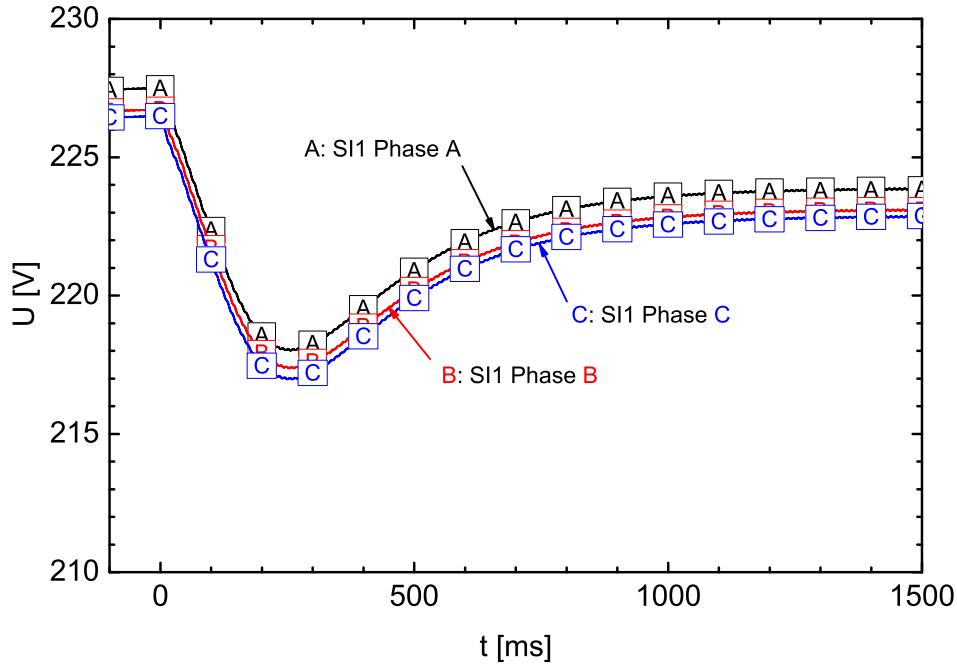

Figure 57: RMS voltages U of the battery inverter Sunny Island 1 (SI1). The connection of the 15 kW asynchronous machine is at the time t = 0 ms.

Additionally, figure 154, figure 155 and figure 156 in the appendix show a comparison of the RMS voltages of the three battery inverters for one phase. They illustrate the same voltage drop and the different voltages of the three battery inverters according to the cables between them.

4.3 Conclusions of the case study

This case study shows that the model of the battery inverter can be used in *PowerFactory* simulations of larger grid configurations. The analysed grid configuration uses more than two battery inverters and comprises additional components of generic *PowerFactory* models. Analyses of simulation results give a better comprehension of the behaviour of the grid. The analysis of the case study grid, for instance, shows that the application of a 15 kW asynchronous machine in the remote grid area results in a voltage drop of 11 % at the connection point and losses of 1.8 kW due to the low-voltage cable. Options to reduce these negative effects are the substitution of the 800 m cable by one with a larger cross section or an operation of the asynchronous machine closer to the Sunny Island battery inverters.

Moreover, the connection of the asynchronous machine has no critical transient behaviour. The transient voltage stabilises rapidly within 3 ms and the transient current within 300 ms.

5 Conclusions

The aim of this thesis is to implement and verify models of decentralised power generation components in the simulation environment of the power system analysis tool *PowerFactory* from DIgSILENT. These models are used for transient simulations in low-voltage grids. The analysed components are a bi-directional battery inverter, an asynchronous generator and loads. These components operate with variable frequency and variable voltage which are controlled by the battery inverter.

Chapter 2 develops a model of a three-phase Sunny Island battery inverter. This model enhances available single-phase models in MATLAB/Simulink and ATP-EMTP and adapts them to the simulation environment of *PowerFactory*. Moreover, the chapter shows the adjustment of the parameters of the available asynchronous generator model in *PowerFactory* to the asynchronous generator in DeMoTec. For this adjustment, the electrical parameters are measured and an optimisation process is performed. Finally, the available load model in *PowerFactory* is adjusted to the loads used in DeMoTec.

Simulations of load changes in grid configurations with these three models are described in chapter 3. The comparison between simulated data in *PowerFactory* and measured data in DeMoTec shows a good fit of the short-term transient simulations. In the scope of these simulations, the *PowerFactory* models are verified, especially the model of the battery inverter which is the main contribution of this work. Changes in active and reactive power in the analysed power grid result in changes of frequency and voltage according to the droop slopes of the connected battery inverters. The analysed power flows of the simulations fit well with the measured data because the active and reactive power as well as the RMS currents have a good correlation. Additionally, unbalanced load changes are simulated well with the implemented battery inverter model. This achievement enables to connect asymmetrical ohmic, inductive, capacitive loads or a mixture of them to the battery inverter. These connection events are simulated well by the *PowerFactory* models. The transient signals after load changes matches qualitatively well. Quantitatively, it is not possible to get an accurate correlation because there are many influences which are not considered in the model. Altogether, the characteristic behaviour of the droop mode of three-phase Sunny Island battery inverters is reproduced well. Even the parallel operation with different droop slopes shows the expected behaviour of power sharing between the battery inverters. However, two main deficits of the simulations have to be considered:

- On the one hand, the battery management, which is not modelled, causes the frequency to deviate between the measurement and the simulation.
- On the other hand, the discretisation effect causes the RMS voltage to deviate between the measurement and the simulation. This effect results from the digital controller of the Sunny Island which influences the amplitude of the voltage. Due to time limitations in this thesis, the discretisation is modelled with simplifications so that the discretisation effect in the simulation is smaller than in the measurement.

Finally, chapter 4 describes the simulation of a connection of an asynchronous machine in an enlarged grid configuration with three battery inverters in parallel operation, asynchronous

machines, loads and cables. This simulation shows an example for an application of the battery inverter model. The load flow analysis shows the loading of the components, especially cables, and the transient signals show the dynamic behaviour of the grid by this exemplary connection of an asynchronous generator. With this case study, the application of a parallel operation of three battery inverters as well as analysis features of *PowerFactory* are demonstrated.

This work shows that *PowerFactory* from DIgSILENT is an appropriate power system analysis tool for transient simulations of decentralised power generation components in low-voltage grids. For transient simulations in low-voltage grids with decentralised components, *PowerFactory* delivers an extensive simulation environment with a variety of functionalities. Three main achievements of the thesis can be derived from its results.

1. A battery inverter model is developed and successfully verified for electromagnetic transients of load changes.

2. Challenges in the determination of accurate parameters for induction generator models are shown by the application of several approaches.

3. The applicability of the developed battery inverter model for studies in island grids is demonstrated with a case study.

For future improvements of the simulation possibilities in *PowerFactory*, two tasks for future works are recommended.

- The available battery inverter model is recommended to be extended by the inclusion of short-circuit behaviour, which changes the battery inverter model from a controlled voltage source to a current source supplying a fixed current in case of too high currents. This additional functionality enables short-circuit analyses which are out of scope of the present contribution.

- However, until now, one disadvantage of *PowerFactory* is the lack of generic models of decentralised power generation components. Consequently, they have to be developed individually. In case that models for photovoltaic generators, diesel generators and small-scale wind energy converters are available, a large variety of island grid configurations can be analysed in detail. Until now, only a battery inverter, which forms the island grid, is developed. Therefore, it is recommended to add models of photovoltaic generators, diesel generators and small-scale wind energy converters to *PowerFactory* in further works.

A Comparison of the measured and simulated data

The figures in appendix A show the comparison between the measured (meas.) values in darker colours (A,B,C) and the simulated (sim.) values in brighter colours (D,E,F). Some of the figures described in chapter 3 and chapter 4 are reproduced in the appendix in order to deliver a complete overview of the comparison between the measurement and the simulation.

A.1 Battery inverter connected with loads

A.1.1 Balanced change in ohmic load

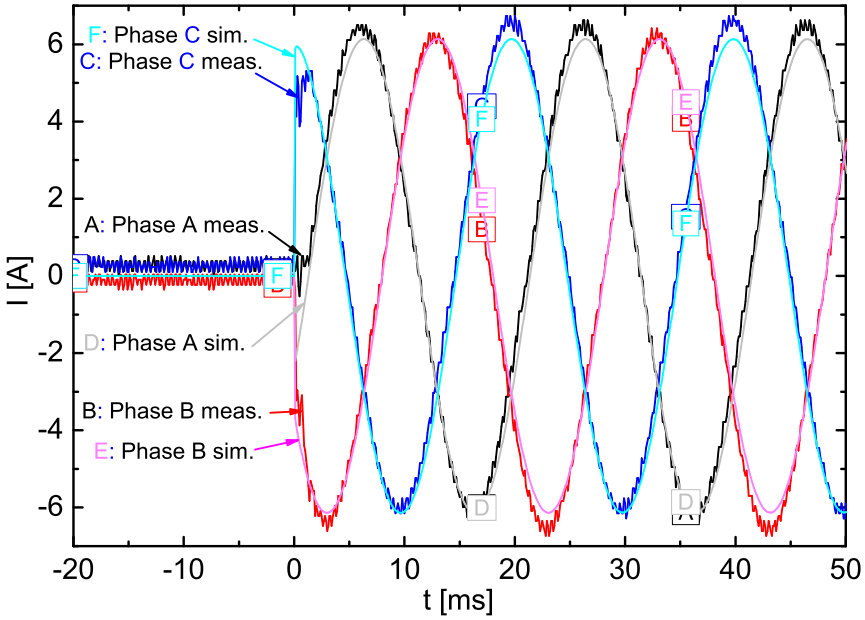

Figure 58: Transient currents I of the battery inverter in open circuit which is connected at the time t = 0 ms to a 3 kW ohmic load.

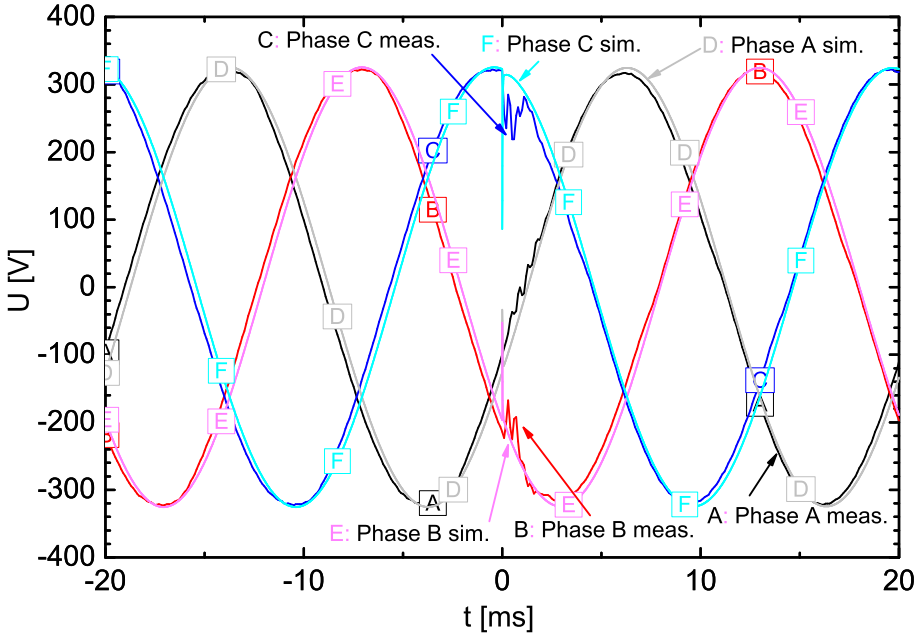

Figure 59: Transient voltages U of the battery inverter in open circuit which is connected at the time t = 0 ms to a 3 kW ohmic load.

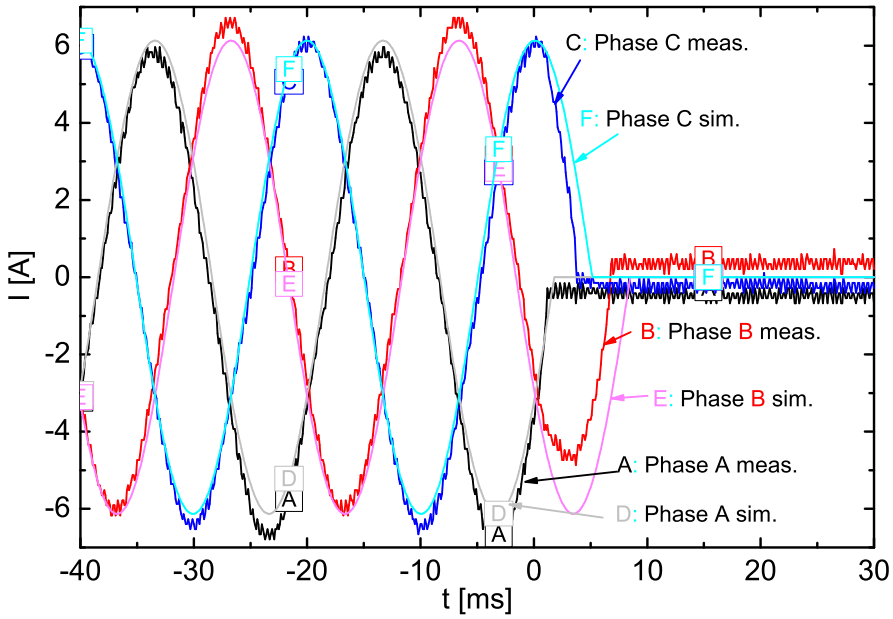

Figure 60: Transient currents I of the battery inverter supplying a 3 kW ohmic which is disconnected at the time t = 0 ms.

A.1.2 Balanced change in inductive load

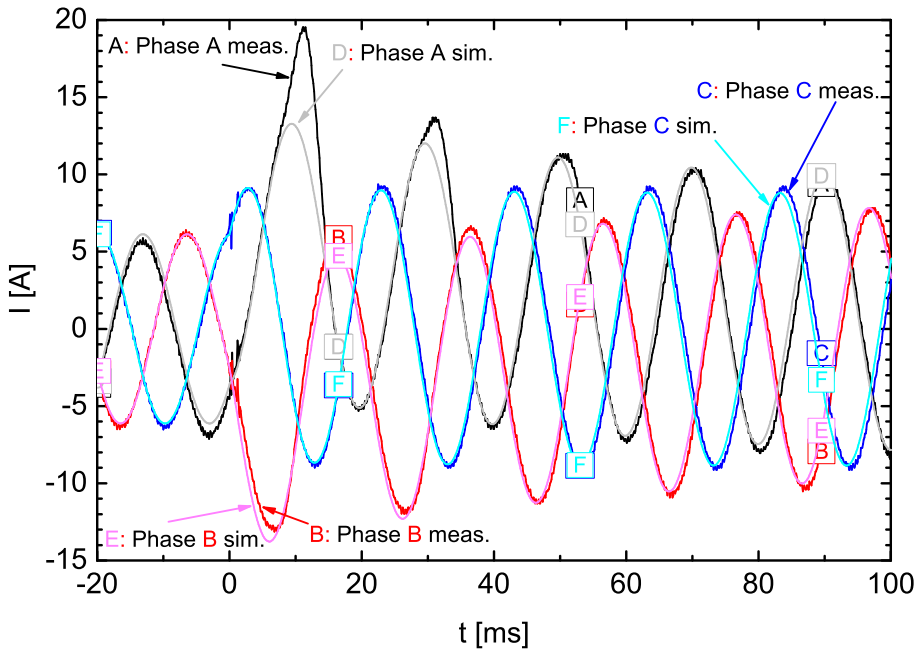

Figure 61: Transient currents I of the battery inverter supplying a 3 kW ohmic load which is connected at the time t = 0 ms to a 3 kVAr inductive load.

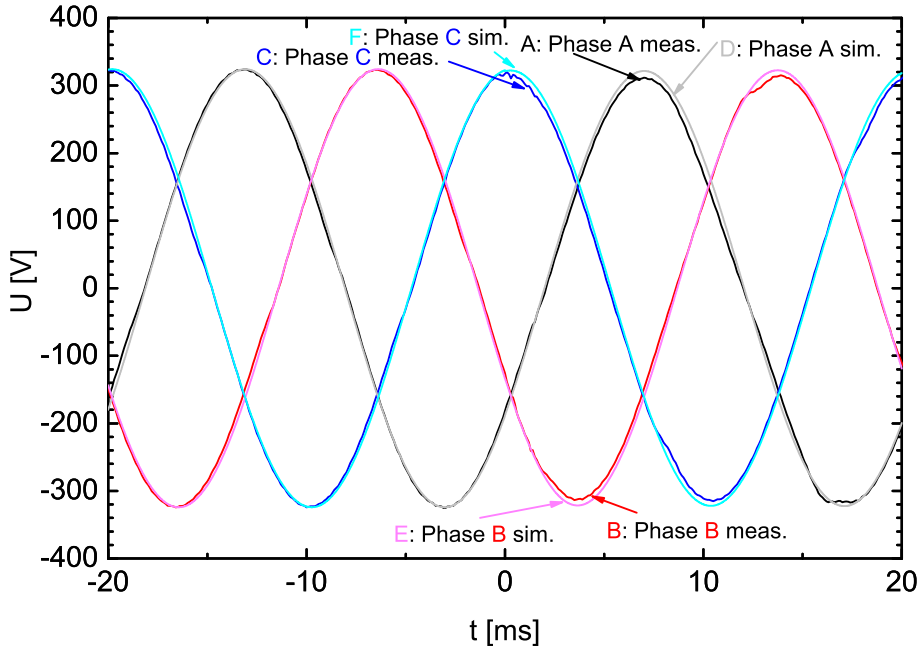

Figure 62: Transient voltages U of the battery inverter supplying a 3 kW ohmic load which is connected at the time t = 0 ms to a 3 kVAr inductive load.

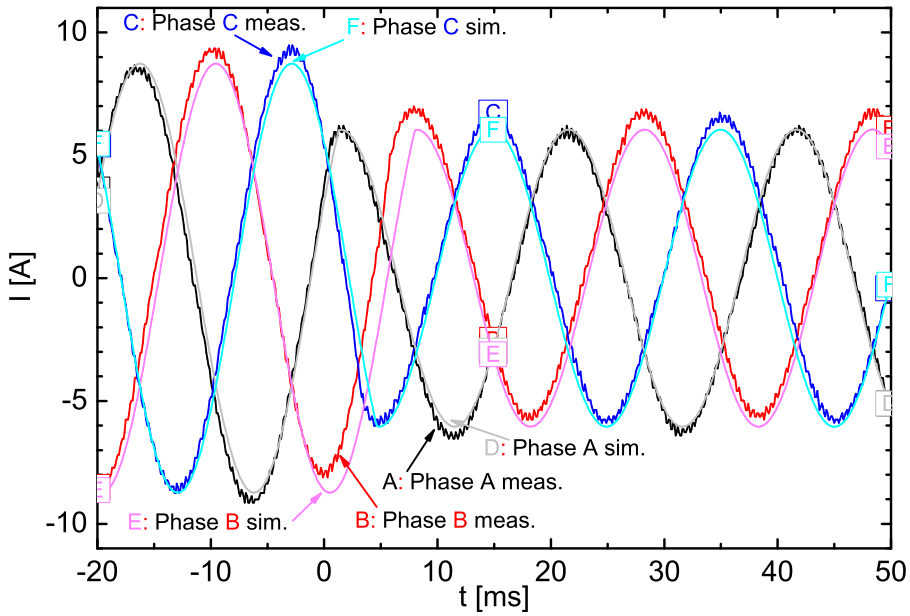

Figure 63: Transient currents I of the battery inverter supplying a 3 kW ohmic and a 3 kVAr inductive load. The 3 kVAr inductive load is disconnected at the time t = 0 ms.

A.1.3 Balanced change in capacitive load

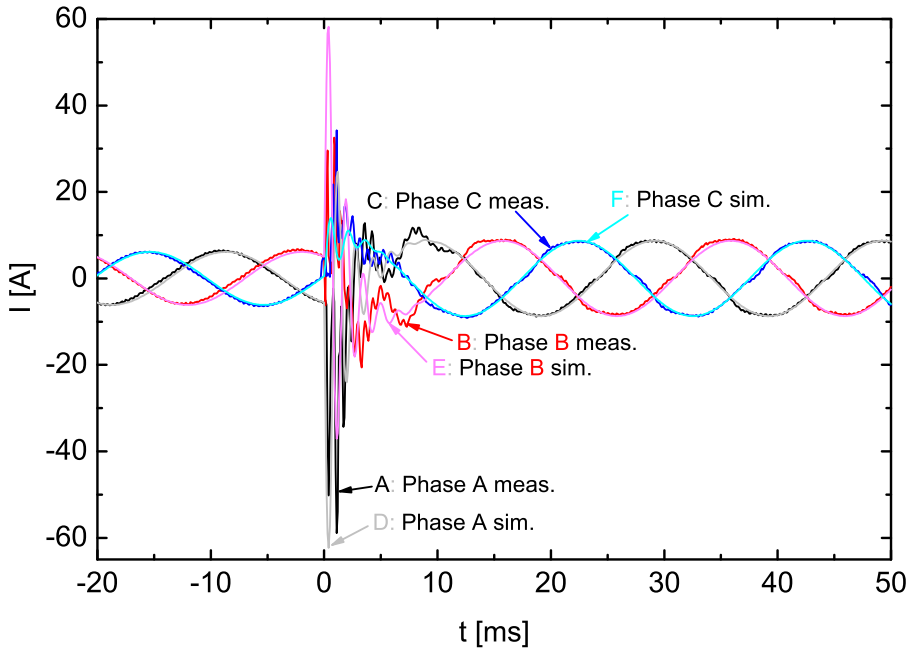

Figure 64: Transient currents I of the battery inverter supplying a 3 kW ohmic load which is connected at the time t = 0 ms to a 3 kVAr capacitive load.

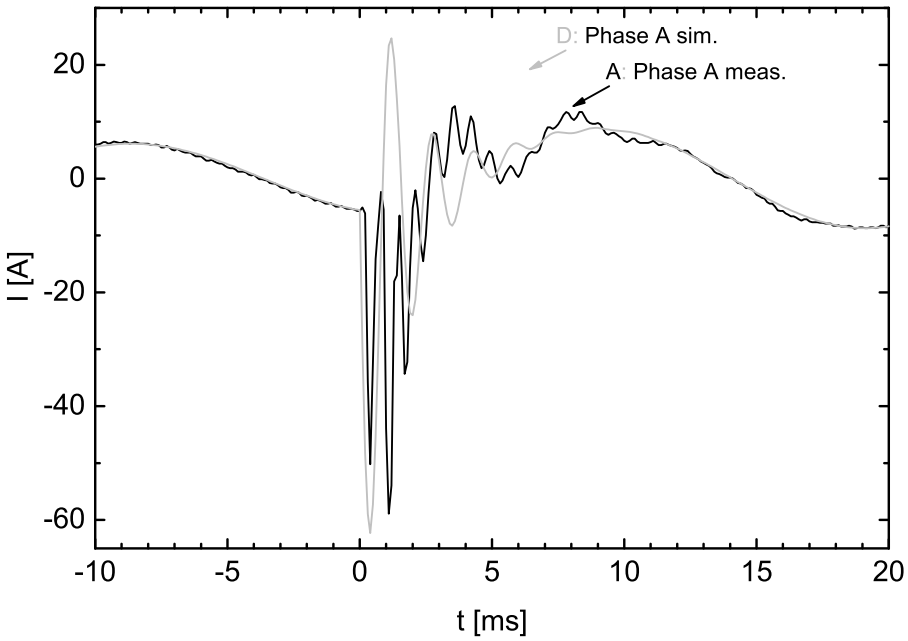

Figure 65: Transient currents I of phase A of the battery inverter supplying a 3 kW ohmic load which is connected at the time t = 0 ms to a 3 kVAr capacitive load.

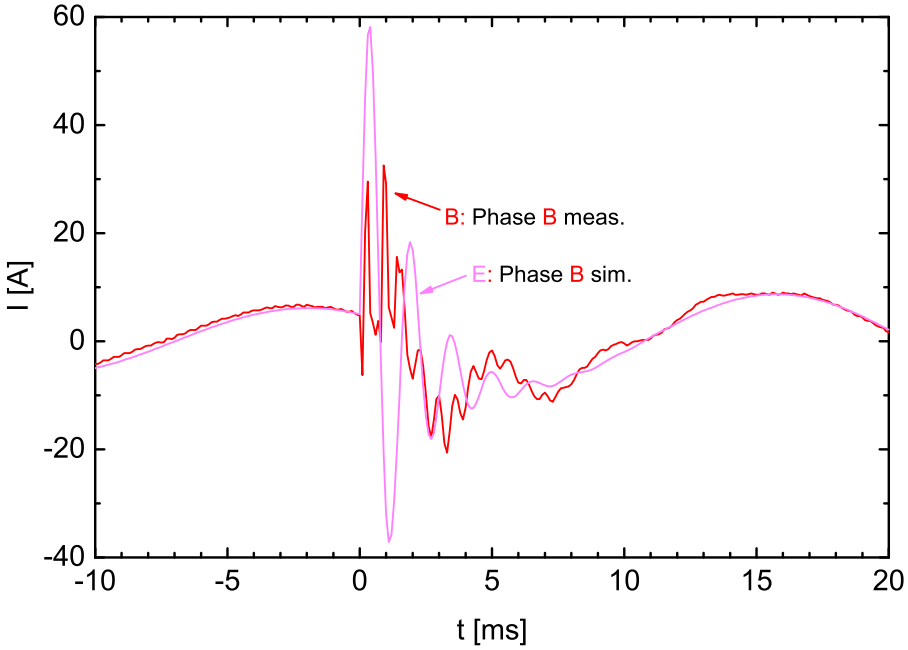

Figure 66: Transient currents I of phase B of the battery inverter supplying a 3 kW ohmic load which is connected at the time t = 0 ms to a 3 kVAr capacitive load.

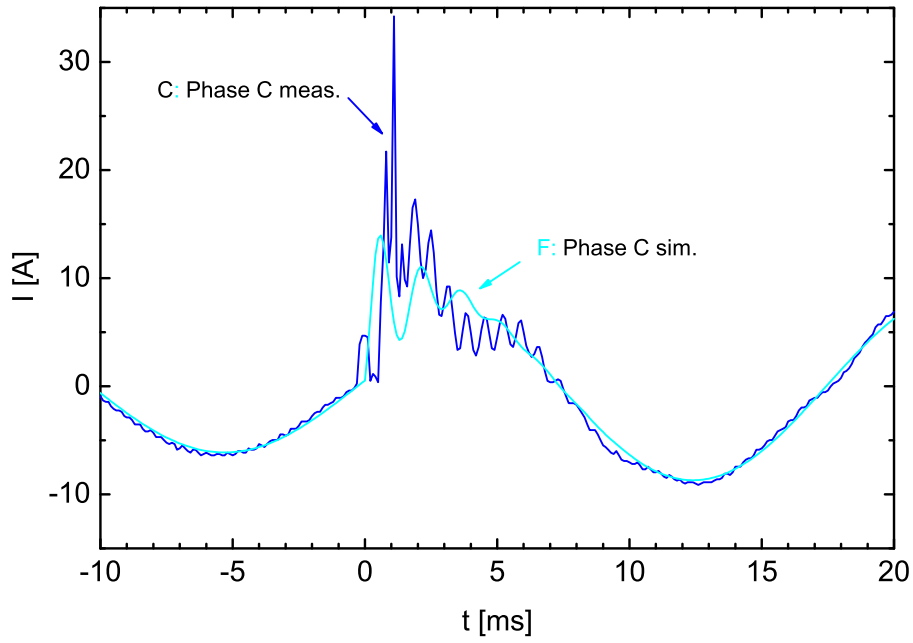

Figure 67: Transient currents I of phase C of the battery inverter supplying a 3 kW ohmic load which is connected at the time t = 0 ms to a 3 kVAr capacitive load.

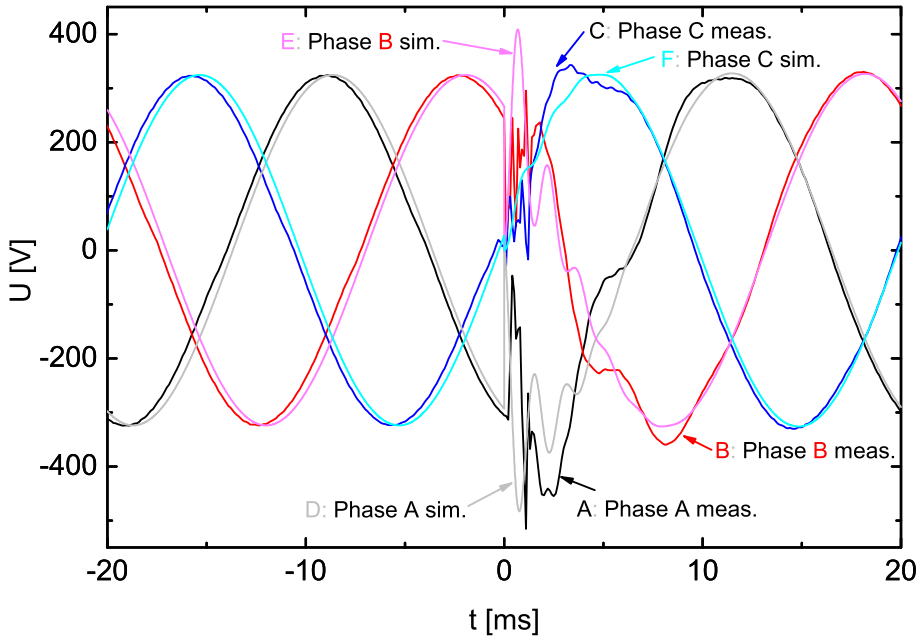

Figure 68: Transient voltages U of the battery inverter supplying a 3 kW ohmic load which is connected at the time t = 0 ms to a 3 kVAr capacitive load.

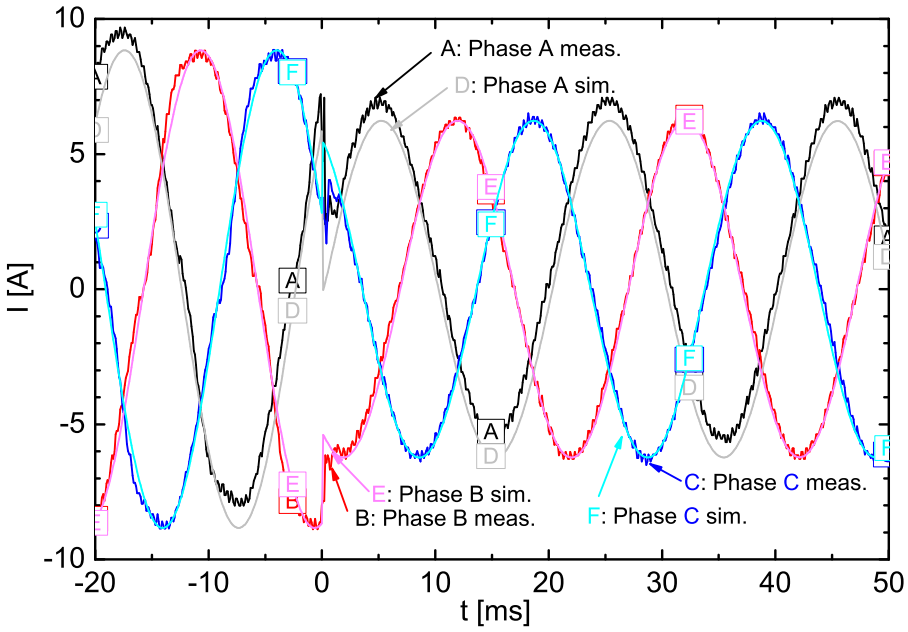

Figure 69: Transient currents I of the battery inverter supplying a 3 kW ohmic and a 3 kVAr capacitive load. The 3 kVAr capacitive load is disconnected at the time t = 0 ms.

A.1.4 Unbalanced change in ohmic load

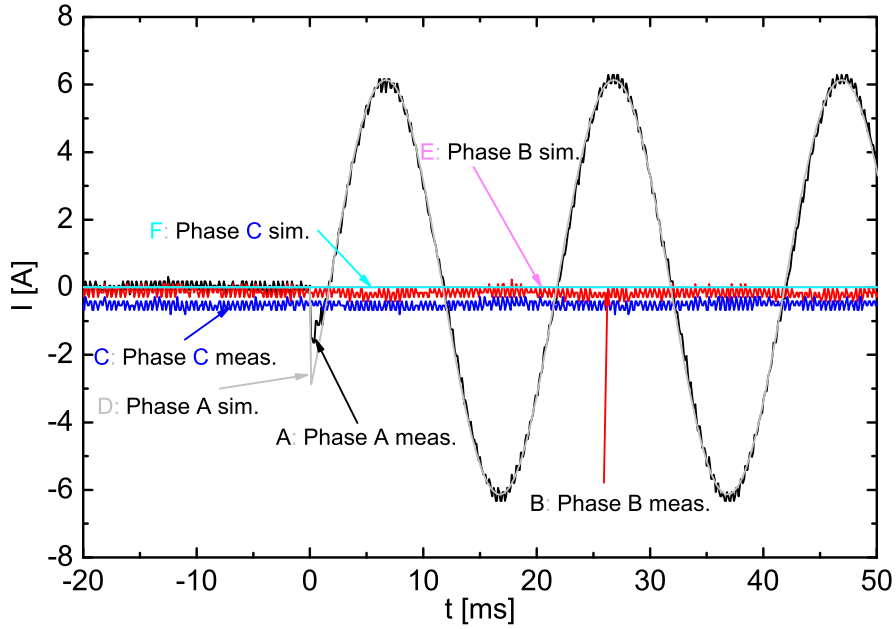

Figure 70: Transient currents I of the battery inverter in open circuit which is connected at the time t = 0 ms to a 1 kW ohmic load at phase A.

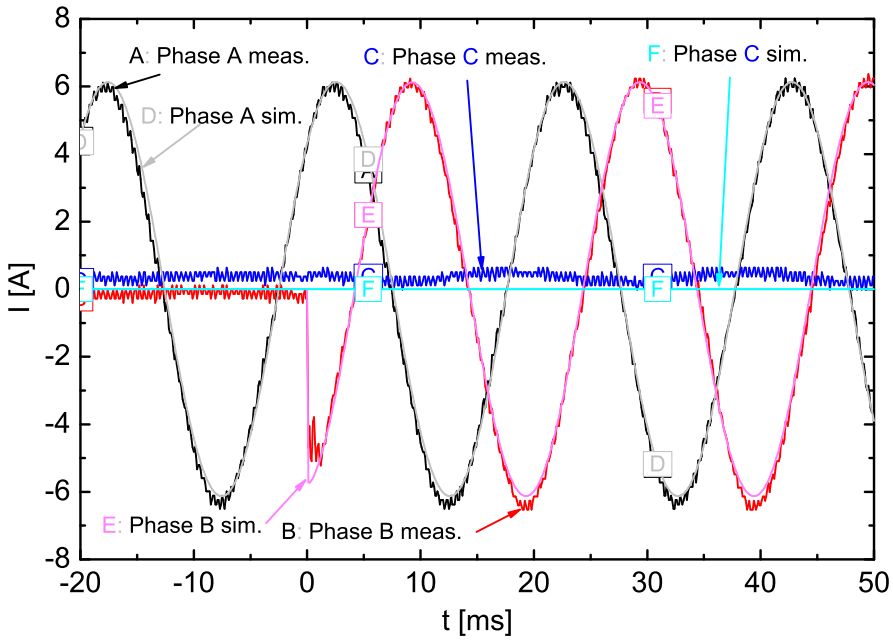

Figure 71: Transient currents I of the battery inverter connected to a 1 kW ohmic load at phase A which is connected at the time t = 0 ms to a 1 kW ohmic load at phase B.

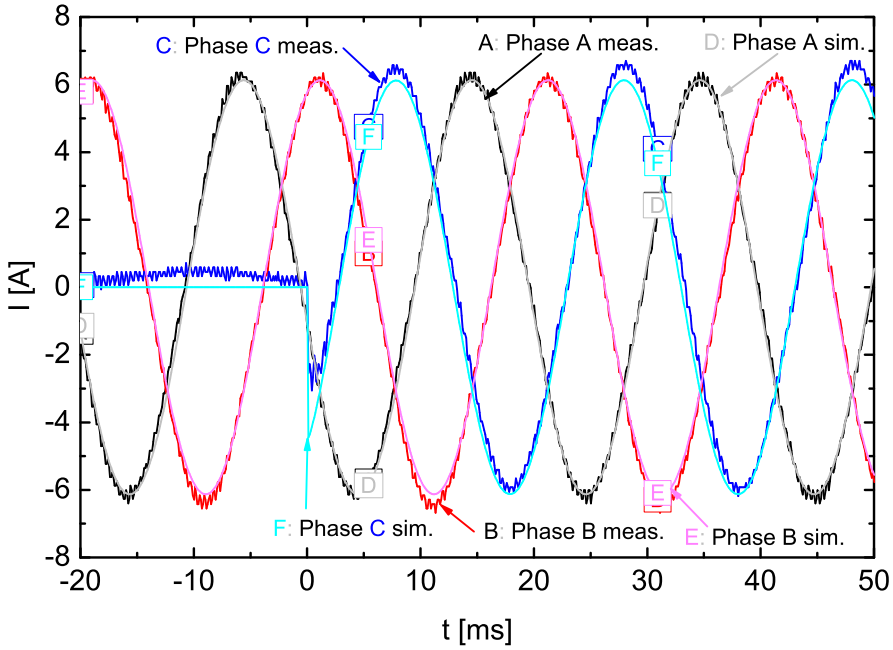

Figure 72: Transient currents I of the battery inverter connected to a 1 kW ohmic load at phase A and a 1 kW ohmic load at phase B which is connected at the time t = 0 ms to a 1 kW ohmic load at phase C.

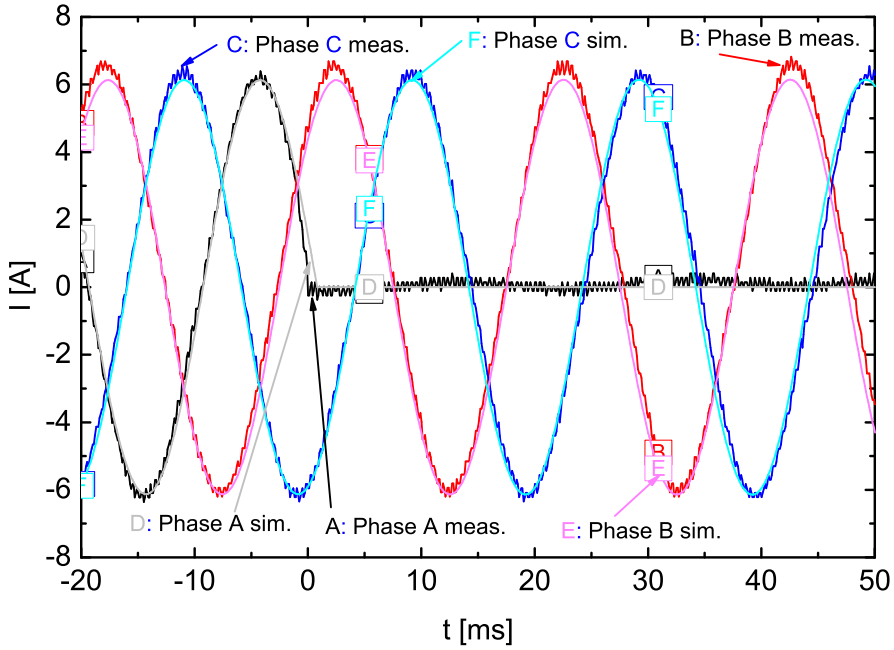

Figure 73: Transient currents I of the battery inverter connected to 1 kW ohmic loads at all three phases. The ohmic load of 1 kW at phase A is disconnected at the time t = 0 ms.

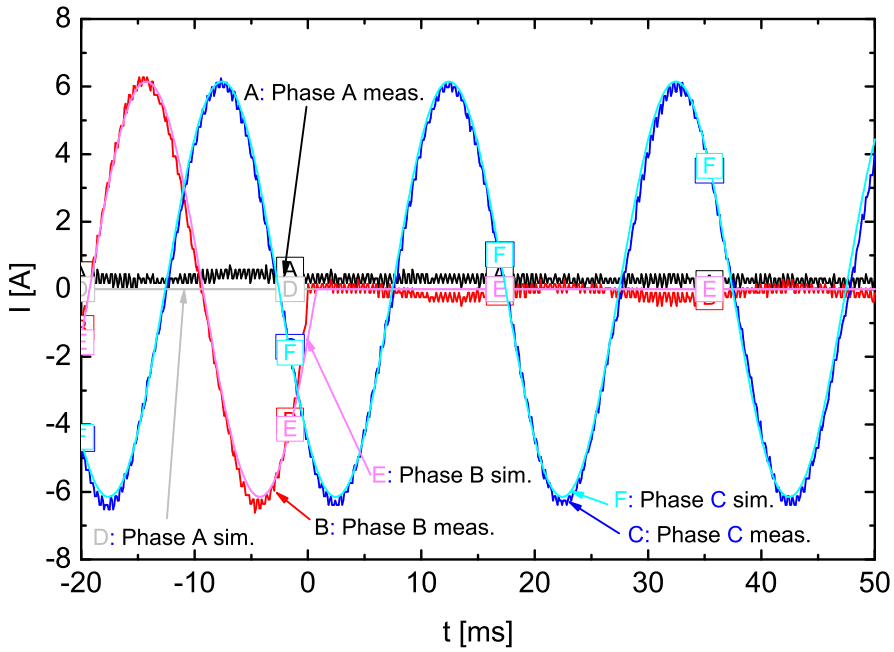

Figure 74: Transient currents I of the battery inverter connected to 1 kW ohmic loads at phase B and phase C. The ohmic load of 1 kW at phase B is disconnected at the time t = 0 ms.

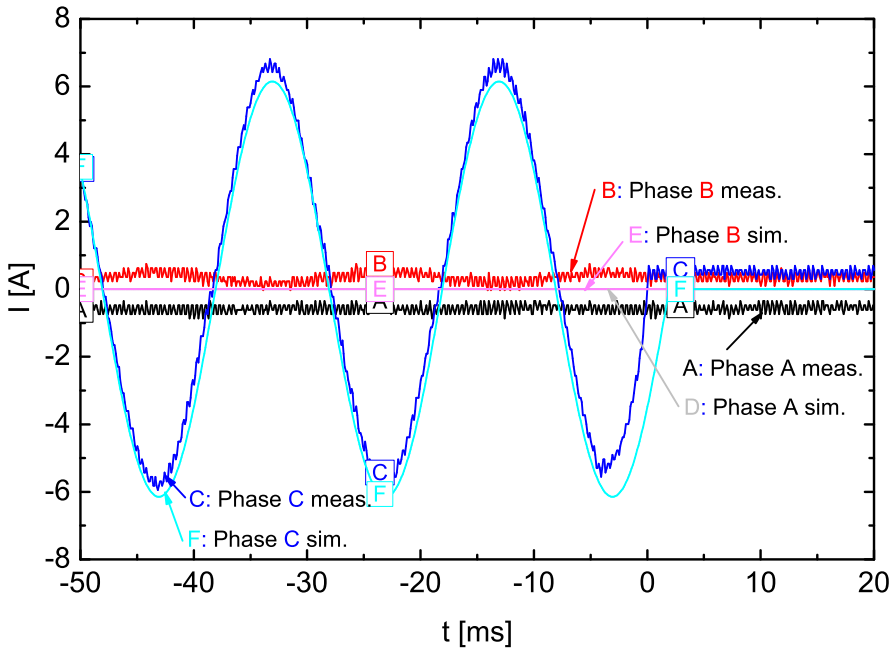

Figure 75: Transient currents I of the battery inverter connected to a 1 kW ohmic load at phase C. The ohmic load is disconnected at the time t = 0 ms.

A.1.5 Unbalanced change in inductive load

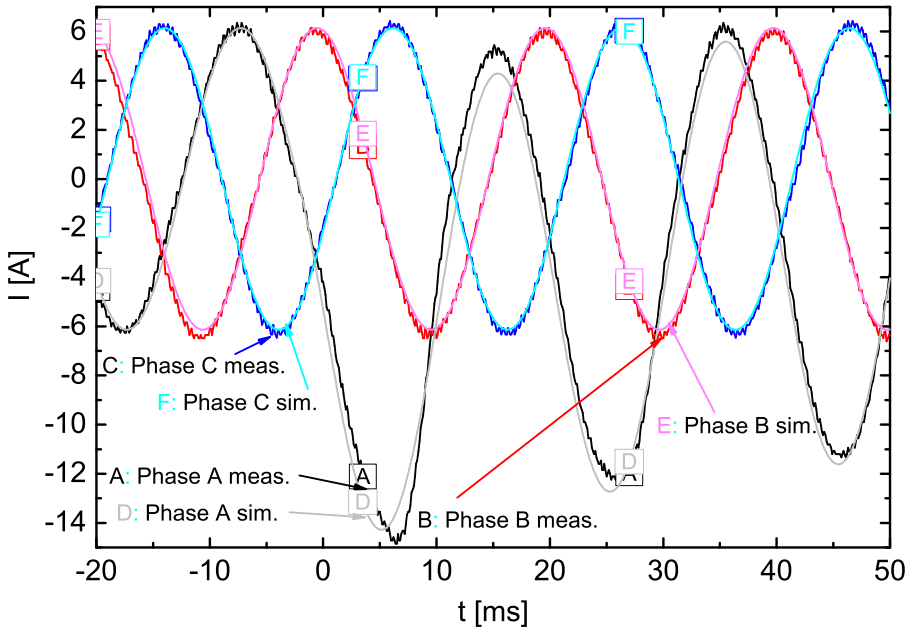

Figure 76: Transient currents I of the battery inverter in connection with a 1 kW ohmic load at each phase. The battery inverter is connected at the time t = 0 ms to a 1 kVAr inductive load at phase A.

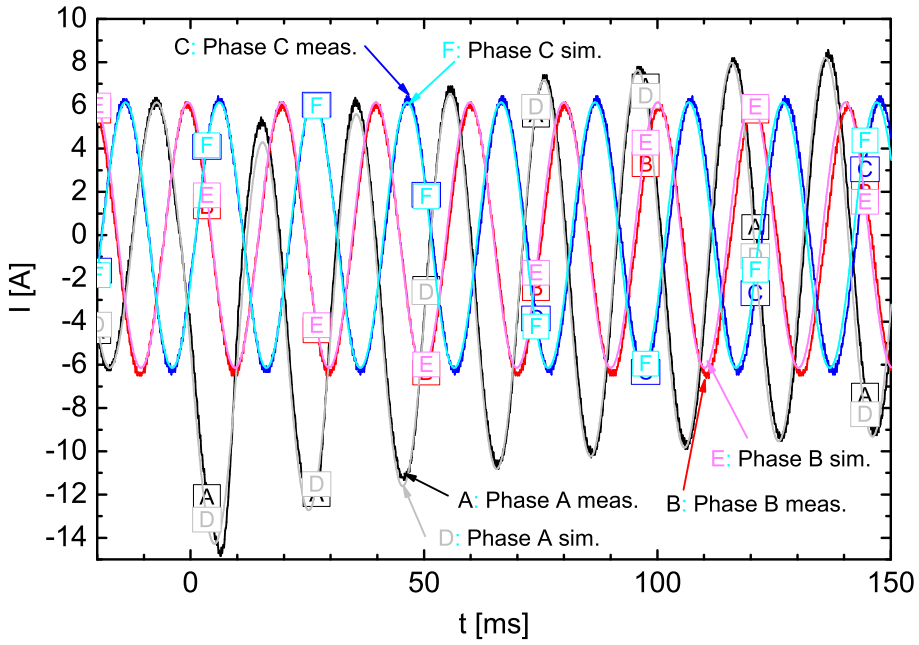

Figure 77: Transient currents I of the battery inverter in connection with a 1 kW ohmic load at each phase. The battery inverter is connected at the time t = 0 ms to a 1 kVAr inductive load at phase A. The enlarged time scale enables to show the decline of the current offset.

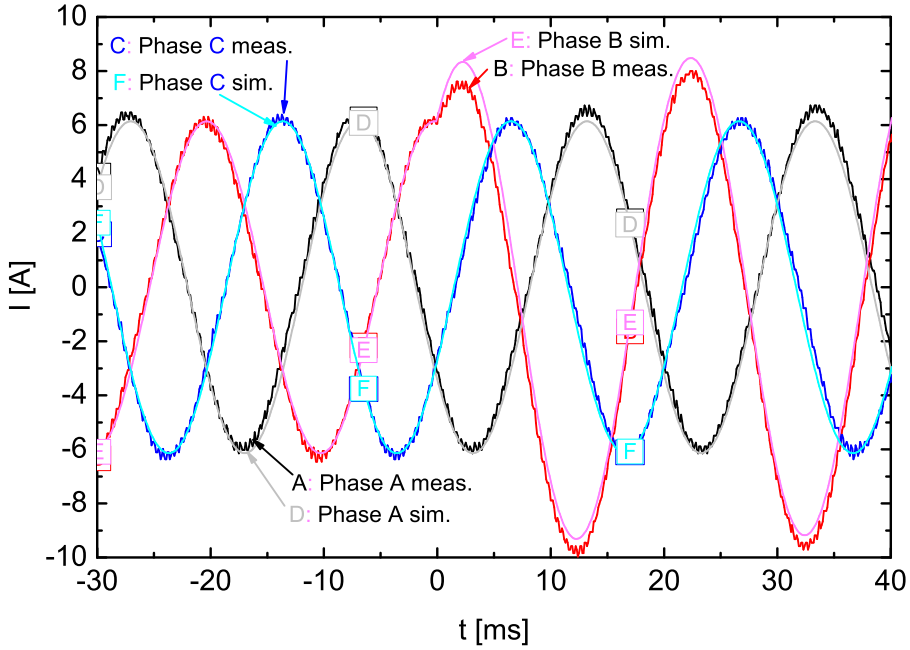

Figure 78: Transient currents I of the battery inverter in connection with a 1 kW ohmic load at each phase. The battery inverter is connected at the time t = 0 ms to a 1 kVAr inductive load at phase B.

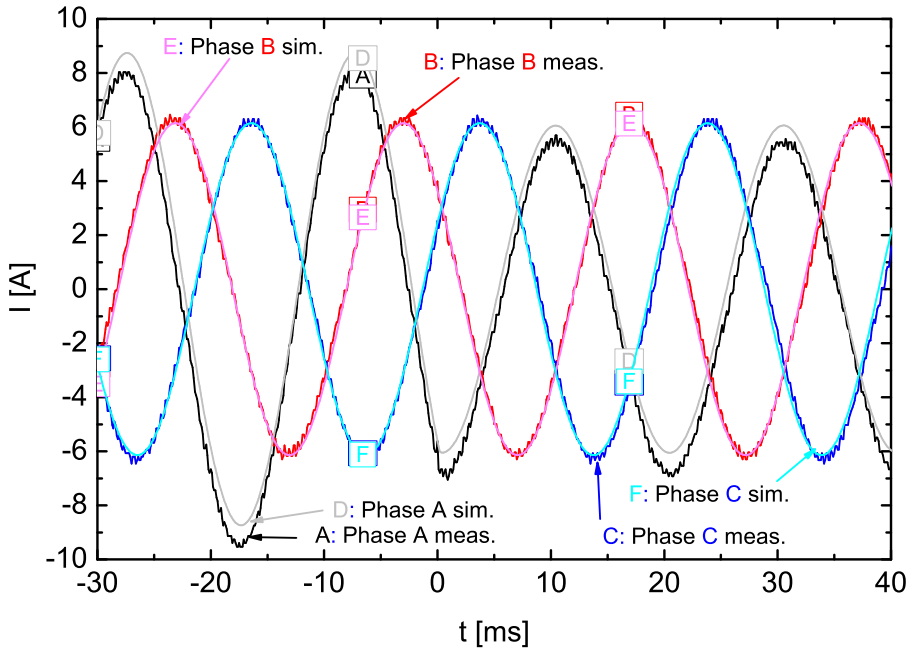

Figure 79: Transient currents I of the battery inverter in connection with a 1 kW ohmic load at each phase and a 1 kVAr inductive load at phase A. The inductive load at phase A is disconnected at the time $t = 0$ ms.

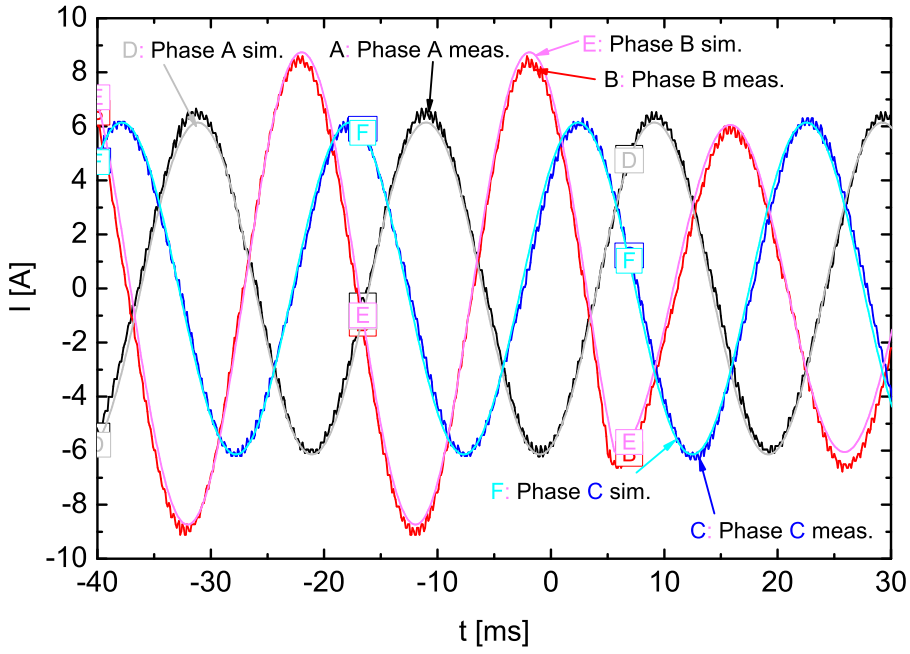

Figure 80: Transient currents I of the battery inverter in connection with a 1 kW ohmic load at each phase and a 1 kVAr inductive load at phase B. The inductive load at phase B is disconnected at the time $t = 0$ ms.

A.1.6 Unbalanced change in capacitive load

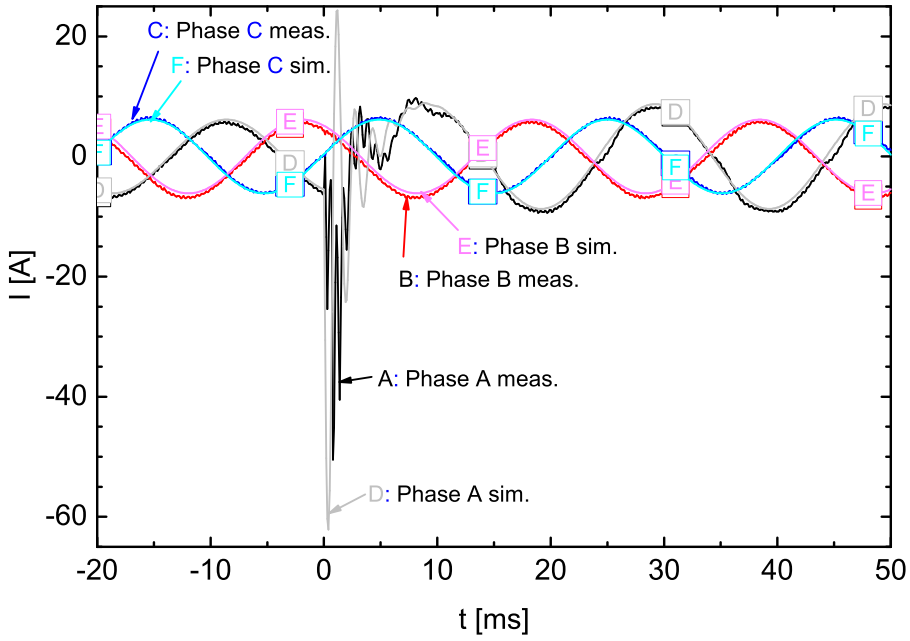

Figure 81: Transient currents I of the battery inverter in connection with a 1 kW ohmic load at each phase. The battery inverter is connected at the time t = 0 ms to a 1 kVAr capacitive load at phase A.

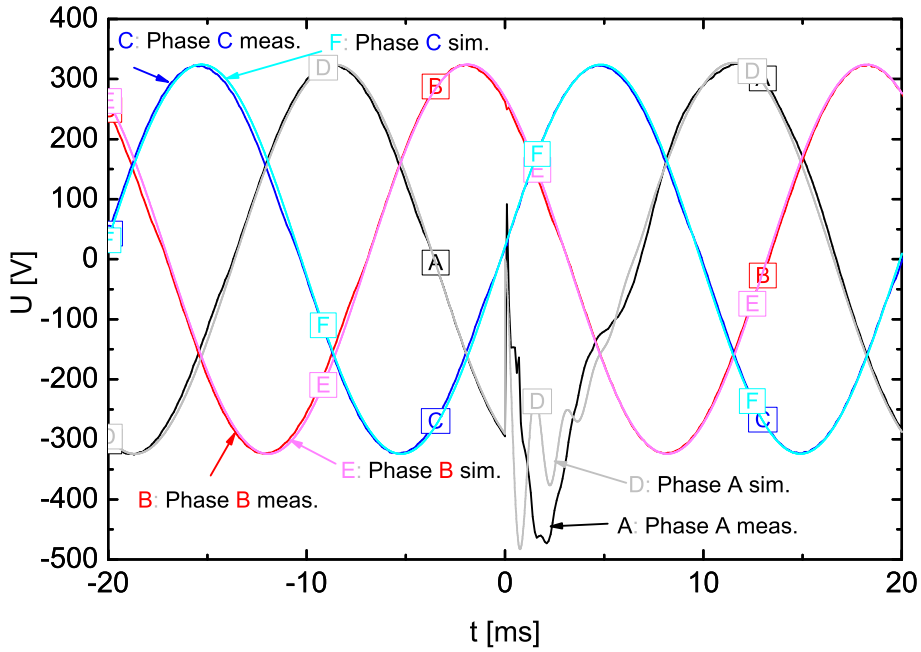

Figure 82: Transient voltages U of the battery inverter in connection with a 1 kW ohmic load at each phase. The battery inverter is connected at the time t = 0 ms to a 1 kVAr capacitive load at phase A.

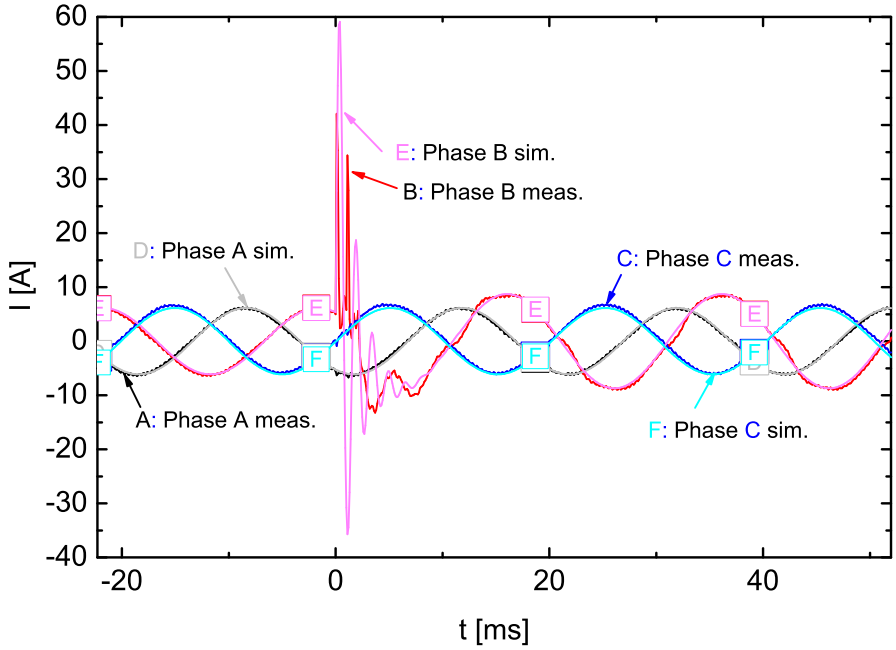

Figure 83: Transient currents I of the battery inverter in connection with a 1 kW ohmic load at each phase. The battery inverter is connected at the time t = 0 ms to a 1 kVAr capacitive load at phase B.

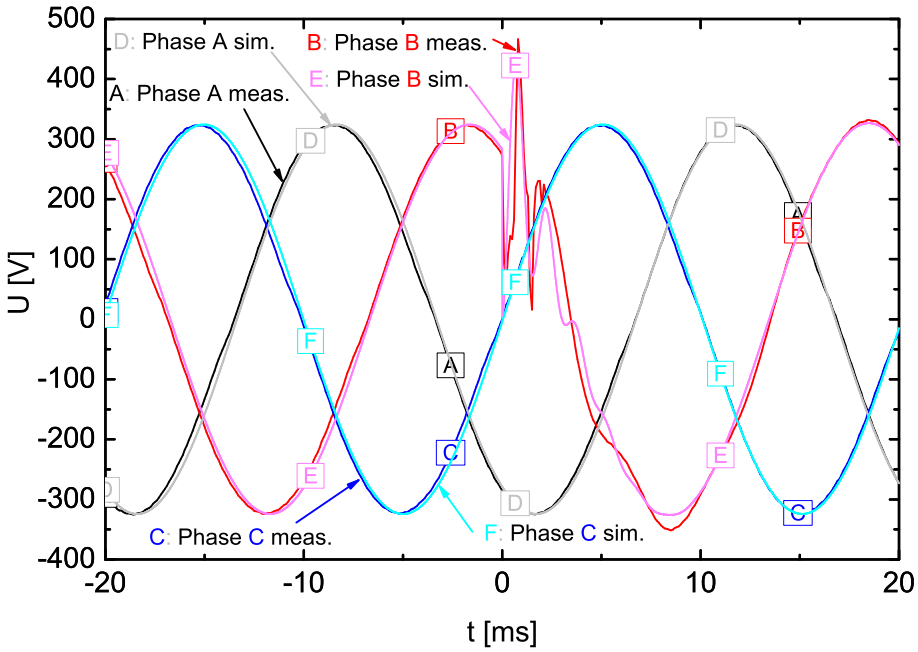

Figure 84: Transient voltages U of the battery inverter in connection with a 1 kW ohmic load at each phase. The battery inverter is connected at the time t = 0 ms to a 1 kVAr capacitive load at phase B.

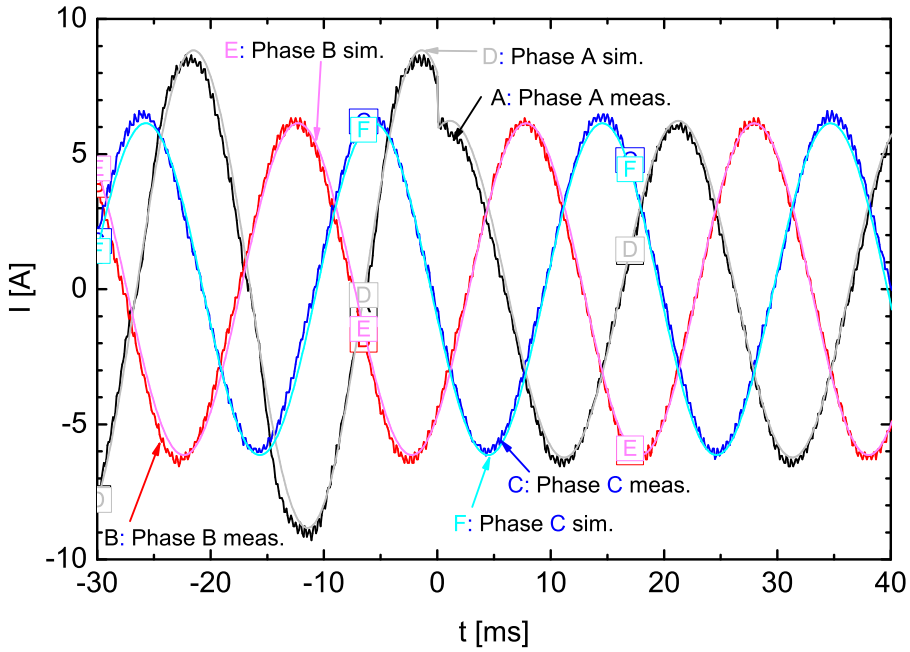

Figure 85: Transient currents I of the battery inverter in connection with a 1 kW ohmic load at each phase and a 1 kVAr capacitive load at phase A. The capacitive load at phase A is disconnected at the time t = 0 ms.

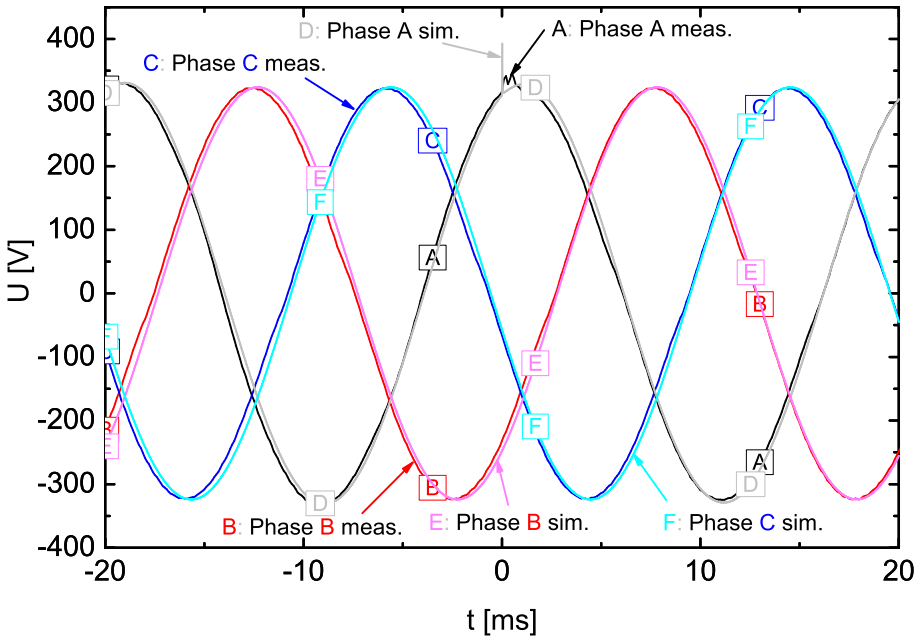

Figure 86: Transient voltages U of the battery inverter in connection with a 1 kW ohmic load at each phase and a 1 kVAr capacitive load at phase A. The capacitive load at phase A is disconnected at the time t = 0 ms.

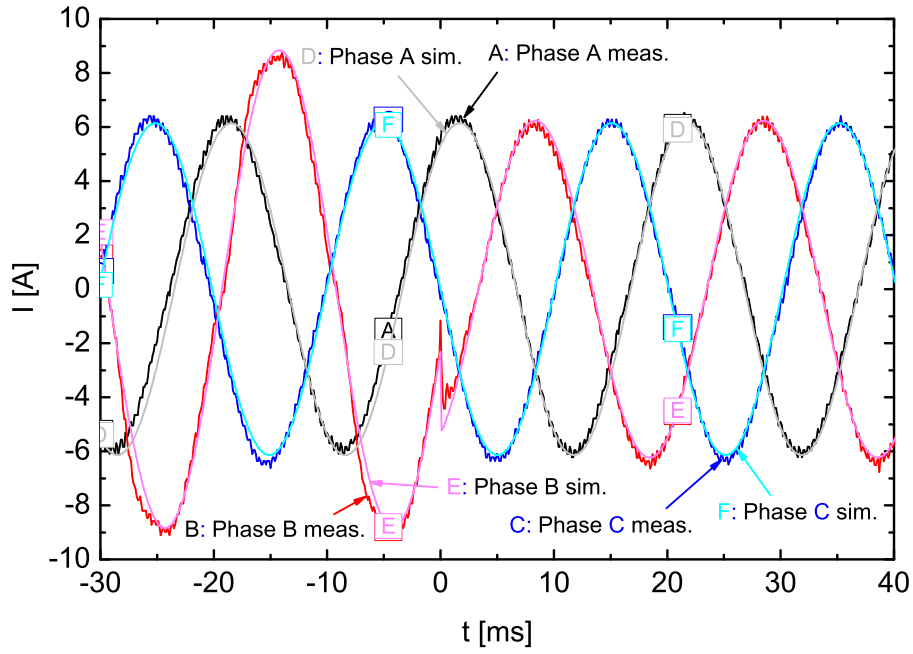

Figure 87: Transient currents I of the battery inverter in connection with a 1 kW ohmic load at each phase and a 1 kVAr capacitive load at phase B. The capacitive load at phase B is disconnected at the time $t = 0$ ms.

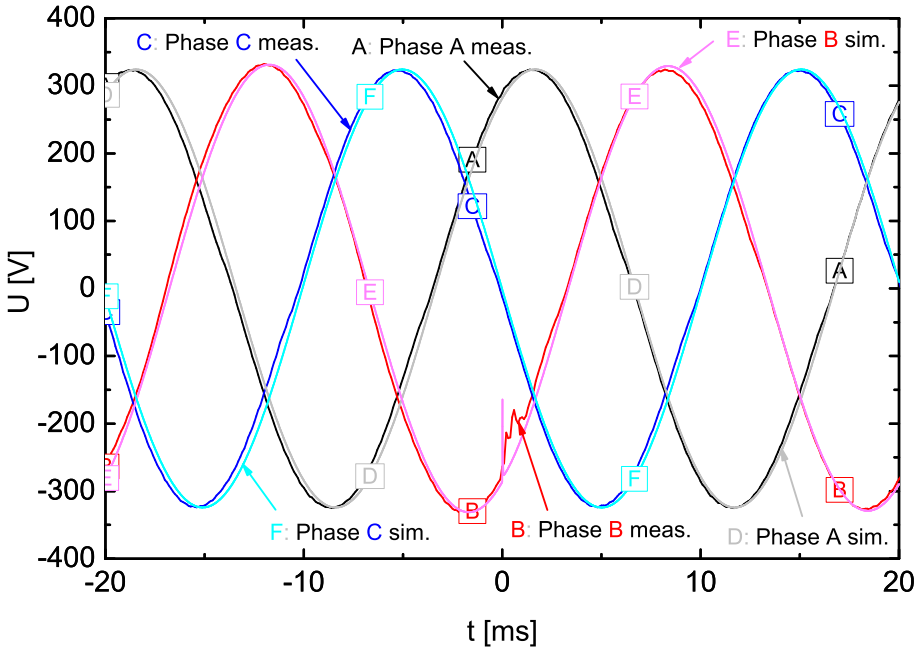

Figure 88: Transient voltage U of the battery inverter in connection with a 1 kW ohmic load at each phase and a 1 kVAr capacitive load at phase B. The capacitive load at phase B is disconnected at the time $t = 0$ ms.

A.2 Battery inverter connected with asynchronous generator and loads

A.2.1 Balanced change in ohmic load

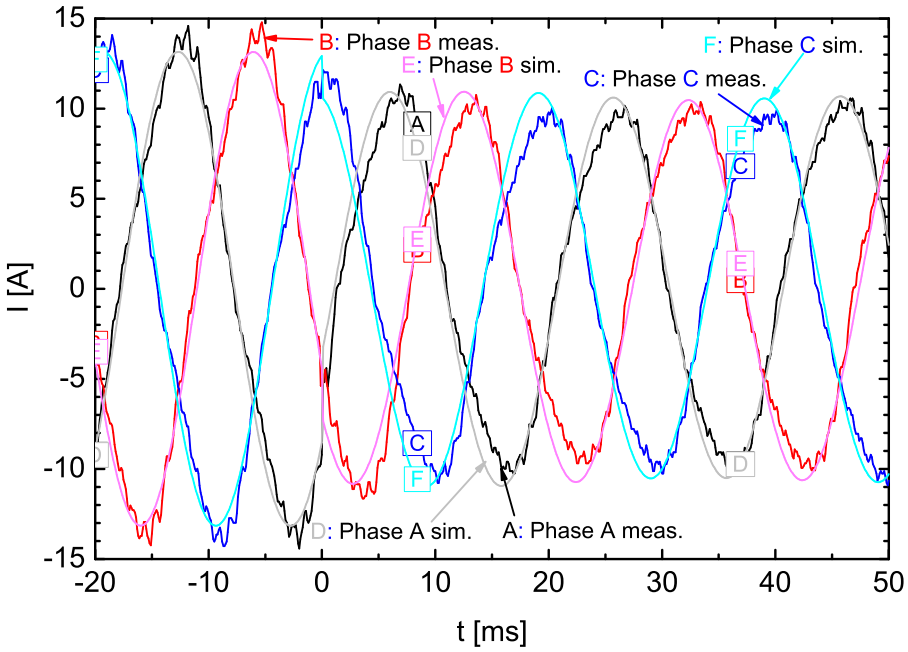

Figure 89: Transient currents I of the battery inverter connected with asynchronous generator which is connected at the time t = 0 ms to a 3 kW ohmic load.

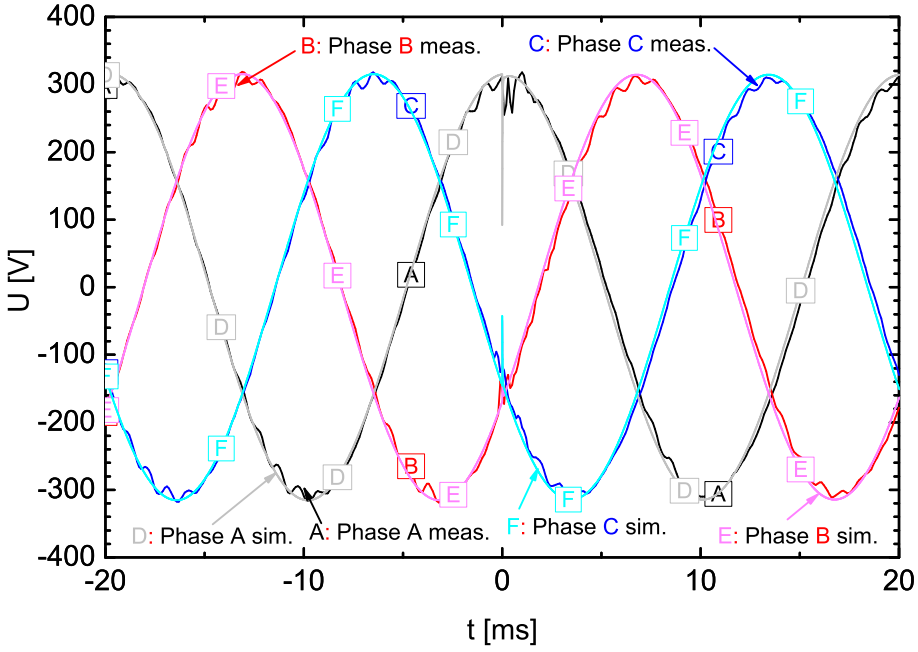

Figure 90: Transient voltages U of the battery inverter connected with asynchronous generator which is connected at the time t = 0 ms to a 3 kW ohmic load.

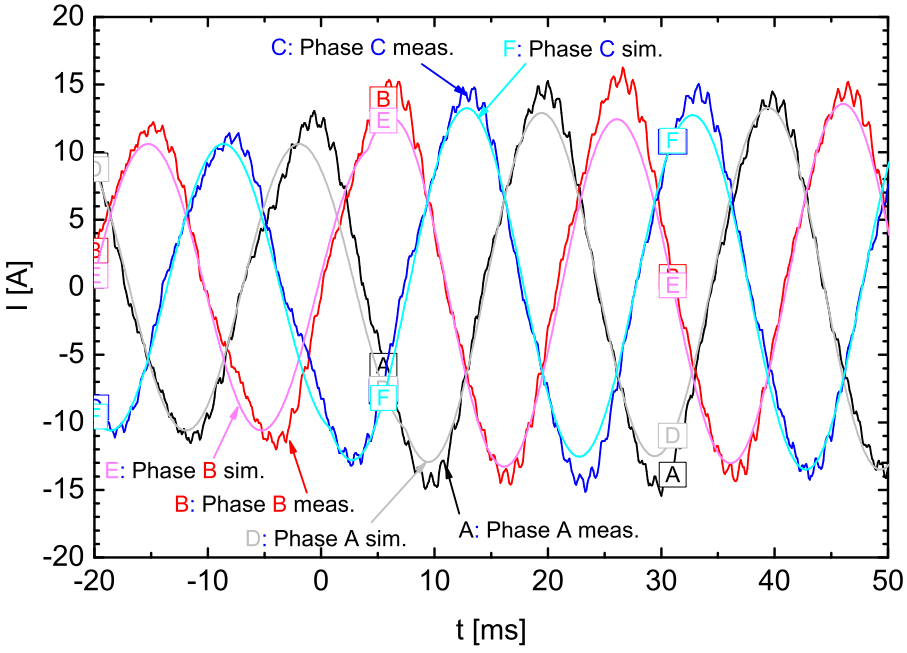

Figure 91: Transient currents I of the battery inverter in connection with the asynchronous generator supplying a 3 kW ohmic load. The 3 kW ohmic load is disconnected at the time t = 0 ms.

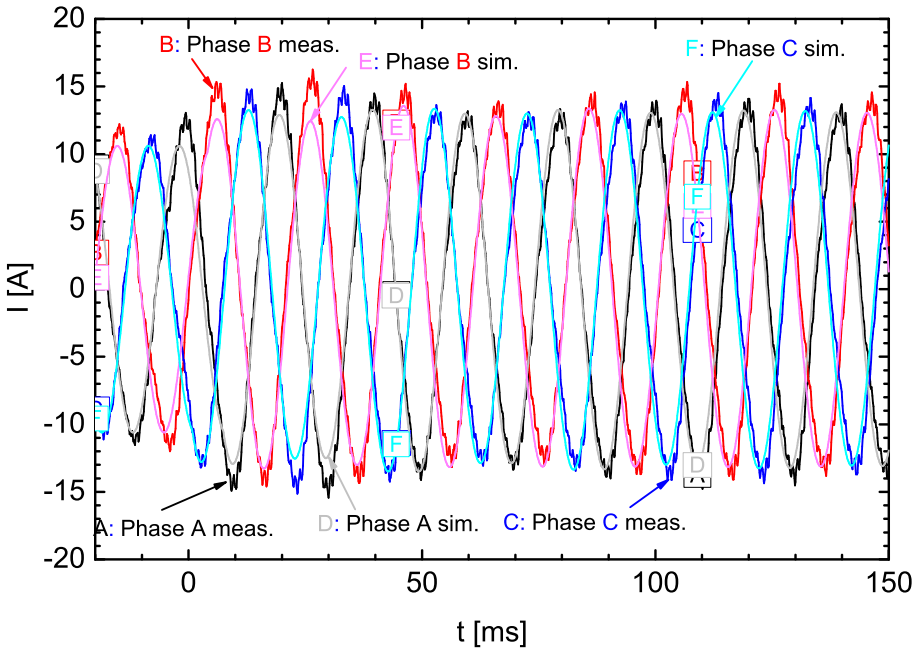

Figure 92: Transient currents I of the battery inverter in connection with the asynchronous generator supplying a 3 kW ohmic load. The 3 kW ohmic load is disconnected at the time t = 0 ms. After the disconnection the currents tune.

A.2.2 Balanced change in inductive load

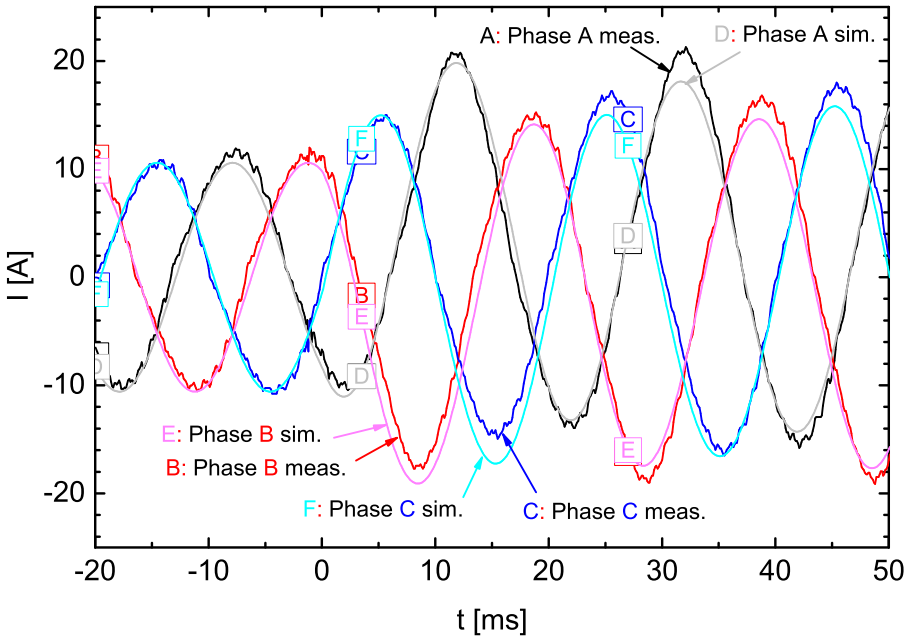

Figure 93: Transient currents I of the battery inverter in connection with the asynchronous generator which is connected at the time t = 0 ms to a 3 kVAr inductive load.

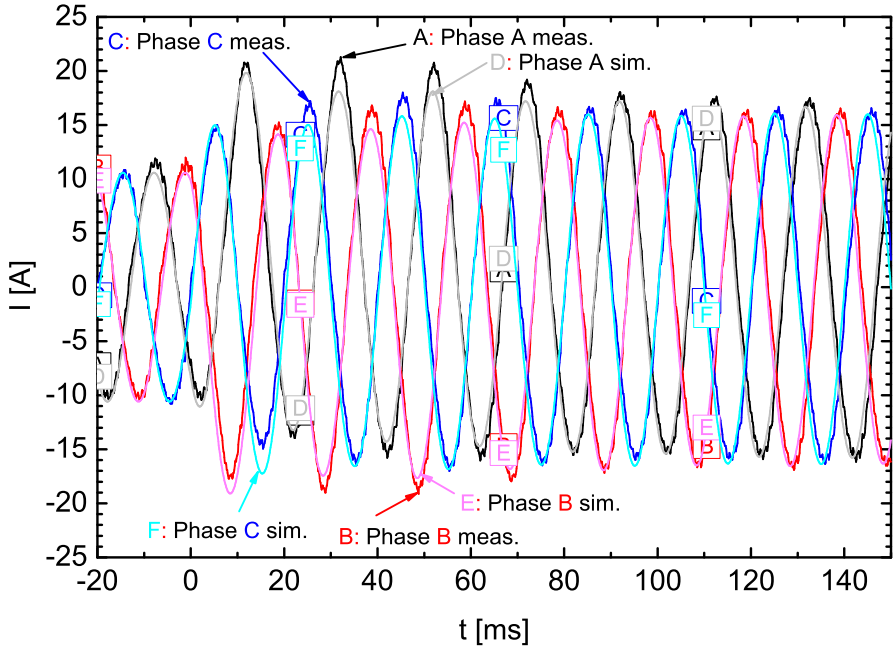

Figure 94: Decay of the transient currents I of the battery inverter in connection with the asynchronous generator which is connected at the time t = 0 ms to a 3 kVAr inductive load.

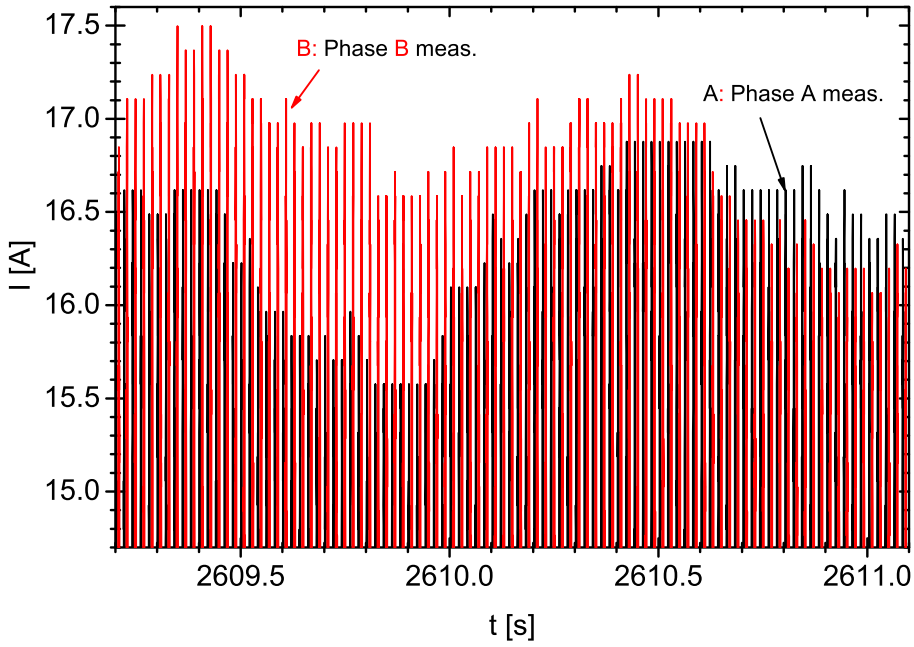

Figure 95: Fluctuations of the transient currents I of phase A and phase B of the battery inverter in connection with the asynchronous generator and a 3 kVAr inductive load.

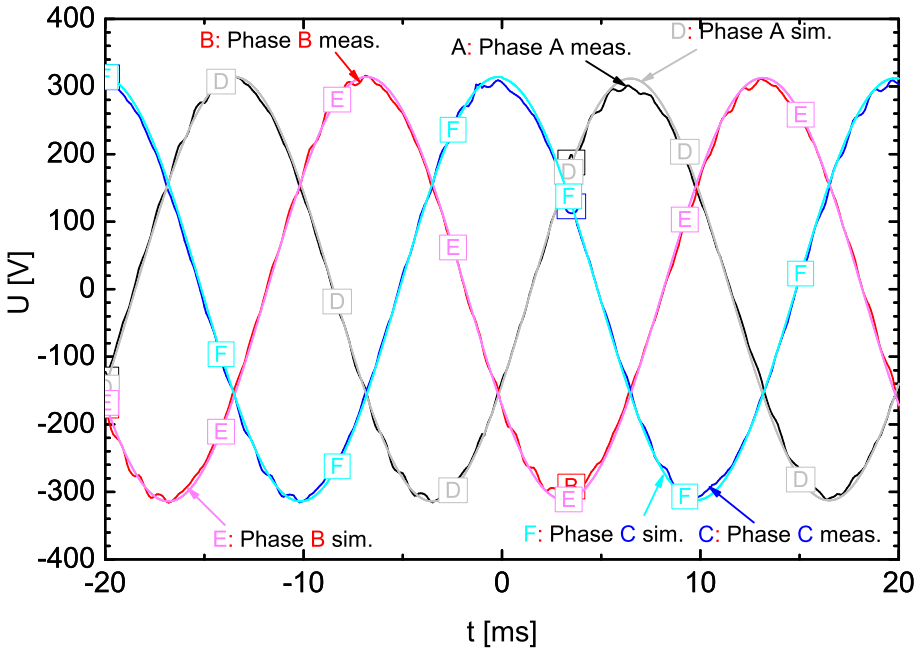

Figure 96: Transient voltages U of the battery inverter connected with asynchronous generator which is connected to a 3 kVAr inductive load.

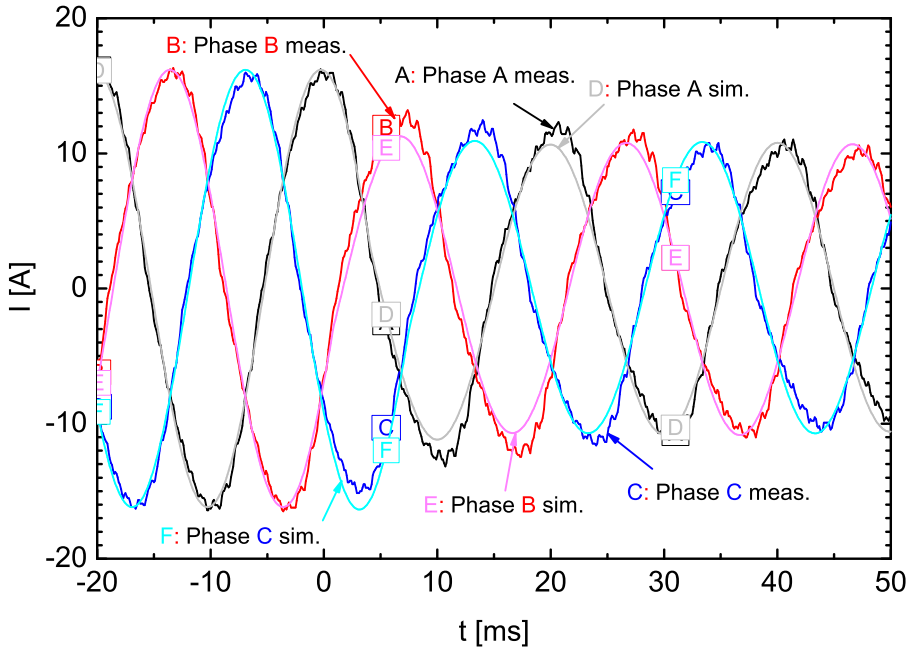

Figure 97: Transient currents I of the battery inverter in connection with the asynchronous generator supplying a 3 kW ohmic load and a 3 kVAr inductive load. The 3 kVAr inductive load is disconnected at the time t = 0 ms.

A.2.3 Balanced change in capacitive load

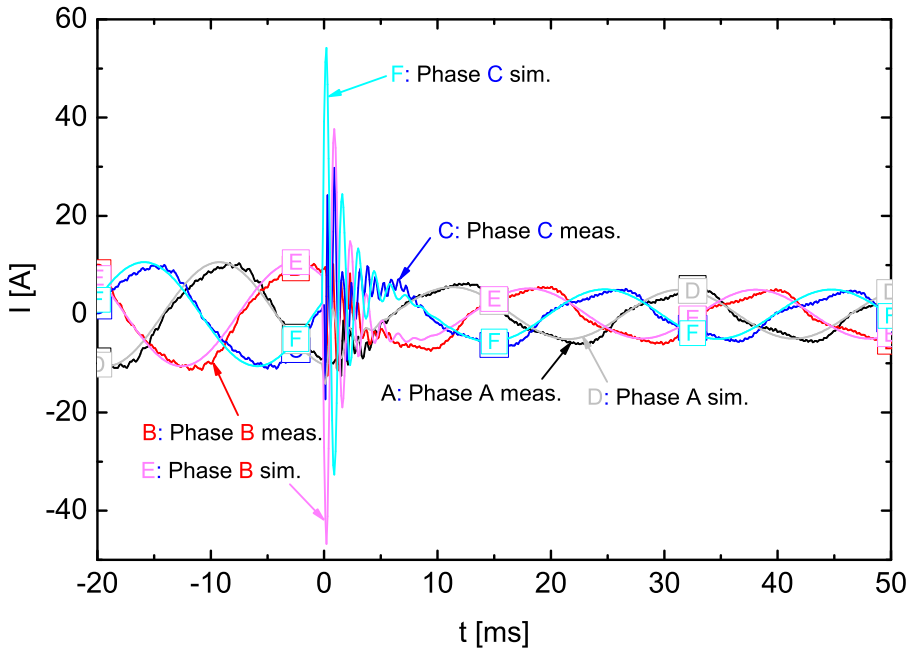

Figure 98: Transient currents I of the battery inverter connected with asynchronous generator which is connected at the time t = 0 ms to a 3 kVAr capacitive load.

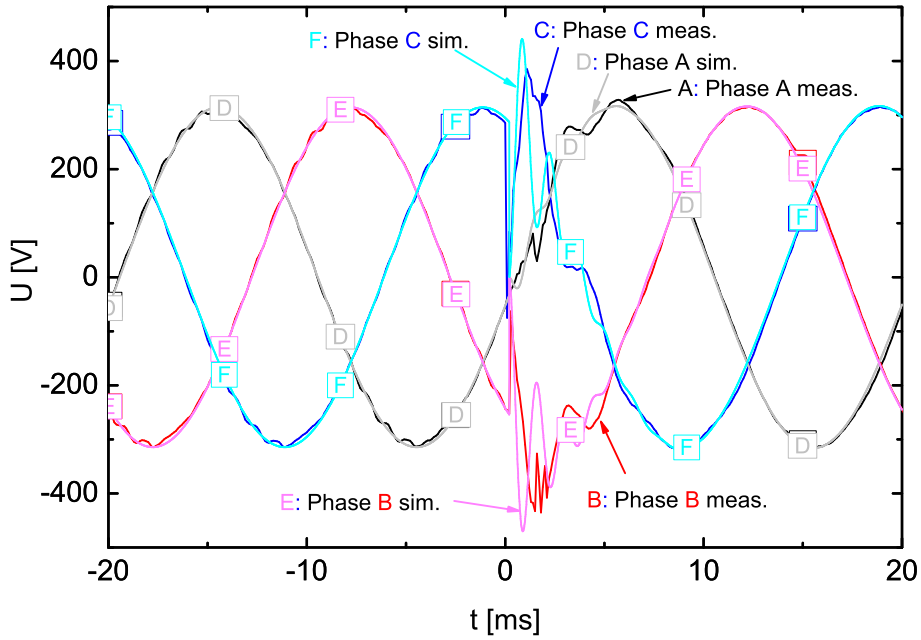

Figure 99: Transient voltages U of the battery inverter connected with asynchronous generator which is connected at the time t = 0 ms to a 3 kVAr capacitive load.

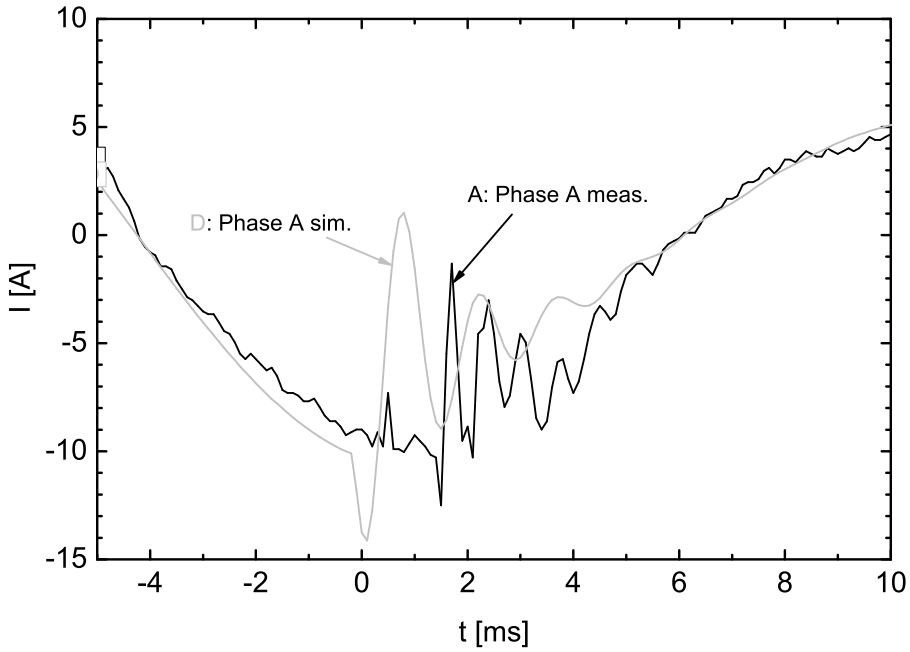

Figure 100: Transient currents I of phase A of the battery inverter connected with asynchronous generator and a 3 kW ohmic load which is connected at the time t = 0 ms to a 3 kVAr capacitive load.

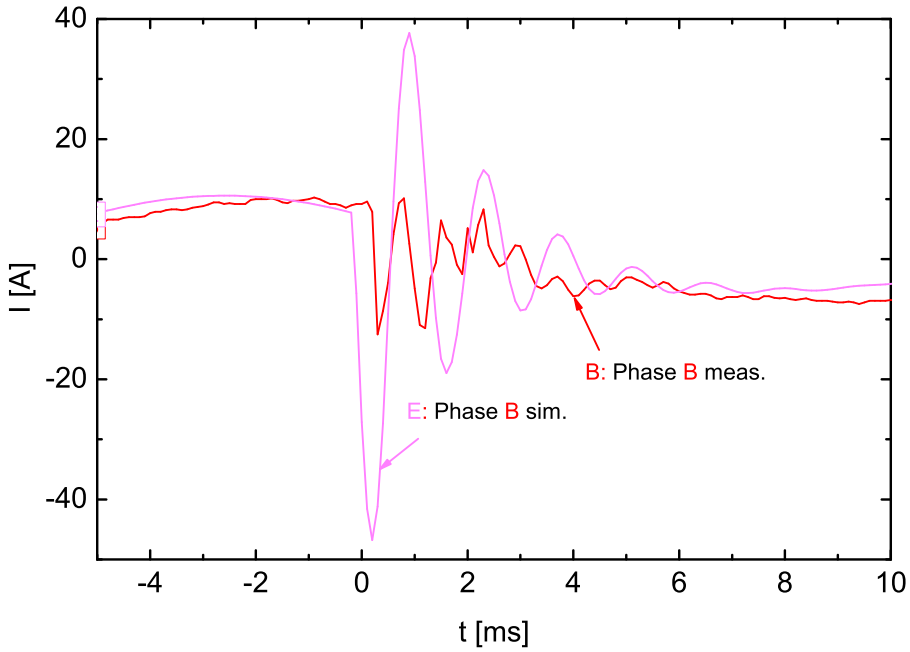

Figure 101: Transient currents I of phase B of the battery inverter connected with asynchronous generator and a 3 kW ohmic load which is connected at the time t = 0 ms to a 3 kVAr capacitive load.

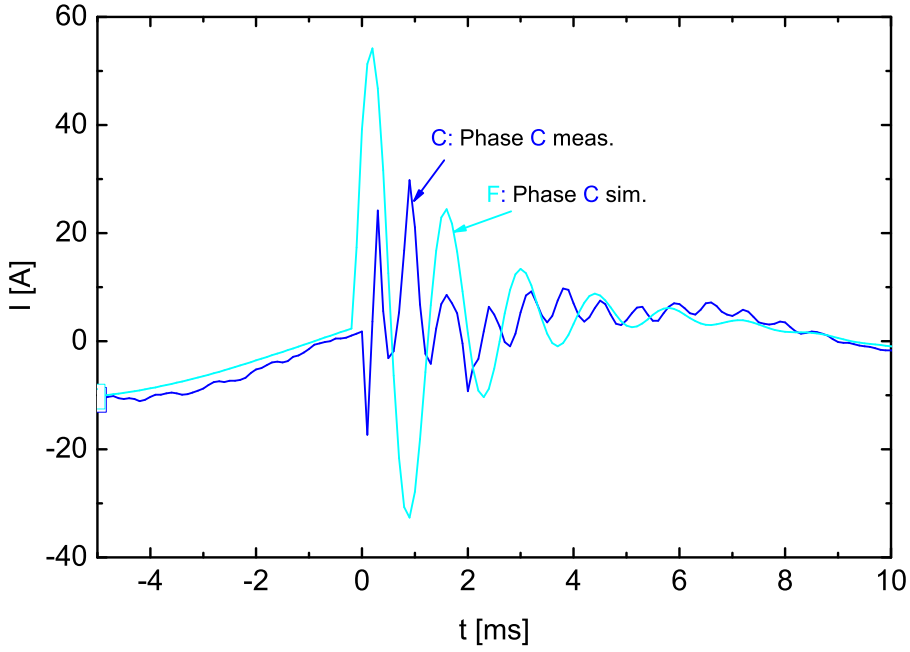

Figure 102: Transient currents I of phase C of the battery inverter connected with asynchronous generator and a 3 kW ohmic load which is connected at the time t = 0 ms to a 3 kVAr capacitive load.

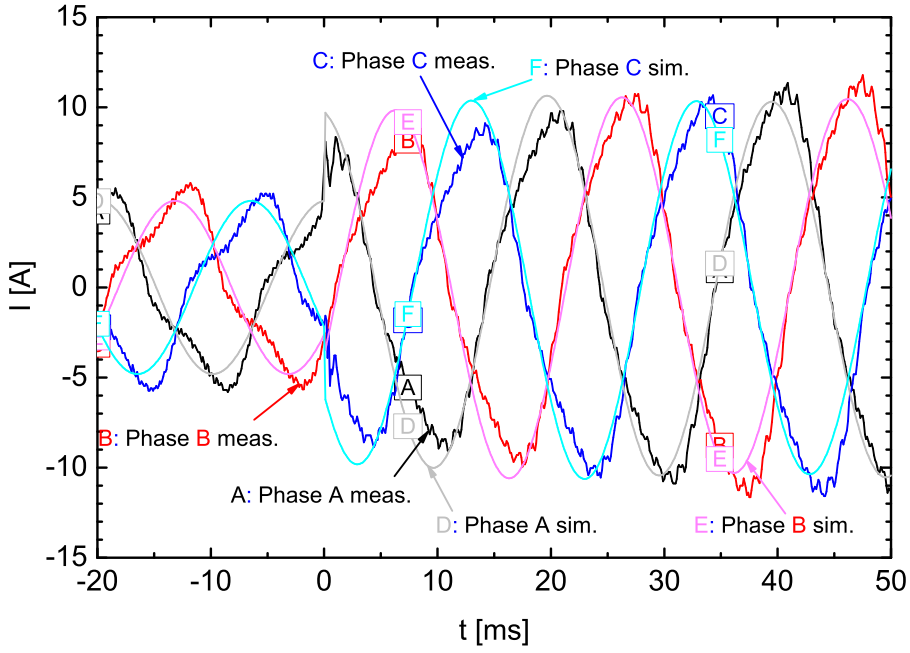

Figure 103: Transient currents I of the battery inverter in connection with the asynchronous generator supplying a 3 kW ohmic and a 3 kVAr capacitive load. The 3 kVAr capacitive load is disconnected at the time t = 0 ms.

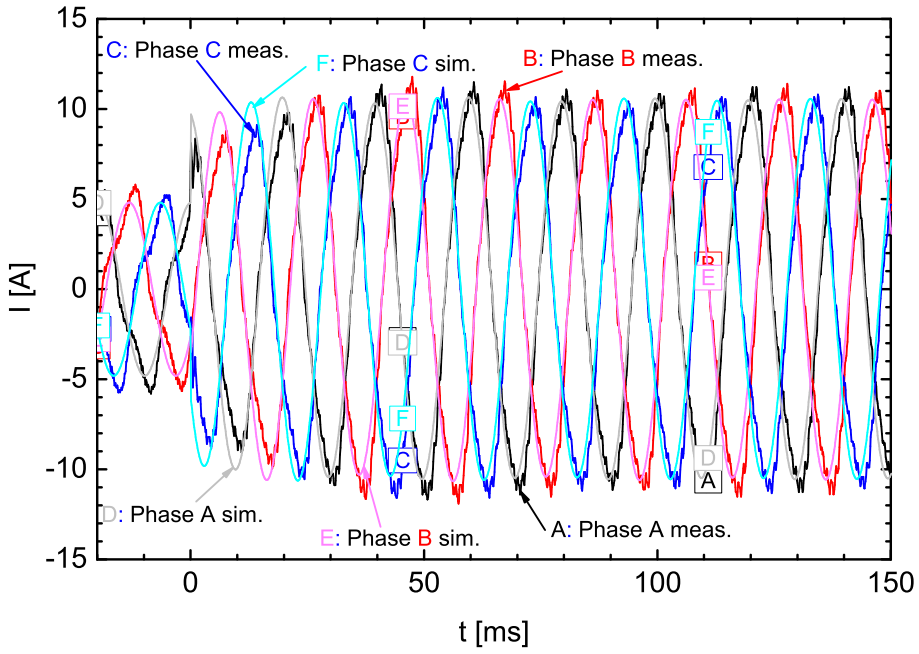

Figure 104: Transient currents I of the battery inverter in connection with the asynchronous generator supplying a 3 kW ohmic and a 3 kVAr capacitive load. The 3 kVAr capacitive load is disconnected at the time t = 0 ms. After the disconnection the currents tune.

A.2.4 Unbalanced change in ohmic load

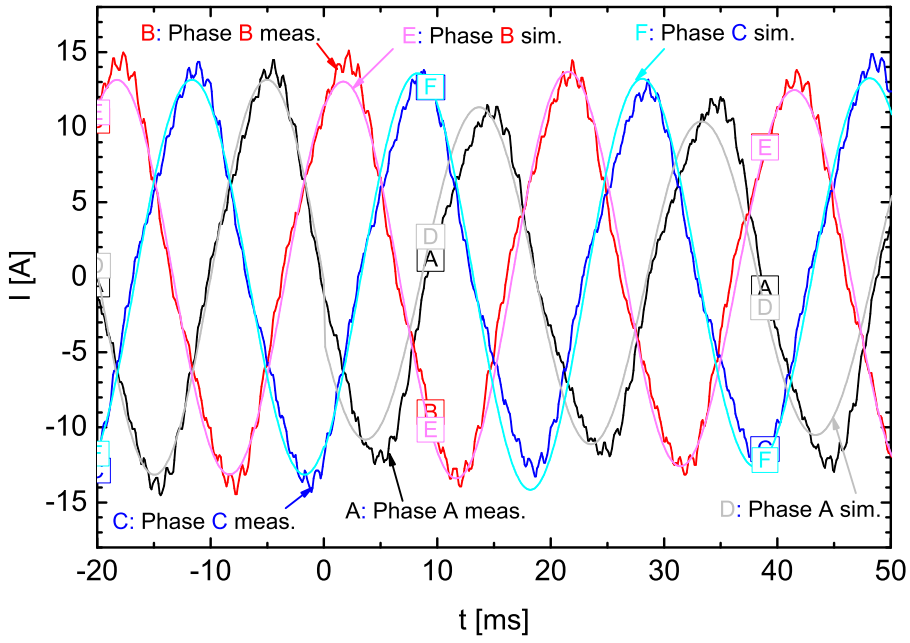

Figure 105: Transient currents I of the battery inverter which is connected with the asynchronous generator. At the time t = 0 ms a 1 kW ohmic load is connected to phase A.

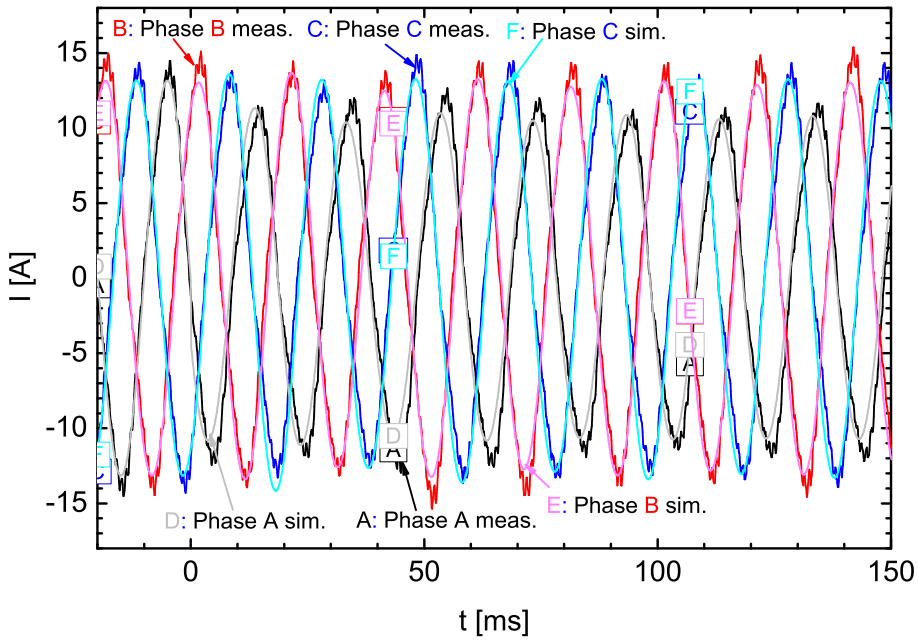

Figure 106: Transient currents I of the battery inverter which is connected with the asynchronous generator. At the time t = 0 ms a 1 kW ohmic load is connected to phase A. The transients of the following 150 ms are displayed.

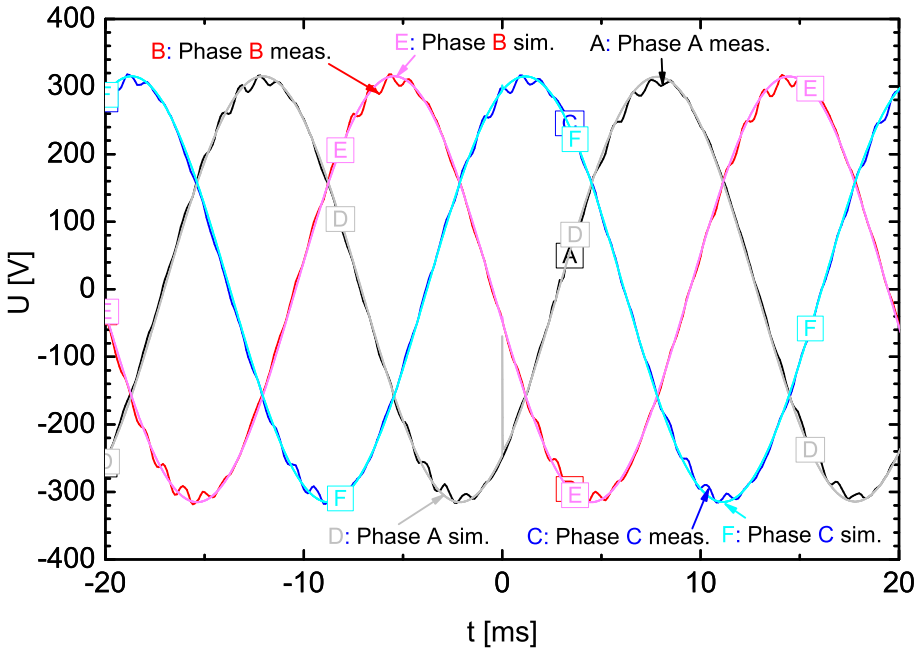

Figure 107: Transient voltages U of the battery inverter which is connected with the asynchronous generator. At the time t = 0 ms a 1 kW ohmic load is connected to phase A.

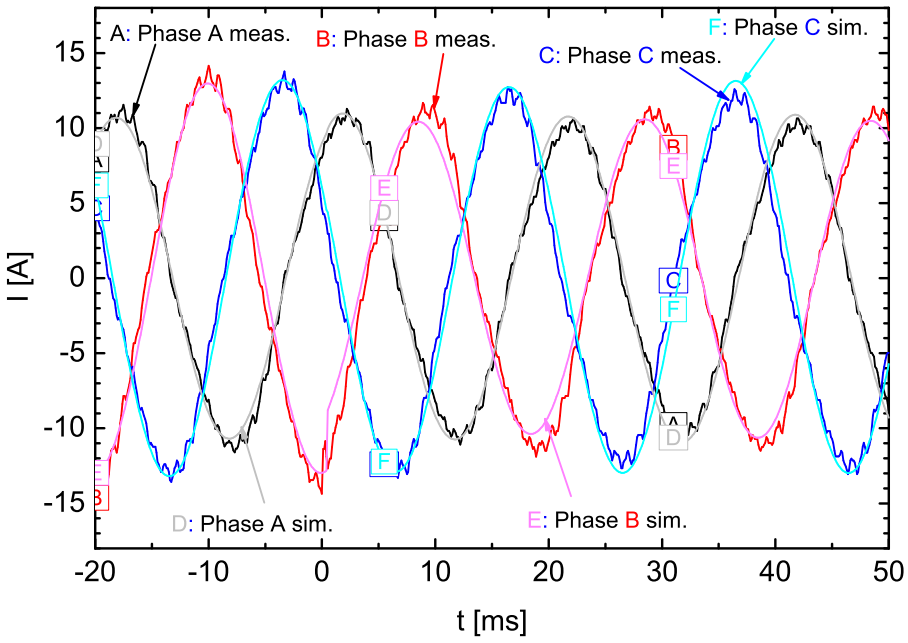

Figure 108: Transient currents I of the battery inverter which is connected with the asynchronous generator supplying a 1 kW ohmic load at phase A. At the time t = 0 ms a 1 kW ohmic load is connected to phase B.

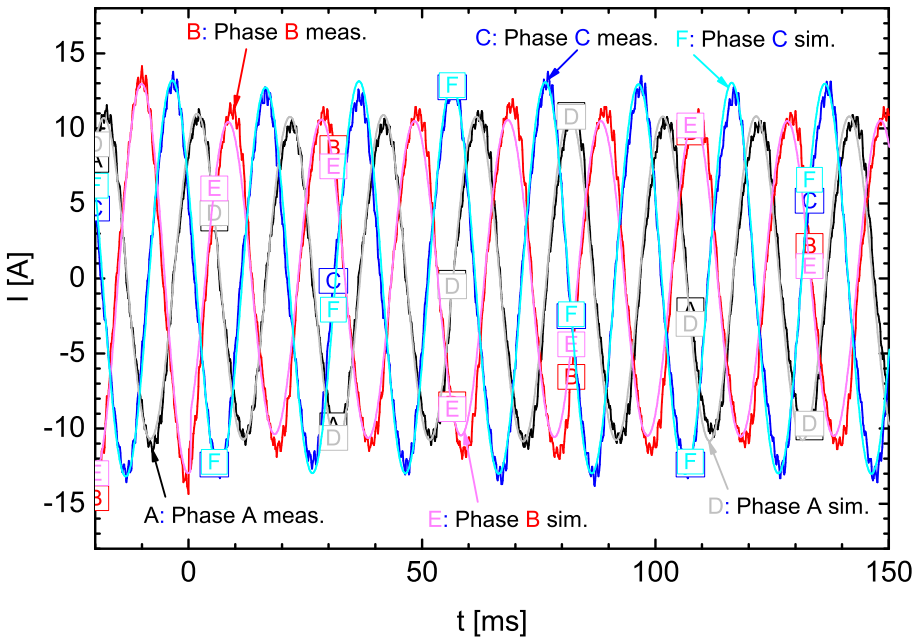

Figure 109: Transient currents I of the battery inverter which is connected with the asynchronous generator supplying a 1 kW ohmic load at phase A. At the time t = 0 ms a 1 kW ohmic load is connected to phase B. The transients of the following 150 ms are displayed.

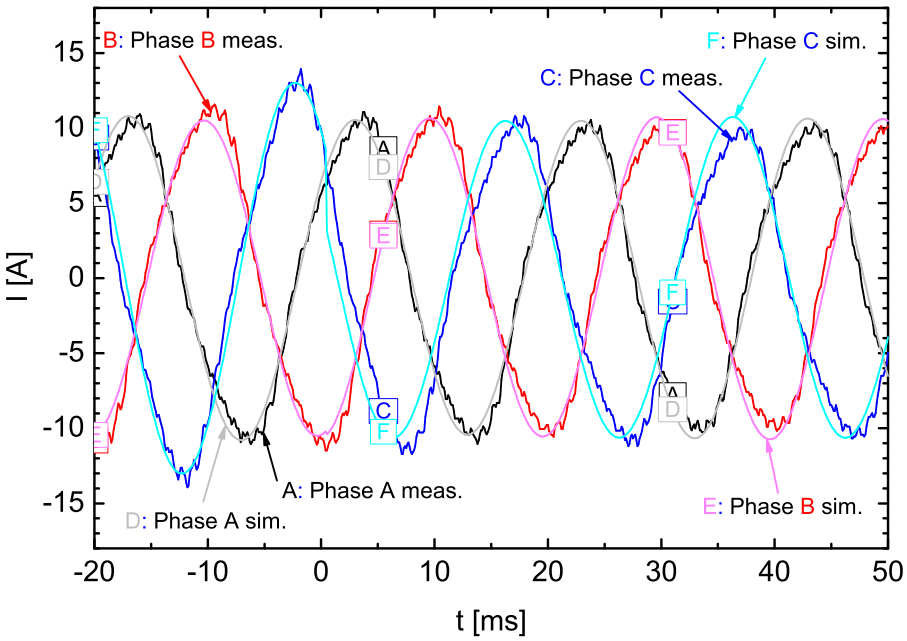

Figure 110: Transient currents I of the battery inverter which is connected with the asynchronous generator supplying a 1 kW ohmic load at phase A and a 1 kW ohmic load at phase B. At the time t = 0 ms a 1 kW ohmic load is connected to phase C.

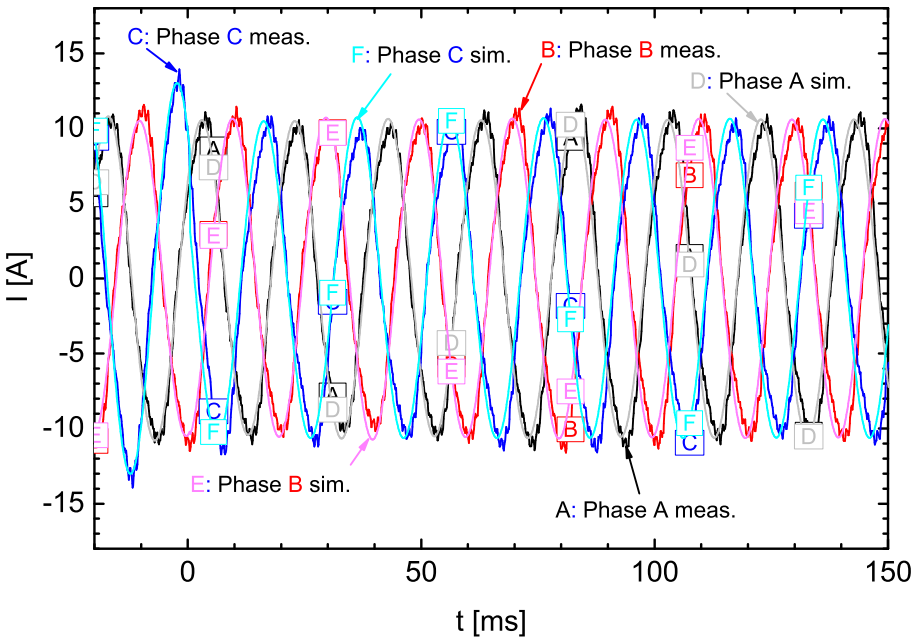

Figure 111: Transient currents I of the battery inverter which is connected with the asynchronous generator supplying a 1 kW ohmic load at phase A and a 1 kW ohmic load at phase B. At the time t = 0 ms a 1 kW ohmic load is connected to phase C. The transients of the following 150 ms are displayed.

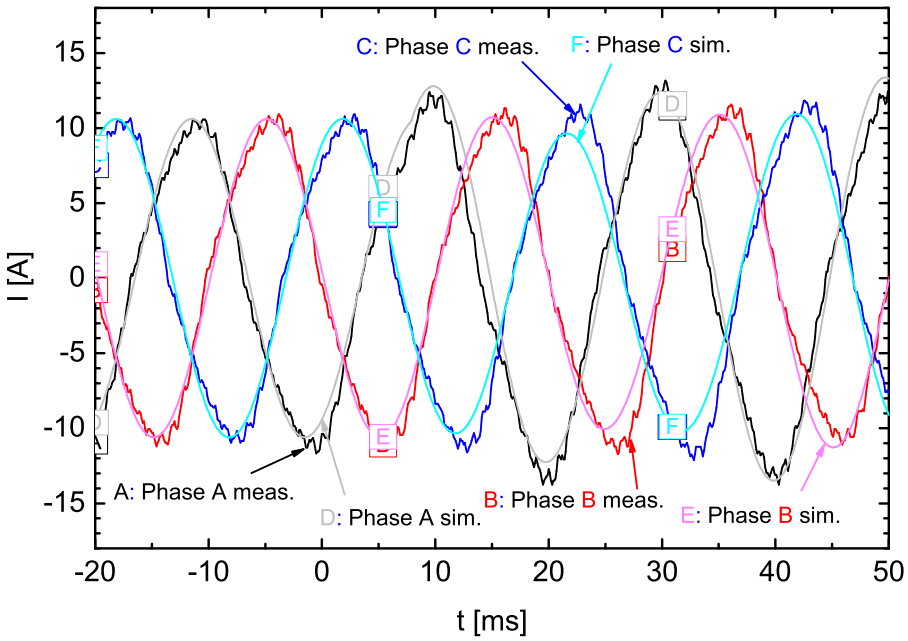

Figure 112: Transient currents I of the battery inverter which is connected with the asynchronous generator supplying 1 kW ohmic loads at all three phases. At the time t = 0 ms the 1 kW ohmic load at phase A is disconnected.

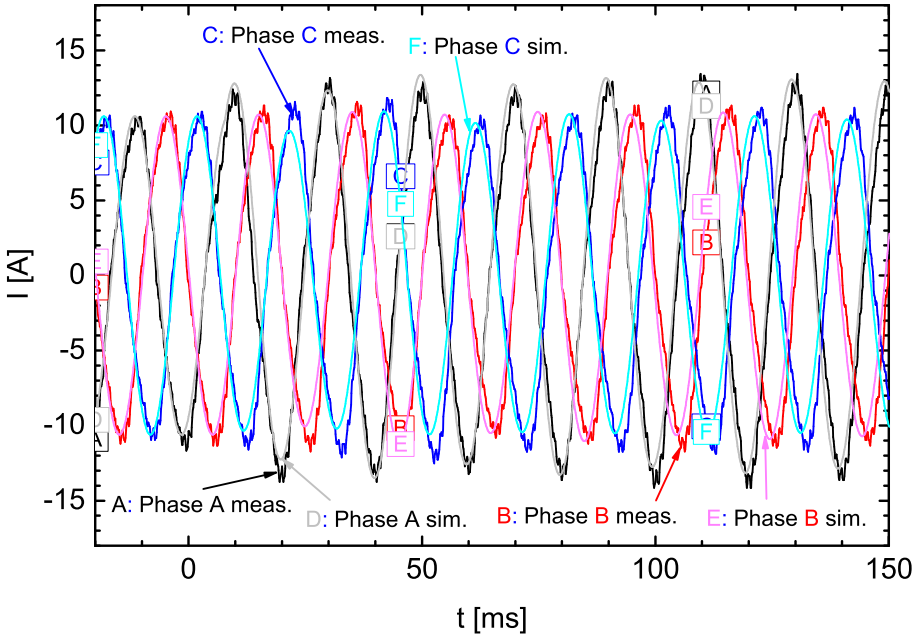

Figure 113: Transient currents I of the battery inverter which is connected with the asynchronous generator supplying 1 kW ohmic loads at all three phases. At the time t = 0 ms the 1 kW ohmic load at phase A is disconnected. The transients of the following 150 ms are displayed.

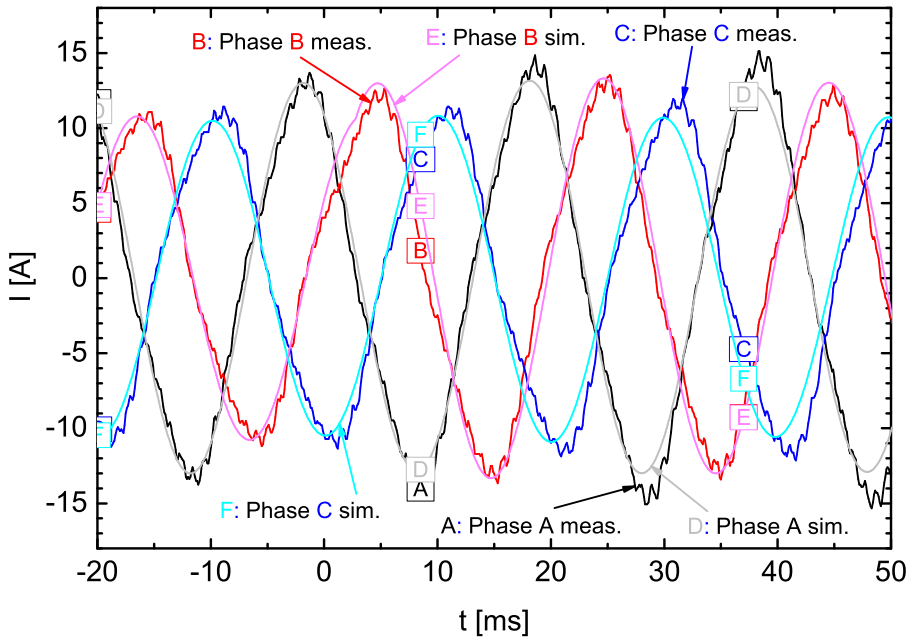

Figure 114: Transient currents I of the battery inverter which is connected with the asynchronous generator supplying 1 kW ohmic loads at phase B and phase C. At the time t = 0 ms the 1 kW ohmic load at phase B is disconnected.

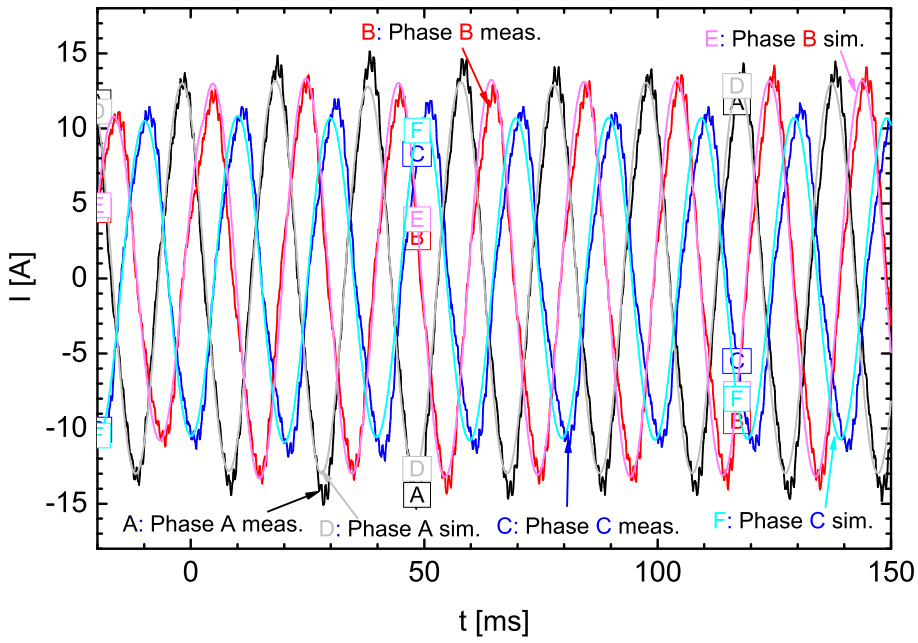

Figure 115: Transient currents I of the battery inverter which is connected with the asynchronous generator supplying 1 kW ohmic loads at phase B and phase C. At the time t = 0 ms the 1 kW ohmic load at phase B is disconnected. The transients of the following 150 ms are displayed.

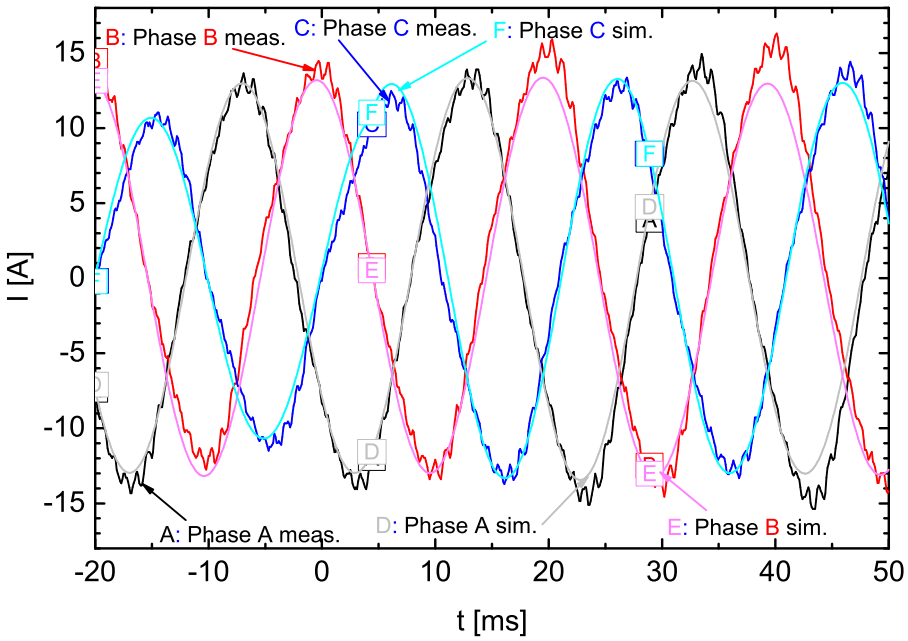

Figure 116: Transient currents I of the battery inverter which is connected with the asynchronous generator supplying a 1 kW ohmic load at phase C. At the time t = 0 ms the 1 kW ohmic load at phase C is disconnected.

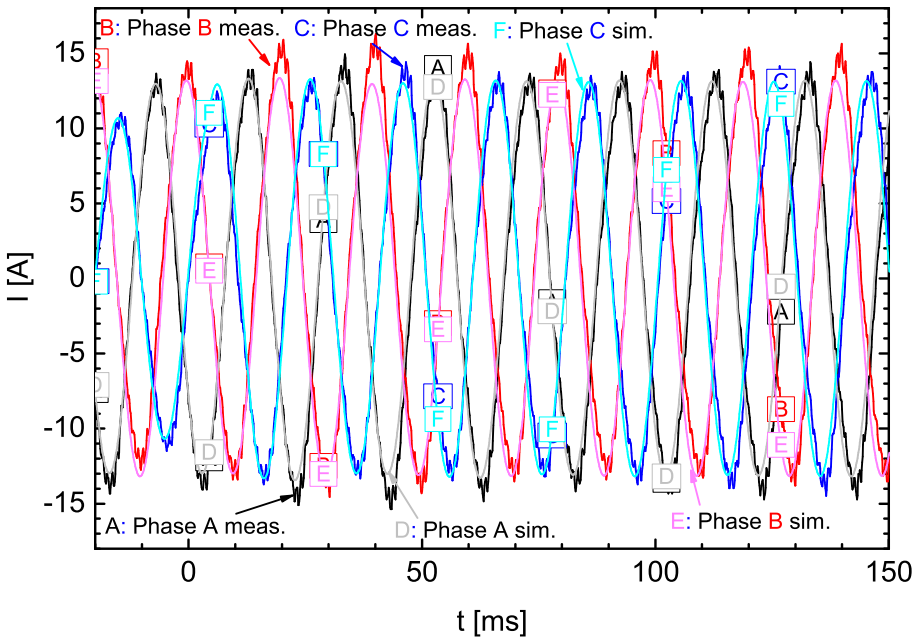

Figure 117: Transient currents I of the battery inverter which is connected with the asynchronous generator supplying a 1 kW ohmic load at phase C. At the time t = 0 ms the 1 kW ohmic load at phase C is disconnected. The transients of the following 150 ms are displayed.

A.2.5 Unbalanced change in inductive load

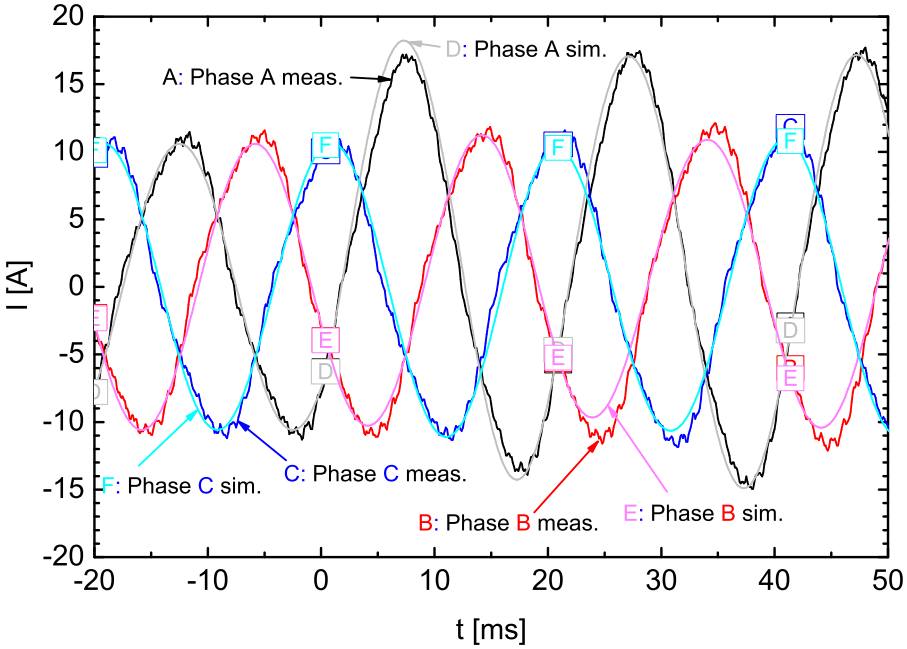

Figure 118: Transient currents I of the battery inverter which is connected with the asynchronous generator supplying a 1 kW ohmic load at each phase. At the time t = 0 ms, a 1 kVAr inductive load is connected to phase A.

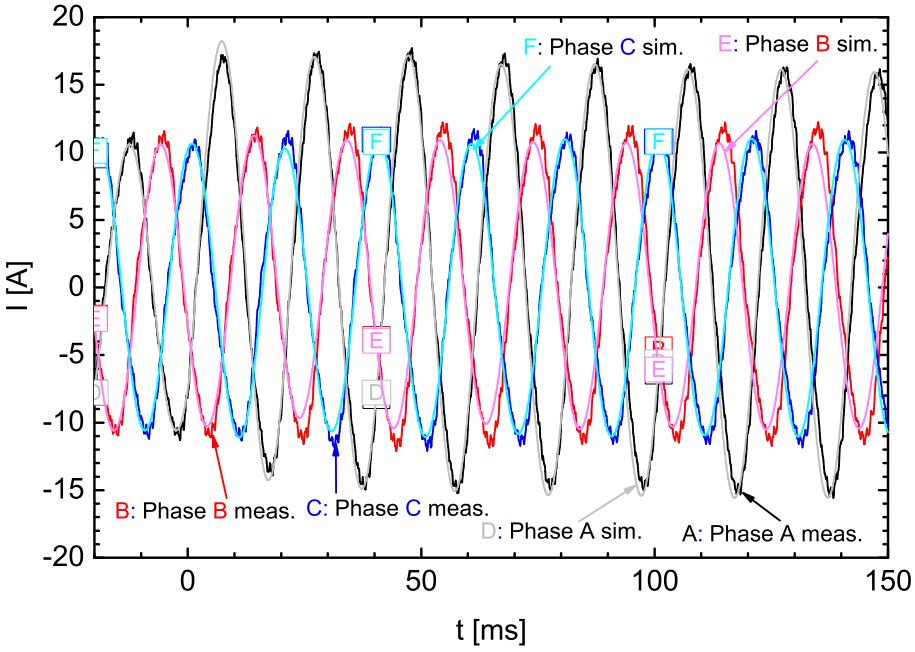

Figure 119: Transient currents I of the battery inverter which is connected with the asynchronous generator supplying a 1 kW ohmic load at each phase. At the time t = 0 ms, a 1 kVAr inductive load is connected to phase A. The transients of the following 150 ms are displayed.

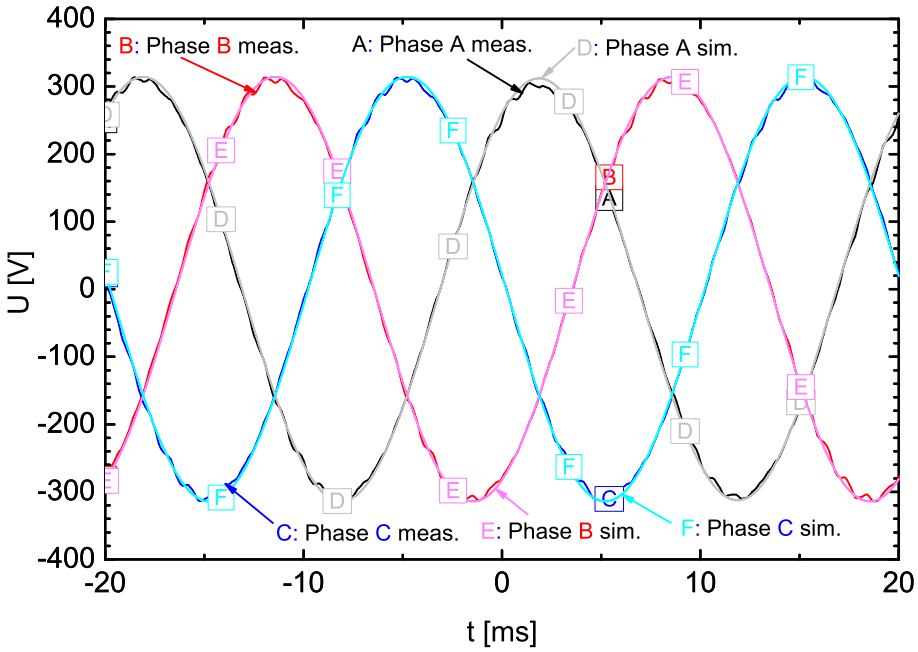

Figure 120: Transient voltages U of the battery inverter which is connected with the asynchronous generator supplying a 1 kW ohmic load at each phase. At the time t = 0 ms, a 1 kVAr inductive load is connected to phase A.

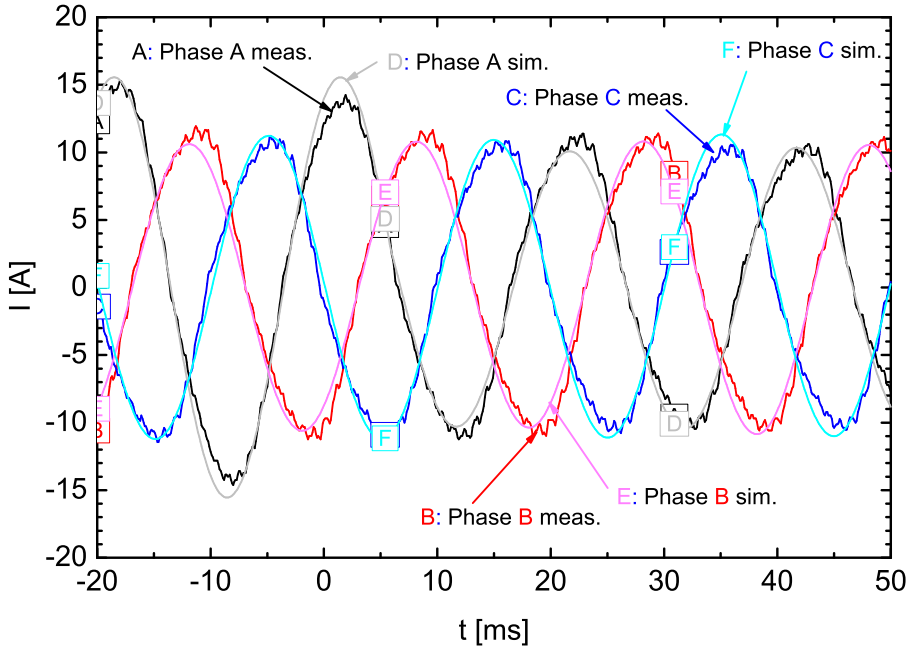

Figure 121: Transient currents I of the battery inverter which is connected with the asynchronous generator supplying a 1 kW ohmic load at each phase and a 1 kVAr inductive load at phase A. The inductive load at phase A is disconnected at the time t = 0 ms.

A.2.6 Unbalanced change in capacitive load

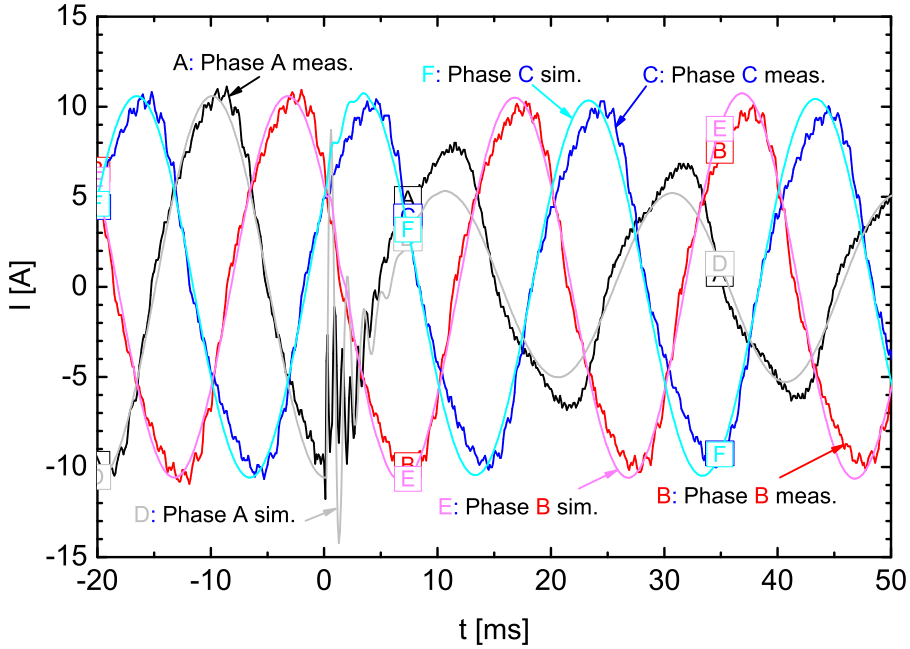

Figure 122: Transient currents I of the battery inverter which is connected with the asynchronous generator supplying a 1 kW ohmic load at each phase. At the time t = 0 ms, a 1 kVAr capacitive load is connected to phase A.

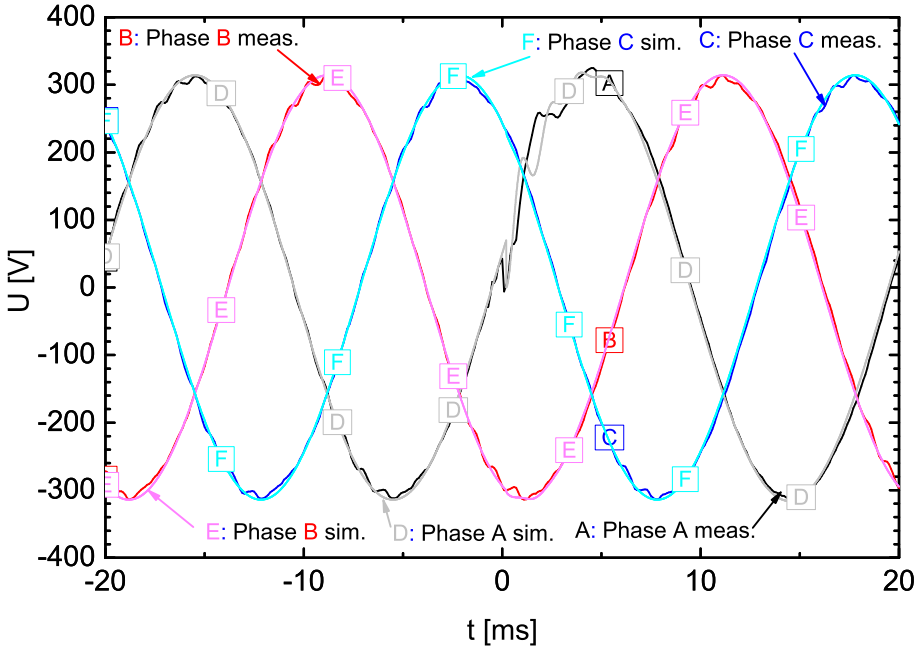

Figure 123: Transient voltages U of the battery inverter which is connected with the asynchronous generator supplying a 1 kW ohmic load at each phase. At the time t = 0 ms, a 1 kVAr capacitive load is connected to phase A.

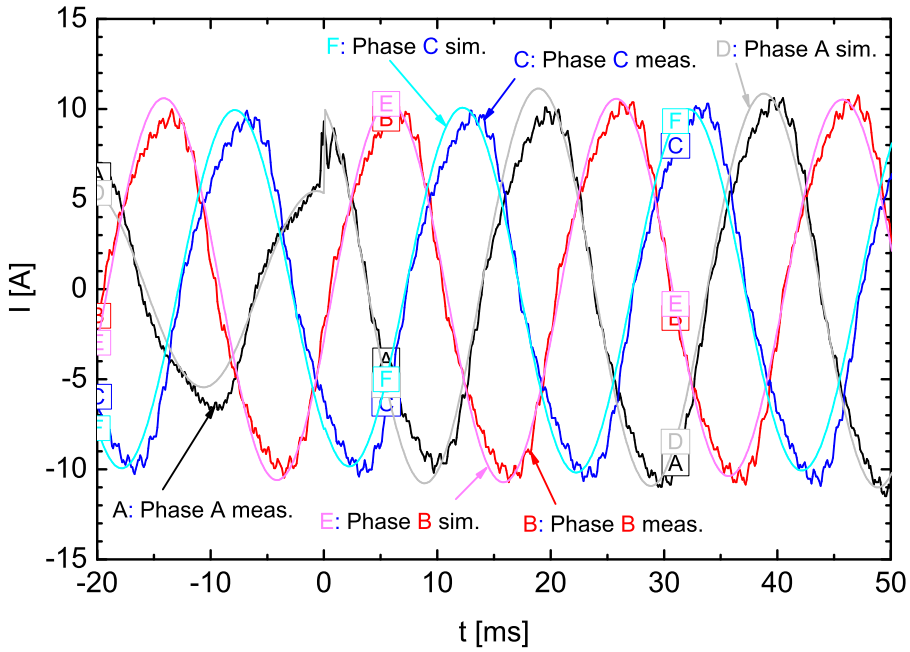

Figure 124: Transient currents I of the battery inverter which is connected with the asynchronous generator supplying a 1 kW ohmic load at each phase and a 1 kVAr capacitive load at phase A. The capacitive load at phase A is disconnected at the time t = 0 ms.

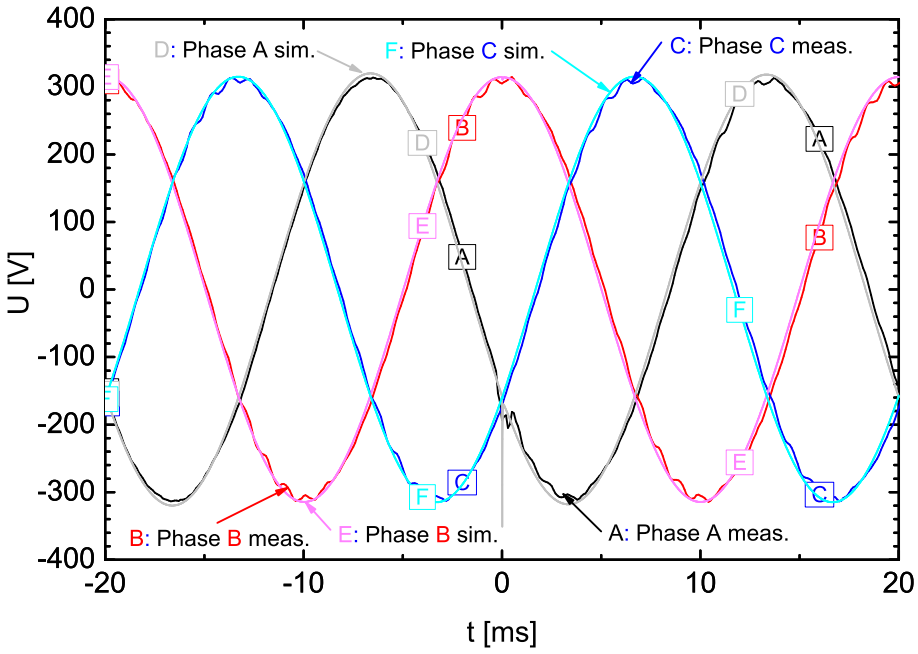

Figure 125: Transient voltages U of the battery inverter which is connected with the asynchronous generator supplying a 1 kW ohmic load at each phase and a 1 kVAr capacitive load at phase A. The capacitive load at phase A is disconnected at the time t = 0 ms.

A.3 Enlarged grid configuration with two battery inverters and a load

A.3.1 Droop ratio 1:1

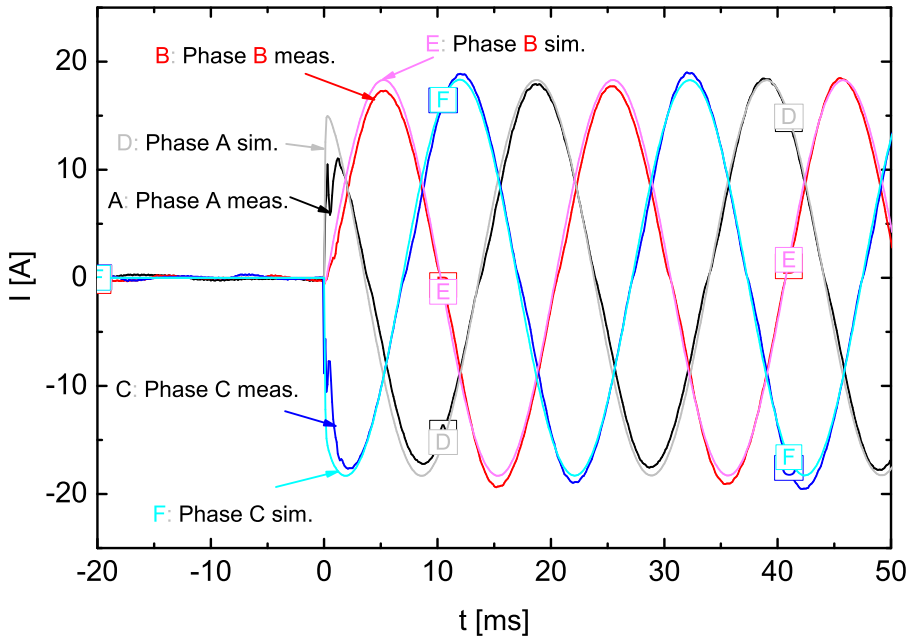

Figure 126: Transient currents I of the battery inverter Sunny Island 1 which operates in parallel with battery inverter Sunny Island 2 with a droop ratio of 1:1. They are connected at the time t = 0 ms to a 18 kW ohmic load.

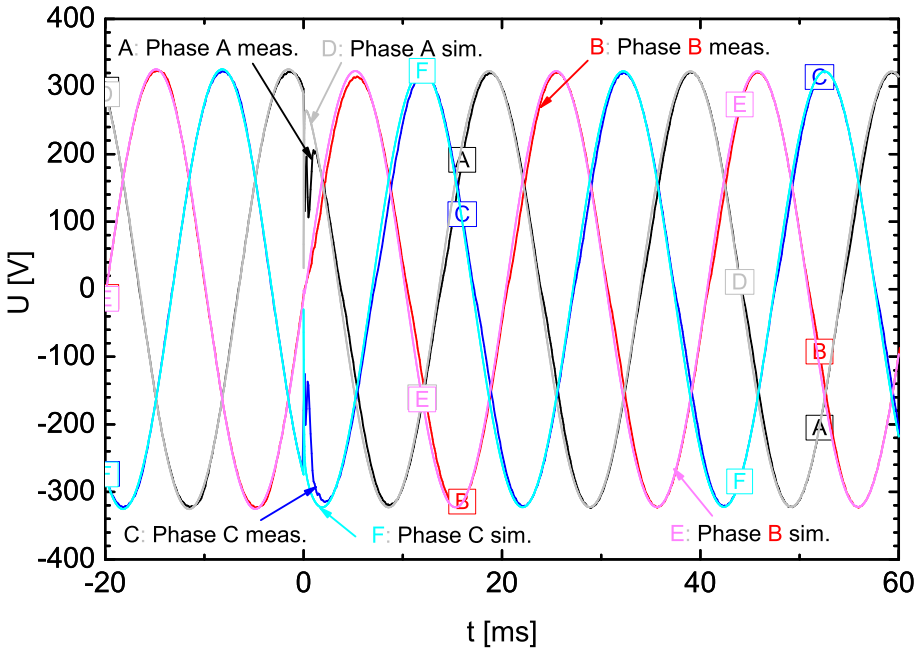

Figure 127: Transient voltages U of the battery inverter Sunny Island 1 which operates in parallel with battery inverter Sunny Island 2 with a droop ratio of 1:1. They are connected at the time t = 0 ms to a 18 kW ohmic load.

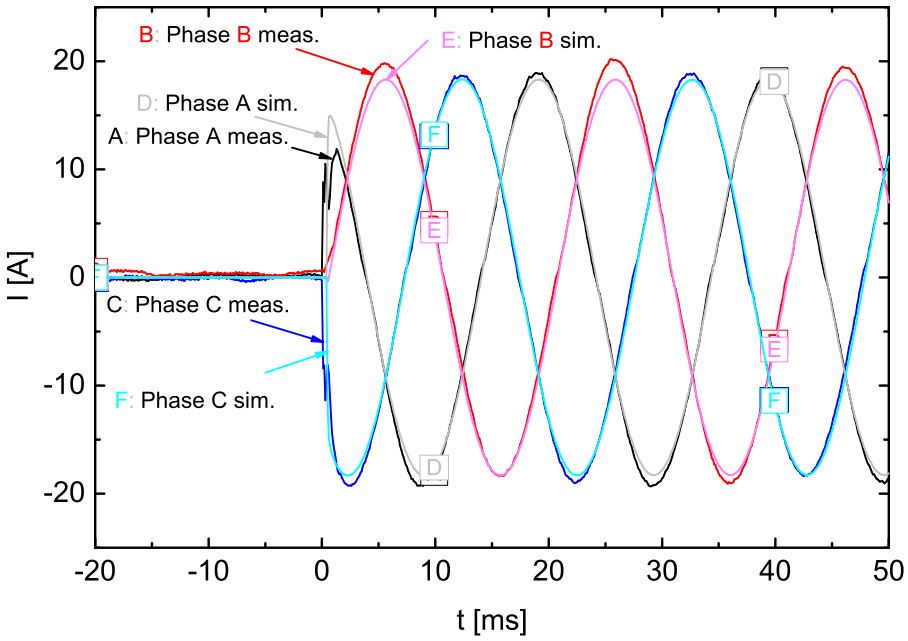

Figure 128: Transient currents I of the battery inverter Sunny Island 2 which operates in parallel with battery inverter Sunny Island 1 with a droop ratio of 1:1. They are connected at the time t = 0 ms to a 18 kW ohmic load.

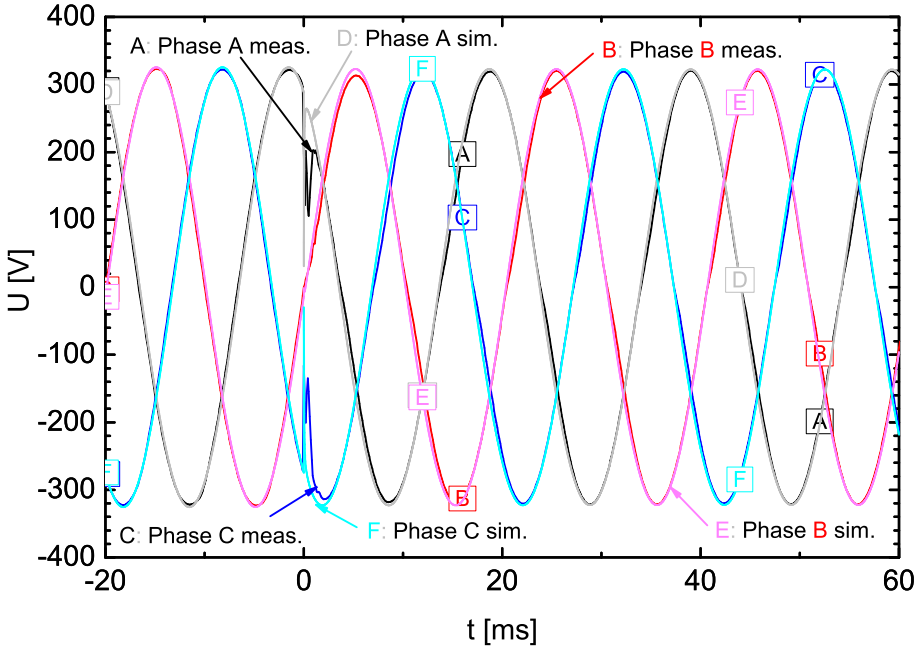

Figure 129: Transient voltages U of the battery inverter Sunny Island 2 which operates in parallel with battery inverter Sunny Island 1 with a droop ratio of 1:1. They are connected at the time t = 0 ms to a 18 kW ohmic load.

A.3.2 Droop ratio 2:1

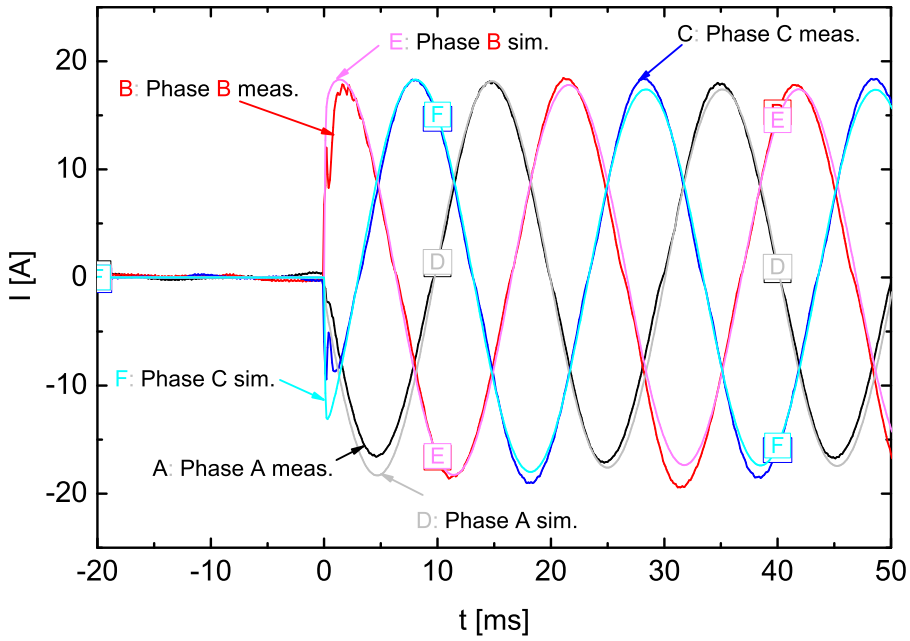

Figure 130: Transient currents I of the battery inverter Sunny Island 1 which operates in parallel with battery inverter Sunny Island 2 with a droop ratio of 2:1. They are connected at the time t = 0 ms to a 18 kW ohmic load.

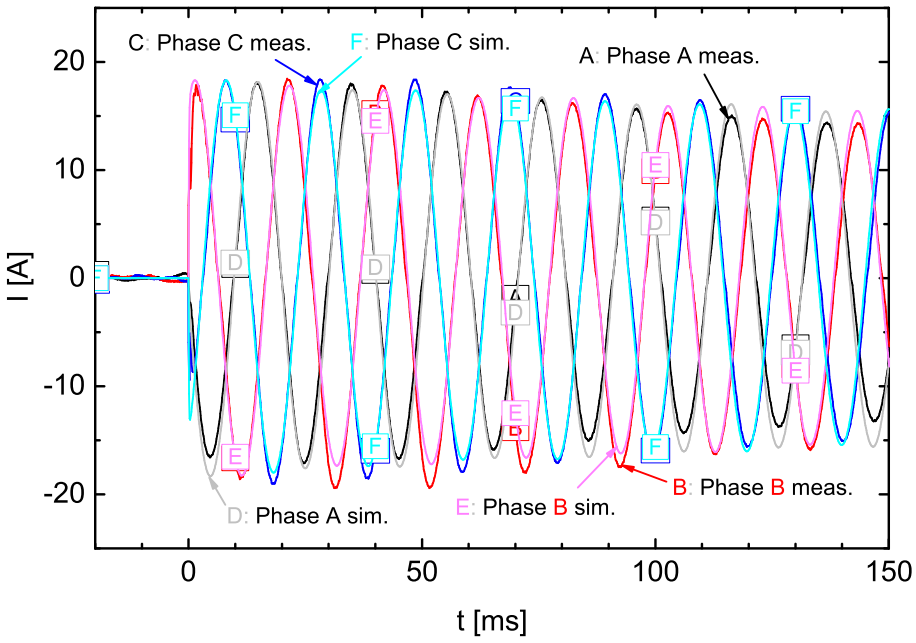

Figure 131: Transient currents I of the battery inverter Sunny Island 1 which operates in parallel with battery inverter Sunny Island 2 with a droop ratio of 2:1. They are connected at the time t = 0 ms to a 18 kW ohmic load. The figure shows the decline of the transient currents.

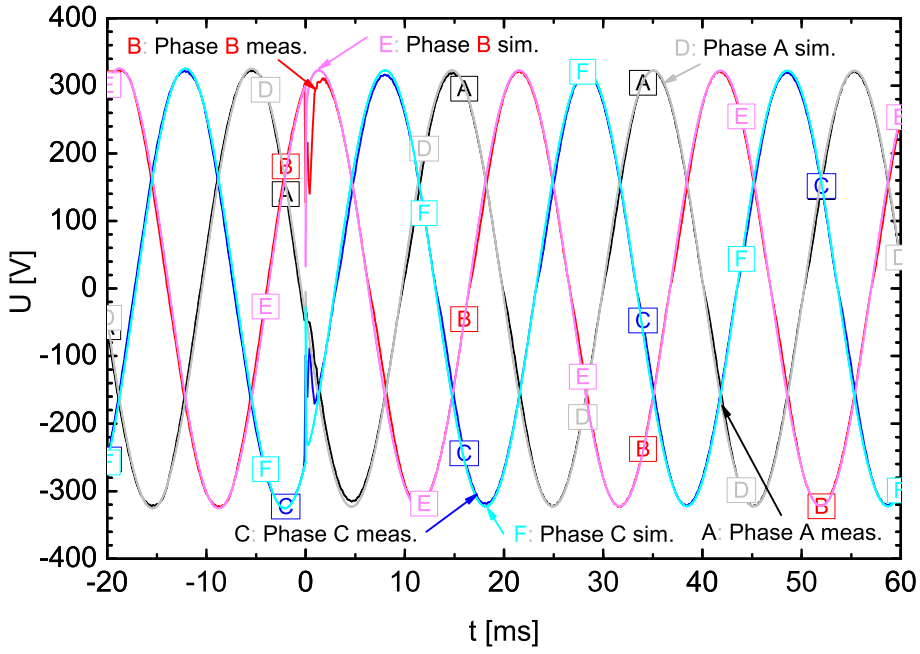

Figure 132: Transient voltages U of the battery inverter Sunny Island 1 which operates in parallel with battery inverter Sunny Island 2 with a droop ratio of 2:1. They are connected at the time t = 0 ms to a 18 kW ohmic load.

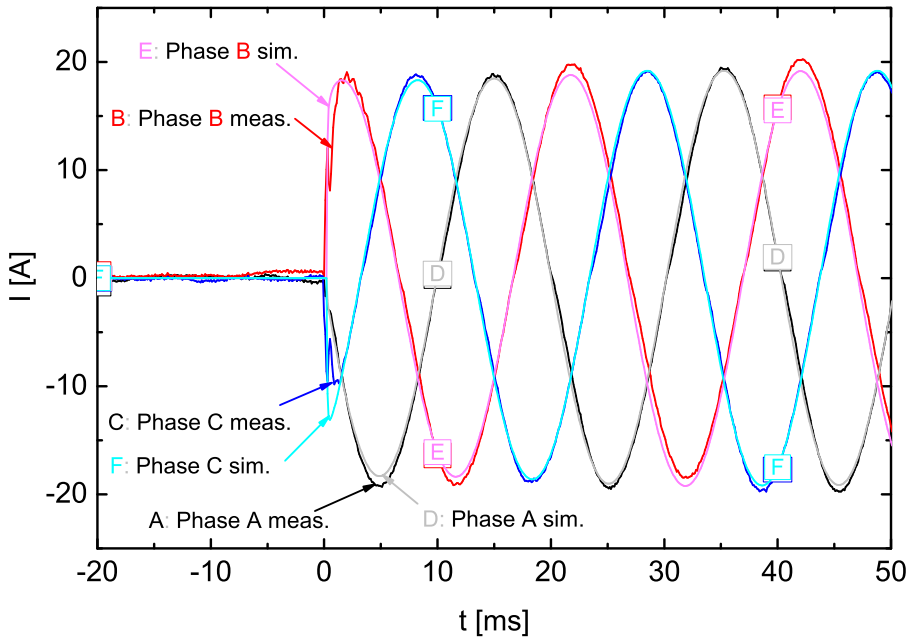

Figure 133: Transient currents I of the battery inverter Sunny Island 2 which operates in parallel with battery inverter Sunny Island 1 with a droop ratio of 1:2. They are connected at the time t = 0 ms to a 18 kW ohmic load.

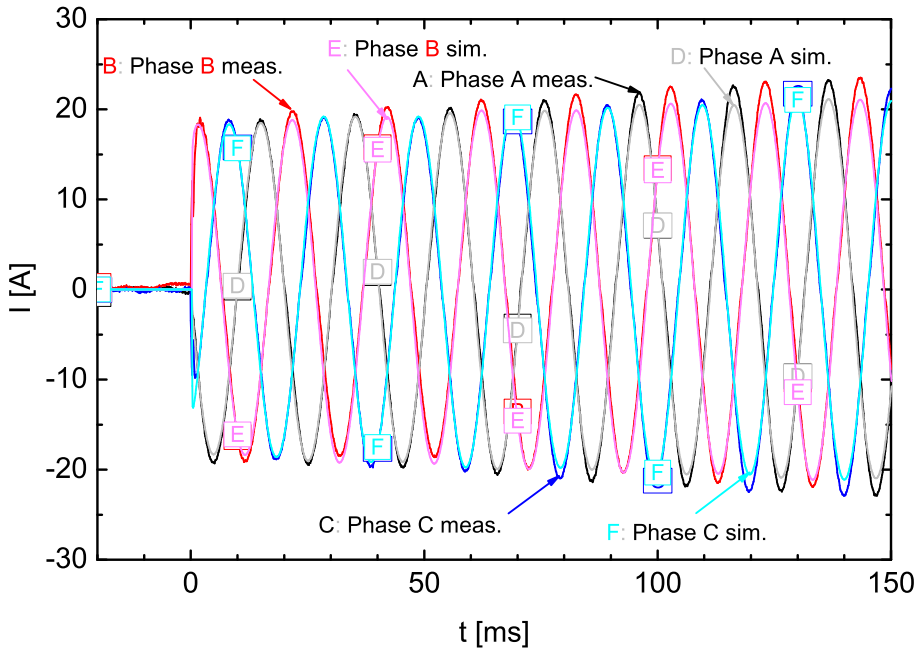

Figure 134: Transient currents I of the battery inverter Sunny Island 2 which operates in parallel with battery inverter Sunny Island 1 with a droop ratio of 1:2. They are connected at the time t = 0 ms to a 18 kW ohmic load. The figure shows the increase of the transient currents.

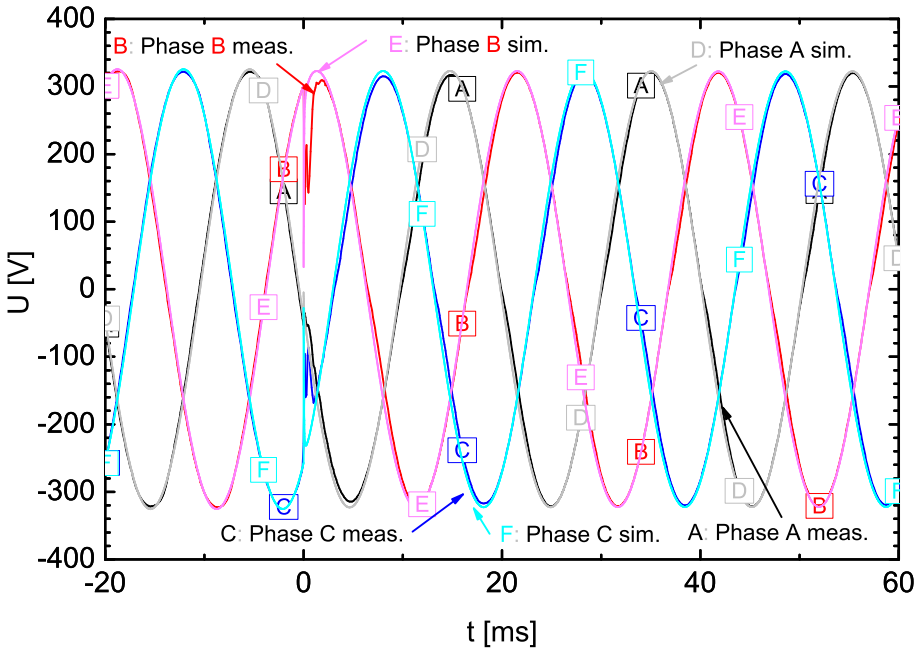

Figure 135: Transient voltages U of the battery inverter Sunny Island 2 which operates in parallel with battery inverter Sunny Island 1 with a droop ratio of 1:2. They are connected at the time t = 0 ms to a 18 kW ohmic load.

A.3.3 Droop ratio 3:1

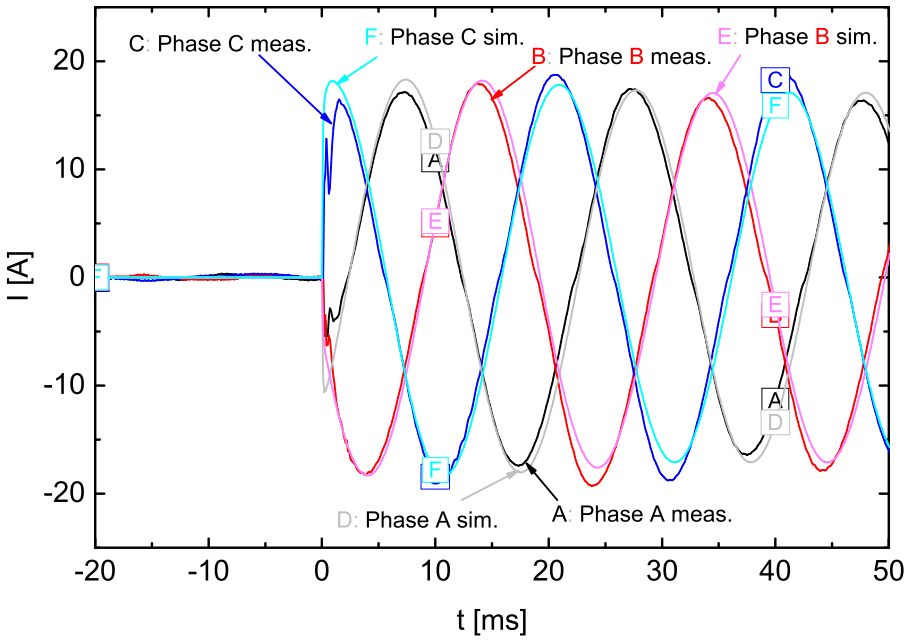

Figure 136: Transient currents I of the battery inverter Sunny Island 1 which operates in parallel with battery inverter Sunny Island 2 with a droop ratio of 3:1. They are connected at the time t = 0 ms to a 18 kW ohmic load.

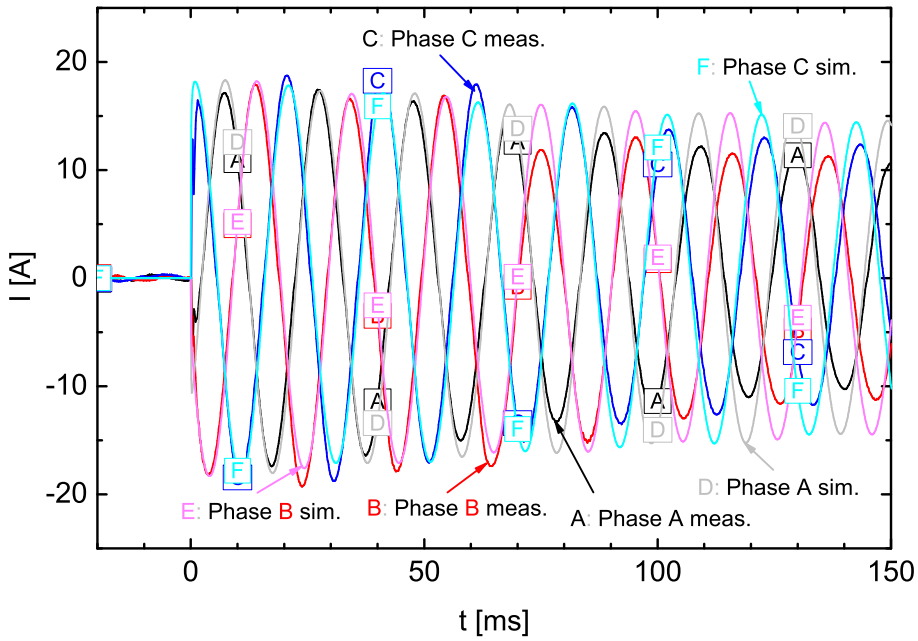

Figure 137: Transient currents I of the battery inverter Sunny Island 1 which operates in parallel with battery inverter Sunny Island 2 with a droop ratio of 3:1. They are connected at the time t = 0 ms to a 18 kW ohmic load. The figure shows the decline of the transient currents.

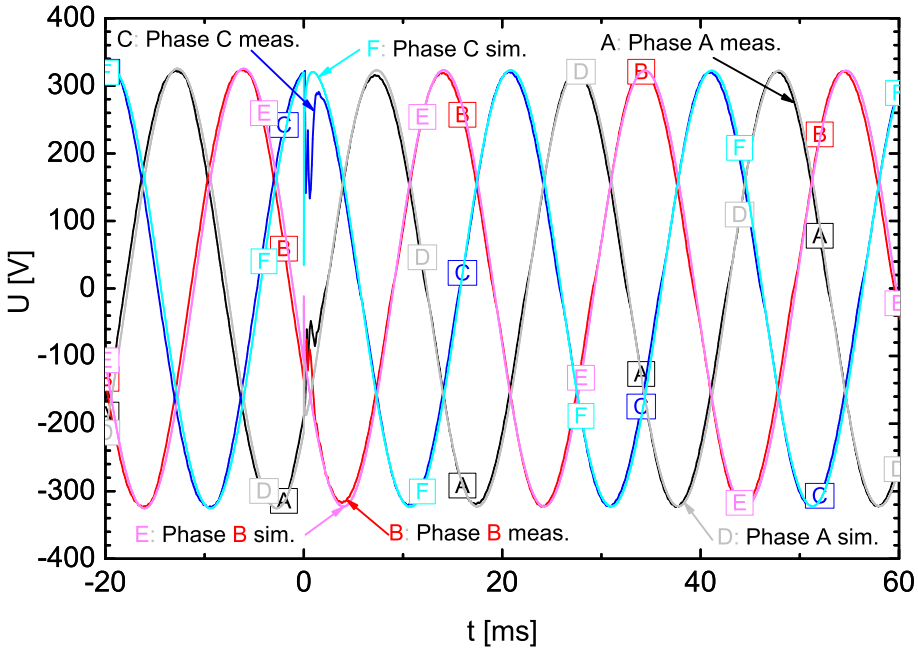

Figure 138: Transient voltages U of the battery inverter Sunny Island 1 which operates in parallel with battery inverter Sunny Island 2 with a droop ratio of 3:1. They are connected at the time t = 0 ms to a 18 kW ohmic load.

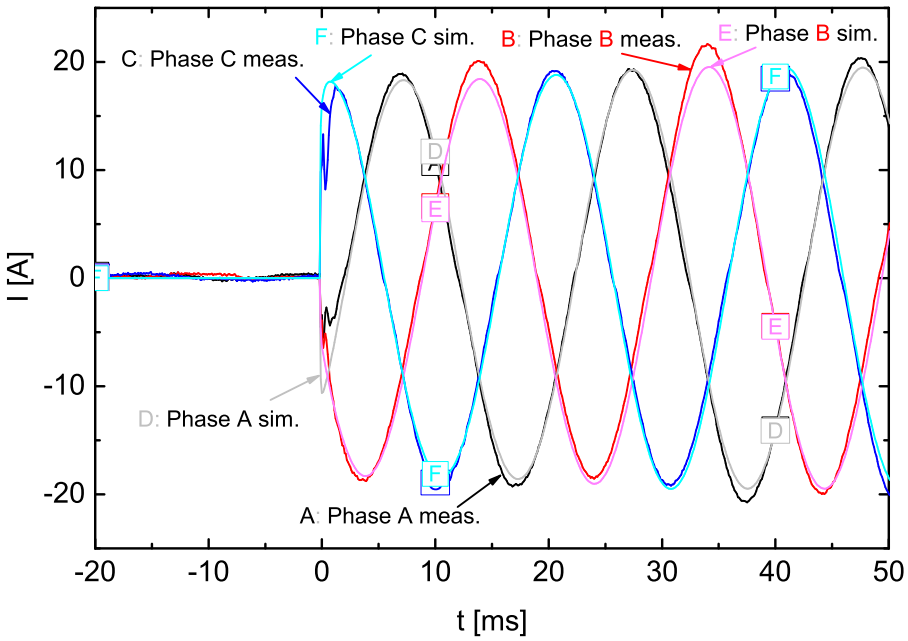

Figure 139: Transient currents I of the battery inverter Sunny Island 2 which operates in parallel with battery inverter Sunny Island 1 with a droop ratio of 1:3. They are connected at the time t = 0 ms to a 18 kW ohmic load.

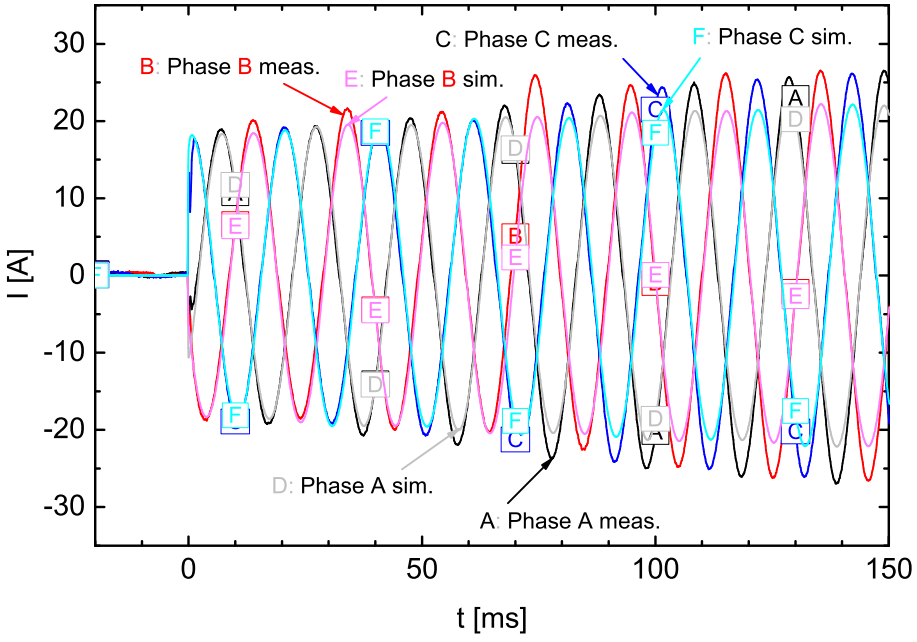

Figure 140: Transient currents I of the battery inverter Sunny Island 2 which operates in parallel with battery inverter Sunny Island 1 with a droop ratio of 1:3. They are connected at the time t = 0 ms to a 18 kW ohmic load. The figure shows the increase of the transient currents.

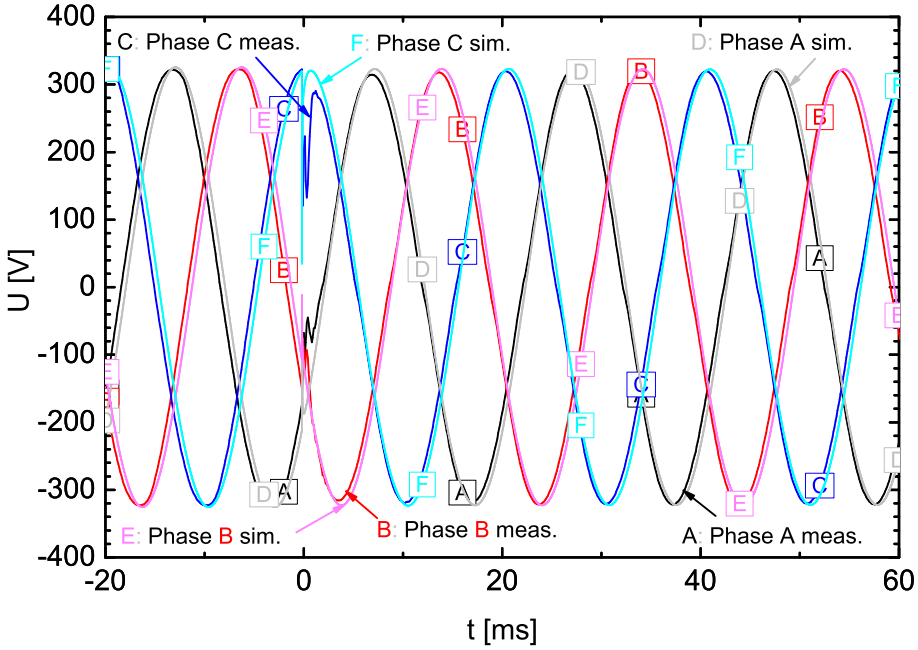

Figure 141: Transient voltages U of the battery inverter Sunny Island 2 which operates in parallel with battery inverter Sunny Island 1 with a droop ratio of 1:3. They are connected at the time t = 0 ms to a 18 kW ohmic load.

B Figures of Case Study

The figures in appendix B show all simulated voltage and current signals of the case study described in chapter 4. Some of the figures in chapter 4 are reproduced in the appendix.

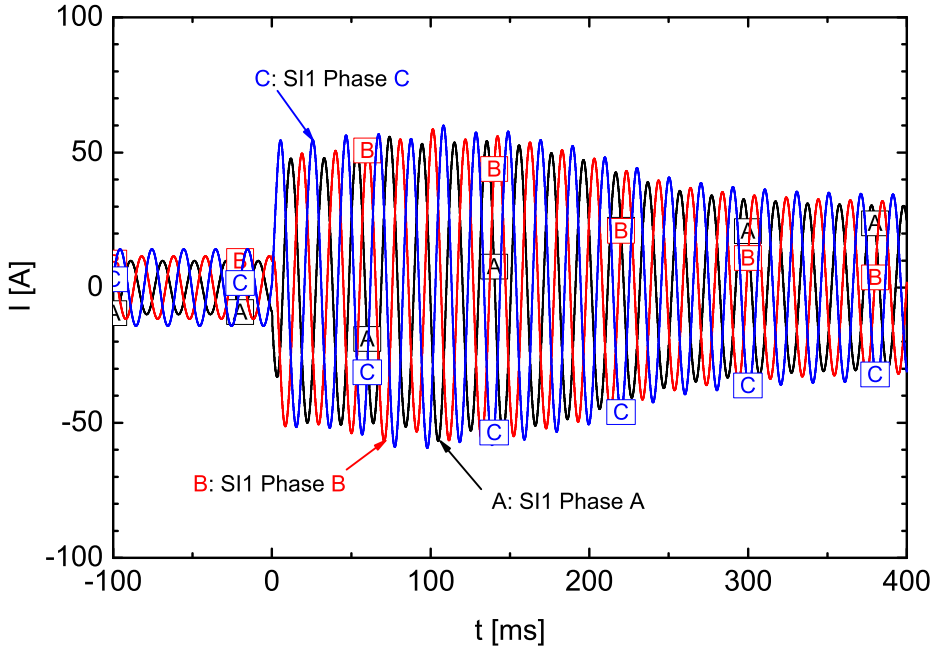

Figure 142: Transient currents I of the battery inverter Sunny Island 1 (SI1). The connection of the 15 kW asynchronous machines is at the time t = 0 ms.

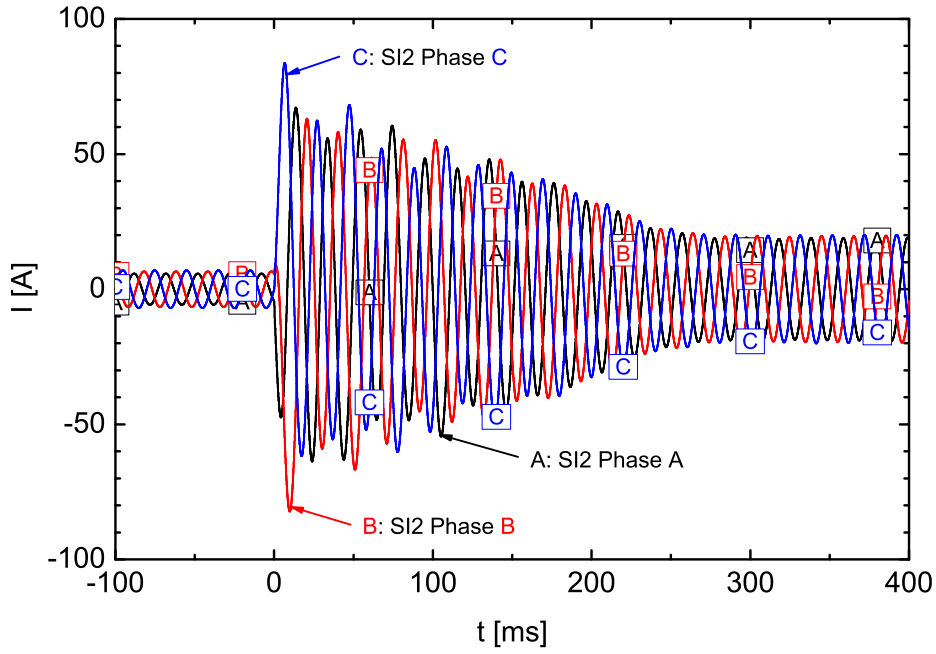

Figure 143: Transient currents I of the battery inverter Sunny Island 2 (SI2). The connection of the 15 kW asynchronous machines is at the time t = 0 ms.

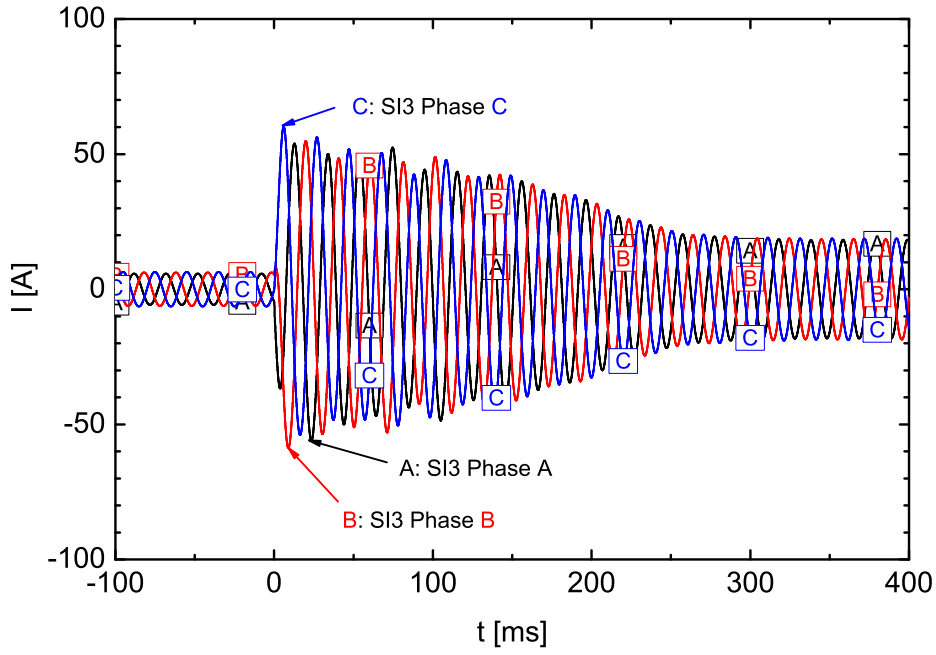

Figure 144: Transient currents I of the battery inverter Sunny Island 3 (SI3). The connection of the 15 kW asynchronous machines is at the time t = 0 ms.

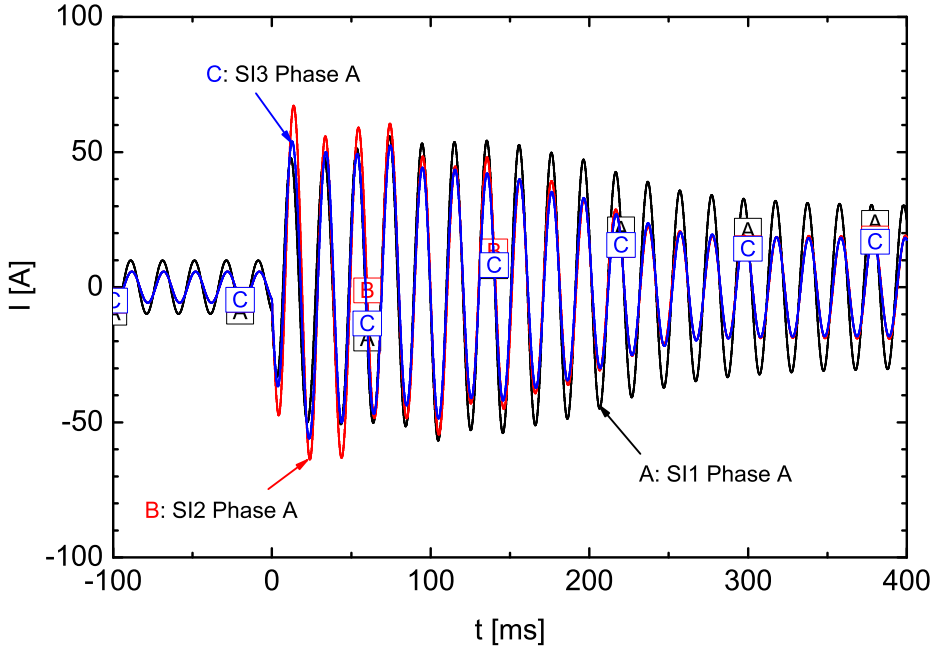

Figure 145: Comparison of the transient currents I of phase A of the three battery inverters SI1, SI2 and SI3. The connection of the 15 kW asynchronous machines is at the time t = 0 ms.

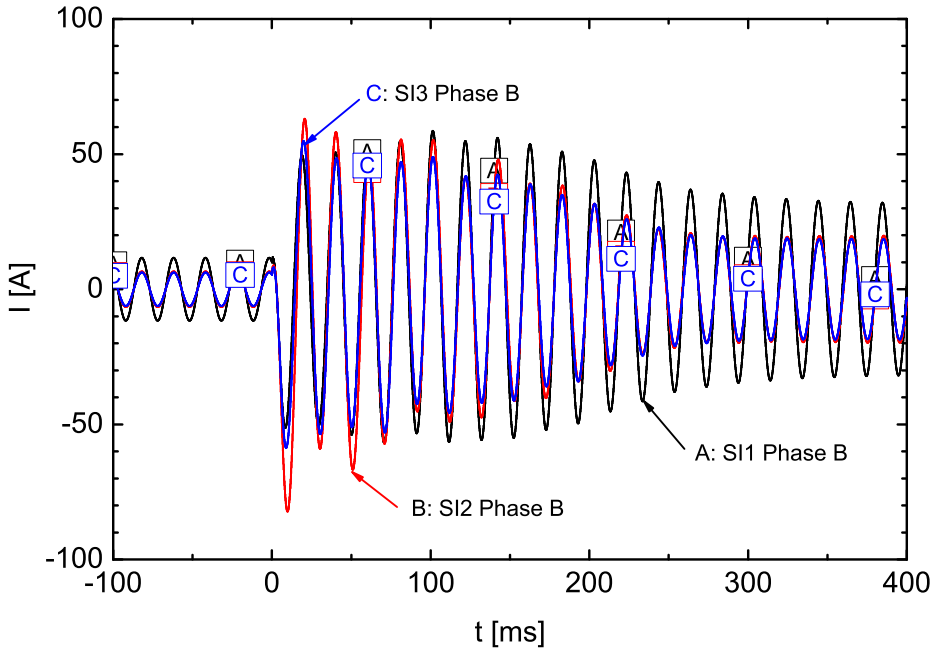

Figure 146: Comparison of the transient currents I of phase B of the three battery inverters SI1, SI2 and SI3. The connection of the 15 kW asynchronous machines is at the time t = 0 ms.

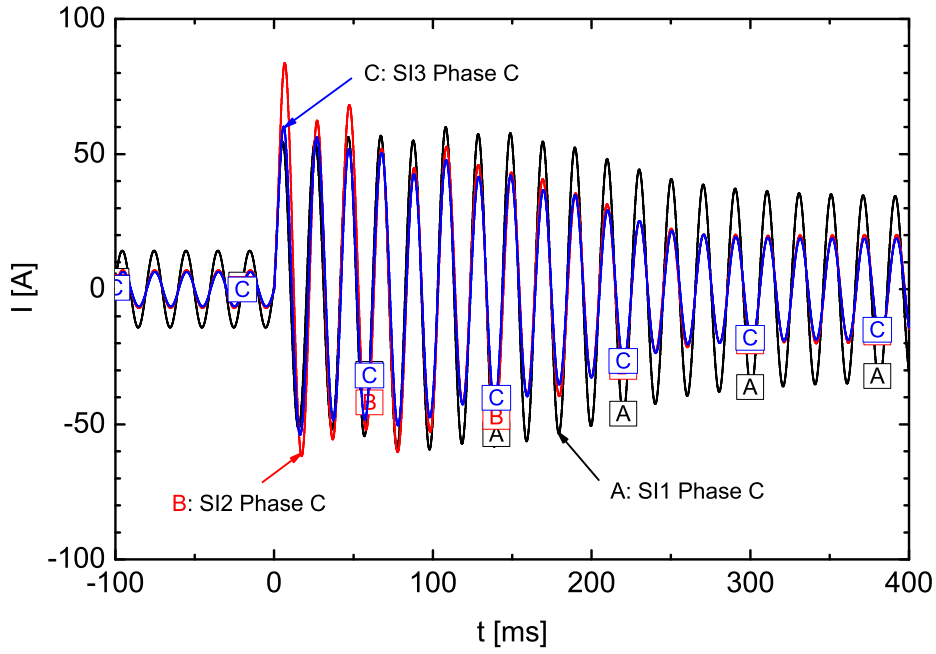

Figure 147: Comparison of the transient currents I of phase C of the three battery inverters SI1, SI2 and SI3. The connection of the 15 kW asynchronous machines is at the time t = 0 ms.

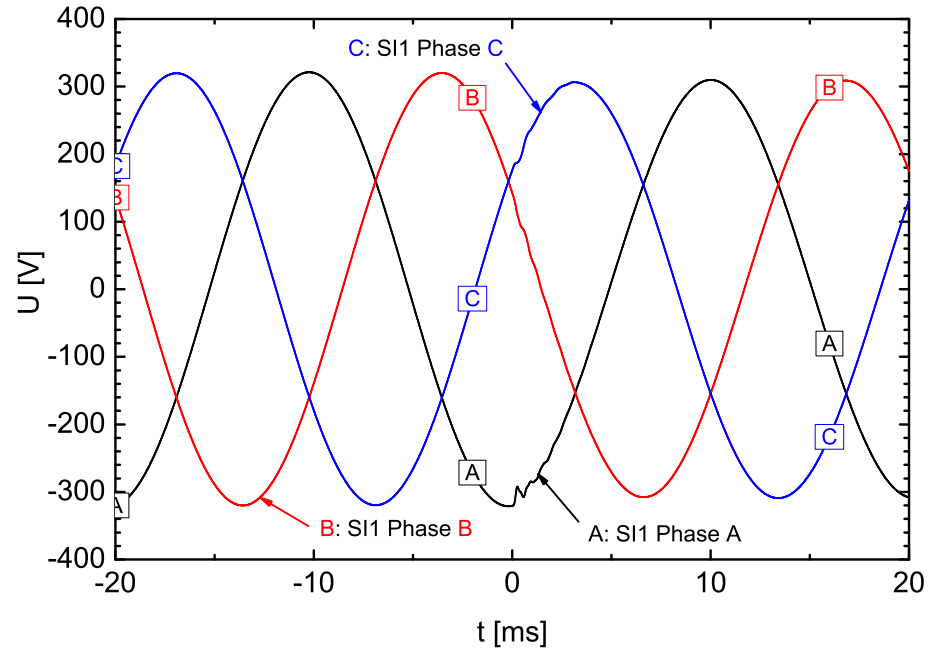

Figure 148: Transient voltages U of the battery inverter Sunny Island 1 (SI1). The connection of the 15 kW asynchronous machines is at the time t = 0 ms.

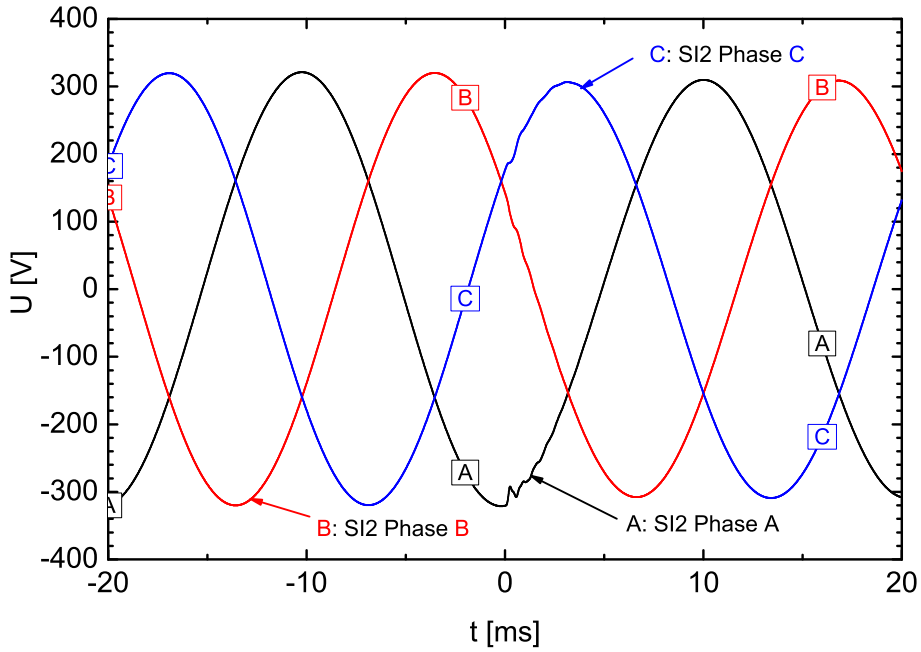

Figure 149: Transient voltages U of the battery inverter Sunny Island 2 (SI2). The connection of the 15 kW asynchronous machines is at the time t = 0 ms.

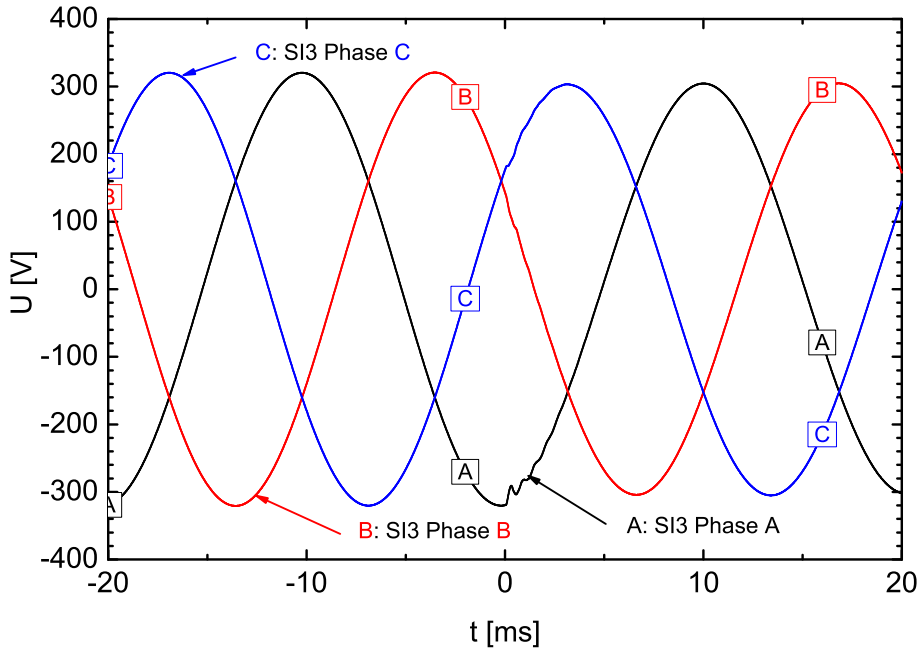

Figure 150: Transient voltages U of the battery inverter Sunny Island 3 (SI3). The connection of the 15 kW asynchronous machines is at the time t = 0 ms.

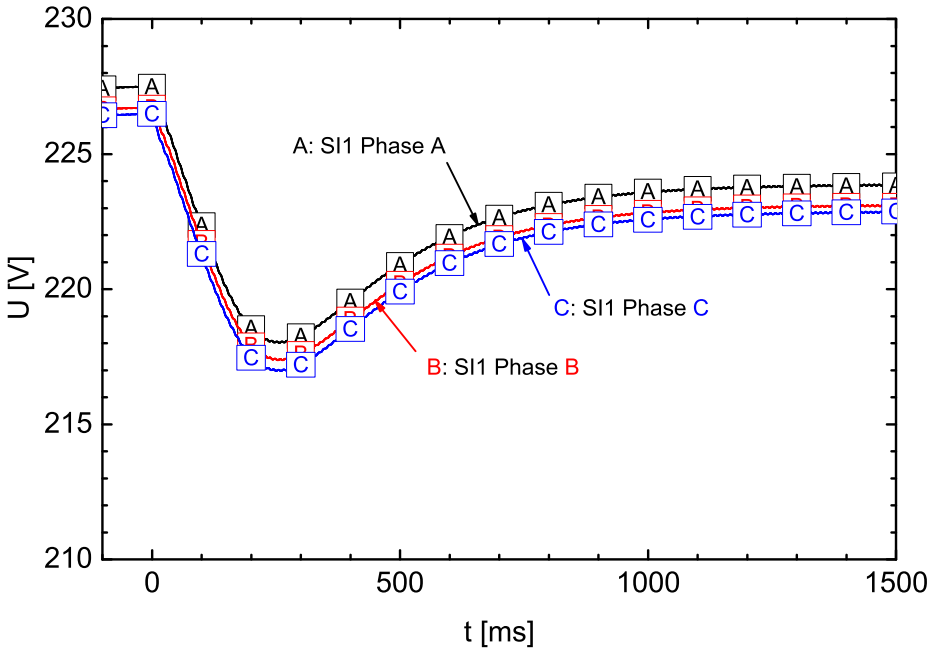

Figure 151: RMS voltages U of the battery inverter Sunny Island 1 (SI1). The connection of the 15 kW asynchronous machines is at the time t = 0 ms.

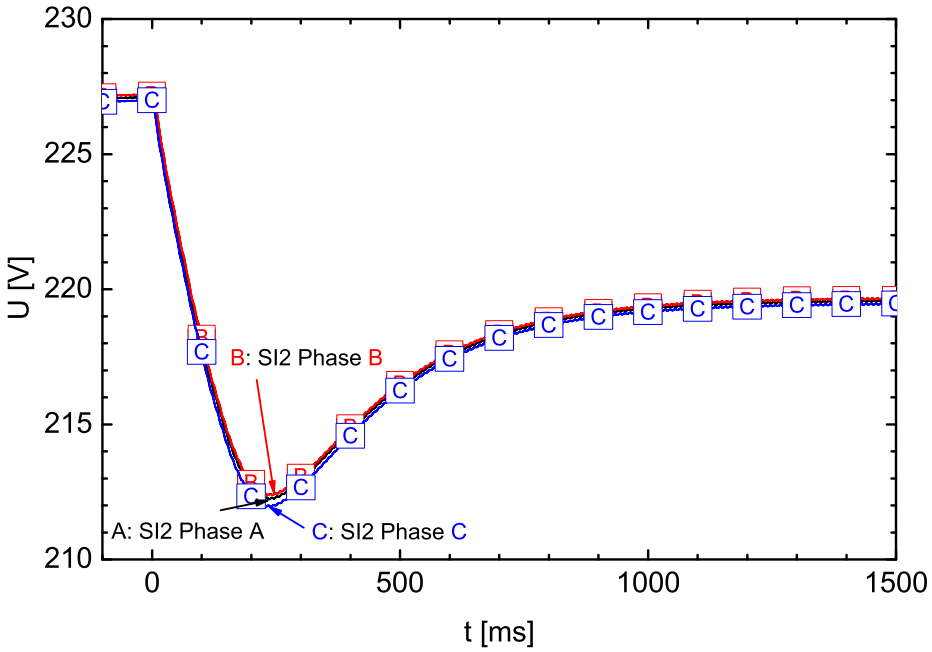

Figure 152: RMS voltages U of the battery inverter Sunny Island 2 (SI2). The connection of the 15 kW asynchronous machines is at the time t = 0 ms.

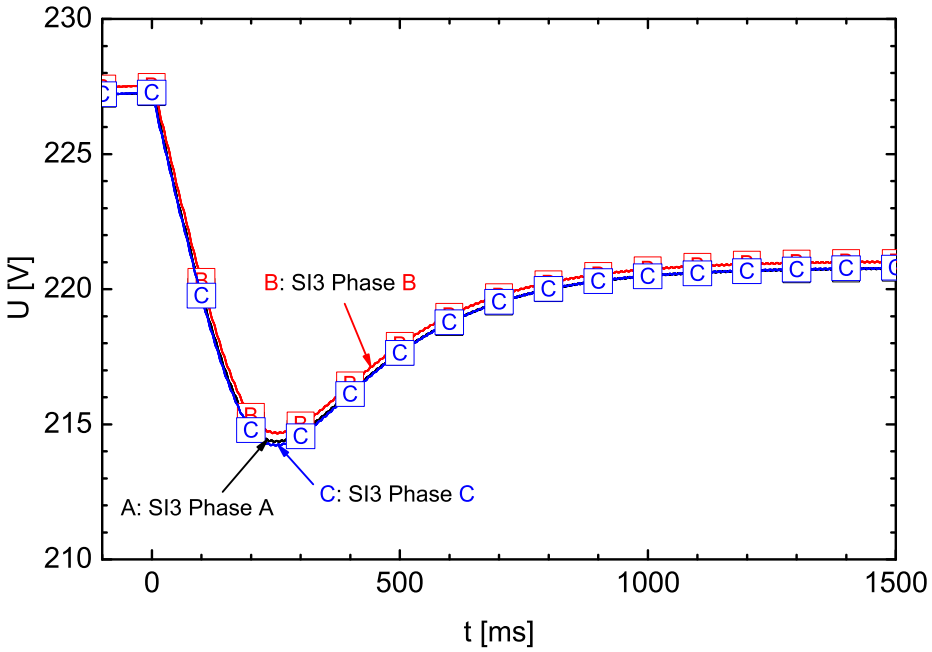

Figure 153: RMS voltages U of the battery inverter Sunny Island 3 (SI3). The connection of the 15 kW asynchronous machines is at the time t = 0 ms.

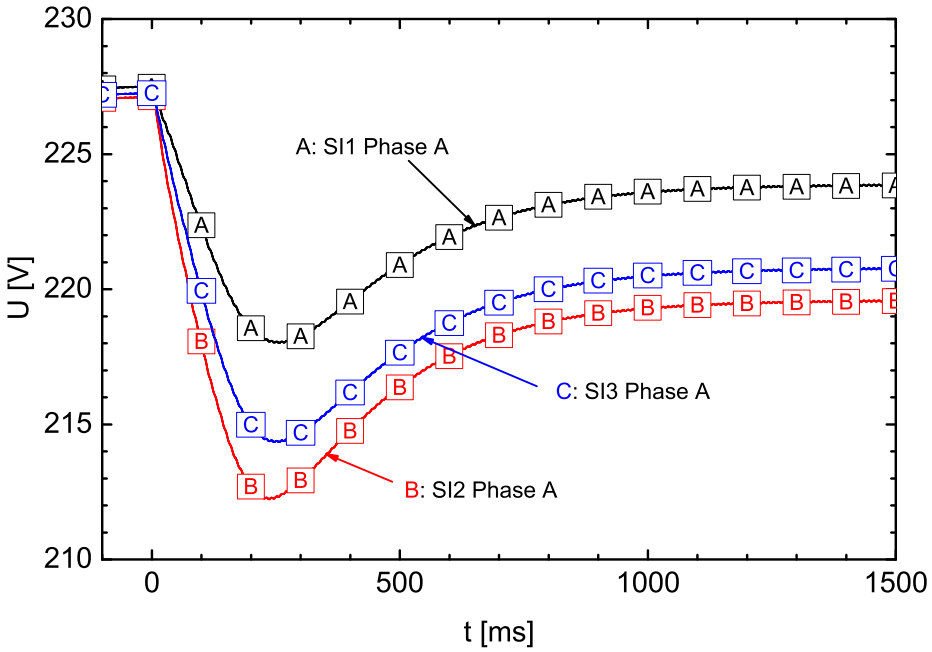

Figure 154: Comparison of the RMS voltages U of phase A of the three battery inverters SI1, SI2 and SI3. The connection of the 15 kW asynchronous machines is at the time t = 0 ms.

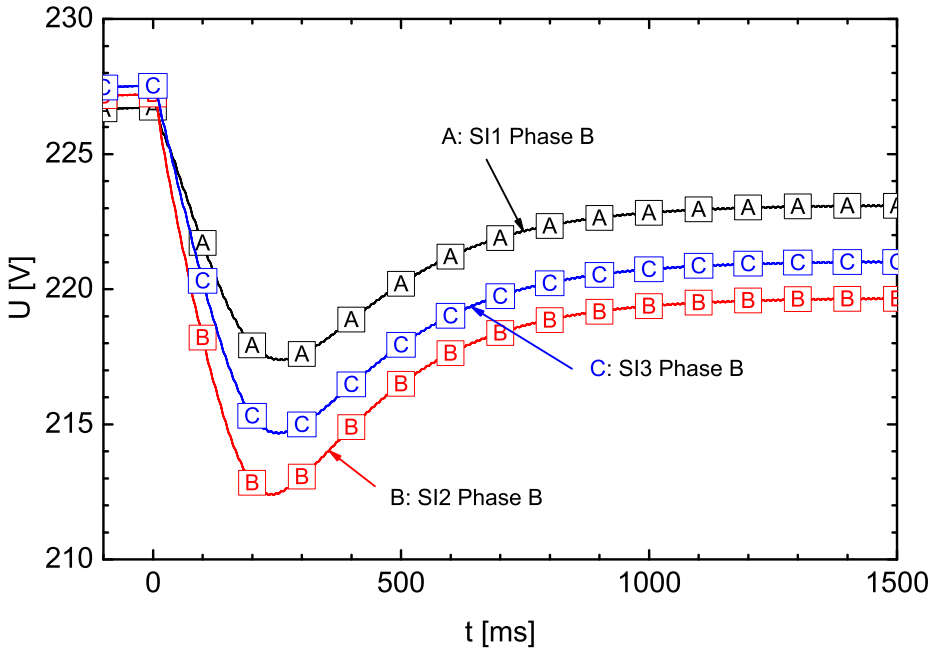

Figure 155: Comparison of the RMS voltages U of phase B of the three battery inverters SI1, SI2 and SI3. The connection of the 15 kW asynchronous machines is at the time t = 0 ms.

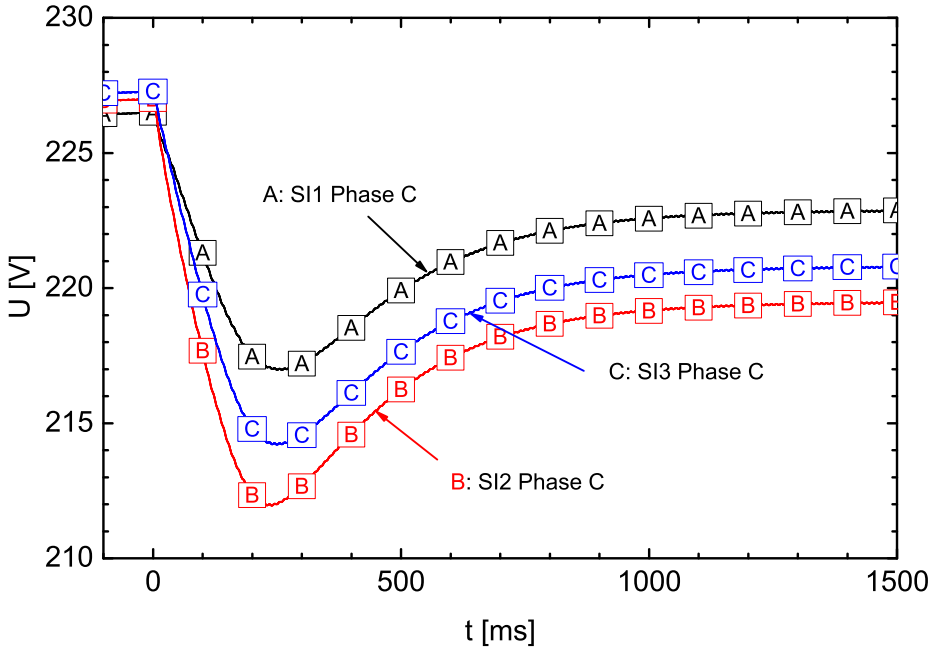

Figure 156: Comparison of the RMS voltages U of phase C of the three battery inverters SI1, SI2 and SI3. The connection of the 15 kW asynchronous machines is at the time t = 0 ms.

List of Tables

List of Figures

List of Abbreviations

AC	Alternating Current
DeMoTec	Design Center for Modular Supply Technology
DC	Direct Current
EMT	Electromagnetic Transients
GIS	Geographic Information System
ISET	Institut für Solare Energieversorgungstechnik
SCADA	Supervisory Control and Data Acquisition
VI	verallgemeinerter Integrator

List of Symbols

α, δ	angle
Δf	frequency reduction
ΔU	difference between the RMS voltages of two voltage sources
η_r	rated efficiency
ω	angular velocity, frequency
ω_r	rated angular velocity
ω_N	resonance frequency
C	capacity
$cos\varphi$	power factor
f	frequency
f_0, f_r	rated electrical frequency
$\underline{i}$	current
$\hat{i}$	magnitude of the current
I	current
i_α, i_β	orthogonal components of the current
I_{oc}	RMS current of the open circuit test
I_r	rated current
I_{sc}	RMS current of the short circuit test
J	torque of inertia
L	inductivity
L_1	inductivity of inverter 1
L_2	inductivity of inverter 2
M_r	rated mechanical torque
M_s	stalling torque
n_1	synchronous speed
n_r	rated mechanical speed
P	active power
P_1	active power of inverter 1
P_2	active power of inverter 2

$P_{e,r}$	rated electrical active power
$P_{m,r}$	rated mechanical active power
P_N	nominal active power
P_{sc}	active power of the short circuit test
p_z	number of pole pairs
Q	reactive power
Q_1	reactive power of inverter 1
Q_2	reactive power of inverter 2
Q_N	rated reactive power
R	resistance
R_{rA}	rotor resistance
R_s	stator resistance
R_{sc}	short circuit resistance
$\vec{S}$	apparent power phasor
s_r	rated slip
S_r	rated electrical apparent power
st_1	slope of the frequency droop
st_1'	slope of the phase control
st_2	slope of the voltage droop
t	time
T_{excite}	excitation time constant
T_{mech}	torque of inertia
$\underline{u}$	voltage
$\hat{u}$	magnitude of the voltage
U	voltage
u_0, U_0	rated RMS voltage
$\underline{U}_1$	voltage phasor of inverter 1
$\underline{U}_2$	voltage phasor of inverter 2
u_α, u_β	orthogonal components of the voltage
U_{oc}	RMS voltage of the open circuit test
U_r	rated voltage
$\underline{u}_{ref}$	voltage reference signal
U_{RMS}	RMS voltage
U_{sc}	RMS voltage of the short circuit test
X_m	magnetizing reactance
X_{rA}	rotor leakage reactance
X_s	stator leakage reactance
X_{sc}	reactance of the short circuit test
Z_r	rated impedance
$Zrot$	rotor impedance
Z_{sc}	impedance of the short circuit test

References

[AG71] Siemens AG. *Handbuch der Elektrotechnik*. W. Girardet, Essen, Berlin, München, 1971.

[Bur97] B. Burger. *Transformatorloses Schaltungskonzept für ein dreiphasiges Inselnetz mit Photovoltaik und Batteriespeicher*. PhD thesis, Universität Karlsruhe, 1997.

[Bur01] A. Engler; B. Burger. Fast signal conditioning in single phase systems. In *9th European Conference on Power Electronics and Applications*, Graz, August 2001.

[Cra00] V. Crastan. *Elektrische Energieversorgung 1: Netzelemente, Modellierung, stationäres Netzverhalten, Bemessung, Schalt- und Schutztechnik*. Springer, Berlin, 2000.

[Cuk77] S. Cuk. *Modelling, Analysis and Design of Switching Conerters*. PhD thesis, California Institute of Technology, Passadena, California, 1977.

[DIg03] DIgSILENT GmbH. *DIgSILENT Technical Documentation - Model Description - Induction Machine*, 220 edition, 2003.

[Eng01] A. Engler. *Regelung von Batteriestromrichtern in modularen und erweiterbaren Inselnetzen*. PhD thesis, Universität Gesamthochschule Kassel, 2001.

[Eng03] O. Osika; A. Engler. Simulation of inverter dominated minigrids. In *2nd European PV-Hybrid and Mini-Grid Conference*, Kassel, September 2003.

[Eng05] A. Engler. Applicability of droops in low voltage grids. *International Journal of Distributed Energy Resources*, 1, 2005.

[HAA03] HAAG Elektronische Messgeräte GmbH. *Die Aufzeichnungsparametrierung des EURO-QUANT (EWS 130) und COMBI-QUANT (EWS 135)*, 28. januar 2003 edition, 2003.

[Har04] S. Papathanassiou; D. Georgakis; N. Hatziargyriou; A. Engler; C. Hardt. Operation of a prototype micro-grid system based on micro-sources equipped with fast-acting power electronic interfaces. In *31th IEEE Power Electronics Specialists Conference*, Aachen, June 2004.

[Leo80] W. Leonhard. *Regelung in der Elektrischen Energieversorgung*. Teubner Studienbücher, Stuttgart, 1980.

[SMA] ISET; SMA. Kythnos island. brochure.

[SMA04] SMA Regelsysteme GmbH. *Sunny Island 4500 - Installation and Operating Instructions*, 3.1 edition, 2004.

[Van01] A. Engler; C. Hardt; P. Strauss; M. Vandenbergh. Parallel operation of generators for stand-alone single-phase hybrid systems - first implementation of a new control technology. In *17th European Photovoltaic Solar Energy Conference and Exhibition*, Munich, October 2001.

[Wil99] B. Burger; P. Zacharias; A. Engler; A. Jansen; B. Kansteiner; M. Rothert; C. Schmitz; C. Siedle; B. Willer. Batteriestromrichter für die modulare systemtechnik in pv-anlagen - entwicklung der steuerungstechnik. FuE-Vorhaben Nr. 0329746 supported by Bundesministerium für Wirtschaft und Technologie, 1999.

[Wue95] F. Jenni; D. Wuest. *Steuerverfahren für selbstgeführte Stromrichter*. vdf Hochschulverlag, Teubner, Zuerich, Stuttgart, 1995.

[Zwi02] T. Zwingmann. Parameterbestimmung für die simulation von asynchronmaschinen mit kurzschlussläufer. Master's thesis, Universität Kassel, Institut für Elektrische Energietechnik, Elektrische Energieversorgungssysteme, 2002.